

SHAPE-DEPENDENT NANOCATALYSIS AND THE EFFECT OF CATALYSIS ON
THE SHAPE AND SIZE OF COLLOIDAL METAL NANOPARTICLES

A Thesis

Presented to

The Academic Family

By

Radha Narayanan

In Partial Fulfillment

of the Requirements for the Degree

Doctor of Philosophy in Chemistry

Georgia Institute of Technology

March 2005

Copyright ©2005 by Radha Narayanan

SHAPE-DEPENDENT NANOCATALYSIS AND THE EFFECT OF CATALYSIS ON
THE SHAPE AND SIZE OF COLLOIDAL METAL NANOPARTICLES

Approved by:

Dr. Mostafa A. El-Sayed, Chairman
School of Chemistry & Biochemistry
Georgia Institute of Technology

Dr. Mohan Srinivasarao
School of Polymer, Textile & Fiber
Engineering
Georgia Institute of Technology

Dr. Paul Wine
School of Chemistry & Biochemistry
Georgia Institute of Technology

Dr. Paul Edmonds
School of Biology
Georgia Institute of Technology

Dr. Z. John Zhang
School of Chemistry & Biochemistry
Georgia Institute of Technology

Date Approved: March 29, 2005

To my family

ACKNOWLEDGMENTS

First and foremost, I would like to thank my advisor, Professor Mostafa A. El-Sayed, for his excellent guidance, encouragement, and support throughout my entire graduate career. I also greatly appreciated the freedom he gave me to pursue my own ideas. I am also very grateful for many rewarding academic, research, professional, and career-related experiences that he has given to me. These experiences have truly enriched my graduate school career and prepared me for my future career.

I thank the Georgia Tech Chemistry department for the Georgia Tech Presidential Fellowship and the GAANN Fellowship I received during the course of my graduate studies. I would like to thank my other committee members (Dr. Paul Wine, Dr. John Zhang, Dr. Mohan Srinivasarao, Dr. Paul Edmonds, Dr. Rick Browner, Dr. Zhong Lin Wang, and Dr. James Gole) for taking some of their valuable time to serve at various stages of my graduate career. I would like to especially thank a former LDL group member, Dr. Yin Li, from whom I have learned a lot during the beginning of my graduate career and also for her genuine friendship during that time. I would also like to thank Ms. Carolyn Dawkins and Ms. Michele Yager for their valuable help when I needed it. I also thank the chemistry department front office staff for their assistance when needed and also for providing me humorous relief at times. I also appreciate the friendships I have made with other graduate students in the department during the course of my graduate career.

I would like to thank the Electron Microscopy Center for the JEOL 100C, Hitachi 2000, and JEOL 4000EX transmission electron microscopes which I have used quite often. I thank Dr. Zhong L. Wang for allowing me the privilege of using the high-

resolution TEM instruments. I also deeply thank Ms. Yolande Berta for training me on all three TEM microscopes and being very helpful when the instruments have problems. I thank Dr. Gary Schuster for allowing me to use his group's HPLC and I thank Ms. Lezah Roberts and Dr. Rick Redic for initially setting up the HPLC with the reversed phase column so I could do my experiments.

Last, but not least, I would like to thank my parents for their complete love, understanding, and support. Without their moral and emotional support, I would not have made it this far.

TABLE OF CONTENTS

	<u>Page</u>
ACKNOWLEDGMENTS	iv
LIST OF TABLES	xv
LIST OF FIGURES	xviii
LIST OF SYMBOLS OR ABBREVIATIONS	xxii
SUMMARY	xxiii
CHAPTER	
1. INTRODUCTION TO NANOCATALYSIS	
1.1 Introduction	1
1.2 Colloidal Metal Nanoparticles as Catalysts in Homogeneous Catalysis	3
1.2.1 Common Synthetic Methods of Colloidal Metal Nanoparticles	4
1.2.1.1 Chemical Reduction Method	6
1.2.1.2 Thermal, Photochemical, or Sonochemical Reduction Methods	7
1.2.1.3 Ligand Displacement Method	9
1.2.1.4 Condensation of Atomic Transition Metal Vapor	9
1.2.1.5 Electrochemical Reduction Method	10
1.2.2 Stabilizers Used in Colloidal Transition Metal Nanoparticles	10
1.2.2.1 Polymers	11
1.2.2.2 Block Copolymer Micelles	12
1.2.2.3 Dendrimers	12
1.2.2.4 Surfactants	13

1.2.2.5 Other Stabilizing Ligands	13
1.2.3 Chemical Reactions Catalyzed by Colloidal Metal Nanoparticles	14
1.2.3.1 Cross-Coupling Reactions	14
1.2.3.2 Electron Transfer Reactions	16
1.2.3.3 Hydrogenation Reactions	17
1.2.3.4 Oxidation Reactions	17
1.3 Supported Transition Metal Nanoparticles in Heterogeneous Catalysis	18
1.3.1 Adsorption of Nanoparticles onto Supports	19
1.3.1.1 Carbon Supports	20
1.3.1.2 Silica Supports	21
1.3.1.3 Alumina Supports	22
1.3.1.4 Titanium Dioxide Supports	22
1.3.2 Grafting of Nanoparticles onto Supports	23
1.3.2.1 Grafting onto Polyacrylamide Gels	23
1.3.2.2 Grafting onto Polystyrene Supports	24
1.3.3 Lithographically Fabricated Transition Metal Nanocatalysts	24
1.3.4 Chemical Reactions Catalyzed Using Transition Metal Nanocatalysts	25
1.3.4.1 Fuel Cell Reactions	26
1.3.4.2 Hydrogenation Reactions	26
1.3.4.3 Reduction and Decomposition Reactions	27
1.4 Outline of the Contents of the Thesis Chapters	27
1.5 References	32
2 EXPERIMENTAL METHODS	

2.1	Preparation of Colloidal Transition Metal Nanoparticles	46
2.1.1	Spherical PVP-Pt Nanoparticles	46
2.1.2	Tetrahedral PVP-Pt Nanoparticles	46
2.1.3	Cubic Polyacrylate-Pt Nanoparticles	47
2.1.4	Spherical PVP-Pd Nanoparticles	48
2.1.5	Spherical Dendrimer-Pd Nanoparticles	49
2.2	Preparation of Supported Transition Metal Nanoparticles	50
2.2.1	Carbon Supported Spherical PVP-Pd Nanoparticles	50
2.3	Transmission Electron Microscopy (TEM)	51
2.3.1	JEOL 100C to Study Size Distribution of Pt and Pd Nanoparticles Under Various Conditions	51
2.3.2	JEOL 100C to Study Shape Distribution of Pt Nanoparticles Under Various Conditions	52
2.3.3	JEM 4000EX HRTEM to Obtain Detailed View of Shape Changes	53
2.3.4	JEM 4000EX HRTEM to Study Size Distribution of Supported Metal Nanoparticles	54
2.4	Catalysis	55
2.4.1	Electron Transfer Reaction	55
2.4.2	Recycling for the Second Cycle of the Electron Transfer Reaction	55
2.4.3	Kinetics of the Electron Transfer Reaction	56
2.4.4	Suzuki Reaction	57
2.4.5	Recycling for the Second Cycle of the Suzuki Reaction	58
2.4.6	Determination of Biphenyl Product by HPLC	58
2.5	References	59
3.	THE EFFECT OF CATALYTIC ACTIVITY ON THE METALLIC	

NANOPARTICLE SIZE DISTRIBUTION: THE ELECTRON TRANSFER
REACTION BETWEEN HEXACYANOFERRATE (III) IONS AND
THIOSULFATE IONS CATALYZED BY PVP-PLATINUM
NANOPARTICLES

3.1 Abstract	60
3.2 Introduction	61
3.3 Experimental Section	64
3.3.1 Synthesis of PVP-Pt Nanoparticles	64
3.3.2 Electron Transfer Reaction	65
3.3.3 Recycling PVP-Pt Nanoparticles for Second Cycle of Electron Transfer Reaction	66
3.3.4 Kinetics of Electron Transfer Reaction	66
3.3.5 Stability of the PVP-Pt Nanoparticles in Various Conditions	67
3.4 Results and Discussion	69
3.4.1 Stability of PVP-Pt Nanoparticles	70
3.4.2 Effect of Catalysis and Recycling	70
3.4.3 Effect of the Individual Reactants on the Nanoparticles	72
3.4.4 Catalytic Activity of PVP-Pt Nanoparticles During First and Second Cycle	77
3.5 Conclusion	82
3.6 References	83
4. EFFECT OF CATALYSIS IN COLLOIDAL SOLUTION ON THE TETRAHEDRAL NANOPARTICLE SHAPE: ELECTRON TRANSFER REACTION CATALYZED BY PVP-PT NANOPARTICLES	
4.1 Abstract	87
4.2 Introduction	88
4.3 Experimental Section	91

4.3.1 Synthesis of Tetrahedral Shaped Platinum Nanoparticles	91
4.3.2 Synthesis of Cubic Shaped Platinum Nanoparticles	91
4.3.3 Studies on the Effect of the Catalytic Reaction	92
4.3.4 TEM Studies	93
4.4 Results and Discussion	94
4.4.1 Effect of the Individual Reactants on the Nanoparticle Shape and the Nanocatalysis Mechanism	102
4.5 Conclusions	108
4.6 References	109
5. SHAPE-DEPENDENT CATALYTIC ACTIVITY OF PLATINUM NANOPARTICLES IN COLLOIDAL SOLUTION	
5.1 Abstract	112
5.2 Introduction	112
5.3 Experimental Section	114
5.4 Results and Discussion	116
5.5 Conclusions	126
5.6 References	127
6. CHANGING CATALYTIC ACTIVITY DURING COLLOIDAL PLATINUM NANOCATALYSIS DUE TO SHAPE CHANGES: ELECTRON TRANSFER REACTION	
6.1 Abstract	129
6.2 Introduction	129
6.3 Experimental Section	131
6.4 Results and Discussion	132
6.5 Conclusions	135

6.6	References	136
7.	EFFECT OF CATALYSIS ON THE STABILITY OF METALLIC NANOPARTICLES: SUZUKI REACTION CATALYZED BY PVP-PD NANOPARTICLES	
7.1	Abstract	137
7.2	Introduction	138
7.3	Experimental Section	141
7.3.1	Synthesis of PVP-Pd Nanoparticles	141
7.3.2	Suzuki Reaction	141
7.3.3	Recycling the PVP-Pd Nanoparticles for the Second Cycle of the Suzuki Reaction	142
7.3.4	The TEM Study to Assess Nanoparticle Stability	142
7.3.5	HPLC Studies to Measure Catalytic Activity	144
7.4	Results and Discussion	145
7.4.1	Effect of Catalysis and Recycling	146
7.4.2	Effect of Excess PVP Stabilizer	151
7.4.3	Effect of Chemicals	154
7.5	Conclusions	157
7.6	References	158
8.	EFFECT OF COLLOIDAL CATALYSIS ON THE METALLIC NANOPARTICLE SIZE DISTRIBUTION: DENDRIMER-PD VS. PVP-PD NANOPARTICLES CATALYZING THE SUZUKI COUPLING REACTION	
8.1	Abstract	162
8.2	Introduction	163
8.3	Experimental Section	166

8.3.1	Synthesis of PAMAM-OH Dendrimer Stabilized Pd Nanoparticles	166
8.3.2	Suzuki Reaction between Phenylboronic Acid and Iodobenzene	167
8.3.3	TEM Studies	167
8.3.4	HPLC Studies	169
8.4	Results and Discussion	170
8.4.1	Effect of Nanoparticle Preparation Method on the Particle Size Growth	170
8.4.2	Mechanism of the Growth of the Palladium Nanoparticles	173
8.4.3	Effect of Capping Agent on Catalytic Mechanism of Suzuki Reaction	178
8.4.4	Effect of Nanoparticle Size during Second Cycle on Biphenyl Yield	181
8.4.5	Effect of Excess Capping Agent	183
8.5	Conclusions	185
8.6	References	186
9.	EFFECT OF COLLOIDAL CATALYSIS ON THE METALLIC NANOPARTICLE SHAPE: THE SUZUKI REACTION	
9.1	Abstract	189
9.2	Introduction	190
9.3	Experimental Section	193
9.3.1	Synthesis of Tetrahedral PVP-Pt Nanoparticles	193
9.3.2	Catalyzing Suzuki Reaction	194
9.3.3	TEM Studies on Size and Shape Stability of Tetrahedral PVP-Pt Nanoparticles	195
9.3.4	HPLC Studies on Catalytic Activity of Nanoparticles	196
9.4	Results and Discussion	196
9.4.1	Catalytic Activity of Tetrahedral PVP-Pt Nanoparticles for Suzuki Reaction	197

9.4.2 Effect of Catalysis and Recycling on Stability of Tetrahedral Shape	200
9.4.3 Effect of the Individual Chemicals Involved in Reaction on Stability of the Tetrahedral Shape	207
9.5 Conclusions	209
9.6 References	210
10. FTIR STUDY ON THE MODE OF BINDING OF THE REACTANTS ON THE PD NANOPARTICLE SURFACE DURING THE CATALYSIS OF THE SUZUKI REACTION	
10.1 Abstract	214
10.2 Introduction	215
10.3 Experimental Section	217
10.3.1 Synthesis of PVP-Pd Nanoparticles	217
10.3.2 FTIR Studies of Dried Films	217
10.4 Results and Discussion	218
10.4.1 FTIR Studies on Phenylboronic Acid	218
10.4.2 FTIR Studies on Films of Iodobenzene and the Pd Nanoparticles	224
10.4.3 Catalytic Mechanism of the Suzuki Reaction	226
10.5 Conclusions	226
10.6 References	227
11. CARBON SUPPORTED PALLADIUM NANOPARTICLES AS POTENTIAL RECYCLABLE CATALYSTS FOR THE SUZUKI REACTION	
11.1 Abstract	229
11.2 Introduction	230
11.3 Experimental Section	234
11.3.1 Synthesis of Colloidal Spherical PVP-Pd Nanoparticles	234

11.3.2	Synthesis of Carbon Supported Spherical PVP-Pd Nanoparticles	235
11.3.3	Catalyzing Suzuki Reaction (First and Second Cycles)	235
11.3.4	HPLC Studies on Catalytic Activity of the Carbon Supported Spherical Pd Nanoparticles	236
11.3.5	HRTEM Studies on the Size Distribution of the Carbon Supported Spherical Palladium Nanoparticles Before and After Catalysis and Recycling	237
11.4	Results and Discussion	238
11.4.1	Catalytic Activity of the Carbon Supported Palladium Nanoparticles	238
11.4.2	Effect of Catalyzing the Suzuki Reaction on the Size of Carbon Supported Spherical Palladium Nanoparticles	242
11.5	Conclusions	245
11.6	References	245
	APPENDIX A--LIST OF PUBLICATIONS	251
	VITA	253

LIST OF TABLES

<u>Table</u>	<u>Page</u>
1.1 Summary of the common reducing agents for the preparation of colloidal transition metal nanoparticles, common stabilizers used to cap transition metal nanoparticles in colloidal solution, and examples of reactions catalyzed using colloidal transition metal nanoparticles in homogeneous catalysis	5
1.2 Summary of the common supports used for the preparation of supported transition metal nanoparticles and examples of reactions catalyzed using supported transition metal nanoparticles in heterogeneous catalysis	19
3.1 Widths and Centers of Gaussian Fits of the Size Distributions of the PVP-Pt Nanoparticles in Various Conditions	69
3.2 Kinetics of Electron Transfer Reaction During First Cycle	78
3.3 Kinetics of Electron Transfer Reaction During the Second Cycle	79
3.4 Activation Energies for Electron Transfer Reaction for First and Second Cycle	80
4.1 Shape Distributions of Dominantly Tetrahedral PVP-Platinum Nanoparticles (Regular Tetrahedral, Distorted Tetrahedral, and Spherical) for Various Perturbations	95
4.2 Shape Distribution of Dominantly Cubic Polyacrylate-Platinum Nanoparticles (Regular Cubes, Distorted Cubes, and Truncated Octahedral) for Various Perturbations	96
5.1 Summary of average size and shape distribution for the dominantly tetrahedral, cubic, and “near spherical” platinum nanoparticles (RT = regular tetrahedral, DT = distorted tetrahedral, S = Spherical, RC = regular cubic, DC = distorted cubic, and TO = truncated octahedral, O = other)	118
5.2 Summary of the average rate constant, activation energy, pre-exponential factor, and entropy of activation for the dominantly tetrahedral, dominantly cubic, and dominantly “near spherical” shaped platinum nanoparticles obtained during the first 40 minutes of the electron transfer reaction	121

6.1	Summary of average size and change in the shape distribution * (%D) for the dominantly tetrahedral, cubic, and spherical platinum nanoparticles and the activation energies (E_a) (kJ/mole) during the course of the catalytic reaction	134
7.1	Summary of Gaussian fits showing the widths and centers of size distributions of PVP-Pd nanoparticles before and after various perturbations	145
7.2	Concentration of the Product Biphenyl After the Various Conditions as Determined by Using HPLC	149
8.1	Summary of widths and centers of size distributions of PAMAM-OH generation 4 dendrimer capped Pd nanoparticles before and after different perturbations	171
8.2	Comparison of the percentage change in the centers and widths of distributions for the PVP-Pd nanoparticles and the PAMAM-OH Generation 4 Dendrimer-Pd nanoparticles as a result of catalyzing the Suzuki reaction	171
8.3	Comparison of center and width of size distributions of dendrimer-Pd nanoparticles synthesized with various reduction times and temperatures before the reaction, after the first cycle, and after the second cycle	176
8.4	Comparison of concentration and reaction yield of biphenyl in the Suzuki reaction catalyzed by the PVP-Pd nanoparticles and dendrimer-Pd nanoparticles	181
8.5	Ratios of biphenyl yields obtained using PVP-Pd nanoparticles and PAMAM-OH Generation 4 Dendrimer-Pd nanoparticles	183
9.1	Summary of the concentration and % yield of biphenyl obtained using the tetrahedral PVP-Pt nanoparticles and the “near spherical” PVP-Pd nanoparticles studied previously	198
9.2	Summary of number (#) of PVP-Pt nanoparticles counted, number and percentage of regular tetrahedral, distorted tetrahedral, and “near spherical” nanoparticles under various conditions	202
10.1	Frequencies of different vibration modes in phenylboronic acid (PA), PA + sodium acetate (SA), PVP-Pd NPs + PA, and PVP-Pd NPS + PA + SA	218

11.1	Biphenyl Yield Obtained with the Carbon Supported Spherical PVP-Pd nanoparticles vs. Colloidal Spherical PVP-Pd nanoparticles studied previously ³⁶	240
11.2	Ratio of biphenyl yields (yield in 2 nd cycle/yield in 1 st cycle) for the case of the carbon supported spherical PVP-Pd nanoparticles and the colloidal spherical PVP-Pd nanoparticles studied previously ³⁶	241
11.3.	Size distributions of the carbon supported spherical PVP-Pd nanoparticles and the colloidal spherical PVP-Pd nanoparticles studied previously ³⁶ before the reaction, after the first cycle, and after the second cycle	244

LIST OF FIGURES

<u>Figure</u>	<u>Page</u>
1.1 Statistics of the number of journal publications per year during the past decade in the area of catalysis with nanoparticles (a) and statistics on the 10 journals with the most publications in the area of catalysis with nanoparticles (b)	2
3.1 TEM images and Gaussian fits of the size distributions [C_D = center of distribution and W_D = width of distribution] of PVP-Pt nanoparticles before the electron transfer reaction (a,b), after the first cycle of the electron transfer reaction (c,d), and after the second cycle of the electron transfer reaction (e,f)	71
3.2 TEM images and Gaussian fits of the size distributions [C_D = center of distribution and W_D = width of distribution] of PVP-Pt nanoparticles before exposure to thiosulfate ions [T] (a,b), after exposure to thiosulfate ions [T] (c,d), before exposure to hexacyanoferrate (III) ions [H] (e,f), and after exposure to thiosulfate ions [H] (g,h)	73
3.3 TEM images and Gaussian fits of the size distributions [C_D = center of distribution and W_D = width of distribution] before electron transfer reaction with PVP-Pt nanoparticles pre-exposed to thiosulfate (a,b), after first cycle of electron transfer reaction with PVP-Pt nanoparticles pre-exposed to thiosulfate (c,d), and after first cycle of the electron transfer reaction with PVP-Pt nanoparticles under normal conditions (e,f)	77
3.4 Plot of activation energy [E_A] as a function of catalyst concentration during the first cycle of the electron transfer reaction (a), Plot of activation energy as a function of catalyst concentration during the second cycle of the electron transfer reaction (b)	82
4.1 Typical TEM image and shape distribution graph of solutions containing dominantly tetrahedral PVP-Pt nanoparticles before electron transfer reaction (a-b), after first cycle of electron transfer reaction (c-d), and after second cycle of electron transfer reaction (e-f) [RT = regular tetrahedral, DT = distorted tetrahedral, and S = spherical]	97
4.2 Typical TEM image and shape distribution of colloidal solutions with dominantly cubic polyacrylate stabilized platinum nanoparticles before the electron transfer reaction (a-b), after the first cycle of electron transfer reaction (c-d), and after the second cycle of electron transfer	

	reaction (e-f) [RC = regular cubes, DC = distorted cubes, and TO = truncated octahedral]	98
4.3	Example of a HRTEM image of a tetrahedral PVP-Pt nanoparticle before electron transfer reaction (a), after second cycle of electron transfer reaction (b), cubic polyacrylate capped Pt nanoparticle before electron transfer reaction (c), and after second cycle of electron transfer reaction (d)	101
4.4	Typical TEM image and shape distribution of solutions with dominantly tetrahedral PVP-Pt nanoparticles before any perturbations (a-b), after exposure to hexacyanoferrate (III) ions for 2 days (c-d), and after exposure to thiosulfate ions for 2 days (e-f) [RT = regular tetrahedral, DT = distorted tetrahedral, and S = spherical]	103
4.5	Typical TEM image and shape distribution of solutions with dominantly cubic polyacrylate capped platinum nanoparticles before any perturbations (a-b), after exposure to hexacyanoferrate (III) ions for 2 days (c-d), and after exposure to thiosulfate ions for 2 days (e-f) [RC = regular cubes, DC = distorted cubes, and TO = truncated octahedral]	104
4.6	Example of a HRTEM image of a tetrahedral PVP-Pt nanoparticle after exposure to hexacyanoferrate (III) ions (a) and dominantly cubic polyacrylate capped platinum nanoparticle after exposure to hexacyanoferrate (III) ions (b)	106
5.1	TEM images and shape distributions of dominantly tetrahedral (a-c), dominantly cubic (d-f), and dominantly “near spherical” (g-i) platinum nanoparticles before and after 40 minutes of electron transfer reaction. This shows that there is no significant change in the shape of the nanoparticles resulting from the catalytic reaction at the highest temperature during the initial 40 minutes of the reaction.	117
5.2	Arrhenius plots obtained using dominantly tetrahedral (a), dominantly cubic (b), and dominantly “near spherical” (c) shaped platinum nanoparticles to catalyze the electron transfer reaction between hexacyanoferrate (III) ions and thiosulfate ions	119
5.3	(a) Plot of average rate constant vs. % surface atoms on edges and corners on the tetrahedral, cubic, and “near spherical” shaped Pt nanoparticles and (b) Plot of $\ln A$ vs. E_A of the Arrhenius equation demonstrating the compensation effect in platinum nanoparticle catalysis. The activation energies and pre-exponential factors are those obtained when using the tetrahedral, cubic, and “near	

	spherical” platinum nanoparticles to catalyze the electron transfer reaction in the first 40 minutes.	123
6.1	TEM images and shape distributions of the nanoparticle solutions used in the catalysis: 6.1a-b is for dominantly tetrahedral, 6.1c-d is for dominantly cubic, and 6.1e-f is for dominantly spherical platinum nanoparticle solutions. (RT = regular tetrahedral, DT = distorted tetrahedral, S = spherical, RC = regular cubic, DC = distorted cubic, TO = truncated octahedral, O = other).	133
6.2	Time dependent changes in the activation energy of the electron transfer reaction (a) and time dependent changes of the initial shape of the platinum nanocatalysts of different shapes (b)	135
7.1	TEM images and Gaussian fits of the size distributions of PVP-Pd NPs before the Suzuki reaction (a,b), after the first cycle (c,d), and after the second cycle (e,f) Figure 8.1e shows a typical TEM image of the nanoparticles after the second cycle	147
7.2	PVP-Pd nanoparticle size as a function of reaction time (a), Biphenyl concentration as a function of reaction time (b)	151
7.3	TEM images and Gaussian fits of PVP-Pd nanoparticles before any perturbations (a,b), after Suzuki reaction with excess PVP (c,d), after refluxing in just solvent (e,f), and after refluxing in just solvent + excess PVP (g,h)	153
7.4	TEM images and Gaussian fits of PVP-Pd nanoparticles before any perturbations (a,b), after just solvent + sodium acetate (c,d), after just solvent + sodium acetate + phenylboronic acid (e,f), and after just solvent + sodium acetate + iodobenzene (g,h)	156
8.1	TEM images and Gaussian fits of size distributions of PAMAM-OH dendrimer capped Pd nanoparticles before the Suzuki reaction (a,b), after the first cycle (c,d), and after the second cycle (e,f)	173
8.2	Typical TEM images and Gaussian fits of the size distributions after the second cycle of the Suzuki reaction for dendrimer-Pd nanoparticles synthesized in the following manners: reduction for 30 minutes at room temperature (a,b), reduction for 1 hour at room temperature (c,d), reduction for 3 hours at room temperature (e,f), and reduction for 1 hour at 100 degrees Celsius (g,h)	177
8.3	TEM images and Gaussian fits of the size distributions of PAMAM-OH Generation 4 dendrimer-Pd nanoparticles after refluxing in solvent (a,b),	

	after refluxing in solvent + SA (c,d), after refluxing in solv. + SA + PA (e,f), and after refluxing in solvent + SA + I (g,h)	179
8.4	TEM images and Gaussian fits of the size distributions of PAMAM-OH Generation 4 dendrimer-Pd nanoparticles before any perturbations (a,b), after refluxing in solvent + excess dendrimer (c,d), and after Suzuki reaction in presence of excess dendrimer (e,f)	184
9.1	Schematic of the Suzuki reaction between phenylboronic acid and iodobenzene to yield biphenyl	194
9.2	TEM images, shape distributions, and size distributions (dominant shape) of PVP-Pt nanoparticles before the Suzuki reaction (a-c), after the first cycle of the Suzuki reaction (d-f), and after the second cycle of the Suzuki reaction (g-i).	203
9.3	Graph of the percentage of regular tetrahedral platinum nanoparticles during the course of the first cycle of the Suzuki reaction and during the course of refluxing the nanoparticles in just the solvent.	205
9.4	HRTEM images of the PVP-Pt nanoparticles before the Suzuki reaction (a) and after the second cycle of the Suzuki reaction (b).	206
9.5	TEM images, shape distributions, and size distributions (dominant shape) of the PVP-Pt nanoparticles after refluxing in solvent alone (a-c), after refluxing in solvent + sodium acetate (d-f), after refluxing in solvent + sodium acetate + phenylboronic acid (g-i), and after refluxing in solvent + sodium acetate + iodobenzene (j-l).	208
10.1	FTIR spectra of PA, SA, SA + PA, PVP-Pd nanoparticles, PVP-Pd nanoparticles + PA, and PVP-Pd nanoparticles + SA + PA in 1800-1200 cm^{-1} region (a), 1200-800 cm^{-1} region (b), and 800-500 cm^{-1} region (c)	220
10.2	Illustration of phenylboronate anion and the two possibilities of binding to the palladium nanoparticle surface which can occur. The binding can occur through one B-O ⁻ group or through both B-O ⁻ groups.	221
10.3	FTIR spectra of I, SA, SA + I, PVP-Pd nanoparticles, and PVP-Pd nanoparticles + SA + I in 1800-1200 cm^{-1} region (a), 1200-800 cm^{-1} region (b), and 800-500 cm^{-1} region (c).	225
11.1	HRTEM images and Gaussian fits of the size distributions of the carbon supported spherical palladium nanoparticles before any perturbations (a-b), after the first cycle of the Suzuki reaction (c-d), and after the second cycle of the Suzuki reaction (e-f)	243

LIST OF SYMBOLS OR ABBREVIATIONS

TEM = Transmission Electron Microscopy

HRTEM = High Resolution Transmission Electron Microscopy

HPLC = High Performance Liquid Chromatography

PVP = polyvinylpyrrolidone

RT = regular tetrahedral

DT = distorted tetrahedral

S = spherical

RC = regular cubic

DC = distorted cubic

TO = truncated octahedral

GC-MS = Gas Chromatography-Mass Spectrometry

E_A = activation energy

A = pre-exponential factor

PAMAM = poly(amidoamine)

ΔS^* = entropy of activation

SUMMARY

From catalytic studies in surface science, it has been shown that the catalytic activity is dependent on the type of metal facet used. Nanocrystals of different shapes have different facets. This raises the possibility that the use of metal nanoparticles of different shapes could catalyze different reactions with different efficiencies. In this thesis, a comparison of the catalytic activity of tetrahedral, cubic, and spherical platinum nanoparticles during the early stages of the electron transfer reaction is conducted. Tetrahedral nanoparticles are composed entirely of (111) facets and have sharp edges and corners. Cubic nanoparticles are composed entirely of (100) facets and have less sharp corners and edges. Spherical nanoparticles are really “near spherical” and composed of both (111) and (100) facets and have corners and edges at the interfaces of these facets. The catalytic activity, as measured by the value of the activation energy, is found to correlate with the fraction of surface atoms located on the corners and edges of the three kinds of nanoparticles. Thus, it is observed that for nanoparticles of comparable size, the tetrahedral nanoparticles have the highest fraction of surface atoms located on the corners and edges and have the lowest activation energy. The cubic nanoparticles have the highest activation energy and the spherical nanoparticles have intermediate activation energy.

Nanoparticles have a high surface-to-volume ratio, which makes them attractive to use compared to bulk catalytic materials. However, their surface atoms are also very active due to their high surface energy. As a result, it is possible that the surface atoms are so active that their size and shape could change during the course of their catalytic function. Would changes in the morphology of the nanoparticles affect their catalytic

activity during the reaction? Studies on how the catalytic process affects the size and shape of the nanocatalyst have been conducted for two reactions: the electron transfer reaction and the Suzuki cross-coupling reaction. The nanoparticle shape (using TEM) and the activation energy are followed during the full course of the electron transfer reaction (2 days). It is found that dissolution of corner and edge atoms occurs for both the tetrahedral and cubic platinum nanoparticles and that there is a corresponding change in the activation energy in which both kinds of nanoparticles strive to behave like spherical nanoparticles. The rate of dissolution of corner and edge atoms is faster for the tetrahedral nanoparticles than the cubic platinum nanoparticles. When spherical platinum nanoparticles are used as catalysts for the electron transfer reaction, there is a small reduction in the size of the nanoparticles after the first and second cycle. When spherical palladium nanoparticles are used as catalysts for the Suzuki reaction, it is found that the nanoparticles grow larger after the first cycle of the reaction due to Ostwald ripening process since it is a relatively harsh reaction due to the need to reflux the reaction mixture for 12 hours at 100 °C. In the case of PVP-capped Pd nanoparticles, the larger nanoparticles formed in the first cycle aggregate and precipitate out of solution resulting in a smaller nanoparticle size distribution remaining in solution. In the case of the PAMAM-OH Generation 4 capped Pd nanoparticles, the nanoparticles continue to grow larger during the second cycle. As a result, the nanoparticle preparation method and capping agent also play a role in the amount of growth that occurs during the catalytic process. In both types of spherical palladium nanoparticles, the nanoparticles were found to have a poor recycling potential, in which the dendrimer-Pd nanoparticles have a slightly higher recycling potential. When the tetrahedral Pt nanoparticles are used to

catalyze this reaction, the tetrahedral nanoparticles transform to spherical ones, which grow larger during the second cycle. The transformed spherical platinum nanoparticles have poor catalytic activity compared to the tetrahedral platinum nanoparticles.

It is also very important to understand the effect of the individual reactants on the nanoparticle size and shape. Can the role of individual reactants on the stability of the nanoparticles provide clues on the mechanism of the reaction? In the case of the electron transfer reaction, it is found that when the platinum nanoparticles are exposed to the thiosulfate ions, the nanoparticle size and shape is maintained for all three nanoparticle shapes. This could be due to binding of the thiosulfate ions to the nanoparticle surface. When the spherical platinum nanoparticles are exposed to the hexacyanoferrate (III) ions, there is a great reduction in the size of the nanoparticles, which could be due to platinum atoms in the surface dissolving due to attack by the CN^- ligand. In the case of the tetrahedral and cubic platinum nanoparticles, distortions in the nanoparticle shape occur due to dissolution of atoms on the corners and edges. As a result, the catalytic mechanism probably involves the thiosulfate ions binding to the nanoparticle surface and reacting with the hexacyanoferrate (III) ions in solution. In the Suzuki reaction, when the spherical palladium nanoparticles are refluxed in the presence of iodobenzene, the nanoparticles continue to grow in size, suggesting that the iodobenzene probably does not interact with the nanoparticle surface. In the case of the tetrahedral platinum nanoparticles, the shape transformation to spherical nanoparticles still occurs, and this also suggests that the iodobenzene does not interact with the nanoparticle surface. However, when the nanoparticles are refluxed in the presence of phenylboronic acid, there is a great inhibition in the growth process in the case of the spherical palladium

nanoparticles and the shape transformation process is greatly inhibited in the case of the tetrahedral platinum nanoparticles. This could be due to the binding of phenylboronic acid to the nanoparticle surface in the deprotonated form. These results suggest that the mechanism of surface catalysis of the Suzuki reaction involves the phenylboronic acid binding to the nanoparticle surface and reacting with iodobenzene via collisional processes. FTIR studies have shown that the mode of binding involves the B-O-Pd bond and the binding is bridged (binding occurs in both B-O groups).

CHAPTER 1

INTRODUCTION TO NANOCATALYSIS

1.1 Introduction

The field of nanocatalysis (the use of nanoparticles to catalyze reactions) has undergone an explosive growth during the past decade, both in homogeneous and heterogeneous catalysis. There have been more than 2800 papers published in both types of nanocatalysis together. Figure 1.1a shows the number of journal publications that have been published in the area of catalysis with nanoparticles for each year in the past decade. It can be seen that catalysis with nanoparticles is a growing field. Since nanoparticles have a large surface-to-volume ratio compared to bulk materials, they are attractive to use as catalysts. Figure 1.1b shows the number of publications that have been published in the area of catalysis with nanoparticles in the top ten journals. The top five journals in this field in terms of the number of publications include *Journal of Physical Chemistry B*, *Langmuir*, *Journal of the American Chemical Society*, *Journal of Catalysis*, and *Chemistry of Materials*. The use of supported nanoparticles in heterogeneous catalysis accounts for majority of the publications, while colloidal nanoparticles in homogeneous catalysis accounts for only about 15-20% of the work. The synthetic methods and stabilizing agents used to prepare colloidal transition metal nanoparticles for homogeneous catalysis applications and the major reactions conducted using these colloidal transition metal nanocatalysts are discussed. The various supports used to prepare supported transition metal nanoparticles for heterogeneous catalysis

applications and the major reactions that have been conducted using the supported transition metal nanocatalysts are also discussed.

In the last section of this chapter, the organization of the thesis and the major findings in each chapter is summarized.

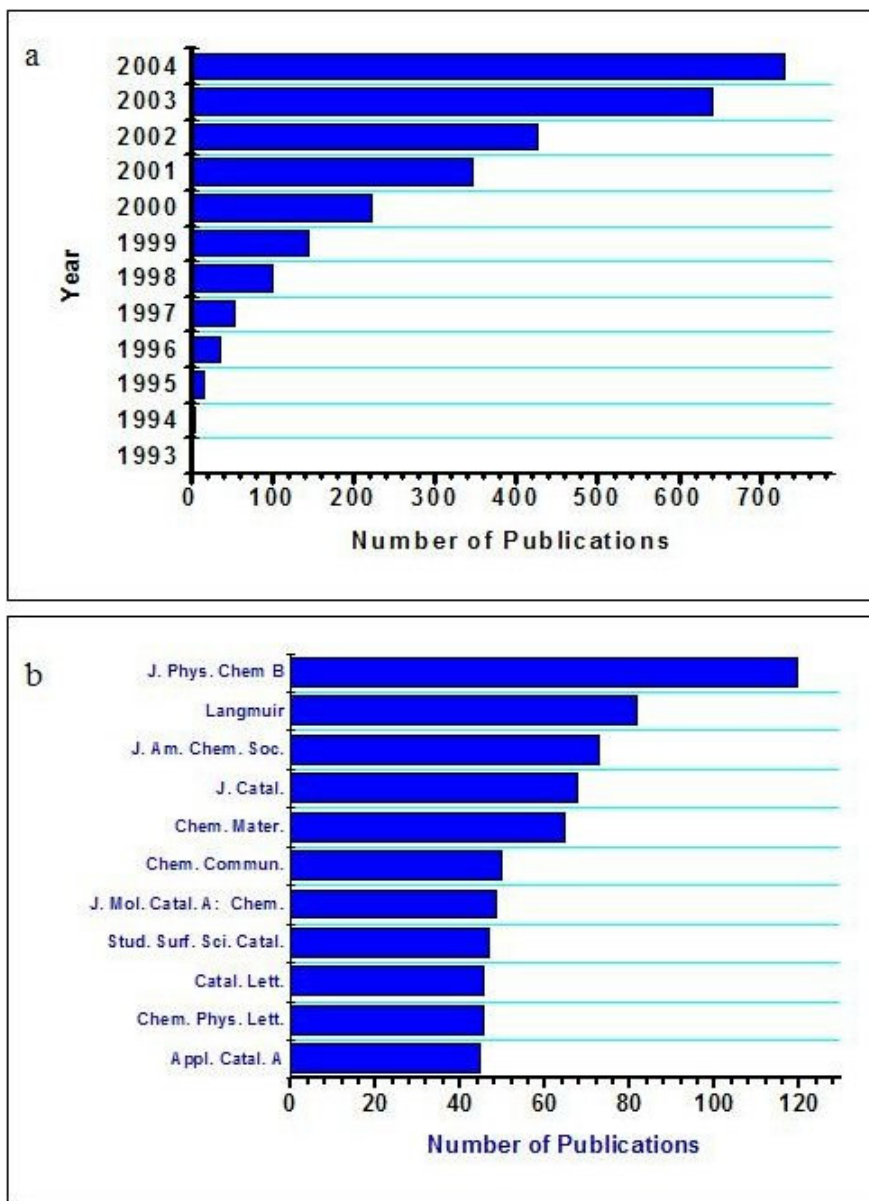


Figure 1.1—Statistics of the number of journal publications per year during the past decade in the area of catalysis with nanoparticles (a) and statistics on the 10 journals with the most publications in the area of catalysis with nanoparticles (b). The statistics are obtained using Scifinder Scholar.

1.2 Colloidal Metal Nanoparticles as Catalysts in Homogeneous Catalysis

In homogeneous catalysis, transition metal nanoparticles in colloidal solution are used as catalysts. In this type of catalysis, the colloidal transition metal nanoparticles are finely dispersed in an organic or aqueous solution or a solvent mixture. The colloidal nanoparticle solutions must be stabilized in order to prevent aggregation of the nanoparticles and also to be good potential recyclable catalysts. Nanoparticles have a large surface-to-volume ratio compared to other bulk materials and this makes them attractive to use as catalysts. The reason why it has been suggested that transition metal colloids are very efficient catalysts is because there is a large number of atoms that are present in the surface of the nanoparticles.

There have been many review articles that discuss the use of colloidal transition metal nanoparticles as catalysts for homogeneous catalysis and also some of the major reactions that this type of nanoparticles has catalyzed¹⁻⁷. One review has focused on whether transition metal colloidal nanoparticles are potential recyclable catalysts¹. The synthesis, structure, and catalytic properties of giant palladium clusters and nanosized palladium complexes stabilized with ligands have also been reported². The use of transition metal nanoparticles stabilized with various polymers as homogeneous catalysts has been reviewed³. The use of monometallic and bimetallic nanoparticles stabilized by solvent and surfactants as catalysts has been surveyed⁴. Bimetallic catalysts in colloidal dispersions that are stabilized with PVP as potential catalysts have also been reviewed⁵. The use of transition metal catalysts in colloidal solution as low temperature oxidation catalysts has been reviewed⁶. There has also been a general review article on nanoscale transition metal nanoparticles and a description of transition metal colloids⁷.

The common synthetic methods that are used to prepare colloidal transition metal nanocatalysts, the common stabilizers that are used to cap the colloidal transition metal nanocatalysts, and some common chemical reactions that have used colloidal transition metal nanoparticles as homogeneous catalysts are discussed. Some of the important concepts in homogeneous catalysis with colloidal transition metal nanoparticles as catalysts are also discussed.

1.2.1 Common Synthetic Methods of Colloidal Metal Nanoparticles

The method that is used in synthesizing transition metal nanoparticles in colloidal solution is very important for catalytic applications. The reduction method that is used controls the size and the shape of the transition metal nanoparticles that are formed. Size and shape control of transition metal nanoparticles is very important in catalytic applications. In this section, many reduction methods that have been used to synthesize transition metal nanoparticles are discussed. Table 1.1 summarizes the different reduction methods that have been used to synthesize colloidal transition metal nanoparticles for homogeneous catalysis. Chemical reduction⁸⁻⁶³ of the precursor transition metal salt is the most widely used method of synthesizing transition metal nanocatalysts in colloidal solution. There are four other synthetic methods to prepare colloidal transition metal nanocatalysts that are not as commonly used. These other synthetic methods include thermal, photochemical, or sonochemical reduction of the precursor transition metal salt⁶⁴⁻⁸³, ligand reduction and displacement from organometallic precursors⁸⁴⁻⁹³, metal vapor synthesis⁹⁴⁻¹⁰², and electrochemical reduction of transition metal precursor salts¹⁰³⁻¹⁰⁵. The common types of chemical reduction

processes that have been used to prepare colloidal transition metal nanocatalysts are discussed in more detail since this is the most widely used method. The other four synthetic methods that are used to generate transition metal nanocatalysts in colloidal solution are also discussed briefly.

Table 1.1—Summary of the common reducing agents for the preparation of colloidal transition metal nanoparticles, common stabilizers used to cap transition metal nanoparticles in colloidal solution, and examples of reactions catalyzed using colloidal transition metal nanoparticles in homogeneous catalysis

Important Factors for Colloidal Transition Metal Nanoparticles	Examples
Reducing Agents	Alcohols ⁸⁻²³ Hydrogen gas ²⁴⁻³⁵ Sodium borohydride ³⁶⁻⁵⁵ Hydrazine ⁵⁶⁻⁶¹ Sodium citrate ⁶²⁻⁶³ Thermal reduction ⁶⁴⁻⁶⁹ Photochemical reduction ⁷⁰⁻⁷⁵ Sonochemical reduction ⁷⁶⁻⁸³ Ligand displacement of organometallics ⁸⁴⁻⁹³ Metal vapor condensation ⁹⁴⁻¹⁰² Electrochemical reduction ¹⁰³⁻¹⁰⁵
Stabilizers	Polymers ^{8-12, 24-28, 106-112} Block copolymers ¹¹³⁻¹¹⁷ Dendrimers ^{114, 118-124} Surfactants ¹²⁵⁻¹²⁹ Other ligands ¹³⁰⁻¹³⁷
Chemical Reactions	Suzuki Reactions ^{9-11, 114, 118, 120, 138-143} Heck Reactions ^{123, 138, 141-142, 144-148} Electron Transfer Reactions ^{12, 26-28, 149-152} Hydrogenations ¹⁵³⁻¹⁵⁷ Oxidations ¹⁵⁸⁻¹⁶⁴

1.2.1.1 Chemical Reduction Method

The chemical reduction of transition metal salts in solution is the most common and simplest method of generating colloidal transition metal nanocatalysts. One common reducing agent used is alcohols⁸⁻²³, mainly ethanol⁸⁻¹⁶ and methanol¹⁷⁻¹⁸. In this reduction method, the alcohol acts both as a solvent and reducing agent and the reduction of the transition metal salt takes place when the solution is refluxed. The use of alcohols as a reducing agent results in a fast reduction of the precursor transition metal salt with colloid formation occurring quickly. In this reduction process, the precursor transition metal salts are reduced to form the transition metal nanoparticles, while the alcohols are oxidized to form the corresponding carbonyl compound. There have been many studies conducted on how the size of the transitional transition metal colloids is dependent on the structure and quantity of alcohol used to reduce the precursor transition metal salt¹⁹⁻²³. It has also been shown that in the case of the formation of platinum, palladium, and rhodium nanoparticles in colloidal solution that the higher the boiling point of the alcohol used as the reducing agent, the smaller the size of the nanoparticles formed¹⁹⁻²¹.

The use of hydrogen gas²⁴⁻³⁵ has also been a common reducing agent for the preparation of colloidal transition metal nanocatalysts. The hydrogen reduction method involves bubbling hydrogen gas into a solution containing the transition metal salt and through a slow reduction process, colloidal nanoparticles are formed. Tetrahedral^{24, 26-28}, cubic^{24, 26-29}, and truncated octahedral²⁴⁻²⁵ shaped platinum nanoparticles have all been formed by the hydrogen reduction method. Tetrahedral shaped nanoparticles, which are composed of (111) facets, are especially attractive to use as catalysts due to the large fraction of surface atoms that are present in the edges and corners. Hydrogen reduction

has also been used to reduce precursor iridium and rhodium organometallic complexes to generate electrosterically stabilized colloidal nanoparticles that have been shown to have a well-defined stoichiometry of formation³³⁻³⁴.

Sodium borohydride³⁶⁻⁵⁵ reduction method is another common method of synthesizing colloidal transition metal nanocatalysts. This method of reduction is generally fast with colloid formation occurring quickly after the addition of sodium borohydride. Sodium borohydride reduction has been used to synthesize platinum, palladium, copper, gold, and silver nanoparticles in the presence of dendrimers^{36,37, 44-50}. Many transition metal nanoparticles such as platinum, palladium, gold and silver have also been synthesized using the sodium borohydride reduction method in the presence of polymer protecting agents⁵¹⁻⁵⁵.

There have also been several other reduction methods that are used to synthesize metal nanoparticles in colloidal solution such as hydrazine⁵⁶⁻⁶¹ and sodium citrate⁶²⁻⁶³ that involve the chemical reduction of the precursor transition metal salt. Hydrazine has been used to synthesize nickel and palladium nanoparticles at room temperature⁵⁶⁻⁵⁷. Hydrazine reduction of platinum and palladium nanoparticles has been conducted in water-in-oil microemulsions^{58, 60-61}. Sodium citrate has also been used as a reducing agent for the preparation of iridium⁶² and platinum⁶³ nanoparticles.

1.2.1.2 Thermal, Photochemical, or Sonochemical Reduction Methods

Thermal reduction⁶⁴⁻⁶⁹ of the precursor transition metal salt is also referred to as thermolysis and is a reduction method that involves the decomposition of the precursor organometallic salt to the zerovalent form. It is another method that is used to synthesize

colloidal transition metal nanocatalysts. Platinum, palladium, and copper nanoparticles have been synthesized by using the thermal reduction method^{64-67, 69}. Bimetallic Pd/Ni nanoparticles have also been synthesized using the thermal reduction method⁶⁸.

The photochemical reduction method⁷⁰⁻⁷⁵ of synthesizing colloidal transition metal nanoparticles can be conducted in two ways: reduction of precursor transition metal salt by radiolytically produced reducing agents or degradation of an organometallic complex by radiolysis. The radiation methods that have been used include X-ray or gamma-ray radiations and also UV-visible radiation by the use of the xenon or mercury lamp. Radiolysis of transition metal salts in aqueous solution produces solvated electrons that result from water radiolysis, which reacts with molecules in solution to form new radicals that are able to reduce the transition metal salts. Radiolytically produced reducing agents have been used to synthesize platinum and palladium nanoparticles in colloidal solution⁷⁰⁻⁷². Photolysis of transition metal salts have also been successfully used to synthesize platinum and palladium nanoparticles using UV-visible radiation⁷³⁻⁷⁵. It has been reported that the use of UV-visible radiation results in smaller and better dispersed transition metal nanoparticles.

Sonochemical reduction⁷⁶⁻⁸³ is another method of synthesizing colloidal transition metal nanoparticles. Sonication is an acoustic cavitation phenomenon that involves the formation, growth, and explosion of bubbles in liquid media. The sonochemical reduction method of precursor transition metal salts involves generation of the active species, reduction of the transition metal, and growth of the colloid in a sonicated liquid medium. These steps occur in different compartments: in gas phase into the cavitation bubbles where high temperature and pressure allow water pyrolysis to form H and OH

radicals, at the interface between the cavitation bubbles and the solution, and finally in the solution. The sonochemical reduction method has been applied for the generation of colloidal platinum, palladium, gold, and silver nanoparticles⁷⁶⁻⁸³. In the case of transition metal salts, the reduction process mainly takes place at the bubble/solution interface and in solution and does not take place in the gas phase due to the low vapor pressure of the precursor transition metal salts.

1.2.1.3 Ligand Displacement Method

The ligand displacement method⁸⁴⁻⁹³ of forming colloidal transition metal nanocatalysts results from the reduction or ligand displacement of organometallic compounds. Platinum and palladium nanoparticles can be generated using this method⁸⁴⁻⁸⁷. The reduction of zerovalent organometallic complexes can also be used to synthesize other transition metal nanoparticles such as ruthenium, nickel, cobalt, or copper nanoparticles⁸⁸⁻⁹³.

1.2.1.4 Condensation of Atomic Transition Metal Vapor

Transition metal vapors can be co-condensed with organic vapors to form transition metal nanocatalysts⁹⁴⁻¹⁰². This method involves the evaporation of relatively volatile transition metals at reduced pressure and a subsequent co-condensation of these transition metals at low temperature with the vapors of organic salts. The colloidal transition metal nanoparticles are formed by nucleation and growth when the frozen metal/organic mixture is warmed to the point of melting. The condensation process has taken place in acetone⁹⁶⁻⁹⁷ to form palladium and gold colloidal nanoparticles and has

also taken place in fluorinated solvents¹⁰⁰⁻¹⁰¹. This method of generating colloidal nanoparticles can lead to particles that are stable for several months, but a limitation of this method is that there is no precise control of the size of the nanoparticles. This is a major limitation in terms of applications in catalysis since control of size of the nanoparticles is necessary to conduct reproducible catalytic reactions.

1.2.1.5 Electrochemical Reduction Method

An electrochemical method¹⁰³⁻¹⁰⁵ for preparing size-controlled transition metal nanoparticles in colloidal solution has been developed. This method involves the use of a sacrificial anode as the metal source, which is oxidized in the presence of a quaternary ammonium salt, which acts as both the electrolyte and the stabilizer. The precursor transition metal ions are reduced at the cathode to yield the colloidal transition metal nanoparticles. This method has been successfully used to synthesize palladium, nickel, copper, platinum, rhodium, and ruthenium nanoparticles¹⁰³⁻¹⁰⁵. An advantage to this method of synthesizing transition metal nanoparticles is that the particle size can be controlled by the current intensity. When the current intensity is increased, smaller transition metal nanoparticles are produced.

1.2.2 Stabilizers Used in Colloidal Transition Metal Nanoparticles

Stabilization of the transition metal nanoparticles in colloidal solution is necessary in order to prevent agglomeration and aggregation. For catalytic applications, the choice of stabilizers for the transition metal nanoparticles is especially important. A good stabilizer is one that protects the nanoparticles during the catalytic process, but does not

passivate the nanoparticle surface fully. If full passivation of the nanoparticles occurs, there will be a drastic loss of catalytic activity since there will be very few active sites available for catalysis. On the other hand, a stabilizer that doesn't passivate the nanoparticle surface well and has many free sites available for catalysis will result in the nanoparticles falling apart during the course of the catalytic process. As a result, in the course of deciding a stabilizer to use for capping transition metal nanoparticles, one must find a balance between the passivation of the nanoparticle surface and the fraction of available sites for catalysis. In addition, the choice of stabilizer will also affect the size and shape of the colloidal transition metal nanoparticles formed. This is another important factor that should play a role in deciding the stabilizer to use to cap transition metal nanoparticles in colloidal solution. Table 1.1 summarizes the different stabilizers that have been used to cap colloidal transition metal nanoparticles used in homogeneous catalysis. Some of the common types of stabilizers that have been used to cap colloidal transition metal nanoparticles such as polymers^{8-12, 24-28, 106-112}, block copolymers¹¹³⁻¹¹⁷, dendrimers^{114, 118-124}, surfactants¹²⁵⁻¹²⁹, and other ligands¹³⁰⁻¹³⁷ are discussed.

1.2.2.1 Polymers

There have been numerous types of polymers that have been used as stabilizers for colloidal transition metal nanoparticles. Some kinds of polymers that have been utilized include PVP^{8-12, 26-28, 106-109}, polyacrylate²⁴⁻²⁸, polystyrene¹¹⁰⁻¹¹², etc. PVP has been used to cap spherical shaped palladium⁸⁻¹¹, platinum^{12, 26-28}, and rhodium¹⁰⁸⁻¹⁰⁹ nanoparticles. It has also been used to prepare tetrahedral shaped platinum nanoparticles²⁶⁻²⁸. Tetrahedral shaped nanoparticles are very attractive as catalysts due to

a large fraction of their surface atoms being present on their edges and corners as opposed to their (111) facets. Polyacrylate has been used to cap cubic^{24, 26-28} and truncated octahedral²⁴⁻²⁵ shaped platinum nanoparticles. Platinum nanoparticles in colloidal solution have also been encapsulated inside the nanocavities of hyper-cross-linked polystyrene¹¹⁰⁻¹¹².

1.2.2.2 Block Copolymer Micelles

The formation of colloidal metal nanoparticles in the micelles of block copolymers¹¹³⁻¹¹⁷ has also been a common method of stabilizing the transition metal nanoparticles. Block copolymers have been used as stabilizers since they provide better protecting action compared to polymers by themselves. There have been many different block copolymer combinations that have been used as catalysts such as poly(ethylene oxide)-block-poly-2-vinylpyridine¹¹³, polystyrene-*b*-poly-(sodium acrylate)¹¹⁴, tert-Bu acrylate-2-cinnamoyloxyethyl methacrylate¹¹⁵, polystyrene-block-Poly-4-vinylpyridine¹¹⁶⁻¹¹⁷, etc. These block copolymers have been used as stabilizers for palladium and platinum nanoparticles.

1.2.2.3 Dendrimers

The use of dendrimers^{114, 118-124} as stabilizers for transition metal nanocatalysts has been a fairly recent phenomenon. The encapsulating action of dendrimers is dependent on the generation of the dendrimers that is used. The higher generation dendrimers have closed, increasingly compact structures which can provide effective encapsulating action for the metal nanoparticles. The most common types of dendrimers

that are used in preparing colloidal metal nanoparticles are PAMAM based dendrimers^{114, 118-124} and PPI based dendrimers^{119, 121, 124}. These types of dendrimers have been used to prepare palladium, platinum, and bimetallic colloidal nanoparticles. Higher generation dendrimers have a strong encapsulating action for the stabilization of the transition metal nanoparticles, but can lead to reduced catalytic activity if the dendrimer generation used is too high. This is an important factor to take into consideration when deciding which generation of dendrimers to use as stabilizers for transition metal nanocatalysts.

1.2.2.4 Surfactants

Surfactants combine both electrostatic and steric stabilization in order to stabilize transition metal nanoparticles in solution. Surfactants have a polar head group that is able to generate an electric double layer and a lipophilic side chain that is able to provide steric repulsion. Some kinds of surfactants¹²⁵⁻¹²⁹ that have been used as stabilizers include N,N-dimethyl-N-cetyl-N-(2-hydroxyethyl)ammonium chloride salt¹²⁵, monoalkyl-monocationic surfactant¹²⁶, N-alkyl-N-(2-hydroxyethyl)ammonium salts¹²⁷, ammonium (Bu₄N⁺)/polyoxoanion¹²⁸⁻¹²⁹, etc. Many colloidal transition metal nanoparticles such as iridium, platinum, and palladium nanoparticles have been prepared by the use of various surfactants as stabilizers.

1.2.2.5 Other Stabilizing Ligands

There are also many other kinds of ligands that have been used to stabilize colloidal metal nanoparticles. Some of these ligands include phosphines¹³⁰⁻¹³², thiols¹³³⁻¹³⁴, and amines¹³⁵⁻¹³⁷. Platinum, palladium, nickel, and gold nanoparticles in colloidal

solution have been stabilized using phosphine ligands. Platinum and palladium nanoparticles have been prepared using octanethiols as ligands.

1.2.3 Chemical Reactions Catalyzed by Colloidal Metal Nanoparticles

Some types of chemical reactions that have been catalyzed using transition metal nanocatalysts in colloidal solution include cross-coupling reactions^{9-11, 114, 118, 120, 123, 138-148}, electron transfer reactions^{12, 26-28, 149-152}, hydrogenations¹⁵³⁻¹⁵⁷, and oxidations¹⁵⁸⁻¹⁶⁴. There are many other types of reaction that have also been catalyzed using transition metal nanoparticles in colloidal solution. Table 1.1 summarizes some of the major reactions that have been catalyzed using colloidal transition metal nanocatalysts.

1.2.3.1 Cross-Coupling Reactions

Two main types of cross-coupling reactions that have been catalyzed using transition metal nanoparticles in colloidal solution are the Suzuki cross-coupling reaction and the Heck cross-coupling reaction. The Suzuki reaction is a C-C bond formation reaction which couples arylboronic acids and aryl halides to form biaryls. The Heck reaction is a C-C bond formation reaction that occurs by the arylation of alkenes with aryl halides.

The use of transition metal nanoparticles to catalyze the Suzuki reaction^{9-11, 114, 118, 120, 138-143} has been a fairly recent phenomenon. Palladium nanoparticles^{9-11, 114, 118, 120, 138-141}, are most commonly used to catalyze the Suzuki reaction while ruthenium¹⁴²⁻¹⁴³, copper¹⁴³, and bimetallic¹⁴³ nanoparticles have also been used to a much smaller extent. Many different capping agents have been used to stabilize the palladium nanoparticles

that are used to catalyze the Suzuki reaction such as PVP^{9-11, 114, 118}, PAMAM-OH dendrimers^{114,118, 120}, polystyrene-*b*-poly-(sodium acrylate)¹¹⁴, poly(N,N-dialkylcarbodiimide¹⁴⁰, G-3 dendrimer¹⁴¹, etc. The Suzuki reaction has been conducted in aqueous solution using the 3:1 acetonitrile:water solvent^{9-11, 114, 118} with palladium nanoparticles. The reaction has also been catalyzed with palladium nanoparticles under microwave heating conditions¹⁴⁰. It has been shown that when PVP-Pd nanoparticles¹¹ and PAMAM-OH Generation 4 dendrimer-stabilized Pd nanoparticles¹¹⁴ are used to catalyze the Suzuki reaction between phenylboronic acid and iodobenzene, the palladium nanoparticles grow larger in size due to the Ostwald ripening process and the presence of unreduced Pd ions, partly reduced Pd ions, and Pd atoms in solution. After the second cycle, the larger nanoparticles aggregate and precipitate out of solution, leaving the smaller nanoparticles left in solution. Also, it is found that the growth process occurs in the presence of iodobenzene, while it is inhibited in the presence of phenylboronic acid, the other reactant. Based on these results, it is proposed that the mechanism of surface catalysis involves phenylboronic acid binding to the nanoparticle surface and reacting with iodobenzene in solution.

Another cross-coupling reaction that has been catalyzed using transition metal nanoparticles in colloidal solution is the Heck reaction^{123, 138, 141-142, 144-148} between alkenes and aryl halides for C-C bond formation. The Heck reaction has also been conducted mainly using palladium nanoparticles^{123, 138, 141, 144-147}. Ruthenium nanoparticles¹⁴² and trimetallic (gold-silver-palladium) nanoparticles¹⁴⁸ have also been used as catalyst for the Heck reaction.

1.2.3.2 *Electron-Transfer Reactions*

Electron transfer reactions^{12, 26-28, 149-152} have also been catalyzed using transition metal nanoparticles in solution. There have been studies using spherical^{12, 27-28}, tetrahedral²⁶⁻²⁸, and cubic²⁶⁻²⁸ shaped platinum nanoparticles to catalyze the electron transfer reaction between hexacyanoferrate (III) ions and thiosulfate ions to understand what happens to the nanoparticles during the course of the reaction^{12, 26-27} and also to determine the catalytic activity²⁷⁻²⁸. The tetrahedral nanoparticles with their (111) facets and also a great fraction of surface atoms on edges and corners are found to be the most catalytically active²⁸. The cubic nanoparticles with their (100) facets and a very small fraction of surface atoms on edges and corners are found to be the least catalytically active. The spherical nanoparticles are actually “near spherical” since they are composed of many (111) and (100) facets with many edges at their interfaces. As a result, the activation energy of the “near spherical” nanoparticles is intermediate to that of the tetrahedral and cubic nanoparticles. All of these results were obtained in the beginning of the reaction where no shape changes were observed²⁸. It has been observed that during the course of the reaction, there are changes in the tetrahedral and cubic shapes with corresponding changes in the activation energies²⁷.

A size-dependent study has also been conducted using platinum nanoparticles¹⁴⁹ to catalyze this electron transfer reaction and it was observed that particles below 38 nanometers exhibit a trend of decreasing reaction rate with decreasing particle size, while those above 38 nanometers show a steady decline of reaction rate with increasing size. Platinum nanoparticles that are stabilized in aerosol-OT (AOT)-water-heptane system¹⁵⁰

have also been used to catalyze this reaction. In addition citrate-stabilized gold nanoparticles¹⁵¹⁻¹⁵² has also been used to catalyze this reaction.

1.2.3.3 Hydrogenation Reactions

Hydrogenation reactions¹⁵³⁻¹⁵⁷ are the most common reactions that have been conducted using transition metal nanoparticles in colloidal solution. Examples of some types of hydrogenation reactions that have been catalyzed with colloidal transition metal nanoparticles include hydrogenation of benzene¹⁵³⁻¹⁵⁴, cyclooctene hydrogenation¹⁵⁵, hydrogenation of dehydrolinalool^{57, 156}, hydrogenation of cinnamaldehyde¹⁵⁷, etc. There are many more kinds of hydrogenation reactions that have also been conducted and are too numerous to list. Hydrogenation reactions have been conducted using many different kinds of colloidal transition metal nanoparticles such as palladium, platinum, and rhodium nanoparticles. Various bimetallic nanoparticles have also been used to catalyze hydrogenation reactions in colloidal solution.

1.2.3.4 Oxidation Reactions

Oxidation reactions¹⁵⁸⁻¹⁶⁴ are very important in many industrial processes and have been catalyzed by colloidal transition metal nanoparticles. Some oxidation processes that are important in the color photography industry include the oxidation of DMPPD¹⁵⁸ and TMPPD¹⁵⁹ which have been shown to be catalyzed by palladium nanoparticles in water/AOT/heptane microemulsions. The oxidation of ethylene has been conducted with silver colloidal nanoparticles¹⁶⁰ that are stabilized with poly (sodium acrylate) and also with gold nanoparticles¹⁶¹⁻¹⁶² stabilized with sodium polyacrylate. The

oxidation of cyclooctane by tBHP¹⁶³⁻¹⁶⁴ has been catalyzed by iron nanoparticles in reverse microemulsions and by ruthenium nanoparticles in a biphasic system.

1.3 Supported Transition Metal Nanoparticles in Heterogeneous Catalysis

In heterogeneous catalysis, transition metal nanoparticles that are supported in various substrates are used as catalysts. There are three major ways that heterogeneous transition metal nanocatalysts are prepared: adsorption of the nanoparticles onto supports, grafting of the nanoparticles onto supports, and fabrication of nanostructures onto supports by lithographic techniques. There have been a number of review articles which discuss various reactions conducted using supported transition metal nanoparticles as catalysts¹⁶⁵⁻¹⁷⁴. There has been a review on highly active supported transition metal nanocatalysts for hydrogenations and enantioselective synthesis of organic compounds¹⁶⁵. Functional resins are reviewed as potential supports for transition metal nanoparticles or complements to traditional supports¹⁶⁶. The effect of the support used on the catalytic activity of monometallic and bimetallic nanoparticles has been surveyed¹⁶⁷. The catalytic properties of transition metal nanoparticles that are supported on oxide supports have been reported¹⁶⁸. A review of supported transition metal nanoparticles as catalysts for oxidations and epoxidations has been conducted¹⁶⁹. The impact of nanoscience on heterogeneous catalysis has been reviewed¹⁷⁰. The use of supported bimetallic nanoparticles for catalyzing a variety of hydrogenation reactions has been reviewed¹⁷¹. A review has been conducted suggesting that the focus of transition metal nanoparticles as catalysts in heterogeneous catalysis should be on 100% selectivity of the product to be formed¹⁷². Adsorbate-induced restructuring of supported transition metal nanocatalysts

has been surveyed¹⁷³. A survey of supported transition nanoparticles fabricated by using electron beam lithography pulsed laser deposition has been conducted¹⁷⁴. In this section of our review, we focus on the three methods of generating supported transition metal nanoparticles, the types of supports used, and reactions that are catalyzed using heterogeneous transition metal nanocatalysts.

Table 1.2—Summary of the common supports used for the preparation of supported transition metal nanoparticles and examples of reactions catalyzed using supported transition metal nanoparticles in heterogeneous catalysis

Important Factors for Supported Transition Metal Nanoparticles	Examples
Supports	Carbon ¹⁷⁵⁻¹⁸⁶ Silica ¹⁸⁷⁻¹⁹⁵ Alumina ¹⁹⁶⁻²⁰⁴ Titanium Dioxide ²⁰⁵⁻²¹⁰ Grafting onto Polymeric Support ²¹¹⁻²¹⁸ Lithographically Fabricated onto Supports ²¹⁹⁻²²⁶
Chemical Reactions	Fuel Cell Reactions ^{175-180, 183, 185, 228-232} Hydrogenations ^{187-188, 193, 195, 197, 199, 204, 210, 219-221, 226, 230} Reduction Reactions ^{196, 198, 200-201, 208, 234} Decompositions ^{181, 209, 235-237}

1.3.1 Adsorption of Nanoparticles onto Supports

Table 1.2 summarizes common supports that have been used to prepare supported transition metal nanocatalysts. The most common method of preparing heterogeneous transition metal nanocatalysts is by the adsorption of transition metal nanoparticles¹⁷⁵⁻²¹⁰ onto different kinds of supports. The adsorption process involves preparing a colloidal

suspension of the transition metal nanoparticles, impregnating the colloidal nanoparticles onto the support, and washing of the solid that is obtained. In the first step, the colloidal nanoparticles are prepared using synthetic methods like those discussed previously. There are many different kinds of supports that the nanoparticles are impregnated onto such as carbon¹⁷⁵⁻¹⁸⁶, silica¹⁸⁷⁻¹⁹⁵, alumina¹⁹⁶⁻²⁰⁴, titanium dioxide²⁰⁵⁻²¹⁰, etc. Carbon supports are the most commonly used support for preparing heterogeneous transition metal nanocatalysts.

1.3.1.1 Carbon Supports

Carbon¹⁷⁵⁻¹⁸⁶ is the most widely used support for the preparation of supported transition metal nanoparticles by the adsorption process. Carbon supports have been commonly used for reactions such as electro-oxidation of methanol^{175, 179-180, 183,185}, oxygen reduction reaction¹⁷⁸, CO oxidation¹⁷⁶⁻¹⁷⁷, etc. Carbon supported transition metal nanoparticles have also been used to catalyze other reactions such as the decomposition of methane¹⁸¹, methanol carbonylation¹⁸⁴, oxidation of glycerol¹⁸⁶, etc. Many different kinds of carbon supports have been used for the adsorption process such as Vulcan XC-72^{175,177, 179-180, 185}, carbon fibers¹⁷⁶, carbon nanotubes¹⁷⁹, diamond¹⁸¹, carbon black¹⁸³, nanoporous carbon¹⁸⁴, graphite¹⁸⁶, activated carbon¹⁸⁶, etc. Many different kinds of transition metal nanoparticles have been prepared using carbon support such as platinum^{175, 178, 180, 186}, platinum-ruthenium^{175, 179-180, 183, 185}, gold^{176-177, 186}, palladium^{181, 186}, nickel¹⁸¹, and rhodium¹⁸⁴. The most common kind of carbon support that is used is the Vulcan XC-72 type. An interesting and unusual carbon support is the one in which palladium and nickel nanoparticles are supported in the diamond form for the

decomposition of methane¹⁸¹. Another interesting type of carbon support is the use of carbon nanotubes as a support for the transition metal nanoparticles. Many of the carbon supported nanoparticles are used to catalyze reactions that are important for fuel cell applications^{175-180, 183, 185} such as the direct methanol fuel cell or the direct ethanol fuel cell. The carbon supported platinum-ruthenium bimetallic nanoparticles and the carbon-supported platinum nanoparticles are the two most common types of nanoparticles used for fuel cell reactions.

1.3.1.2 Silica Supports

Silica based supports¹⁸⁷⁻¹⁹⁵ have also been used for the adsorption of transition metal nanoparticles for the preparation of heterogeneous nanocatalysts. Some types of silica based supports that have been used include low surface area silica¹⁸⁷, silica monolith¹⁸⁸, SBA-15¹⁸⁹⁻¹⁹⁰, high surface area silica¹⁹¹, silica gel¹⁹², mesoporous silica¹⁹³, MCM-41¹⁹⁴, Aerosil 200¹⁹⁵, etc. Silica supported transition metal nanoparticles have been used to catalyze reactions such as hydrogenation of benzene^{187, 195}, hydrogenation of cinnamaldehyde¹⁸⁸, Heck reaction between butyl acrylate and iodobenzene¹⁸⁸, CO oxidation^{189,191}, Fischer-Tropsch synthesis^{190, 194}, toluene hydrogenation¹⁹¹, oxidative acetoxylation of toluene¹⁹², oxidative acetoxylation of 1,3-butadiene¹⁹², hydrogenation of N-heterocycles¹⁹³, etc. Some common transition metal nanoparticles that are supported on silica include nickel¹⁸⁷, palladium^{188,192, 195}, gold¹⁸⁹, cobalt¹⁹⁰, platinum¹⁹¹, ruthenium¹⁹³, iron¹⁹⁴, etc. Silica supported nanoparticles have been used to catalyze a wide variety of reactions such as hydrogenations, oxidations, and other organic synthetic reactions. A wide variety of transition metal nanoparticles have also been adsorbed onto

silica supports to form heterogeneous nanocatalysts. Also, there have been many forms of silica that have been used to form silica supported transition metal nanoparticles.

1.3.1.3 Alumina Supports

Alumina¹⁹⁶⁻²⁰⁴ has also been used as a support for the preparation of heterogeneous transition metal nanocatalysts. Some reactions that have been catalyzed using alumina supported transition metal nanoparticles include NO reduction^{196,198, 200-201}, hydrogenation of arenes¹⁹⁷, hydrogenation of propene^{199, 204}, CO oxidation²⁰², ammonia synthesis²⁰³, etc. Some transition metal nanoparticles that have been supported on alumina include platinum^{196, 198-200, 202, 204}, ruthenium^{197, 201, 203}, etc. Cubic platinum nanoparticles supported on alumina have been used to catalyze the NO reduction reaction¹⁹⁶. It is observed that there is a conversion of the low index facets of the cubic nanoparticles to higher index planes that occurs during the reaction conditions, which is attributed to substantial changes in the catalytic activity and selectivity to reaction products¹⁹⁶. A large morphological evolution of large platinum nanoparticles is also observed during the NO reduction reaction²⁰⁰. Platinum and ruthenium are the most common metal nanoparticles that are supported on alumina. A wide variety of reactions have been conducted on alumina-supported metal nanoparticles.

1.3.1.4 Titanium Dioxide Supports

Titanium dioxide (titania) supports²⁰⁵⁻²¹⁰ have also been used for adsorption of transition metal nanoparticles in the process of forming heterogeneous nanocatalysts. Some reactions that have been catalyzed using titanium dioxide supported transition

metal nanoparticles include CO oxidation²⁰⁵⁻²⁰⁷, reduction of SO₂²⁰⁸, decomposition of formic acid²⁰⁹, hydrogenation of crotonaldehyde²¹⁰, etc. Some types of transition metal nanoparticles that have been supported on titanium dioxide include gold²⁰⁵⁻²⁰⁷, palladium^{207, 209}, gold-palladium²⁰⁷, ruthenium²⁰⁸, silver²¹⁰, etc. Titanium dioxide supported transition metal nanocatalysts have also been used to catalyze a variety of chemical reactions.

1.3.2 Grafting of Nanoparticles onto Supports

Another less common method of preparing supported transition metal nanocatalysts is to graft transition metal nanoparticles onto a solid support. There has been many different chemical bonds that have been used to immobilize the transition metal nanoparticles onto the support. Some kinds of supports that have been used in the grafting method of generating supported transition metal nanocatalysts include polyacrylamide gel²¹¹⁻²¹⁴, polystyrene microspheres²¹⁵⁻²¹⁸, etc.

1.3.2.1 Grafting onto Polyacrylamide gels

One support that is used in the grafting method of preparing supported transition metal nanocatalysts is polyacrylamide gels²¹¹⁻²¹⁴. Platinum and rhodium colloids have been immobilized onto polyacrylamide gels with aminoethyl groups²¹¹⁻²¹⁴. The immobilization process occurs by the formation of amide bonds by the reaction of the ester functional groups of the protecting polymer copolymer PVP/methyl polyacrylate copolymer with the amine functions of the gel. The immobilization process does not

affect the morphology of the grafted process and metal leaching does not occur during the immobilization process.

1.3.2.2 Grafting onto Polystyrene Supports

Another support that has been used in the grafting method of preparing supported transition metal nanocatalysts is the use of polystyrene microspheres²¹⁵⁻²¹⁸. Platinum nanoparticles have been supported on polystyrene microspheres that contain surface grafted PNIPAAm²¹⁵⁻²¹⁷. In this method, the precursor transition metal salt is reduced in the presence of the polystyrene nanospheres. As a result, the PNIPAAm chains will stabilize the platinum nanoparticles onto the surface of the polystyrene microspheres. Polystyrene nanospheres that contain surface grafted poly(p-hydroxystyrene) have been used to synthesize supported silver and ruthenium nanoparticles²¹⁸.

1.3.3 Lithographically Fabricated Supported Transition Metal Nanocatalysts

Electron beam lithography²¹⁹⁻²²⁶ has been used to fabricate arrays of transition metal nanoparticles onto different supports such as silica and alumina. Platinum nanoparticles that are 50 nanometers have been fabricated onto silicon wafers and have been used to catalyze the ethylene hydrogenation at high pressures^{219, 221}. Studies on the reaction intermediates and surface restructuring of platinum nanoparticle arrays formed on silica, alumina, and titania that are used to catalyze olefin hydrogenations have been conducted²²⁰. The stability of lithographically fabricated supported silver arrays in both oxidizing and reducing conditions has been investigated²²². Twenty nanometer silver arrays supported on a silicon wafer has been used to catalyze the ethylene epoxidation

reaction²²³. The thermal, chemical, and adhesion stability of platinum nanoparticle arrays supported on silica were studied²²⁴. It was found that in the presence of high temperature (1000 K), high vacuum (10^{-7} torr), and in the presence of 1 atm hydrogen gas, the domain sizes within individual particles grew larger, without any noticeable deformation of the arrays. Platinum nanoparticles that are lithographically fabricated and supported on silica have been used to catalyze the hydrogenation and dehydrogenation of cyclohexane²²⁵. The ethylene hydrogenation reaction catalyzed by platinum arrays supported on alumina can be used to determine the active metal surface area in this type of nanocatalyst²²⁶.

1.3.4 Chemical Reactions Catalyzed Using Supported Transition Metal Nanocatalysts

Many different kinds of chemical reactions have been catalyzed using heterogeneous transition metal nanocatalysts. A major industrial area that utilizes supported transition metal nanocatalysts is the fuel cell industry for catalyzing fuel cell reactions. Some types of reactions that have been catalyzed using heterogeneous metal nanocatalysts include fuel cell reactions^{175-180, 183, 185, 228-232}, hydrogenations^{187-188, 193, 195, 197, 199, 204, 210, 219-221, 226, 230}, reductions^{196, 198, 200-201, 208, 234}, decompositions^{181, 209, 235-237}, etc. There are many other types of chemical reactions that have been conducted using supported transition metal nanoparticles in heterogeneous catalysis, but due to the huge volume of literature, we will focus only on the above reactions in this review. Table 1.2 summarizes some of the major reactions that have been catalyzed using supported transition metal nanoparticles.

1.3.4.1 Fuel Cell Reactions

Supported metal nanoparticles have been widely used in catalyzing many reactions associated with direct methanol and ethanol fuel cells. A majority of the fuel cell reactions^{175-180, 183, 185, 228-232} have been conducted using transition metal nanoparticles that are supported on various forms of carbon. Some fuel cell reactions that have been conducted using heterogeneous supported transition metal nanoparticles include methanol oxidation^{175, 179-180, 183, 185, 228, 230-232}, ethanol oxidation²²⁷, oxidation reduction¹⁷⁸, CO oxidation^{176-177, 229}, etc. Platinum and platinum-ruthenium nanoparticles supported on various forms of carbon are the most commonly used supported transition metal nanoparticles for catalyzing a variety of fuel cell reactions. A highly active electrocatalytic architecture consisting of colloidal platinum-modified carbon-silica composite aerogels has been shown to have electrocatalytic activity that is 4 orders of magnitude greater than that of a native Pt-modified carbon powder²²⁸. Gold supported titanium dioxide composite aerogels have also been shown to have high catalytic activity for the CO oxidation reaction²²⁹.

1.3.4.2 Hydrogenation Reactions

Numerous hydrogenation reactions^{187-188, 193, 195, 197, 199, 204, 210, 219-221, 226, 230} have been also been catalyzed by many different types of heterogeneous supported transition metal nanoparticles. Some specific hydrogenation reactions that have been catalyzed using supported transition metal nanocatalysts include hydrogenation of benzene^{187, 195}, hydrogenation of cinnamaldehyde¹⁸⁸, hydrogenation of N-heterocycles¹⁹³, hydrogenation of arenes¹⁹⁷, hydrogenation of propene^{199, 204}, hydrogenation of crotonaldehyde²¹⁰,

ethylene hydrogenation^{219, 221, 226}, hydrogenation of olefins^{220, 230}, etc. There are many more kinds of hydrogenation reactions which have been catalyzed using supported transition metal nanoparticles, and the above reactions mentioned are examples of some typical hydrogenation reactions. Many different kinds of supported transition metal nanoparticles have been used such as platinum, palladium, rhodium, and also many different kinds of bimetallic nanoparticles.

1.3.4.3 Reduction and Decomposition Reactions

There are many kinds of reduction^{196, 198, 200-201, 208, 234} and decomposition^{181, 209, 235-237} reactions that have been catalyzed by heterogeneous supported transition metal nanocatalysts. Some types of reduction reactions include NO reduction^{196, 198, 200-201, 234}, reduction of SO₂²⁰⁸, etc. Some decomposition reactions that have been catalyzed using heterogeneous supported transition metal nanoparticles include decomposition of methane¹⁸¹, decomposition of formic acid²⁰⁹, decomposition of chlorodifluoromethane²³⁵, ammonia decomposition²³⁶, decomposition of acetylene²³⁷, etc. Many different kinds of supported transition metal nanoparticles have been used to catalyze reduction and decomposition reactions such as palladium and platinum nanocatalysts.

1.4 Outline of the Contents of the Thesis Chapters

Nanocatalysis is a rapidly growing field that has undergone an explosive growth during the past decade. Nanoparticles have a large surface-to-volume ratio compared to bulk catalytic materials, which make them attractive to use as catalysts. The surface atoms of nanoparticles are very active due to their high surface energy. This raises the

possibility that the surface atoms could be so active that they could cause changes in the size and shape of the nanoparticles during the course of catalysis. In the bulk of the literature in the nanocatalysis field, there has not been an examination of what happens to the nanocatalysts during the course of its catalytic function. This kind of examination is necessary in order to truly examine the usefulness of nanoparticles as catalysts. In addition, these kinds of studies could also provide clues on how to design better catalysts.

Spherical, tetrahedral, and cubic shaped platinum nanoparticles in colloidal solution have been used to catalyze the electron transfer reaction between hexacyanoferrate and thiosulfate ions. The stability of the spherical PVP-Pt nanoparticles during the electron transfer reaction has been examined in **Chapter 3**. The nanoparticles become slightly smaller after the first and second cycles of the reaction. In the presence of just the hexacyanoferrate (III) ions, it is observed that there is a large reduction in the size of the nanoparticles while in the presence of thiosulfate ions, the nanoparticles maintain their size. The hexacyanoferrate (III) ions could dissolve Pt atoms from the surface of the nanoparticles and form a complex via the cyanide group and this could explain the reduction in the nanoparticle size. The thiosulfate binds to the nanoparticle surface via the sulfur group. Based on these observations, we propose that the surface catalytic mechanism involves thiosulfate ions binding to the nanoparticle surface and reacting with hexacyanoferrate (III) ions in solution.

We have also conducted this reaction using tetrahedral PVP-Pt nanoparticles and cubic polyacrylate-Pt nanoparticles as catalysts as shown in **Chapter 4**. It is observed that dissolution of Pt atoms on the corners and edges occur after the first and second cycle of the reaction for both tetrahedral and cubic Pt nanoparticles. The dissolution of

the corner and edge atoms is faster for the tetrahedral Pt nanoparticles than for the cubic Pt nanoparticles. Dissolution of atoms in the corners and edges of the tetrahedral and cubic nanoparticles also occur in the presence of hexacyanoferrate (III) ions and the nanoparticles maintain their shape in the presence of thiosulfate ions. This supports the mechanism of surface catalysis we proposed for this reaction.

During the first forty minutes of the reaction, it is observed that there are no shape changes and as a result the shape dependence on the catalytic activity can be examined. The activation energy obtained using the spherical, tetrahedral, and cubic platinum nanoparticles are correlated with the fraction of surface atoms on the corners and edges of each type of particle in **Chapter 5**. It is observed that the tetrahedral nanoparticles with the greatest fraction of atoms on their defective corners and edges are the most catalytically active while the cubic nanoparticles with the smallest fraction of atoms on the defective corners and edges are the least catalytically active. The spherical nanoparticles have a catalytic activity that is intermediate to that observed with the tetrahedral and cubic nanoparticles and have an intermediate fraction of atoms on the defective corners and edges. During the course of the entire reaction (2 days), it is observed that dissolution of atoms on the corners and edges of the tetrahedral and cubic nanoparticles result in distorted tetrahedral and distorted cubic nanoparticles as shown in **Chapter 6**. It is observed that with the distortion in the shape of the tetrahedral and cubic nanoparticles, there is a corresponding change in the activation energy of the reaction.

A detailed examination of the stability of spherical palladium nanoparticles in colloidal solution used to catalyze the Suzuki reaction has also been conducted as shown in **Chapter 7**. In the case of the Suzuki reaction with the spherical PVP-Pd

nanoparticles as catalysts, it is observed that the Pd nanoparticles grow larger after the first cycle of the reaction due to Ostwald ripening processes. After the second cycle, the larger nanoparticles aggregate and precipitate out of solution leaving the smaller nanoparticles left in solution. In addition, studies in the presence of individual reactants have shown that the nanoparticles grow larger in the presence of iodobenzene and that the Ostwald ripening process is severely diminished in the presence of phenylboronic acid. These observations provide clues to the surface catalytic mechanism in which phenylboronic acid binds to the nanoparticle surface and reacts with iodobenzene via collisional processes. A comparison between the use of PVP-Pd and dendrimer-Pd nanoparticles as catalysts was conducted in order to find out the effect of the stabilizer on the stability of the nanoparticles in **Chapter 8**. It is observed that when PAMAM-OH Generation 4 dendrimer is used as the stabilizer for the Pd nanoparticles, the nanoparticles continue to grow during the second cycle of the Suzuki reaction. The higher the generation of the dendrimer, the better its capping action is. As a result, the strong capping action of the dendrimer results in the nanoparticles being more resistant to aggregation and precipitation. Studies in the presence of individual reactants support the mechanism of surface catalysis developed with the studies on the PVP-Pd nanoparticles.

In the literature, there have been recent studies that have shown that platinum complexes can catalyze the Suzuki reaction, but spherical platinum nanoparticles were found to not catalyze the Suzuki reaction. Since we have shown previously that the tetrahedral PVP-Pt nanoparticles can catalyze the electron transfer reaction, we decided to see if the colloidal tetrahedral Pt nanoparticles can catalyze the Suzuki reaction in **Chapter 9**. It is observed that the tetrahedral Pt nanoparticles can catalyze the Suzuki

reaction, but is not as catalytically active as the spherical palladium nanoparticles. In addition, it is observed that the tetrahedral platinum nanoparticles transform into the more stable spherical shape during the Suzuki reaction and in the presence of the all conditions except in the presence of phenylboronic acid. After the second cycle of the Suzuki reaction, it is observed that the transformed spherical nanoparticles become larger in size. In the presence of phenylboronic acid, the Pt nanoparticles maintain their tetrahedral shape and are similar in size to the tetrahedral Pt nanoparticles before any perturbations. As a result, these results also support the catalytic mechanism we have proposed for the Suzuki reaction.

FTIR has been used to investigate the mode of binding of phenylboronic acid to the palladium nanoparticle surface in **Chapter 10**. It was determined that the phenylboronate anion binds to the palladium nanoparticle surface by the bridged mode of binding through the O⁻ group. It was also determined that iodobenzene does not interact with the nanoparticle surface since there are no shifts in the characteristic infrared vibrational modes associated with iodobenzene. The FTIR studies confirm the mechanism of surface catalysis we proposed previously and also show the mode of binding of the phenylboronic acid to the nanoparticle surface.

Since these studies have shown that colloidal metal nanoparticles are unstable and undergo changes in their morphology (changes in the size and shape) during their catalytic function, there is a need to use alternative types of nanocatalysts. One possibility is to use supported metal nanoparticles as catalysts for a variety of reactions. Since carbon is a very common support material used for the preparation of supported nanoparticles, we have used this in our investigations. The use of carbon supported

spherical palladium nanoparticles as catalysts for the Suzuki reaction has been compared to that of the colloidal spherical palladium nanoparticles studied previously in **Chapter 11**. It is observed that the carbon supported spherical palladium nanoparticles are less catalytically active than the colloidal spherical palladium nanoparticles during the first cycle of the Suzuki reaction, but the supported palladium nanoparticles demonstrate almost double the recycling potential than that observed with the colloidal spherical palladium nanoparticles. It is observed that the carbon supported spherical palladium nanoparticles continue to grow in size after the first and second cycle and the width of the size distribution is not very broad unlike the colloidal spherical palladium nanoparticles. The presence of the large amount of the carbon support could account for the continued growth of the nanoparticles that occur and also the preservation of the catalytic activity during the second cycle of the Suzuki reaction.

1.5 References

1. Roucoux, A.; Schulz, J.; Patin, H., *Chem. Rev.*, **2002**, *102*(10), 3757.
2. Moiseev, I. I.; Vargatfik, M. N., *Russ. J. Gen. Chem.*, **2002**, *72*(4), 512.
3. Mayer, A. B. R. *Polym. Adv. Technol.* **2001**, *12*(1-2), 96.
4. Boennemann, H.; Braun, G.; Brijoux, G.; Brinkman, R.; Tilling, A.; Seevogal, K.; Siepen, K., *J. Organomet. Chem.*, **1996**, *520*(1-2), 143.
5. Toshima, N. *NATO ASI Ser., Ser. 3* **1996**, *12*, 371.
6. Duff, D. G.; Baiker, A. *Stud. Surf. Sci. Catal.* **1995**, *91*, 505.
7. Bradley, J. S. In *Clusters and Colloids: From Theory to Application*; Schmid, G., Ed.; VCH: New York, 1994; pp 459-536.
8. Teranishi, T.; Miyake, M. *Chem. Mat.*, **1998**, *10*, 594.

9. Li, Y.; Hong, X. M.; Collard, D. M.; El-Sayed, M. A. *Org. Lett.* **2000**, *2*(15), 2385.
10. Li, Y.; Boone, E.; El-Sayed, M. A. *Langmuir* **2002**, *18*, 4921.
11. Narayanan, R.; El-Sayed, M. A. *J. Am. Chem. Soc.*, **2003**, *125*(27), 8340.
12. Narayanan, R.; El-Sayed, M. A. *J. Phys. Chem. B*, **2003**, *107*(45), 12416.
13. Chen, C. W.; Tano, D.; Akashi, M., *J. Coll. Interf. Sci.*, **2000**, *225*(2), 349.
14. Shiraishi, Y.; Nakayama, M.; Takagi, E.; Tominaga, T.; Toshima, M., *Inorganica Chimica Acta*, **2000**, *300-302*, 964.
15. Chen, C. W.; Akashi, M., *Langmuir*, **1997**, *13*(24), 6465.
16. Toshima, N., *NATO ASI Ser.*, **1996**, *12*, 371.
17. Adlim, M.; Abu Bakar, M.; Liew, K. Y.; Ismail, J., *J. Molec. Catal. A: Chem.*, **2004**, *212*(1-2), 141.
18. Yu, W.; Liu, M.; Liu, H.; Zheng, J. *J. Colloid Interface Sci.* **1999**, *210*, 218.
19. Teranishi, T.; Miyake, M. *Chem. Mater.* **1998**, *10*, 594.
20. Teranishi, T.; Hosoe, M.; Miyake, M. *Adv. Mater.* **1997**, *9*, 65.
21. Busser, G. W.; Van Ommen, J. G.; Lercher, J. A. *Adv. Catal. Nanostruct. Mater.* **1996**, 213.
22. Porta, F.; Ragaini, F.; Cenini, S.; Scari, G. *Gazz. Chim. Ital.* **1992**, *122*, 361.
23. Bonet, F.; Delmas, V.; Grugeon, S.; Herrera Urbina, R.; Silvert, P.-Y.; Tekaiia-Elhsissen, K. *Nanostruct. Mater.* **2000**, *11*, 1277.
24. Ahmadi, T. S.; Wang, Z. L.; Green, T. C.; Henglein, A.; El-Sayed, M. A. *Science*, **1996**, *272*, 1924.
25. Li, Y.; Petroski, J.; El-Sayed, M. A. *J. Phys. Chem. B*, **2000**, *104*(47), 10956.
26. Narayanan, R.; El-Sayed, M. A. *J. Phys. Chem. B*, **2004**, *108*(18), 5726.
27. Narayanan, R.; El-Sayed, M. A., *J. Am. Chem. Soc.*, **2004**, ASAP Article.
28. Narayanan, R.; El-Sayed, M. A., *Nano Lett.*, **2004**, in press.

29. Fu, X.; Wang, Y.; Wu, N.; Gui, L.; Tan, Y., *Langmuir*, **2002**, *18*(12), 4619.
30. Ohde, H.; Wai, C. M.; Kim, H.; Kim, J., Ohde, M., *J. Am. Chem. Soc.*, **2002**, *124*(17), 4540.
31. Troitski, S. Y.; Serebriakova, M. A.; Fedotov, M. A.; Ignashin, S. V.; Chuvilin, A. L.; Moroz, E. M.; Novgorodov, B. N.; Kochubey, D. I.; Likholobov, V. A.; Blanc, B.; Gallezot, P., *J. Molec. Catal. A: Chem.*, **2000**, *158*(1), 461.
32. Henglein, A., *J. Phys. Chem. B*, **2000**, *104*(10), 2201.
33. Aiken, J. D. III; Finke, R. G., *Chem. Mat.*, **1999**, *11*(4), 1035.
34. Aiken, J. D., III; Finke, R. G. *J. Am. Chem. Soc.* **1999**, *121*, 8803.
35. Yu, W.; Liu, H. *Chem. Mater.* **1998**, *10*, 1205.
36. Li, Y.; El-Sayed, M. A., *J. Phys. Chem. B*, **2001**, *105*, 8938.
37. Narayanan, R.; El-Sayed, M. A., *J. Phys. Chem. B*, **2004**, ASAP Article.
38. Tamura, M.; Fujihara, H., *J. Am. Chem. Soc.*, **2003**, *125*(51), 15742.
39. Pittelkov, M.; Moth-Poulsen, K.; Boas, U.; Christensen, J. B., *Langmuir*, **2003**, *19*(18), 7682.
40. Tabuani, D.; Monticelli, O.; Chincarinni, A.; Bianchini, C.; Vizza, F.; Moneti, S.; Russo, S., *Macromol.*, **2003**, *36*(12), 4294.
41. Porta, F.; Prati, L.; Rossi, M.; Scari, G., *J. Catal.*, **2002**, *211*(2), 464.
42. Sau, T. K.; Pal, A.; Pal, T., *J. Phys. Chem. B*, **2001**, *105*(38), 9266.
43. Schulz, J.; Roucoux, A.; Patin, H., *Chem. Eur. J.*, **2000**, *6*(4), 618.
44. Zhao, M.; Sun, L.; Crooks, R. M., *J. Am. Chem. Soc.* **1998**, *120*, 4877.
45. Zhao, M.; Crooks, R. M. *Angew. Chem., Int. Ed. Engl.* **1999**, *38*, 364.
46. Zhao, M.; Sun, L.; Crooks, R. M. *Polym. Prepr.* **1999**, *40*, 400.
47. Chechik, V.; Crooks, R. M. *J. Am. Chem. Soc.* **2000**, *122*, 1243.
48. Crooks, R. M.; Zhao, M.; Sun, L.; Chechik, V.; Yeung, L. K. *Acc. Chem. Res.* **2001**, *34*, 181.

49. Zhao, M.; Crooks, R. M. *Adv. Mater.* **1999**, *11*, 217.
50. Garcia, M. E.; Baker, L. A.; Crooks, R. M. *Anal. Chem.* **1999**, *71*, 256.
51. Mayer, A. B. R.; Johnson, R. W.; Hausner, S. H.; Mark, J. E. *J. Macromol. Sci. Pure Appl. Chem.* **1999**, *A36*, 1427.
52. Mayer, A. B. R.; Hausner, S. H.; Mark, J. E. *Polym. J.* **2000**, *32*, 15.
53. Mayer, A. B. R.; Mark, J. E. *Eur. Polym. J.* **1998**, *34*, 103.
54. Mayer, A. B. R.; Mark, J. E. *J. Macromol. Sci., Pure Appl. Chem.* **1997**, *A34*, 2151.
55. Mayer, A. B. R.; Antonietti, M. *Colloid Polym. Sci.* **1998**, *276*, 769.
56. Wu, S. H.; Chen, D.H., *Chem. Lett.*, **2004**, *33(4)*, 406.
57. Demir, M. M.; Gulgun, M. A.; Menciloglu, Y. Z.; Erman, B.; Abramchuk, S. S.; Makhaeva, E. E.; Khokhlov, A. R.; Matveeva, V. G.; Sulman, M. G., *Macromol.*, **2004**, *37(5)*, 1787.
58. Solla-Gullon, J.; Rodes, A.; Montiel, V.; Aldaz, A.; Clavilier, J., *J. Electroanal. Chem.*, **2003**, *554-555*, 273.
59. Wu, S. H.; Chen, D.H., *J. Coll. Interf. Sci.*, **2003**, *259(2)*, 282.
60. Solla-Gullon, J.; Montiel, V.; Aldaz, A.; Clavilier, J., *J. Electrochem. Soc.*, **2003**, *150(2)*, E104.
61. Zhang, X.; Chang, K. Y., *Chem. Mat.*, **2003**, *15(2)*, 451.
62. Harriman, A.; Thomas, J. M.; Millward, G. R. *New J. Chem.* **1987**, *11*, 757.
63. Furlong, D. N.; Launikonis, A.; Sasse, W. H. F.; Sanders, J. V. *J. Chem. Soc., Faraday Trans. 1* **1984**, *80*, 571.
64. Tano, T.; Esumi, K.; Meguro, K. *J. Colloid Interface Sci.* **1989**, *133*, 530.
65. Esumi, K.; Suzuki, M.; Tano, T.; Torigoe, K.; Meguro, K. *Colloids Surf.* **1991**, *55*, 9.
66. Esumi, K.; Tano, T.; Meguro, K. *Langmuir* **1989**, *5*, 268.
67. Esumi, K.; Sadakane, O.; Torigoe, K.; Meguro, K. *Colloids Surf.* **1992**, *62*, 255.

68. Son, S. U.; Jang, Y.; Park, J.; Na, H. B.; Park, H. M.; Yun, H. J.; Lee, J.; Hyeon, T., *J. Am. Chem. Soc.*, **2004**, *126*(16), 5026.
69. Son, S. U.; Park, I. K.; Park, J.; Hyeon, T., *Chem. Comm.*, **2004**, 7, 778.
70. Michaelis, M.; Henglein, A. *J. Phys. Chem.* **1992**, *96*, 4719.
71. Rafaeloff, R.; Haruvy, Y.; Binenboym, J.; Baruch, G.; Rajbenbach, L. A. *J. Mol. Catal.* **1983**, *22*, 219.
72. Kurihara, K.; Kizling, J.; Stenius, P.; Fendler, J. H. *J. Am. Chem. Soc.* **1983**, *105*, 2574.
73. Toshima, N.; Takahashi, T.; Hirai, H. *Chem. Lett.* **1986**, 35.
74. Toshima, N.; Takahashi, T.; Hirai, H. *Chem. Lett.* **1985**, 1245.
75. Toshima, N.; Takahashi, T. *Bull. Chem. Soc. Jpn.* **1992**, *65*, 400.
76. Nagata, Y.; Watanabe, Y.; Fujita, S.; Dohmaru, T.; Taniguchi, S. *J. Chem. Soc., Chem. Commun.* **1992**, 1620.
77. Fujimoto, T.; Mizukoshi, Y.; Oshima, R.; Nagata, Y.; Maeda, Y. *Trans. Mater. Res. Soc. Jpn.* **2000**, *25*, 95.
78. Maeda, Y.; Mizukoshi, Y.; Takagi, E.; Fujimoto, T.; Oshima, R.; Nagata, Y. *Trans. Mater. Res. Soc. Jpn.* **2000**, *25*, 99.
79. Caruso, R. A.; Ashokkumar, M.; Grieser, F. *Colloids Surf., A* **2000**, *169*, 219.
80. Fujimoto, T.; Terauchi, S.; Umehara, H.; Kojima, I.; Henderson, W. *Chem. Mater.* **2001**, *13*, 1057.
81. Mizukoshi, Y.; Takagi, E.; Okuno, H.; Oshima, R.; Maeda, Y.; Nagata, Y. *Ultrason. Sonochem.* **2001**, *8*, 1.
82. Fujimoto, T.; Mizukoshi, Y.; Nagata, Y.; Maeda, Y.; Oshima, R. *Scr. Mater.* **2001**, *44*, 2183.
83. Takagi, E.; Mizukoshi, Y.; Oshima, R.; Nagata, Y.; Bandow, H.; Maeda, Y. *Stud. Surf. Sci. Catal.* **2001**, *132*, 335.
84. Bradley, J. S.; Hill, E. W.; Behal, S.; Klein, C.; Chaudret, B.; Duteil, A. *Chem. Mater.* **1992**, *4*, 1234.
85. De Caro, D.; Bradley, J. S. *New J. Chem.* **1998**, *22*, 1267.

86. Duteil, A.; Queau, R.; Chaudret, B.; Mazel, R.; Roucau, C.; Bradley, J. S. *Chem. Mater.* **1993**, *5*, 341.
87. Bradley, J. S.; Millar, J. M.; Hill, E. W.; Behal, S.; Chaudret, B.; Duteil, A. *Faradays Discuss.* **1991**, *92*, 255.
88. Duteil, A.; Queau, R.; Chaudret, B.; Mazel, R.; Roucau, C.; Bradley, J. S. *Chem. Mater.* **1993**, *5*, 341.
89. Bradley, J. S.; Millar, J. M.; Hill, E. W.; Behal, S.; Chaudret, B.; Duteil, A. *Faradays Discuss.* **1991**, *92*, 255.
90. De Caro, D.; Bradley, J. S. *Langmuir* **1997**, *13*, 3067.
91. Ould Ely, T.; Amiens, C.; Chaudret, B.; Snoeck, E.; Verelst, M.; Respaud, M.; Broto, J. M. *Chem. Mater.* **1999**, *11*, 526.
92. De Caro, D.; Agelou, V.; Duteil, A.; Chaudret, B.; Mazel, R.; Roucau, C.; Bradley, J. S. *New J. Chem.* **1995**, *19*, 1265.
93. Osuna, J.; De Caro, D.; Amiens, C.; Chaudret, B.; Snoeck, E.; Respaud, M.; Broto, J. M.; Fert, A. *J. Phys. Chem.* **1996**, *100*, 14571.
94. Klabunde, K. J.; Cardenas-Trevino, G. In *Active Metals: Preparation, Characterization, Applications*; Furstner, A., Ed.; VCH:New York, 1996; pp 237-278.
95. Klabunde, K. J. *Platinum Met. Rev.* **1992**, *36*, 80.
96. Lin, S. T.; Franklin, M. T.; Klabunde, K. J. *Langmuir* **1986**, *2*, 259.
97. Cardenas-Trivino, G.; Klabunde, K. J.; Brock Dale, E. *Langmuir* **1987**, *3*, 986.
98. Kilner, M.; Mason, N.; Lambrick, D.; Hooker, P. D.; Timms, P. L. *J. Chem. Soc., Chem. Commun.* **1987**, 356.
99. Bradley, J. S.; Hill, E.; Leonowicz, M. E.; Witzke, H. *J. Mol. Catal.* **1987**, *41*, 59.
100. Devenish, R. W.; Goulding, T.; Heaton, B. T.; Whyman, R. *J. Chem. Soc., Dalton Trans.* **1996**, 673.
101. Collier, P. J.; Iggo, J. A.; Whyman, R. *J. Mol. Catal. A: Chem.* **1999**, *146*, 149.
102. Cardenas, G. T.; Oliva, R. C. *Mater. Res. Bull.* **2000**, *35*, 2227.

103. Reetz, M. T.; Helbig, W.; Quaiser, S. A. In *Active Metals: Preparation, Characterization, Applications*; Furstner, A., Ed.; VCH: New York, 1996; pp 279-297.
104. Reetz, M. T.; Helbig, W. *J. Am. Chem. Soc.* **1994**, *116*, 7401.
105. Reetz, M. T.; Quaiser, S. A. *Angew. Chem., Int. Ed. Engl.* **1995**, *34*, 2240.
106. Shiraishi, Y.; Ikenaga, D.; Toshima, N., *Aust. J. Chem.*, **2003**, *56(10)*, 1025.
107. Hirai, H.; Yakurat, N., *Polym. Adv. Tech.*, **2001**, *12(11-12)*, 724.
108. Pellegatta, J. L.; Blandy, C.; Colliere, V.; Choukroun, R.; Chaudret, B.; Cheng, P.; Philippot, K., *J. Mol. Catal. A: Chem.*, **2002**, *178(1-2)*, 55.
109. Borsla, A.; Wilhelm, A. M.; Delmas, H., *Catal. Today*, **2001**, *66(2-4)*, 389.
110. Sidorov, S. N.; Volkov, I. V.; Davankov, V. A.; Tsyurupa, M. P.; Valetsky, P. M.; Bronstein, L. M.; Karlinsey, R.; Zwanziger, J. W.; Matveeva, V. G.; Sulman, E. M.; Lakina, N. V.; Wilder, E. A.; Spontak, R. J., *J. Am. Chem. Soc.*, **2001**, *123(43)*, 10502.
111. Lakina, N. V.; Sul'man, E. M.; Matveeva, V. G.; Mikhailov, I. A, *Pharm. Chem. J.*, **2000**, *34(3)*, 138.
112. Sulman, E.; Lakina, N.; Sulman, M.; Ankudinova, T.; Matveeva, V.; Sidorov, A.; Sidorov, S., *Stud. Surf. Sci. Catal.*, **2000**, *130B*, 1787.
113. Semagina, N. V.; Bykov, A. V.; Sulman, E. M.; Matveeva, V. G.; Sidorov, S. N.; Dubrovina, L. V.; Valetsky, P. M.; Kiselyova, O. I.; Khokhlov, A. R.; Stein, B.; Bronstein, L. M., *J. Molec. Catal. A: Chem.*, **2004**, *208(1-2)*, 273.
114. Li, Y.; El-Sayed, M.A., *J. Phys. Chem. B* **2001**, *105*, 8938-8943
115. Lu, Z.; Liu, G.; Phillips, H.; Hill, J. M.; Chang, J.; Kydd, R. A., *Nano Lett.*, **2001**, *1(12)*, 683.
116. Bronstein, L. M.; Chernyshov, D. M.; Volkov, I. O.; Ezernitskaya, M. G.; Valetsky, P. M.; Matveeva, V. G.; Sulman, E. M., *J. Catal.*, **2000**, *196(2)*, 302.
117. Sulman, E.; Bodrova, Y.; Matveeva, V.; Semagina, N.; Cerveny, L.; Kurtc, V.; Bronstein, L.; Platonova, O.; Valetsky, P., *Appl. Catal. A: Gen.*, **1999**, *176(1)*, 75.
118. Narayanan, R.; El-Sayed, M. A., *J. Phys. Chem. B*, **2004**, ASAP Article.

119. Esumi, K.; Isono, R.; Yoshimura, T., *Langmuir*, **2004**, *20*(1), 237.
120. Pittelkow, M.; Moth-Poulsen, K.; Boas, U.; Christensen, J. B., *Langmuir*, **2003**, *19*(18), 7682.
121. Hayakawa, K.; Yoshimura, T.; Esumi, K., *Langmuir*, **2003**, *19*(13), 5517.
122. Scott, Robert W. J.; Datye, Abhaya K.; Crooks, Richard M., *J. Am. Chem. Soc.*, **2003**, *125*(13), 3708.
123. Rahim, E. H.; Kamounah, F. S.; Frederiksen, J.; Christensen, J. B., *Nano Lett.*, *1*(9), 499.
124. Crooks, R. M.; Lemon, B. I., III; Sun, L.; Yeung, L. K.; Zhao, M., *Topics Curr. Chem.*, **2001**, *212*, 81.
125. Mevellec, V.; Roucoux, A.; Ramirez, E.; Philippot, K.; Chaudret, B., *Adv. Synth. Catal.*, **2004**, *346*(1), 72.
126. Yonezawa, T.; Toshima, N.; Wakai, C.; Nakahara, M.; Nishinaka, M.; Tominaga, T.; Nomura, H., *Coll. Surf. A: Physicochem. Engin. Asp.*, **2000**, *169*(1-3), 35.
127. Schulz, J.; Roucoux, A.; Patin, H., *Chem. Eur. J.*, **2000**, *6*(4), 618.
128. Aiken, J. D., III; Finke, R. G. *J. Mol. Catal. A: Chem.* **1999**, *145*, 1.
129. Lin, Y.; Finke, R. G. *J. Am. Chem. Soc.* **1994**, *116*, 8335.
130. Schmid, G.; Pfeil, R.; Boese, R.; Bandermann, F.; Meyers, S.; Calis, G. H. M.; Van Der Velden, J. W. A. *Chem. Ber.* **1981**, *114*, 3634.
131. Amiens, C.; De Caro, D.; Chaudret, B.; Bradley, J. S.; Mazel, R.; Roucau, C. *J. Am. Chem. Soc.* **1993**, *115*, 11638.
132. Duteil, A.; Schmid, G.; Meyer-Zaika, W. *J. Chem. Soc., Chem. Commun.* **1995**, 31.
133. Dassenoy, F.; Philippot, K.; Ould Ely, T.; Amiens, C.; Lecante, P.; Snoeck, E.; Mosset, A.; Casanove, M. J.; Chaudret, B. *New J. Chem.* **1998**, *22*, 703.
134. Chen, S.; Kimura, K. *J. Phys. Chem. B* **2001**, *105*, 5397.
135. Schmid, G.; Morun, B.; Malm, J. O. *Angew. Chem., Int. Ed. Engl.* **1989**, *28*, 778.

136. Schmid, G.; Maihack, V.; Lantermann, F.; Peschel, S. *J. Chem. Soc., Dalton Trans.* **1996**, 589.
137. Schmid, G.; Emde, S.; Maihack, V.; Meyer-Zaika, W.; Peschel, S. *J. Mol. Catal. A: Chem.* **1996**, *107*, 95.
138. Moreno-Manas, M.; Pleixats, R.; Villarroya, S., *Organomet.*, **2001**, *20(22)*, 4524.
139. Kogan, V.; Aizenshtat, Z.; Popovitz-Biro, R.; Neumann, R., *Org. Lett.*, **2002**, *4(20)*, 3529.
140. Liu, Y.; Khemtong, C.; Hu, J., *Chem. Comm.*, **2004**, *4*, 398.
141. Gopidas, K. R.; Whitesell, J. K.; Fox, M. A., *Nano Lett.*, **2003**, *3(12)*, 1757.
142. Na, Y.; Park, S.; Han, S. B.; Han, H.; Ko, S.; Chang, S., *J. Am. Chem. Soc.*, **2004**, *126(1)*, 250.
143. Thathagar, M. B.; Beckers, J.; Rothenberg, G. *J. Am. Chem. Soc.* **2002** *124(40)*, 11858.
144. Sanji, T.; Ogawa, Y.; Nakatsuka, Y.; Tanaka, M.; Sakurai, H., *Chem. Lett.*, **2003**, *32(10)*, 980.
145. Calo, V.; Nacci, A.; Monopoli, A.; Detomaso, A.; Iliade, P., *Organomet.*, **2003**, *22(21)*, 4193.
146. Calo, V.; Nacci, A.; Monopoli, A.; Laera, S.; Cioffi, N., *J. Org. Chem.*, **2003**, *68(7)*, 2929.
147. Yeung, L. K.; Crooks, R. M., *Nano Lett.*, **2001**, *1(1)*, 14.
148. Tsai, S. H.; Liu, Y. H.; Wu, P. L.; Yeh, C. S., *J. Mat. Chem.*, **2003**, *13(5)*, 978.
149. Sharma, R. K.; Sharma, P.; Maitra, A., *J. Coll. Interf. Sci.*, **2003**, *265(1)*, 134.
150. Clint, J. H.; Collins, I. R.; Williams, J. A.; Robinson, B. H.; Towey, T. F.; Cajean, P.; Khan-Lodhi, A. *Faraday Discuss.* **1993**, *95*, 219.
151. Freund, P. L.; Spiro, M. *J. Phys. Chem.* **1985**, *89*, 1074.
152. Freund, P. L.; Spiro, M. *J. Chem. Soc., Faraday Trans. 1* **1986**, *82*, 2277.
153. Ohde, H.; Ohde, M.; Wai, C. M., *Chem. Comm.*, **2004**, *8*, 930.

154. Fonseca, G. S.; Umpierre, A. P.; Fichtner, P. F. P.; Teixeira, S. R.; Dupont, J., *Chem. Eur. J.*, **2003**, *9*(14), 3263.
155. Adlim, M.; Abu Bakar, M.; Liew, K. Y.; Ismail, J., *J. Molec. Catal. A: Chem.*, **2004**, *212*(1-2), 141.
156. Semagina, N. V.; Bykov, A. V.; Sulman, E. M.; Matveeva, V. G.; Sidorov, S. N.; Dubrovina, L. V.; Valetsky, P. M.; Kiselyova, O. I.; Khokhlov, A. R.; Stein, B.; Bronstein, L. M., *J. Molec. Catal. A: Chem.*, **2004**, *208*(1-2), 273.
157. Anderson, K.; Cortinas Fernandez, S.; Hardacre, C.; Marr, P. C., *Inorg. Chem. Comm.*, **2003**, *7*(1), 73.
158. Spiro, M.; De Jesus, D., *Langmuir*, **2000**, *16*(6), 2464.
159. De Jesus, D.; Spiro, M. *Langmuir*, **2000**, *16*(11), 4896.
160. Shiraishi, Y.; Toshima, N., *Coll. Surf. A: Physico. Eng. Asp.*, **2000**, *169*(1-3), 59.
161. Shiraishi, Y.; Toshima, N. *J. Mol. Catal. A: Chem.* **1999**, *141*, 187.
162. Shiraishi, Y.; Toshima, N. *Colloids Surf., A* **2000**, *169*, 59.
163. Launay, F.; Patin, H. *New J. Chem.* **1997**, *21*, 247.
164. Launay, F.; Roucoux, A.; Patin, H. *Tetrahedron Lett.* **1998**, *39*, 1353.
165. Johnson, Brian F. G., *Top. Catal.*, **2003**, *24*(1-4), 147.
166. Corain, B.; Centomo, P.; Lora, S.; Kralik, M., *J. Mol. Catal. A: Chem.*, **2003**, *204-205*, 755.
167. Wieckowski, A.; Savinova, E. R.; Vayenas, C. G., *Catal. Electrocatal. Nano. Surf.*, **2003**, 847.
168. Santra, A. K.; Goodman, D. W., *Catal. Electrocatal. Nano. Surf.*, **2003**, 281.
169. Haruta, M., *Chem. Rec.*, **2003**, *3*(2), 75.
170. Bell, A. T., *Science*, **2003**, *299*(5613), 1688.
171. Thomas, J. M.; Johnson, B. F. G.; Raja, R.; Sankar, G.; Midgley, P. A., *Acc. Chem. Res.*, **2003**, *36*(1), 20.
172. Somorjai, G. A.; Borodko, Y. G., *Catal. Lett.*, **2001**, *76*(1-2), 1.

173. Rupprechter, G.; Freund, H.-J., *Top. Catal.*, **2001**, *14*(1-4), 3.
174. Eppler, A.; Rupprechter, G.; Gucci, L.; Somorjai, G. A., *J. Phys. Chem. B*, **1997**, *101*(48), 9973.
175. Liu, Z.; Ling, X. Y.; Su, X.; Lee, J. Y., *J. Phys. Chem. B*, **2004**, ASAP Article.
176. Bulushev, D. A.; Yuranov, I.; Suvorova, E. I.; Buffat, P. A.; Kiwi-Minsker, L., *J. Catal.*, **2004**, *224*(1), 8.
177. Lopez, N.; Janssens, T. V. W.; Clausen, B. S.; Xu, Y.; Mavrikakis, M.; Bligaard, T.; Norskov, J. K., *J. Catal.*, **2004**, *223*(1), 232.
178. Chen, S.; Kucernak, A., *J. Phys. Chem. B*, **2004**, *108*(10), 3262.
179. Liu, Z.; Lee, J. Y.; Chen, W.; Han, M.; Gan, L. M., *Langmuir*, **2004**, *20*(1), 181.
180. Liu, Z.; Ling, X. Y.; Lee, J. Y.; Su, X.; Gan, L. M., *J. Mat. Chem.*, **2003**, *13*(12), 3049.
181. Nakagawa, K.; Yamagishi, M.; Nishimoto, H.; Ikenaga, N.; Suzuki, T.; Kobayashi, T.; Nishitani-Gamo, M.; Ando, T., *Chem. Mat.*, **2003**, *15*(24), 4571.
182. Fachini, E. R.; Diaz-Ayala, R.; Casado-Rivera, E.; File, S.; Cabrera, C. R., *Langmuir*, **2003**, *19*(21), 8986.
183. Takasu, Y.; Itaya, H.; Kawaguchi, T.; Sugimoto, W.; Murakami, Y., *Stud. Surf. Sci. Catal.*, **2003**, *145*, 279.
184. Li, F.; Zou, J.; Yuan, G., *Catal. Lett.*, **2003**, *89*(1-2), 115.
185. Dubau, L.; Coutanceau, C.; Garnier, E.; Leger, J.-M.; Lamy, C., *J. Appl. Electrochem.*, **2003**, *33*(5), 419.
186. Carrettin, S.; McMorn, P.; Johnston, P.; Griffin, K.; Kiely, C. J.; Hutchings, G. J., *Phys. Chem. Chem. Phys.*, **2003**, *5*(6), 1329.
187. Boudjahem, A. G.; Monteverdi, S.; Mercy, M.; Bettahar, M. M., *J. Catal.*, **2004**, *221*(2), 325.
188. Anderson, K.; Cortinas Fernandez, S.; Hardacre, C.; Marr, P. C., *Inorg. Chem. Comm.*, **2003**, *7*(1), 73.
189. Yang, C.; Kalwei, M.; Schuth, F.; Chao, K., *Appl. Catal. A: Gen.*, **2003**, *254*(2), 289.

190. Khodakov, A. Y.; Bechara, R.; Griboval-Constant, A., *Appl. Catal. A: Gen.*, **2003**, 254(2), 273.
191. Lang, H.; May, R. A.; Iversen, B. L.; Chandler, B. D., *J. Am. Chem. Soc.*, **2003**, 125(48), 14832.
192. Komatsu, T.; Inaba, K.; Uezono, T.; Onda, A.; Yashima, T., *Appl. Catal. A: Gen.*, **2003**, 251(2), 315.
193. Bianchini, C.; Dal Santo, V.; Meli, A.; Moneti, S.; Moreno, M.; Oberhauser, W.; Psaro, R.; Sordelli, L.; Vizza, F., *J. Catal.*, **2003**, 213(1), 47.
194. Marchetti, S. G.; Cagnoli, M. V.; Alvarez, A. M.; Bengoa, J. F.; Gallegos, N. G.; Yeramian, A. A.; Mercader, R. C., *Hyperfine Interact.*, **2002**, 139/140(1-4/1-4), 33.
195. Horvath, A.; Beck, A.; Koppány, Z.; Sarkány, A.; Gucci, L., *J. Mol. Catal. A: Chem.*, **2002**, 182-183, 295.
196. Balint, I.; Miyazaki, A.; Aika, K., *Phys. Chem. Chem. Phys.*, **2004**, 6(9), 2000.
197. Marconi, G.; Pertici, P.; Evangelisti, C.; Caporusso, A. M.; Vitulli, G.; Capannelli, G.; Hoang, M.; Turney, T. W., *J. Organomet. Chem.*, **2004**, 689(3), 639.
198. Miyazaki, A.; Balint, I.; Nakano, Y., *J. Nano. Res.*, **2003**, 5(1-2), 69.
199. Yoo, J. W.; Hathcock, D. J.; El-Sayed, M. A., *J. Catal.*, **2003**, 214(1), 1.
200. Balint, I.; Miyazaki, A.; Aika, K., *Chem. Comm.*, **2002**, 10, 1044.
201. Balint, I.; Miyazaki, A.; Aika, K., *J. Catal.*, **2002**, 207(1), 66.
202. Ingelsten, H. H.; Beziat, J.; Bergkvist, K.; Palmqvist, A.; Skoglundh, M.; Hu, Q.; Falk, L. K. L.; Holmberg, K., *Langmuir*, **2002**, 18(5), 1811.
203. Miyazaki, A.; Balint, I.; Aika, K.; Nakano, Y., *Chem. Lett.*, **2001**, 12, 1332.
204. Yoo, J. W.; Hathcock, D.; El-Sayed, M. A., *J. Phys. Chem. A*, **2002**, 106(10), 2049.
205. Konova, P.; Naydenov, A.; Venkov, Cv.; Mehandjiev, D.; Andreeva, D.; Tabakova, T., *J. Mol. Catal. A: Chem.*, **2004**, 213(2), 235.
206. Mallick, Kaushik; Scurrall, Mike S., *Appl. Catal. A: Gen.*, **2003**, 253(2), 527.

207. Gucci, L.; Beck, A.; Horvath, A.; Koppany, Zs.; Stefler, G.; Frey, K.; Sajo, I.; Geszti, O.; Bazin, D.; Lynch, J., *J. Molec. Catal. A: Chem.*, **2003**, 204-205, 545.
208. Ishiguro, A.; Nakajima, T.; Iwata, T.; Fujita, M.; Minato, T.; Kiyotaki, F.; Izumi, Y.; Aika, K.; Uchida, M.; Kimoto, K.; Matsui, Y.; Wakatsuki, Y., *Chem. Eur. J.*, **2002**, 8(14), 3260.
209. Bowker, M.; Stone, P.; Bennett, R.; Perkins, N., *Surf. Sci.*, **2002**, 511(1-3), 435.
210. Claus, P.; Hofmeister, H., *J. Phys. Chem. B*, **1999**, 103(14), 2766.
211. Toshima, N.; Ohtaki, M.; Teranishi, T. *React. Polym.* **1991**, 15, 135.
212. Hirai, H.; Ohtaki, M.; Komiyama, M. *Chem. Lett.* **1986**, 269.
213. Hirai, H.; Ohtaki, M.; Komiyama, M. *Chem. Lett.* **1987**, 149.
214. Ohtaki, M.; Toshima, N.; Komiyama, M.; Hirai, H. *Bull. Chem. Soc. Jpn.* **1990**, 63, 1433.
215. Suzuki, K.; Yumura, T.; Mizuguchi, M.; Tanaka, Y.; Chen, C.-W.; Akashi, M. *J. Appl. Polym. Sci.* **2000**, 77, 2678.
216. Chen, C.-W.; Chen, M.-Q.; Serizawa, T.; Akashi, M. *Chem. Commun.* **1998**, 831.
217. Chen, C.-W.; Serizawa, T.; Akashi, M. *Chem. Mater.* **1999**, 11, 1381.
218. Greci, M. T.; Pathak, S.; Mercado, K.; Prakash, G. K. S.; Thompson, M. E.; Olah, G. A., *J. Nanosci. Nanotech.*, **2001**, 1(1), 3.
219. Jacobs, P. W.; Wind, S. J.; Ribeiro, F. H.; Somorjai, G. A., *Surf. Sci.*, **1997**, 372(1-3), L249.
220. Somorjai, G. A., *Appl. Surf. Sci.*, **1997**, 121/122, 1.
221. Eppler, A.; Rupprechter, G.; Gucci, L.; Somorjai, G. A., *J. Phys. Chem. B*, **1997**, 101(48), 9973.
222. Yang, M. X.; Gracias, D. H.; Jacobs, P. W.; Somorjai, G. A., *Langmuir*, **1998**, 14(6), 1458.
223. Avoyan, A.; Rupprechter, G.; Eppler, A. S.; Somorjai, G. A., *Top. Catal.*, **2000**, 10(1,2), 107.

224. Eppler, A. S.; Rupprechter, G.; Anderson, E. A.; Somorjai, G. A., *J. Phys. Chem. B*, **2000**, *104*(31), 7286.
225. Eppler, A. S.; Zhu, J.; Anderson, E. A.; Somorjai, G. A., *Top. Catal.*, **2000**, *13*(1,2), 33.
226. Grunes, J.; Zhu, J.; Anderson, E. A.; Somorjai, G. A., *J. Phys. Chem. B*, **2002**, *106*(44), 11463.
227. Zhou, W. J.; Li, W. Z.; Song, S. Q.; Zhou, Z. H.; Jiang, L. H.; Sun, G. Q.; Xin, Q.; Poulianitis, K.; Kontou, S.; Tsiakaras, P., *J. Power Sources*, **2004**, *131*(1-2), 217.
228. Anderson, M. L.; Stroud, R. M.; Rolison, D. R., *Nano Lett.*, **2002**, *2*(3), 235.
229. Pietron, J. J.; Stroud, R. M.; Rolison, D. R., *Nano Lett.*, **2002**, *2*(5), 545.
230. Long, J. W.; Stroud, R. M.; Swider-Lyons, K. E.; Rolison, D. R., *J. Phys. Chem. B*, **2000**, *104*, 9772.
231. Moore, J. T.; Corn, J. D.; Chu, D.; Jiang, R.; Boxall, D. L.; Kenik, E. A.; Lukehart, C. M., *Chem. Mater.*, **2003**, *15*(17), 3320.
232. Moore, J. T.; Chu, D.; Jiang, R.; Deluga, G. A.; Lukehart, C. M., *Chem. Mater.*, **2003**, *15*(5), 1119.
233. Ye, X.; Lin, Y.; Wang,.; Engelhard, M. H.; Wang, Y.; Wai, C. M., *J. Mat. Chem.*, **2004**, *14*(5), 908.
234. Lyman, C. E.; Lakis, R. E.; Stenger, , H. G. Jr., *Ultramicros.*, **1995**, *58*(1), 25.
235. Lai, S. Y.; Zhang, H.; Ng, C. F., *Catal. Lett.*, **2004**, *92*(3-4), 107.
236. Yin, S.; Xu, B.; Ng, C.; Au, C., *Appl. Catal. B: Environ.*, **2004**, *48*(4),
237. Delpeux, S.; Szostak, K.; Frackowiak, E.; Bonnamy, S.; Beguin, F., *J. Nanosci. Nanotech.*, **2002**, *2*(5), 481.

CHAPTER II

EXPERIMENTAL METHODS

2.1 Preparation of Colloidal Transition Metal Nanoparticles

2.1.1 Spherical PVP-Pt Nanoparticles

The spherical PVP-Pt nanoparticles were synthesized by the reduction of the Pt^{+2} ions with ethanol similar to a method described previously¹⁻³ except that the K_2PtCl_4 precursor salt was used instead of PdCl_2 . The method described previously¹⁻³ was used to prepare PVP-capped palladium nanoparticles. A 0.01 M stock solution of the precursor K_2PtCl_4 salt was prepared in a volumetric flask, sonicated for three hours, and allowed to age for one day prior to use. During the aging process, the volumetric flask was covered with aluminum foil and kept in a dark place. A solution containing 3 mL of the 0.01 M K_2PtCl_4 precursor salt, 33 mL of doubly deionized water, 0.0667 g PVP, and 4 drops of 1 M HCl was heated. The concentration of Pt^{+2} ions present in the solution is 6×10^{-4} M. When the solution refluxes, 14 mL of ethanol was added. The solution is refluxed for three hours and the resulting colloidal solution is dark brown. A drop of the colloidal solution is placed onto a Formvar stabilized copper grid and allowed to dry for 2 hours. The 100C TEM is used to image the nanoparticles.

2.1.2 Tetrahedral PVP-Pt Nanoparticles

The PVP stabilized tetrahedral Pt nanoparticles were prepared using H_2 reduction methods described previously⁴⁻⁵ with some modifications. The precursor platinum salt

used is K_2PtCl_6 and the stabilizer used is PVP (mw = 360,000). A 500 mL 3-neck flask equipped with a gas trap was used for the synthesis of the nanoparticles. A 0.01 M stock solution of the K_2PtCl_6 precursor salt was prepared, sonicated for three hours, and allowed to age for one day prior to use. During the aging process, the volumetric flask was covered with aluminum foil and stored in a dark place. Two hundred fifty mL of doubly deionized water, 2 mL of 0.01 M K_2PtCl_6 , and 0.25 g of PVP was added to the flask. No adjustment of the pH of the solution is needed and the synthesis is conducted at the solution's "natural pH". After the solution is thoroughly mixed, argon is bubbled for 20 minutes and then hydrogen gas is bubbled for 5 minutes. The argon can be bubbled at any flow rate desired since the main purpose of bubbling argon is to get rid of oxygen present in the solution prior to the synthesis. The hydrogen gas is bubbled at a flow rate of 15 psi for 5 minutes. The flask is then sealed, wrapped in aluminum foil, and stored in the dark for 24 hours. The resulting colloidal solution is light brown. A drop of the colloidal solution is placed onto a Formvar stabilized copper grid and allowed to dry for 2 hours. The 100C TEM is used to image the nanoparticles.

2.1.3 Cubic Polyacrylate-Pt Nanoparticles

The polyacrylate stabilized Pt nanoparticles were prepared using the H_2 reduction method described previously⁴ with a few modifications. The precursor platinum salt used is K_2PtCl_4 and the stabilizer used is polyacrylate (mw = 2,100). A 500 mL 3-neck flask equipped with a gas trap was used for the synthesis and this flask was thoroughly cleaned with Aqua Regia for 2 hours immediately before the synthesis. Cleaning the flask with fresh Aqua Regia is extremely important for the successful production of dominantly

cubic platinum nanoparticles. A 0.01 M stock solution of the K_2PtCl_4 precursor salt was prepared, sonicated for three hours, and allowed to age for one day prior to use. A 0.1 M stock solution of the sodium polyacrylate was prepared and sonicated for 30 minutes prior to synthesis. It is important to prepare the polyacrylate immediately prior to the synthesis since so that it is a fresh solution. During the aging process, the volumetric flask was covered with aluminum foil and stored in a dark place. Two hundred fifty mL of doubly deionized water, 2 mL of 0.01 M K_2PtCl_4 , and 1 mL of 0.1 M polyacrylate were added to the flask. The solution was adjusted to a pH of 9 prior to synthesis. After the solution is thoroughly mixed, argon is bubbled for 20 minutes and then hydrogen gas is bubbled for 5 minutes. The argon can be bubbled at any flow rate desired since the main purpose of bubbling argon is to get rid of oxygen present in the solution prior to the synthesis. The hydrogen gas is bubbled at a flow rate of 15 psi for 5 minutes. The flask is then sealed, wrapped in aluminum foil, and stored in the dark for 24 hours. The resulting colloidal solution is light brown. A drop of the colloidal solution is placed onto a Formvar stabilized copper grid and allowed to dry for 2 hours. The 100C TEM is used to image the nanoparticles.

2.1.4 Spherical PVP-Pd Nanoparticles

The spherical PVP-Pd nanoparticles were synthesized by the reduction of the Pd ions with ethanol similar to that described previously¹⁻³. The palladium precursor stock solution (H_2PdCl_4) was prepared by adding 0.0887 g of $PdCl_2$, 6 mL of 0.2 M HCl, and diluting to 250 mL with doubly distilled water. The concentration of the palladium precursor stock solution was 2 mM and it was prepared in a volumetric flask, sonicated

for three hours, and allowed to age for one day prior to use. A solution containing 15 mL of 2 mM of H_2PdCl_4 , 21 mL of doubly deionized water, 0.0667 g PVP, and 4 drops of 1 M HCl was heated. When the solution began to reflux, 14 mL of ethanol was added. The solution was then refluxed for three hours and this resulted in a dark brown colloidal Pd solution. A drop of the colloidal solution is placed onto a Formvar stabilized copper grid and allowed to dry for 2 hours. The 100C TEM is used to image the nanoparticles.

2.1.5 Spherical Dendrimer-Pd Nanoparticles

The PAMAM-OH dendrimer stabilized Pd nanoparticles were synthesized in a similar manner to that described previously⁵. It is important to keep the PAMAM-OH Generation 4 dendrimer refrigerated at all times prior to use. The dendrimer solution was rotovaped in order to remove the methanol solvent. A 1 mM aqueous stock solution of the dendrimer and a 3 mM stock solution of the K_2PdCl_4 precursor salt were prepared. To prepare the nanoparticles, 90 mL of the dendrimer stock solution was added to 30 mL of the K_2PdCl_4 stock solution in a round-bottom flask. The solution is stirred under nitrogen for five minutes prior to synthesis and this is accomplished by inserting a needle attached to the tubing connected to the nitrogen gas tank onto the rubber stopper sealing the round bottom flask. An empty needle is also inserted onto the rubber stopper to prevent pressure buildup and to allow accumulated gas to exit. A stock solution of sodium borohydride with a concentration of 0.36 M was prepared and it is important to prepare a fresh sodium borohydride stock solution immediately prior to the synthesis. Then, 2 mL of 0.36 M of sodium borohydride is added to the round-bottom flask. The solution is stirred vigorously under nitrogen atmosphere for 1 hour. The resulting

colloidal solution is dark brown. A drop of the colloidal solution is placed onto a Formvar stabilized copper grid and allowed to dry for 2 hours. The 100C TEM is used to image the nanoparticles.

2.2 Preparation of Supported Transition Metal Nanoparticles

2.2.1 Carbon Supported Spherical PVP-Pd Nanoparticles

The carbon supported spherical PVP-Pd nanoparticles are prepared using the adsorption method. First, 25 mL of the colloidal spherical PVP-Pd nanoparticle solution is diluted to 50 mL by adding 25 mL of doubly distilled water. Next, 50 mL of the diluted palladium nanoparticles is mixed with 1.0 gram of activated carbon. The solution is then stirred vigorously at room temperature for 24 hours. After this, the solution is centrifuged at 19,000 rpm for 30 minutes at 25° C in order to separate the liquid from the carbon support containing the adsorbed Pd nanoparticles. The centrifugation process is continued for two more cycles in order to make sure that only the adsorbed nanoparticles remain in the carbon support and to remove as much of the reducing agent, metal ions, and metal atoms as possible. The resulting slurry, which is the carbon support containing the adsorbed Pd nanoparticles, is poured onto a piece of filter paper and allowed to dry overnight. The solid is gently crushed into a powder in order to use in catalytic processes. The resulting solid is the spherical PVP-Pd nanoparticles adsorbed onto the activated carbon support. In order to observe the nanoparticles by TEM, it is necessary to place a small amount of the powder into a solution of ethanol and sonicate it for an hour prior to spotting the solution onto a Formvar stabilized copper TEM grid. The carbon-

supported palladium nanoparticles are imaged by using the JEM 4000EX HRTEM since the use of high-resolution transmission electron microscopy results in the supported nanoparticles being seen more clearly than in the case of conventional transmission electron microscopy.

2.3 Transmission Electron Microscopy (TEM)

2.3.1 JEOL 100C to Study Size Distribution of Pt and Pd Nanoparticles Under Various Conditions

The JEOL 100C TEM is used to determine any changes in the width and center of the size distributions of the transition metal nanoparticles after the first and second cycle of the reaction being studied. In addition, TEM images are obtained after exposure to individual reactants involved in the reaction.

The metal nanoparticle samples were spotted by placing a drop of the solution onto a Formvar stabilized copper grid and allowing the drop to evaporate in air. The spotted samples take approximately 2 hours to dry for aqueous solutions and approximately 30 minutes to dry for organic solutions. Since the same deposition conditions are employed for all of the samples, the evaporation rate of the solvent is fairly reproducible from one sample to another. For each experiment, the internal reproducibility of the observed particle size and distribution was verified by spotting the sample onto three separate TEM grids. Also, TEM images were taken from different sections of the TEM grids to verify the particle size and distribution. The general reproducibility of the observed particle size and distribution was verified by repeating

each experiment three times. As a result, it is possible to compare the particle size and distribution changes under the various conditions.

The nanoparticle size and distribution was determined by counting approximately 1800 nanoparticles from 9 enlarged TEM images (approximately 200 nanoparticles from each TEM image). The size distribution plots were fit using a Gaussian model with the Microcal Origin 5.0 graphing software in order to determine the widths and centers of the size distributions. The widths of the size distributions give an idea of how narrow or wide the size distributions are. The centers of the size distributions are the most probable or average size of the nanoparticles (depending on the shape of the distribution).

2.3.2 JEOL 100C to Study Shape Distribution of Pt Nanoparticles Under Various Conditions

The stability of the platinum nanoparticle shapes before and after the different conditions is assessed by using TEM. The nanoparticle samples were spotted by placing a drop of the solution onto a Formvar stabilized copper grid and allowing the drop to evaporate in air. The spotted aqueous samples take approximately 2 hours to dry. Since the same deposition conditions are employed for all of the samples, the evaporation rate of the solvent is fairly reproducible from one sample to another. For each experiment, the internal reproducibility of the observed nanoparticle shape distribution was examined by spotting the sample onto three separate TEM grids. Also, TEM images were taken from different sections of the TEM grids to verify the shape distribution. The general reproducibility of the observed shape distribution was verified by conducting each of the experiments three times. As a result, it is possible to compare the shape distribution changes under the various conditions.

For each experiment, approximately 1800 nanoparticles were counted (9 enlarged TEM images with approximately 200 nanoparticles in each image). In the case of the dominantly tetrahedral PVP-Pt nanoparticles, the shapes that were counted are regular tetrahedral, distorted tetrahedral, and spherical nanoparticles. The goal is to see if there are changes in the distribution of the nanoparticle shape under the different conditions. In these experiments, the size distributions of the nanoparticles were not conducted since when there are distorted tetrahedral nanoparticles, the size depends on the type of the distortion. As a result, the shape distribution is used as a better indication of the stability of the nanoparticles after catalysis, recycling, or in the presence of the individual chemicals used in the reaction. In the case of the dominantly cubic polyacrylate stabilized platinum nanoparticles, the shapes that were counted are regular cubes, distorted cubes, and truncated octahedral. Here also, the size distribution was not conducted since in the case of distorted cubic nanoparticles, the size of the particle would depend on the type of distortion.

2.3.3 JEM 4000EX HRTEM to Obtain Detailed View of Shape Changes

The JEOL 4000EX HRTEM can be used to obtain high-resolution TEM images of the platinum nanoparticles and to observe their lattice fringes. HRTEM images were obtained for a typical tetrahedral and cubic nanoparticle before the reaction, after the first cycle, and after exposing the nanoparticles to just the hexacyanoferrate (III) ions in the case of the electron transfer reaction. In the case of the Suzuki reaction, HRTEM images were obtained before the reaction and after the second cycle of the reaction. Images that have lattice fringes that can be clearly seen are obtained and are outlined for better

visualization of the shape. These images are used to obtain proof of whether there are changes in the corners and edges of the tetrahedral and cubic nanoparticles under various conditions.

2.3.4 JEM 4000EX HRTEM to Study Size Distribution of Supported Metal Nanoparticles

The reaction mixture solutions containing the carbon supported spherical PVP-Pd nanoparticles are sonicated for an hour before spotting them onto TEM grids. For spotting the samples, a dilute solution of the supported nanoparticles is used. A drop of the dilute solution is placed onto a Formvar stabilized copper grid and the drop is allowed to evaporate in air. The spotted samples take approximately 30 minutes to dry. Since the same deposition conditions are employed for all samples, the evaporation rate of the solvent is fairly reproducible from one sample to another. For each of the experiments, the internal reproducibility of the observed size distribution is verified by spotting the sample onto three separate TEM grids. HRTEM images are also obtained from different sections of the TEM grids in order to verify the reproducibility of the size distribution. The general reproducibility of the size distribution is verified by conducting each of the experiments three times. The nanoparticle size distribution is determined by counting approximately 1800 nanoparticles from nine enlarged HRTEM images (approximately 200 nanoparticles from each HRTEM image). The size distribution plots were fit using a Gaussian model with the Microcal Origin 5.0 graphing software in order to determine the widths and centers of the size distributions. The widths of the size distributions give an idea of how narrow or wide the size distributions are. The centers of the size

distributions are the most probable or average size of the nanoparticles (depending on the shape of the distribution).

2.4 Catalysis

2.4.1 Electron Transfer Reaction

The platinum nanoparticle solution is adjusted to a pH of 7 by the addition of NaOH or HCl as appropriate before conducting the reaction. A 0.01 M stock solution of hexacyanoferrate (III) ions was prepared using the potassium hexacyanoferrate (III) salt. A 0.1 M stock solution of thiosulfate ions was prepared using the sodium thiosulfate salt. The pH of both stock solutions was adjusted to 7 in order to conduct the reaction at a pH of 7. The electron transfer reaction between hexacyanoferrate (III) ions and thiosulfate ions was carried out by adding 200 μ L of 0.01 M potassium hexacyanoferrate (III) ions and 200 μ L of 0.1 M sodium thiosulfate to 2 mL of the platinum nanoparticles. To do a control experiment without the presence of a catalyst, 2 mL of doubly distilled water is added instead of 2 mL of the catalyst.

2.4.2 Recycling for the Second Cycle of the Electron Transfer Reaction

In order to recycle the nanoparticles, the absorption spectra is taken to make sure that all of the hexacyanoferrate (III) ions are used up signaling that the first cycle of the reaction is over. Basically, the hexacyanoferrate (III) ions absorb at 420 nm, and if there is no peak present in this region, this signals that there is no more hexacyanoferrate (III) ions present in the reaction mixture or the amount present is lower than the detection

limit of the Shimadzu UV-VIS-NIR spectrophotometer. After the first cycle of the electron transfer reaction is completed, the second cycle of electron transfer reaction is initiated by adding 2 μL of 1 M potassium hexacyanoferrate (III) and 2 μL of 1 M sodium thiosulfate to the solution. Both the 1 M potassium hexacyanoferrate (III) stock solution and the 1 M sodium thiosulfate stock solution are adjusted to a pH of 7 prior to their use. Since the volume increase is only 4 μL for a total volume of 2.404 mL, the concentrations of the platinum nanoparticle solutions are about the same as in the first cycle. Since there is negligible difference in the concentrations, the stability and catalytic activity of the nanoparticles can be compared for the first and second cycle.

2.4.3 Kinetics of the Electron Transfer Reaction

The kinetics of the electron transfer reaction was monitored by using absorption spectroscopy with a Shimadzu UV-VIS-NIR spectrophotometer. The disappearance of the hexacyanoferrate (III) peak as a function of time was monitored by subtracting the absorption at 500 nm from the absorption at 420 nm. At 420 nm, both the hexacyanoferrate (III) ions and the platinum nanoparticles absorb and at 500 nm, only the platinum nanoparticles absorb with an absorption coefficient very close to that at 420 nm. The absorbance was monitored every 10 minutes for 40 minutes. The slope of the graph of $-\ln A$ vs. Time is the rate constant, k . The rate constant of the reaction was determined at four different temperatures (25°C, 30°C, 40°C, and 45°C) for the four different concentrations of the catalyst. In order to carry out the reaction at different temperatures, a brass cuvette holder connected with tubes to the ethylene glycol bath was placed inside the spectrophotometer. The quartz cell was placed in the brass holder and

heated to the desired temperature. A thermocouple was placed in the brass holder to monitor the temperature throughout the whole experiment. From the slope of the graph $\ln k$ vs. $1000/T$, the activation energy of the reaction was determined. The activation energy of the reaction was determined for all 4 different concentrations of the spherical platinum nanocatalysts for the first and second cycle of the reaction. A comparison of the activation energy was also conducted for the tetrahedral, cubic, and spherical platinum nanoparticles.

2.4.4 Suzuki Reaction

The Suzuki reaction between phenylboronic acid and iodobenzene was catalyzed using the spherical PVP-Pd nanoparticles as described previously^{1-2, 6}. For this reaction, 0.49 g (6 mmol) of sodium acetate, 0.37 g (3 mmol) of phenylboronic acid, and 0.20 g (1 mmol) of iodobenzene was added to 150 mL of 3:1 acetonitrile:water solvent. It is very important to conduct this reaction using HPLC grade acetonitrile, which is the most pure form of the solvent. In addition, the water used to generate the solvent mixture must be doubly distilled. The use of other kinds of acetonitrile (non-HPLC grade) can sometimes result in no reaction taking place and this could be due to impurities that are present. In addition, the sodium acetate is necessary to activate the reaction. When the sodium acetate is not present, the reaction does not take place. The reaction mixture was heated to 100 °C and 5 mL of the PVP-Pd nanoparticles was added to start the reaction. The reaction mixture was refluxed for a total of 12 hours. In the case of the dendrimer-Pd nanoparticles used as catalysts for the Suzuki reaction, 5 mL of the nanoparticles was added to start the reaction. In the case of the tetrahedral PVP-Pt nanoparticles as

catalysts for the Suzuki reaction, 15 mL of the nanoparticles are added in order to start the reaction.

2.4.5 Recycling for the Second Cycle of the Suzuki Reaction

The same reaction mixture solution was used for recycling after the addition of fresh amounts of the reactants. For recycling, an assumption was made that all of the iodobenzene was used up since it is the limiting reactant. Initially there is 1 mmol iodobenzene and 3 mmol phenylboronic acid present in the reaction mixture. After the first cycle, it is assumed that there is no iodobenzene left and 2 mmol phenylboronic acid left. As a result, for the second cycle, 1 mmol iodobenzene and 1 mmol phenylboronic acid were added. The reaction mixture was then refluxed for another 12 hours to complete the second cycle. The same procedure for recycling the catalysts for the Suzuki reaction was followed for all three types of nanocatalysts (spherical PVP-Pd nanoparticles, spherical PAMAM-OH Generation 4 Pd nanoparticles, tetrahedral PVP-Pt nanoparticles).

2.4.6 Determination of Biphenyl Product Yield by HPLC

HPLC measurements were conducted on a Hitachi-4500 HPLC equipped with a L4500A diode array detector in which the absorbance was monitored at 254 nm. The separation was carried out on a reversed-phase packed column (Rainin Microsorb-MV C18, 300 Angstroms, dim 4.6 x 250 mm) using a 60:40 acetonitrile-water mixture and a flow rate of 1 mL/min. The area of the chromatographic peaks was calculated with a D-6000 interface-integrator. A calibration curve for determining the concentration of

biphenyl was constructed by plotting the peak area vs. concentration of biphenyl standards. The standards prepared were 0.0005 M, 0.001 M, 0.0015 M, 0.002 M, 0.0025 M, and 0.003 M biphenyl. For all of the HPLC measurements, the samples were diluted to $\frac{1}{4}$ of the original concentration so that the peak areas will be within the range of the calibration curve. The actual concentration present in the sample was determined by taking the concentration of the diluted sample and multiplying by 4. The concentration of biphenyl was determined before the first cycle, after the first cycle, before the second cycle, and after the second cycle. Also, the effect of PVP on the amount of biphenyl formed was also determined. In addition, the impact of the presence of biphenyl in the Suzuki reaction mixture on the formation of additional biphenyl product was also investigated by using HPLC.

2.5 References

1. Li, Y.; Hong, X. M.; Collard, D. M.; El-Sayed, M. A. *Org. Lett.* **2000**, *2(15)*, 2385.
2. Li, Y.; Boone, E.; El-Sayed, M. A. *Langmuir* **2002**, *18*, 4921.
3. Teranishi, T.; Miyake, M. *Chem. Mater.* **1998**, *10*, 594.
4. Ahmadi, T. S.; Wang, Z. L.; Green, T. C.; Henglein, A.; El-Sayed, M. A. *Science*, **1996**, *272*, 1924.
5. Yu, Y.; Xu, B., *Chin. Sci. Bull.*, **2003**, *48(23)*, 2589.
6. Li, Y.; El-Sayed, M. A. *J. Phys. Chem. B*, **2001**, *105*, 8938.

CHAPTER 3

THE EFFECT OF CATALYTIC ACTIVITY ON THE METALLIC SIZE DISTRIBUTION: THE ELECTRON TRANSFER REACTION BETWEEN HEXACYANOFERRATE (III) IONS AND THIOSULFATE IONS CATALYZED BY PVP-PLATINUM NANOPARTICLES

3.1 Abstract

The electron transfer reaction between hexacyanoferrate (III) ions and thiosulfate ions is known to be catalyzed by platinum nanoparticles. In the present study, the stability and catalytic activity of the PVP-Pt nanoparticles during its catalytic function for this electron transfer reaction is studied. The stability of the nanoparticles after various perturbations was assessed using TEM and the kinetics of the reaction was followed using absorption spectroscopy. The studies were conducted on four different concentrations of PVP-Pt nanoparticles.

It was found that the average size and width of the PVP-Pt nanoparticles decreases slightly after the first and second cycle of the electron transfer reaction. The size and distribution width do not change in the presence of just the thiosulfate reactant while the presence of just the hexacyanoferrate reactant results in a reduction of the nanoparticle size. The reduction in the nanoparticle size in the presence of hexacyanoferrate (III) ions is proposed to result from dissolving surface Pt atoms by complexation with the strong cyanide ligand. Thiosulfate ions bind to the nanoparticle surface and acts as a capping material resulting in the stability of the nanoparticles. From these observations, it is possible that the surface catalytic mechanism involves the thiosulfate ions binding to the free sites on the surface of the nanoparticles followed by

the reaction with hexacyanoferrate ions approaching the nanoparticle surface from the solution. Conducting the reaction with the nanoparticles pre-exposed to thiosulfate results in very little change in the centers and widths of the size distributions of the nanoparticles, thus suggesting that thiosulfate ions bind to the nanoparticle surface and inhibits desorption of Pt atoms by hexacyanoferrate (III) ions. The kinetics of the electron transfer reaction during the first and second cycle is similar. The activation energy of the nanoparticle catalytic reaction is found to decrease linearly with increasing nanoparticle concentration during both the first and second cycle. If increasing the nanoparticle concentration leads to more aggregation, then these results suggest that the aggregated Pt has more catalytic activity than the individual nanoparticles.

3.2 Introduction

Due to their large surface to volume ratio, nanoparticles offer higher catalytic efficiency per gram than larger size materials. The field of nanocatalysis has been very active lately with numerous review articles published during the past decade in both heterogeneous catalysis in which the nanoparticles are supported on solid surfaces (e.g. silica or alumina)¹⁻¹³ and in homogeneous catalysis with colloidal nanoparticles¹⁴⁻²¹. Being small in size is expected to increase the nanoparticle surface tension. This makes surface atoms very active. The question is now raised as to how active they become. Are they active beyond their catalytic function and thus become reactants rather than catalysts? Are they active enough to change their own shape or size during the catalysis?

In the bulk of the catalysis with colloids, TEM characterization of the nanoparticles before and after catalysis is not given. However, there are a few studies in

the literature where the size distribution of the nanoparticles after recycling along with the catalytic activity is reported for characterization. Such studies have been conducted on reactions such as the hydrogenation of ethyl pyruvate²², hydrogenation of arenes²³, carbonylation of methanol²⁴, the intra- and inter-molecular Paulson-Khand reactions²⁵, hydrogenation of alkenes²⁶, and the Suzuki reaction between phenylboronic acid and iodobenzene²⁷. There also have been some papers that discuss the catalytic activity of the nanoparticles upon recycling, but which do not examine the stability of the nanoparticles after catalysis. Such studies were conducted for reactions like hydrogenation of alkenes²⁸, Heck reaction between aryl halides and n-butylacrylate²⁹, hydrogenation of olefins³⁰, and hydrogenation of unsaturated fatty acid esters³¹. In the review article on transition metal colloids³², it was pointed out that the major interest of reusability of the nanoparticle catalysts has not been systematically studied or published in the metal colloid literature.

For reactions catalyzed by metal nanoparticles in colloidal solution, there has been very few detailed examinations in the literature of what causes size distribution changes, the effect of the various chemicals, and whether the changes in the nanoparticles affects the catalytic activity upon recycling. A detailed examination is necessary in order to evaluate the nanoparticles' usefulness in catalyses and to understand in detail the mechanism of "nanocatalysis". This will enable a much better understanding of what kind of nanoparticles are the best for catalysis and also provide insight on how to make the nanoparticles more stable and maintain their catalytic activity.

We have previously conducted a detailed examination of the stability of PVP-Pd nanoparticles catalyzing the Suzuki reaction between phenylboronic acid and

iodobenzene²⁷. We found that the nanoparticles increased in size after the first cycle of the reaction and decreased in size after the second cycle of the reaction. The increase in the size of the nanoparticles was attributed to Ostwald ripening of the nanoparticles and the decrease in size after the second cycle was blamed on the aggregation and precipitation of the large nanoparticles. The effect of the individual chemicals involved in the reaction was also examined. It was also found that the catalytic activity greatly diminished upon recycling which is due to a lower number of nanoparticles present in solution due to the larger nanoparticles aggregating and precipitating out of solution and also due to biphenyl product poisoning the active sites.

The electron transfer reaction between hexacyanoferrate (III) ions and thiosulfate ions results in the formation of hexacyanoferrate (II) ions and tetrathionate ions. The reaction can even proceed without a catalyst, but occurs at a very slow rate. The electron transfer reaction has been recently catalyzed using various metal nanoparticles as catalysts. Citrate-capped gold nanoparticles³³⁻³⁴, platinum nanoparticles prepared in situ in water-in-oil microemulsions by the aerosol-OT (AOT)-water-heptane system³⁵, and polyacrylate stabilized platinum nanoparticles³⁶ have all been used to catalyze the electron transfer reaction between hexacyanoferrate (III) ions and thiosulfate ions to form hexacyanoferrate (II) ions and tetrathionate ions.

In this paper, the stability of PVP-Pt nanoparticles after catalyzing the electron transfer reaction between hexacyanoferrate (III) and thiosulfate ions and after recycling for the second cycle was assessed by using TEM to see if there are any changes in the widths and centers of the size distributions of the nanoparticles. The effect of the individual chemicals involved in the reaction on the stability of the nanoparticles was

also studied. The catalytic activity of the nanoparticles during the first and second cycle of the reaction was assessed using absorption spectroscopy to follow the kinetics and determine the activation energy.

We found that after the first and second cycle of the electron transfer reaction, the centers and widths of the size distributions of the PVP-Pt nanoparticles decrease slightly. The presence of hexacyanoferrate (III) ions results in a great reduction in the size of the nanoparticles which could be due to it reacting with the Pt atoms in the nanoparticle surface and dissolving the atoms. The presence of thiosulfate ions results in the nanoparticles maintaining their size which could be due to it binding to the nanoparticle surface. As a result, it is proposed that the surface catalytic mechanism involves thiosulfate ions binding to the nanoparticle surface and reacting with hexacyanoferrate (III) ions in solution. Conducting the reaction with the nanoparticles pre-exposed to thiosulfate resulted in very little change in the nanoparticle size suggesting that the binding of the thiosulfate ions onto the nanoparticle surface inhibits desorption of Pt atoms by hexacyanoferrate (III) ions during catalysis. The kinetics of the reaction is found to be similar in both cycles and in both cases, the activation energy decreases linearly with increasing nanoparticle concentration.

3.3 Experimental Section

3.3.1 Synthesis of PVP-Pt Nanoparticles

The PVP-Pt nanoparticles were synthesized by the reduction of the Pt^{+2} ions with ethanol similar to a method described previously³⁷⁻³⁹ except that the K_2PtCl_4 salt was

used. A solution containing 15 mL of 2 mM of K_2PtCl_4 , 21 mL of doubly deionized water, 0.0667 g PVP, and 4 drops of 1 M HCl was heated. The concentration of Pt^{+2} ions present in the solution is 6×10^{-4} M. When the solution refluxes, 14 mL of ethanol was added. The solution is refluxed for three hours and the resulting colloidal solution is dark brown. A drop of the colloidal solution is placed onto a Formvar stabilized copper TEM grid and JEOL 100C TEM is used to determine the average size of the nanoparticles. Based on the average size and width of the nanoparticles, the average concentration of the PVP-Pt nanoparticles formed is $13.9 \text{ nM} \pm 1.9 \text{ nM}$. The concentration is determined using the formula of $([Pt^{+2} \text{ ions}] * N_A) / (V_{NP} / V_{Pt \text{ atom}})$ where NP is nanoparticle and V is volume.

3.3.2 Electron Transfer Reaction

Four PVP-Pt nanoparticle solutions of lower concentrations were prepared from the stock nanoparticle solution ($3.2 \pm 0.4 \text{ nM}$, $2.2 \pm 0.3 \text{ nM}$, $1.8 \pm 0.3 \text{ nM}$, and $1.5 \pm 0.2 \text{ nM}$). All of the nanoparticle solutions were adjusted to a pH of 7 by the addition of NaOH. For the electron transfer reaction between hexacyanoferrate (III) ions and thiosulfate ions, 200 μL of 0.01 M potassium hexacyanoferrate (III) and 200 μL of 0.1 M sodium thiosulfate was added to 2 mL of the PVP-Pt nanoparticles. Since the total volume is 2.40 mL, the final concentrations of the PVP-Pt nanoparticle solutions are $2.7 \pm 0.4 \text{ nM}$, $1.9 \pm 0.3 \text{ nM}$, $1.5 \pm 0.2 \text{ nM}$, and $1.2 \pm 0.2 \text{ nM}$ respectively.

3.3.3 Recycling PVP-Pt Nanoparticles for Second Cycle of Electron Transfer Reaction

In order to recycle the nanoparticles, the absorption spectra is taken to make sure that all of the hexacyanoferrate (III) ions are used up signaling that the first cycle of the reaction is over. After the first cycle of the electron transfer reaction is completed, the second cycle of electron transfer reaction is initiated by adding 2 μL of 1 M potassium hexacyanoferrate (III) and 2 μL of 1 M sodium thiosulfate to the solution. Since the volume increase is only 4 μL for a total volume of 2.404 mL, the concentrations of the PVP-Pt nanoparticle solutions are about the same as in the first cycle (2.7 ± 0.4 nM, 1.9 ± 0.3 nM, 1.5 ± 0.2 nM, and 1.2 ± 0.2 nM). Since there is negligible difference in the concentrations, the stability and catalytic activity of the nanoparticles can be compared for the first and second cycle. The effect of recycling the catalyst on the stability of the nanoparticles was assessed using TEM and the kinetics and activation energy of the reaction with the recycled nanoparticles was compared to those during the first cycle by using absorption spectroscopy.

3.3.4 Kinetics of Electron Transfer Reaction

The kinetics of the reaction was monitored by using absorption spectroscopy with a Shimadzu UV-VIS-NIR spectrophotometer. The disappearance of the hexacyanoferrate (III) peak as a function of time was monitored by subtracting the absorption at 500 nm from the absorption at 420 nm. At 420 nm, both the hexacyanoferrate (III) ions and the platinum nanoparticles absorb and at 500 nm, only the platinum nanoparticles absorb with an absorption coefficient very close to that at 420 nm. The absorbance was monitored every 10 minutes for 40 minutes. The slope of the graph

of $-\ln A$ vs. Time is the rate constant, k . The rate constant of the reaction was determined at four different temperatures (25°C, 30°C, 40°C, and 45°C) for the four different concentrations of the catalyst. In order to carry out the reaction at different temperatures, a brass cuvette holder connected with tubes to the ethylene glycol bath was placed inside the spectrophotometer. The quartz cell was placed in the brass holder and heated to the desired temperature. A thermocouple was placed in the brass holder to monitor the temperature throughout the whole experiment. From the slope of the graph $\ln k$ vs. $1000/T$, the activation energy of the reaction was determined. The activation energy of the reaction was determined for all 4 different concentrations of the catalyst for the first and second cycle of the reaction.

3.3.5 Stability of the PVP-Pt Nanoparticles in Various Conditions

The JEOL 100C TEM is used to determine any changes in the width and center of the size distributions of the PVP-Pt nanoparticles after the first and second cycle of the reaction. This was done for all four concentrations of the nanoparticle catalyst. The effect of hexacyanoferrate (III) ions on the PVP-Pt nanoparticles and the effect of thiosulfate ions on the PVP-Pt nanoparticles were also assessed by using TEM to find out if any changes occur due to the presence of either of the reactants by itself. The absorption spectra of the nanoparticles in the presence of hexacyanoferrate (III) ions were also followed at 0 min and after 2 days to see if there are any changes in the spectra. Also, the effect of catalyzing the reaction with PVP-Pt nanoparticles pre-exposed to thiosulfate ions on the nanoparticle size was examined.

The PVP-Pt nanoparticle samples were spotted by placing a drop of the solution onto a Formvar stabilized copper grid and allowing the drop to evaporate in air. The spotted samples take approximately 2 hours to dry since they are aqueous. Since the same deposition conditions are employed for all of the samples, the evaporation rate of the solvent is fairly reproducible from one sample to another. For each experiment, the internal reproducibility of the observed particle size and distribution was verified by spotting the sample onto three separate TEM grids. Also, TEM images were taken from different sections of the TEM grids to verify the particle size and distribution. The general reproducibility of the observed particle size and distribution was verified by repeating each experiment three times. As a result, it is possible to compare the particle size and distribution changes under the various conditions.

The nanoparticle size and distribution was determined by counting approximately 1800 nanoparticles from 9 enlarged TEM images (approximately 200 nanoparticles from each TEM image). The size distribution plots were fit using a Gaussian model with Microcal Origin 5.0 graphing software in order to determine the widths and centers of the size distributions. The widths of the size distributions give an idea of how narrow or wide the size distributions are. The centers of the size distributions are the most probable or average size of the nanoparticles (depending on the shape of the distribution).

3.4 Results and Discussion

3.4.1 Stability of PVP-Pt Nanoparticles

The stability of the PVP-Pt nanoparticles after the first and second cycle of the electron transfer reaction is investigated to find out whether there are any changes in the width and center of the size distributions of the nanoparticles after a mild reaction. The TEM images and Gaussian fits of the size distributions of the 2.7 ± 0.4 nM PVP-Pt nanoparticles for the various conditions are obtained and discussed here and the results for the other three concentrations of PVP-Pt nanoparticles are summarized in Table 3.1.

Table 3.1—Widths (W) and Centers (C) of Gaussian Fits of the Size Distributions of the PVP-Pt Nanoparticles in Various Conditions

Condition	Width and Center (nm) 1.2 ± 0.2 nM PVP-Pt NPs	Width and Center (nm) 1.5 ± 0.2 nM PVP-Pt NPs	Width and Center (nm) 1.9 ± 0.3 nM PVP-Pt NPs	Width and Center (nm) 2.7 ± 0.4 nM PVP-Pt NPs
Before 1 st Cycle	W: 0.7 ± 0.1 C: 5.0 ± 0.1	W: 0.7 ± 0.1 C: 4.9 ± 0.1	W: 0.7 ± 0.1 C: 4.9 ± 0.1	W: 0.7 ± 0.1 C: 4.9 ± 0.1
After 1 st Cycle	W: 0.7 ± 0.1 C: 4.8 ± 0.1	W: 0.6 ± 0.1 C: 4.8 ± 0.1	W: 0.7 ± 0.1 C: 4.8 ± 0.1	W: 0.6 ± 0.1 C: 4.8 ± 0.1
After 2 nd Cycle	W: 0.5 ± 0.1 C: 4.7 ± 0.1	W: 0.5 ± 0.1 C: 4.7 ± 0.1	W: 0.6 ± 0.1 C: 4.7 ± 0.1	W: 0.5 ± 0.1 C: 4.7 ± 0.1
Before Presence of $S_2O_3^{-2}$	W: 0.8 ± 0.1 C: 4.9 ± 0.1	W: 0.7 ± 0.1 C: 4.9 ± 0.1	W: 0.7 ± 0.1 C: 4.9 ± 0.1	W: 0.8 ± 0.1 C: 4.9 ± 0.1
After Presence of $S_2O_3^{-2}$	W: 0.7 ± 0.1 C: 4.9 ± 0.1	W: 0.7 ± 0.1 C: 4.9 ± 0.1	W: 0.7 ± 0.1 C: 4.9 ± 0.1	W: 0.7 ± 0.1 C: 4.9 ± 0.1
Before Presence of $Fe(CN)_6^{-3}$	W: 0.7 ± 0.1 C: 4.9 ± 0.1	W: 0.7 ± 0.1 C: 4.9 ± 0.1	W: 0.7 ± 0.1 C: 4.8 ± 0.1	W: 0.7 ± 0.1 C: 4.9 ± 0.1
After Presence of $Fe(CN)_6^{-3}$	W: 0.6 ± 0.1 C: 3.8 ± 0.1	W: 0.6 ± 0.1 C: 3.7 ± 0.1	W: 0.5 ± 0.1 C: 3.8 ± 0.1	W: 0.6 ± 0.1 C: 3.8 ± 0.1

3.4.2 Effect of Catalysis and Recycling

Figure 3.1a shows a typical TEM image of the PVP-Pt nanoparticles immediately after the addition of the reactants, hexacyanoferrate (III) ions and thiosulfate ions (time = 0). Figure 3.1b shows the Gaussian fits of the size distributions of the PVP-Pt nanoparticles at time = 0. It can be seen that the PVP-Pt nanoparticles are monodisperse with the centers of distributions = 4.9 ± 0.1 nm and widths of distributions = 0.7 ± 0.1 nm. Figure 3.1c shows a typical TEM image of the PVP-Pt nanoparticles after the first cycle of the reaction while Figure 3.1d shows the Gaussian fits of the size distributions of the PVP-Pt nanoparticles after the first cycle of the reaction. By comparing the widths and centers of distributions after the first cycle to those before the reaction, it can be seen that there is a 2% decrease in the centers and 14% decrease in the widths of the distributions. The trend of the slight decrease in the size of the nanoparticles after the first cycle of the reaction occurs at all four concentrations of the PVP-Pt nanoparticle catalyst as shown in Table 3.1.

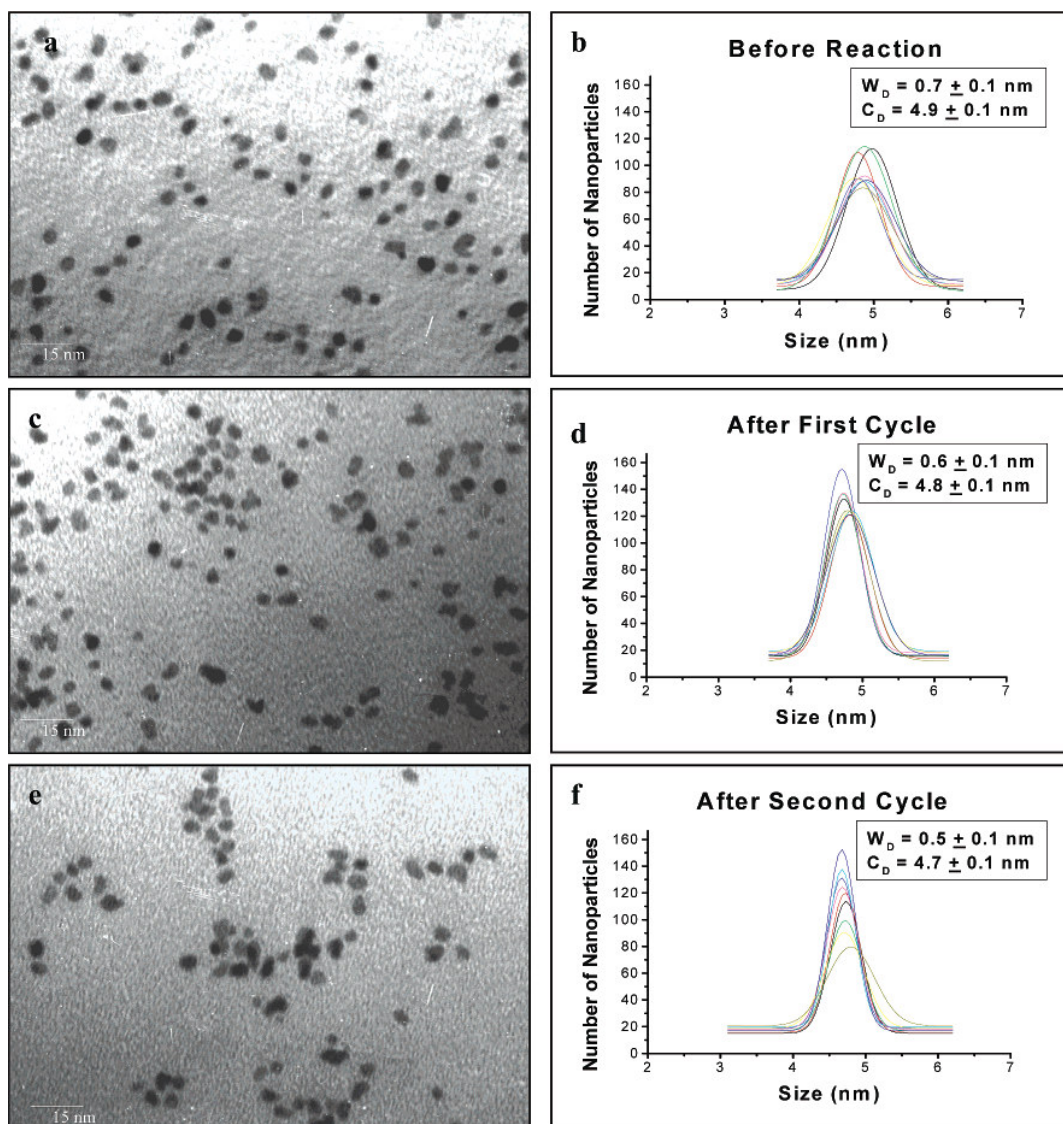


Figure 3.1—TEM images and Gaussian fits of the size distributions (C_D center of distribution and W_D width of distribution) of PVP-Pt nanoparticles (a,b) before the electron-transfer reaction, (c,d) after the first cycle of the electron-transfer reaction, (e,f) and after the second cycle of the electron-transfer reaction.

Figure 3.1e shows the TEM images after recycling the PVP-Pt nanoparticles for the second cycle of the electron transfer reaction and Figure 3.1f shows the Gaussian fits of the size distributions of the nanoparticles after recycling them. By comparing the widths and centers of the distributions with those before the reaction, it can be seen that the centers and widths of the distributions decrease by 4% and 29%, respectively after the

second cycle of the reaction. An explanation of the slight decrease in the size of the nanoparticles is discussed later on in the section on the effect of chemicals. This trend of the slight decrease in size after the second cycle is observed for all four concentrations of the PVP-Pt nanoparticles as shown in Table 3.1.

3.4.3 Effect of the Individual Reactants on the Nanoparticles

The effects of the presence of individual reactants on the PVP-Pt nanoparticles have also been investigated. The effect of exposing the nanoparticles to just thiosulfate ions was investigated. Figure 3.2a shows a representative TEM image of the PVP-Pt nanoparticles prior to exposing them to thiosulfate ions and Figure 3.2b shows Gaussian fits of the size distributions of the nanoparticles. Figure 3.2c shows a typical TEM image of the PVP-Pt nanoparticles after exposing them to thiosulfate ions for 2 days at 25 °C and Figure 3.2d shows Gaussian fits of the size distributions of these nanoparticles. It can be seen that the presence of the thiosulfate ions does not affect the centers or the widths of the size distributions of the nanoparticles. This is true for all the four concentrations of the PVP-Pt nanoparticle catalyst as can be seen in Table 3.1. The reason why the nanoparticles maintain their stability in the presence of the thiosulfate ions might be that the thiosulfate ions bind to the free sites on the nanoparticle surface and acts as a capping material. It is well known in the literature⁴⁰⁻⁴⁷ that thiosulfate binds to metal surfaces such as silver, cadmium, palladium, nickel, aluminum, zinc, platinum, etc. As a result, it is very logical to propose that the thiosulfate is binding to the free sites of the PVP-Pt nanoparticle surface.

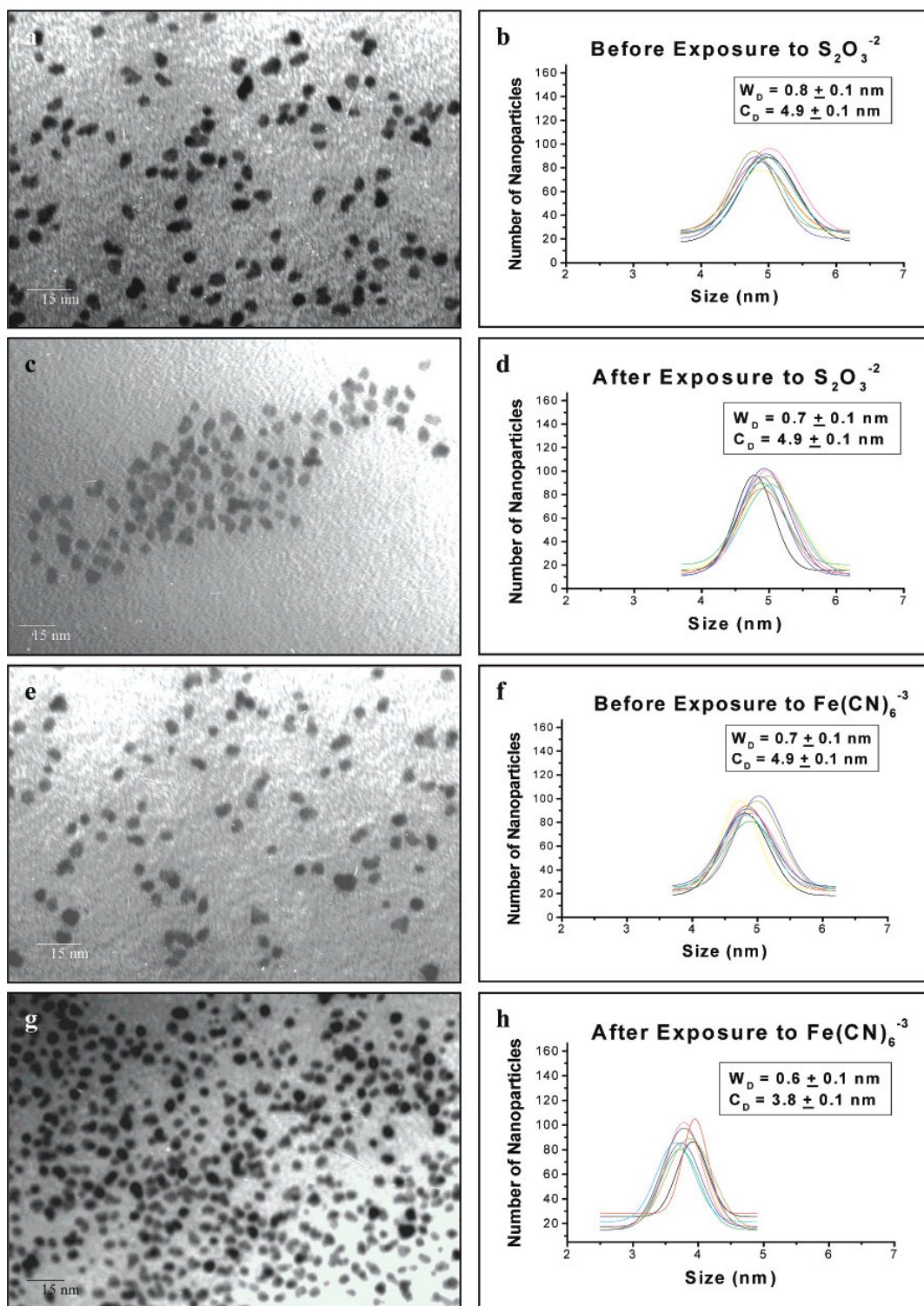


Figure 3.2— TEM images and Gaussian fits of the size distributions (C_D) center of distribution and W_D) width of distribution) of PVP-Pt nanoparticles (a,b) before exposure to thiosulfate ions [T], (c,d) after exposure to thiosulfate ions [T], (e,f) before exposure to hexacyanoferrate(III) ions [H], and (g,h) after exposure to thiosulfate ions [H].

The effect of the presence of hexacyanoferrate (III) ions on the PVP-Pt nanoparticles has also been studied. Figure 3.2e shows a representative TEM image of the PVP-Pt nanoparticles before exposing them to hexacyanoferrate (III) ions. Figure 3.2f shows Gaussian fits of the size distributions of the nanoparticles before exposing them to hexacyanoferrate (III) ions. Figure 3.2g shows typical TEM images of the PVP-Pt nanoparticles after exposing them to hexacyanoferrate (III) ions for 2 days at 25 °C. Figure 3.2h shows Gaussian fits of the size distributions of the nanoparticles. The presence of just the hexacyanoferrate (III) ions causes the nanoparticles to become smaller in size, which can be seen by the shift in the center of the size distribution toward smaller sized nanoparticles by 22% and a decrease in the width of the size distribution by 14%. This shift in the center of the distributions is evident for all four concentrations of the catalyst as can be seen in Table 3.1.

It is proposed that the reduction in size is due to the dissolving of surface Pt atoms by complexation with the strong cyanide ligand in hexacyanoferrate (III) ions. The stability constants⁴⁸ for $\text{Fe}(\text{CN})_6^{-3}$ and $\text{Pt}(\text{CN})_4^{-2}$ are 10^{31} and 10^{41} respectively. Since the stability constant for the platinum complex is much higher than the iron complex, it is quite possible that the hexacyanoferrate (III) ions could decomplex and form the more stable platinum complex. In order to examine this proposal, the absorption spectra of hexacyanoferrate (III) ions in the presence of the PVP-Pt nanoparticles were obtained at 0 min and after 2 days. No change in the intensity of the hexacyanoferrate (III) absorption peak at 420 nm was detected. This might be due to a low value of the concentration lost causing the observed reduction in the size of the nanoparticles in solution. Let us calculate the expected change in the hexacyanoferrate (III) concentration. The

concentration of hexacyanoferrate (III) ions that could be lost is calculated in the presence of the highest concentration nanoparticles studied which is 2.7 ± 0.4 nM. First, the decrease in the volume of one nanoparticle in the solution before and after exposure to hexacyanoferrate (III) ions was calculated using the following formula; $\Delta V = \frac{4}{3} \pi r_1^3 - \frac{4}{3} \pi r_2^3$, where r_1 and r_2 are the radii of the nanoparticle before and after exposure to hexacyanoferrate ions. Using the density of Pt metal, the atomic volume of platinum is calculated to be 0.0151 nm^3 . The number of Pt atoms lost by a nanoparticle is then calculated by dividing ΔV by the atomic volume of the platinum atom and is found to be 2126 atoms per particle. To find the molar concentration of hexacyanoferrate (III) ions lost, the following formula is used: Molar Concentration of Nanoparticles*(2126/6). Based on the stoichiometry, it is assumed that each $\text{Fe}(\text{CN})_6^{-3}$ dissolves 6 Pt ions. Thus, lost hexacyanoferrate concentration = Nanoparticle concentration *((2126 atoms of Pt/nanoparticle)/(6 Pt atoms/molecule of hexacyanoferrate)). This gives $1.0 \pm 0.2 \text{ } \mu\text{M}$. The initial concentration of hexacyanoferrate ions present is $833 \text{ } \mu\text{M}$ and as a result the amount of hexacyanoferrate (III) ions lost is only 0.12% of the initial concentration, which is too small to be detected.

The small changes in the centers and widths of the distributions after the first and second cycle compared to the large changes occurring in the presence of hexacyanoferrate ions alone could very well result from passivating the surface with the thiosulfate. The hexacyanoferrate can then react with the thiosulfate as it cannot reach the surface Pt atoms. Based on the tendency of thiosulfate ions to bind to the nanoparticle surface and to act as a capping agent, it is proposed that the mechanism of surface catalysis involves the thiosulfate ions binding to the free metal sites on the

surface of the nanoparticles followed by the reaction with hexacyanoferrate (III) ions approaching the nanoparticle surface from solution.

In order to test this catalytic mechanism, we first exposed the PVP-Pt nanoparticles to thiosulfate ions and then initiated the electron transfer reaction by the addition of hexacyanoferrate (III) ions. Figure 3.3a and 3.3b show typical TEM image and Gaussian fits of the nanoparticles before the electron transfer reaction with pre-exposed Pt nanoparticles while Figure 3.3c and 3.3d show representative TEM image and Gaussian fits of the nanoparticles after the first cycle of the electron transfer reaction with the pre-exposed Pt nanoparticles. Figure 3.3e and 3.3f shows the TEM image and Gaussian fits of the nanoparticles after the first cycle of the electron transfer reaction under normal conditions (repeat of Figure 3.1c and 3.1d) for comparison purposes. It can be seen that there is very little change in the centers and widths of the size distributions after the reaction with the pre-exposed nanoparticles while under normal conditions, there is a narrowing of the size distribution, supporting the passivation effect of the pre-exposed nanoparticles to thiosulfate.

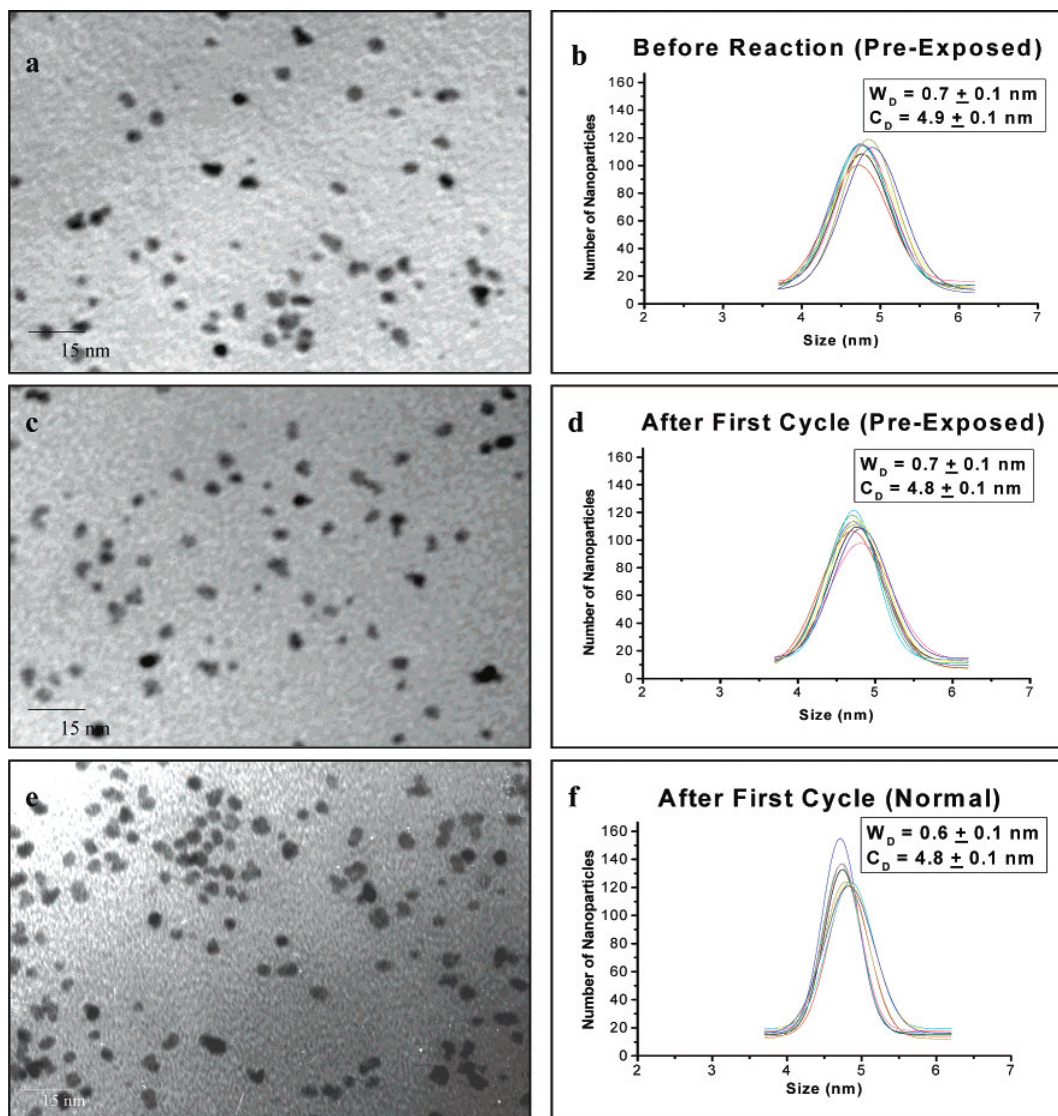


Figure 3.3—TEM images and Gaussian fits of the size distributions (C_D center of distribution and W_D width of distribution) (a,b) before electron-transfer reaction with PVP-Pt nanoparticles pre-exposed to thiosulfate, (c,d) after first cycle of electron-transfer reaction with PVP-Pt nanoparticles pre-exposed to thiosulfate, and (e,f) after first cycle of the electron-transfer reaction with PVP-Pt nanoparticles under normal conditions.

3.4.4 Catalytic Activity of PVP-Pt Nanoparticles During First and Second Cycle

The kinetics of the electron transfer reaction with PVP-Pt nanoparticles was followed by absorption spectroscopy in which the disappearance of the hexacyanoferrate (III) ion at 420 nm was monitored as a function of time at different temperatures. The activation energy of the reaction was determined for each of the four concentrations of

the catalyst in the temperature range between 25 and 45 degrees C. The kinetics of the reaction was followed at 25, 30, 40, and 45 degrees Celsius. Table 3.2 and Table 3.3 compare the kinetics of the reaction at the four different temperatures at four different concentrations of the catalyst for the first and second cycle.

In order to follow the kinetics at the second cycle, the reaction was allowed to proceed completely at room temperature, more amount of fresh reactants were added, and the kinetics were followed at the different temperatures for the second cycle. It can be seen that the kinetics of the reaction during the second cycle is similar to that of the first cycle. This observation is consistent with the observation that very little changes in the nanoparticle size or its distribution occur and as a result, the catalytic activity could remain unchanged for the second cycle of the reaction.

Table 3.2—Kinetics of Electron Transfer Reaction During First Cycle

Concentration of PVP-Pt Nanoparticle Solution (nM)	Rate Constant (min⁻¹) at 25° C	Rate Constant (min⁻¹) at 30° C	Rate Constant (min⁻¹) at 40° C	Rate Constant (min⁻¹) At 45° C
1.2 ± 0.2	0.00110 ± 0.000012	0.00137 ± 0.000017	0.00180 ± 0.000035	0.00221 ± 0.000051
1.5 ± 0.2	0.00123 ± 0.000051	0.00164 ± 0.000035	0.00213 ± 0.000104	0.00260 ± 0.000101
1.9 ± 0.3	0.00179 ± 0.000072	0.00219 ± 0.000082	0.00278 ± 0.000087	0.00317 ± 0.000055
2.7 ± 0.4	0.00273 ± 0.000060	0.00293 ± 0.00014	0.00344 ± 0.00010	0.00382 ± 0.000071

Table 3.3—Kinetics of Electron Transfer Reaction during the Second Cycle

Concentration of PVP-Pt Nanoparticle Solution (nM)	Rate Constant (min⁻¹) at 25° C	Rate Constant (min⁻¹) at 30° C	Rate Constant (min⁻¹) at 40° C	Rate Constant (min⁻¹) At 45° C
1.2 ± 0.2	0.00104 ± 0.000035	0.00129 ± 0.000020	0.00170 ± 0.000031	0.00208 ± 0.000076
1.5 ± 0.2	0.00130 ± 0.000034	0.00154 ± 0.000026	0.00191 ± 0.000025	0.00236 ± 0.000040
1.9 ± 0.3	0.00169 ± 0.000054	0.00208 ± 0.000035	0.00264 ± 0.000057	0.00293 ± 0.000051
2.7 ± 0.4	0.00265 ± 0.000045	0.00281 ± 0.000029	0.00331 ± 0.000042	0.00369 ± 0.000039

It is worth noting that the effect of catalyst concentration on the activation energy of the reaction has not been studied using nanoparticle based catalysts. However, in homogeneous catalysis (not nanoparticle based), there are a few papers⁴⁹⁻⁵⁵ that discussed the effect of the catalyst concentration on the activation energy of the reaction. Out of these studies, some showed that the activation energy was dependent on the catalyst concentration such as the solid-state polycondensation of poly(ethylene terephthalate) catalyzed by antimony trioxide⁴⁹, zinc octoate/nonylphenol catalyzed thermal cure of bisphenol A dicyanate⁵⁰, and the thermal cure reaction in the presence of various transition metal acetyl acetonates and dibutyl tin dilaurate (DBTDL)⁵¹. Also, some showed that the activation energy was independent of the catalyst concentration such as the reaction of epoxy resin with an acrylic copolymer catalyzed by dimethylbenzylamine⁵², the formation of polyurethanes catalyzed by dibutyltin dilaurate (DBTDL)⁵³, the reaction of hydroxyl terminated polybutadiene with isophorone

diisocyanate with the ferric tris (acetyl acetonate) (FeAA) catalyst⁵⁴, and the polycyclotrimerization of 4,4'-thiodiphenylcyanate catalyzed by n-nonylphenol⁵⁵.

Table 3.4 compares the activation energy at the different concentrations of the PVP-Pt nanoparticle solutions for the first and second cycles of the electron transfer reaction. It can be seen that the activation energies for the four concentrations of catalysts during the second cycle are similar to those in the first cycle. Figure 3.4a shows the plot of activation energy as a function of the catalyst concentration for the first cycle of the reaction. A very interesting observation is that the activation energy decreases linearly with increasing concentration of the PVP-Pt nanoparticles. Figure 3.4b shows a plot of the activation energy vs. concentration of the PVP-Pt nanoparticle solution for the second cycle of the reaction. It can be seen that the activation energy also decreases linearly with increasing concentration of the PVP-Pt nanoparticles for the second cycle. The changes in the activation energy are similar for both cycles of the reaction.

Table 3.4—Activation Energies for Electron Transfer Reaction for First and Second Cycle

Concentration of PVP-Pt Nanoparticle Solution (nM)	Activation Energy (First Cycle) (kJ/mole)	Activation Energy (Second Cycle) (kJ/mole)
1.2 ± 0.2	25.3 ± 2.1	24.2 ± 1.3
1.5 ± 0.2	22.6 ± 1.2	22.2 ± 1.6
1.9 ± 0.3	20.5 ± 0.8	20.0 ± 1.6
2.7 ± 0.4	12.4 ± 0.8	13.3 ± 0.9

The observed decrease in the activation energy can only be explained if the nature of the catalytic particles changes with concentration. One important change that is known to occur in the colloidal nanoparticle solutions is aggregation. As a result, the type of catalytic particles changes as new sites created at the intersection of the aggregated nanoparticles are formed. It is possible that atoms at these sites are more active catalytically giving rise to reduction in the activation energy. The mechanism of surface catalysis involves the thiosulfate ions binding to the active sites of the nanoparticles and the hexacyanoferrate ions approaching the nanoparticle surface from the solution.

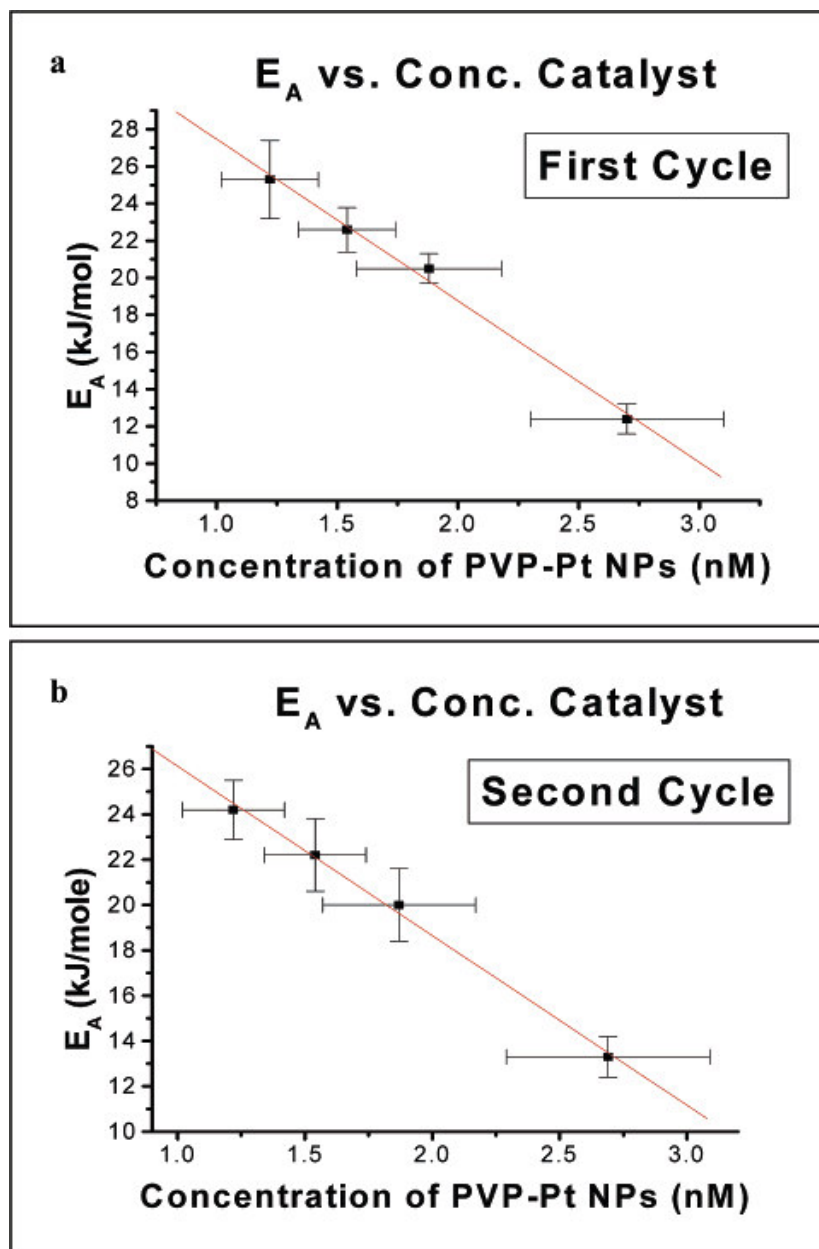


Figure 3.4—Plot of activation energy (E_A) as a function of catalyst concentration (a) during the first cycle of the electron-transfer reaction and (b) during the second cycle of the electron-transfer reaction.

3.5 Conclusions

The PVP-Pt nanoparticles decrease greatly if mixed with only the hexacyanoferrate (III) ions but is not affected if mixed with only the thiosulfate ions and slightly decreases during the reaction between hexacyanoferrate (III) ions and thiosulfate

ions. The results suggest that the hexacyanoferrate (III) ions alone dissolve the Pt from the nanoparticle surface to form a cyano complex as expected from thermodynamic considerations. Thiosulfate seems to bind to the surface thus passivate it against attack by the hexacyanoferrate, which instead, reacts with the surface bound thiosulfate to give the reaction products.

The kinetics of the reaction during the second cycle of the electron transfer reaction is similar to those in the first cycle. In both cycles, the activation energy of the reaction decreases linearly with increasing the concentration of the nanoparticle solution. If increasing concentration leads to more aggregation, these results suggest that aggregated Pt nanoparticles have more catalytic activity than individual nanoparticles.

3.6 References

1. Eppler, A.; Rupprechter, G.; Gucci, L.; Somorjai, G. A. *J. Phys. Chem. B* **1997**, *101*(48), 9973.
2. Toshima, N.; Yonezawa, T. *New J. Chem.* **1998**, *22*(11), 1179.
3. Schmid, G. *Met. Clus. Chem.* **1999**, *3*, 1325.
4. Puddephatt, R. J. *Met. Clus. Chem.* **1999**, *2*, 605.
5. Henry, C. R. *Appl. Surf. Sci.* **2000**, *164*, 252.
6. St. Clair, T. P.; Goodman, D. W. *Top. Catal.* **2000**, *13*(1,2), 5.
7. Kralik, M.; Corain, B.; Zecca, M. *Chem. Pap.* **2000**, *54*(4), 254.
8. Chusuei, C. C.; Lai, X.; Luo, K.; Goodman, D. W. *Top. Catal.* **2001**, *14*(1-4), 71.
9. Bowker, M.; Bennett, R. A.; Dickinson, A.; James, D.; Smith, R. D.; Stone, P. *Stud. Surf. Sci. Catal.* **2001**, *133*, 3.
10. Kralik, M.; Biffis, A. *J. Mol. Catal. A: Chem.* **2001**, *177*(1), 113.
11. Thomas, J. M.; Raja, R. *Chem. Rec.* **2001**, *1*(6), 448.

12. Mohr, C.; Claus, P. *Sci. Prog.* **2001**, *84(4)*, 311.
13. Thomas, J. M.; Johnson, B. F. G.; Raja, R.; Sankar, G.; Midgley, P. A. *Acc. Chem. Res.* **2003**, *36(1)*, 20.
14. Bradley, J. S. *Clus. Colloids* **1994**, 459.
15. Duff, D. G.; Baiker, A. *Stud. Surf. Sci. Catal.* **1995**, *91*, 505.
16. Toshima, N. *NATO ASI Ser., Ser. 3* **1996**, *12*, 371.
17. Boenermann, H.; Braun, G.; Brijoux, G. B.; Brinkman, R.; Tilling, A. S.; Schulze, S. K.; Siepen, K. *J. Organomet. Chem.* **1996**, *520(1-2)*, 143.
18. Fugami, K. *Organomet. News* **2000**, *1*, 25.
19. Mayer, A. B. R. *Polym. Adv. Technol.* **2001**, *12(1-2)*, 96.
20. Bonnemann, H.; Richards, R. *Syn. Meth. Organom. Inorg. Chem.* **2002**, *10*, 209.
21. Moiseev, I. I.; Vargaftik, M. N. *Russ. J. Chem.* **2002**, *72(4)*, 512.
22. Collier, P. J.; Iggo, J. A.; Whyman, R. *J. Mol. Catal. A: Chem.* **1999**, *146 (1-2)*, 149.
23. Schulz, J.; Roucoux, A.; Patin, H. *Chem. Eur. J.* **2000**, *6(4)*, 618.
24. Wang, Q.; Liu, H.; Han, M.; Li, X.; Jiang, D. *J. Mol. Catal. A: Chem.* **1997**, *118(2)*, 145.
25. Kim, S.; Son, S. U.; Lee, S. S.; Hyeon, T.; Chung, Y. K. *Chem. Commun.* **2001**, 2212.
26. Larpent, C.; Menn, B. F.; Patin, H. *J. Mol. Catal.* **1991**, *65*, L35.
27. Narayanan, R.; El-Sayed, M. A. *J. Am. Chem. Soc.*, **2003**, *125(27)*, 8340.
28. Chechik, V.; Crooks, R. M. *J. Am. Chem. Soc.* **2000**, *122*, 1243.
29. Yeung, L. K.; Crooks, R. M. *Nano Letters* **2001**, *1(1)*, 14.
30. Dupont, J.; Fonseca, G. S.; Umpierre, A. P.; Fichtner, P. F. P.; Teixeira, S. R. *J. Am. Chem. Soc.* **2002**, *124*, 4228.
31. Hirai, H.; Chawanya, H.; Toshima, N. *Nip. Kag. Kai.* **1984**, *6*, 1027.
32. Roucoux, A.; Schulz, J.; Patin, H. *Chem. Rev.* **2002**, *102*, 3757.

33. Freund, P. L.; Spiro, M. *J. Phys. Chem.* **1985**, *89*, 1074.
34. Freund, P. L.; Spiro, M. *J. Chem. Soc., Faraday Trans.* **1986**, *82*, 2277.
35. Clint, J. H.; Collins, I. R.; Williams, J. A.; Robinson, B. H.; Towey, T. F.; Cajean, P.; Khan-Lodhi, A. *Faraday Discuss.* **1993**, *95*, 219.
36. Li, Y.; Petroski, J.; El-Sayed, M. A. *J. Phys. Chem. B* **2000**, *104*, 10956.
37. Li, Y.; Hong, X. M.; Collard, D. M.; El-Sayed, M. A. *Org. Lett.* **2000**, *2(15)*, 2385.
38. Li, Y.; Boone, E.; El-Sayed, M. A. *Langmuir* **2002**, *18*, 4921.
39. Teranishi, T.; Miyake, M. *Chem. Mater.* **1998**, *10*, 594.
40. Ong, C. G.; Leckie, J. O. *Adsorpt. Met. Geo.*, **1998**, 317.
41. Baggio, S.; Pardo, M. I.; Baggio, R.; Garland, M. T. *Acta Crystallogr., Sect. C: Cryst. Struct. Commun.* **1997**, *C53(6)*, 727.
42. Rizov, I.; Ilcheva, L. *Analyst* **1995**, *120(6)*, 1651.
43. Aruga, R. *Inorg. Chem.* **1978**, *17(9)*, 2503.
44. Cusomano, M.; Giannetto, A.; Cavasino, P. F.; Sbriziolo, C. *Inorg. Chim. Acta* **1992**, *201(1)*, 49.
45. Itabashi, E. *Chem. Lett.* **1978**, *2*, 211.
46. Foye, W. O., Hu, J. *J. Pharm. Sci.* **1979**, *68(2)*, 202.
47. Foye, W. O.; Kaewchansilp, V. **1979**, *68(9)*, 1131.
48. Sillen, L. S.; Martell, A. E., "Stability Constants of Metal-Ion Complexes", Metcalfe & Cooper Limited, England, 1964.
49. Duh, B. *Polym.* **2002**, *43*, 3147.
50. Mathew, D.; Nair, C. P. R.; Krishnan, K.; Ninan, K. N. *J. Polym. Sci. Part A-Polym. Chem.* **1999**, *37(8)*, 1103.
51. Catherine, K. B.; Krishnan, K.; Ninan, K. N. *J. of Therm. Anal. Calorim.* **2000**, *59(1-2)*, 93.
52. Chu, F.; McKenna, T.; Lu, S. *Eur. Polym. J.* **1997**, *33(6)*, 837.

53. Mayr, A. E.; Cook, W. D.; Edward, G. H.; Murray, G. J. *Polym. Int.* **2000**, *49*(3), 293.
54. Nair, C. P. R.; Gopalakrishnan, C.; Ninan, K. N. *Polym. Polym. Compos.* **2001**, *9*(8), 531.
55. Lin, R. H.; Hong, J. L.; Su, A. C. *Polym.* **1995**, *36*(17), 3349.

CHAPTER 4

EFFECT OF NANOCATALYSIS IN COLLOIDAL SOLUTION ON THE TETRAHEDRAL AND CUBIC NANOPARTICLE SHAPE: ELECTRON TRANSFER REACTION CATALYZED BY PLATINUM NANOPARTICLES

4.1 Abstract

The stability of tetrahedral and cubic platinum nanoparticles during the catalysis of the electron transfer reaction between hexacyanoferrate (III) and thiosulfate ions in colloidal solution at room temperature was studied by using TEM and HRTEM. Before the reaction, the dominantly tetrahedral nanoparticles have a shape distribution of $55 \pm 4\%$ regular tetrahedral, $22 \pm 2\%$ distorted tetrahedral, and $23 \pm 2\%$ spherical nanoparticles, and the dominantly cubic nanoparticles have an initial shape distribution of $56 \pm 4\%$ regular cubes, $13 \pm 1\%$ distorted cubes, and $31 \pm 3\%$ truncated octahedral nanoparticles. The amount of tetrahedral nanoparticles decreases by $60 \pm 5\%$ after the first cycle and by $62 \pm 4\%$ after the second cycle of the reaction. In the case of cubic nanoparticles, the amount of cubic nanoparticles decreases by $39 \pm 5\%$ after the first cycle and by $66 \pm 5\%$ after the second cycle compared to before the reaction. After the first and second cycles of the reaction, there are a greater percentage of distorted tetrahedral and distorted cubic nanoparticles present. The rate of the dissolution of the surface Pt atoms is faster for the tetrahedral nanoparticles than for the cubic nanoparticles. This suggests that tetrahedral nanoparticles, with their sharp corners and edges, are more sensitive and more liable to shape changes during nanocatalysis. The presence of just hexacyanoferrate ions in the solution with the nanoparticles is found to

increase the amount of distorted tetrahedral and distorted cubes present much more than during the reaction. The presence of only the thiosulfate ions does not seem to affect the size or shape distribution which might result from the capping ability of this anion and thus protects the nanoparticles.

4.2 Introduction

Nanoparticles offer higher catalytic efficiency per gram than larger size materials due to their large surface-to-volume ratio. This makes them an attractive choice to use as catalysts. The nanocatalysis field has been very active with numerous review articles in both heterogeneous catalysis with supported nanoparticles²⁻¹⁴ and in homogeneous catalysis with colloidal nanoparticles¹⁵⁻²¹. However, being small in size is expected to increase the nanoparticle surface tension, which makes their surface atoms very active. This raises the question of whether the surface atoms are sufficiently unstable to result in an observable change in the size and shape of the nanoparticles during catalysis. TEM characterization of the nanoparticles before and after catalysis is not given in the bulk of catalysis conducted with nanoparticles in colloidal solution. It is also worth noting that there has not been any characterization of the nanoparticle shape before and after catalysis. However, there are few studies in the literature where size distribution of the nanoparticles after recycling along with the catalytic activity is reported²²⁻²⁶. There are also some papers that discuss the catalytic activity of the nanoparticles upon recycling, but which do not examine the stability of the nanoparticles after catalysis²⁷⁻³⁰. The major interest of the reusability of nanoparticle catalysts has not been systematically studied or published in the metal colloid literature³¹.

Previously, we have conducted detailed studies on the effect of catalysis on the *size* distribution of Pd and Pt nanoparticles catalyzing the Suzuki³² and electron transfer reaction³³. In a previous study³² conducted with spherical PVP-Pd nanoparticles catalyzing the Suzuki reaction between phenylboronic acid and iodobenzene, it was found that after the first cycle of the reaction, the nanoparticles increased in size, and this was attributed to the presence of free metal atoms in solution and also to Ostwald ripening processes. After the second cycle of the reaction, the nanoparticle size decreases and this was attributed to the aggregation and precipitation of the larger nanoparticles. It was also found that the nanoparticle size increases in the presence of iodobenzene, but their size was not affected in the presence of phenylboronic acid. From this observation, it was proposed that the surface catalytic mechanism involved phenylboronic acid binding to the nanoparticle surface followed by the reaction with iodobenzene in solution via collisional processes.

In the study of the electron transfer reaction between hexacyanoferrate (III) ions and thiosulfate ions catalyzed by spherical PVP-Pt nanoparticles, it was found³³ that the nanoparticles decrease slightly in size after the first and second cycle of the reaction. The nanoparticles greatly decrease in size in the presence of hexacyanoferrate (III) ions alone but maintain their size in the presence of thiosulfate ions. This is proposed to be due to the reaction between hexacyanoferrate (III) ions and the surface Pt atoms of the nanoparticle resulting in dissolving them to form cyanide complexes. Also, the mechanism of surface catalysis is proposed to involve thiosulfate ions binding to the nanoparticle surface followed by the reaction with hexacyanoferrate (III) ions via collisional processes.

The previous studies³²⁻³³ involved the use of spherical nanoparticles and as a result has focused on what happens to the size distribution of the nanoparticles after catalysis. Another important study is to examine shape changes of the nanoparticles after catalysis. Tetrahedral nanoparticles are the best to use for two reasons. They have (111) facets which are known to be the most catalytically active³⁴⁻³⁶ and thus suggests that they are the most sensitive to shape changes. They also have sharp corners and edges with least surface energy that would easily be reconstructed under chemical perturbations. This would lead to large shape changes that could be detected by TEM. In addition, for comparison, cubic nanoparticles with their (100) facets was also investigated. Since the (100) facets are not as catalytically active and their edges and corners are not as sharply pointed as in the tetrahedral particles, they probably will not be as sensitive to shape changes as the tetrahedral particles.

The aim in this work is to examine and compare the shape stability of tetrahedral and cubic platinum nanoparticles used to catalyze the electron transfer reaction between hexacyanoferrate (III) ions and thiosulfate ions to form hexacyanoferrate (II) ions and tetrathionate ions. The effect of catalysis, recycling, and presence of the individual reactants on the *shape* distribution of these different nanoparticles is examined by using TEM and HRTEM.

4.3 Experimental Section

4.3.1 Synthesis of Tetrahedral Shaped Platinum Nanoparticles

The PVP stabilized Pt nanoparticles were prepared using the H₂ reduction method described previously³⁷ with some modifications. The precursor platinum salt used is K₂PtCl₆ and the stabilizer used is PVP (mw = 360,000). A 500 mL 3-neck flask equipped with a gas trap was used for the synthesis. Two hundred fifty mL of doubly deionized water, 2 mL of 0.01 M K₂PtCl₆, and 0.25 g of PVP was added to the flask. After the solution is thoroughly mixed, argon is bubbled for 20 minutes and then hydrogen gas is bubbled for 5 minutes. The flask is then sealed, wrapped in aluminum foil, and stored in the dark for 24 hours. The resulting colloidal solution is light brown. A drop of the colloidal solution was placed onto a Formvar stabilized carbon grid and allowed to evaporate in air. JEOL 100C TEM and JEM 4000EX HRTEM are used to characterize the nanoparticle shape.

4.3.2 Synthesis of Cubic Shaped Platinum Nanoparticles

The polyacrylate stabilized Pt nanoparticles were prepared using the H₂ reduction method described previously³⁷ with a few modifications. The precursor platinum salt used is K₂PtCl₄ and the stabilizer used is polyacrylate (mw = 2,100). A 500 mL 3-neck flask equipped with a gas trap was used for the synthesis and this flask was thoroughly cleaned with Aqua Regia before the synthesis. Two hundred fifty mL of doubly deionized water, 2 mL of 0.01 M K₂PtCl₄, and 1 mL of 0.1 M polyacrylate were added to the flask. The solution was adjusted to a pH of 9. After the solution is thoroughly mixed,

argon is bubbled for 20 minutes and then hydrogen gas is bubbled for 5 minutes. The flask is then sealed, wrapped in aluminum foil, and stored in the dark for 24 hours. The resulting colloidal solution is light brown. A drop of the colloidal solution was placed onto a Formvar stabilized carbon grid and allowed to evaporate in air. JEOL 100C TEM and JEM 4000EX HRTEM are used to characterize the nanoparticle shape.

4.3.3 Studies of the Effect of the Catalytic Reaction

The electron transfer reaction between hexacyanoferrate (III) ions and thiosulfate ions was catalyzed in a similar manner described previously^{33,38}. PVP capped platinum nanoparticles with a dominantly tetrahedral shape and polyacrylate stabilized platinum nanoparticles with a dominantly cubic shape are both used as the catalysts for the reaction. Two mL of the platinum nanoparticles, 200 μ L of 0.01 M potassium hexacyanoferrate, and 200 μ L of 0.1 M sodium thiosulfate were mixed together for a total volume of 2.4 mL. The hexacyanoferrate (III) ions absorb at 420 nm and the progress of the reaction can be monitored by the disappearance of the hexacyanoferrate (III) peak over time. The complete disappearance of the hexacyanoferrate (III) peak is an indication that the first cycle of the reaction is complete. To begin the second cycle of the reaction, 2 μ L of 1 M potassium hexacyanoferrate and 2 μ L of 1 M sodium thiosulfate was added to the reaction mixture. The new total volume is 2.404 mL and as a result, there is very little difference in the concentration of the nanoparticles during the second cycle compared to the first cycle. As a result, it is possible to compare the stability of the nanoparticles before the first cycle, after the first cycle, and after the second cycle.

4.3.4 TEM Studies

The stability of the platinum nanoparticle shapes before and after the different conditions is assessed by using TEM. The nanoparticle samples were spotted by placing a drop of the solution onto a Formvar stabilized copper grid and allowing the drop to evaporate in air. The spotted aqueous samples take approximately 2 hours to dry. Since the same deposition conditions are employed for all of the samples, the evaporation rate of the solvent is fairly reproducible from one sample to another. For each experiment, the internal reproducibility of the observed nanoparticle shape distribution was examined by spotting the sample onto three separate TEM grids. Also, TEM images were taken from different sections of the TEM grids to verify the shape distribution. The general reproducibility of the observed shape distribution was verified by conducting each of the experiments three times. As a result, it is possible to compare the shape distribution changes under the various conditions.

For each experiment, approximately 1800 nanoparticles were counted (9 enlarged TEM images with approximately 200 nanoparticles in each image). In the case of the dominantly tetrahedral PVP-Pt nanoparticles, the shapes that were counted are regular tetrahedral, distorted tetrahedral, and spherical nanoparticles. The goal is to see if there are changes in the distribution of the nanoparticle shape under the different conditions. In these experiments, the size distributions of the nanoparticles were not conducted since when there are distorted tetrahedral nanoparticles, the size depends on the type of the distortion. As a result, the shape distribution is used as a better indication of the stability of the nanoparticles after catalysis, recycling, or in the presence of the individual

chemicals used in the reaction. In the case of the dominantly cubic polyacrylate stabilized platinum nanoparticles, the shapes that were counted are regular cubes, distorted cubes, and truncated octahedral. Here also, the size distribution was not conducted since in the case of distorted cubic nanoparticles, the size of the particle would depend on the type of distortion.

In addition, HRTEM images were obtained for a typical tetrahedral and cubic nanoparticle before the reaction, after the second cycle, and after exposing the nanoparticles to just the hexacyanoferrate (III) ions. Images that have lattice fringes that can be clearly seen are obtained and are outlined for better visualization of the shape.

4.4 Results and Discussion

The stability of tetrahedral and cubic platinum nanoparticles under different conditions was investigated using TEM by examining the changes in the shape distribution of solutions containing dominantly tetrahedral and dominantly cubic nanoparticle shapes. Table 4.1 and 4.2 summarize the shape distribution of the dominantly tetrahedral and dominantly cubic nanoparticle solutions before the electron transfer reaction, after the first cycle of the electron transfer reaction, after the second cycle of the electron transfer reaction, after exposure to just the hexacyanoferrate (III) ions, and after exposure to just the thiosulfate ions.

Table 4.1—Shape Distributions of Dominantly Tetrahedral PVP-Platinum Nanoparticles (Regular Tetrahedral, Distorted Tetrahedral, and Spherical) for Various Perturbations

Condition	Number of Nanoparticles Counted	# and % of Regular Tetrahedral NPs	# and % of Distorted Tetrahedral NPs	# and % of Spherical NPs
Before Electron Transfer Reaction	1735	953 ± 68 55 ± 4%	382 ± 37 22 ± 2%	401 ± 34 23 ± 2%
After First Cycle of Electron Transfer Reaction	1765	387 ± 33 22 ± 2%	919 ± 38 52 ± 2%	460 ± 32 26 ± 2%
After Second Cycle of Electron Transfer Reaction	1842	385 ± 55 21 ± 3%	1048 ± 74 57 ± 4%	405 ± 19 22 ± 1%
After Just Thiosulfate Ions	1816	869 ± 34 48 ± 2%	472 ± 38 26 ± 2%	470 ± 35 26 ± 2%
After Just Hexacyanoferrate Ions	1782	284 ± 36 16 ± 2%	1103 ± 72 62 ± 4%	373 ± 34 21 ± 2%

Table 4.2—Shape Distribution of Dominantly Cubic Polyacrylate-Platinum Nanoparticles (Regular Cubes, Distorted Cubes, and Truncated Octahedral) for Various Perturbations

Condition	Number of Nanoparticles Counted	# and % of Regular Cubic NPs	# and % of Distorted Cubic NPs	# and % of Truncated Octahedral NPs
Before Electron Transfer Reaction	1786	1002 \pm 73 56 \pm 4	231 \pm 19 13 \pm 1	554 \pm 51 31 \pm 3
After First Cycle of Electron Transfer Reaction	1802	614 \pm 34 34 \pm 2	722 \pm 56 40 \pm 3	469 \pm 37 26 \pm 2
After Second Cycle of Electron Transfer Reaction	1769	337 \pm 54 19 \pm 3	901 \pm 91 51 \pm 5	533 \pm 36 30 \pm 2
After Just Thiosulfate Ions	1794	1057 \pm 52 59 \pm 3	267 \pm 37 15 \pm 2	465 \pm 19 26 \pm 1
After Just Hexacyanoferrate Ions	1809	381 \pm 53 21 \pm 3	939 \pm 73 52 \pm 4	508 \pm 56 28 \pm 3

Figure 4.1a-f and Figure 4.2a-f show typical TEM images and shape distribution graphs of the tetrahedral shaped and cubic shaped platinum nanoparticles before the reaction, after the first cycle of the reaction, and after the second cycle of the reaction. Table 4.1 and 4.2 also summarizes the shape distributions observed for these solutions. In the case of the dominantly tetrahedral nanoparticle solutions, as shown in Figure 4.1a-b and Table 4.1, it can be seen that before the reaction, the regular tetrahedral nanoparticles are dominant (55 \pm 4%). There are also some distorted tetrahedral

nanoparticles ($22 \pm 2\%$) and spherical nanoparticles ($23 \pm 2\%$) present. For the dominantly cubic nanoparticle solutions, as shown in Figure 4.2a-b and Table 4.2, it can be seen that the cubic nanoparticles are dominant ($56 \pm 4\%$) with some distorted cubic nanoparticles ($13 \pm 1\%$) and truncated octahedral nanoparticles ($31 \pm 3\%$) also being present.

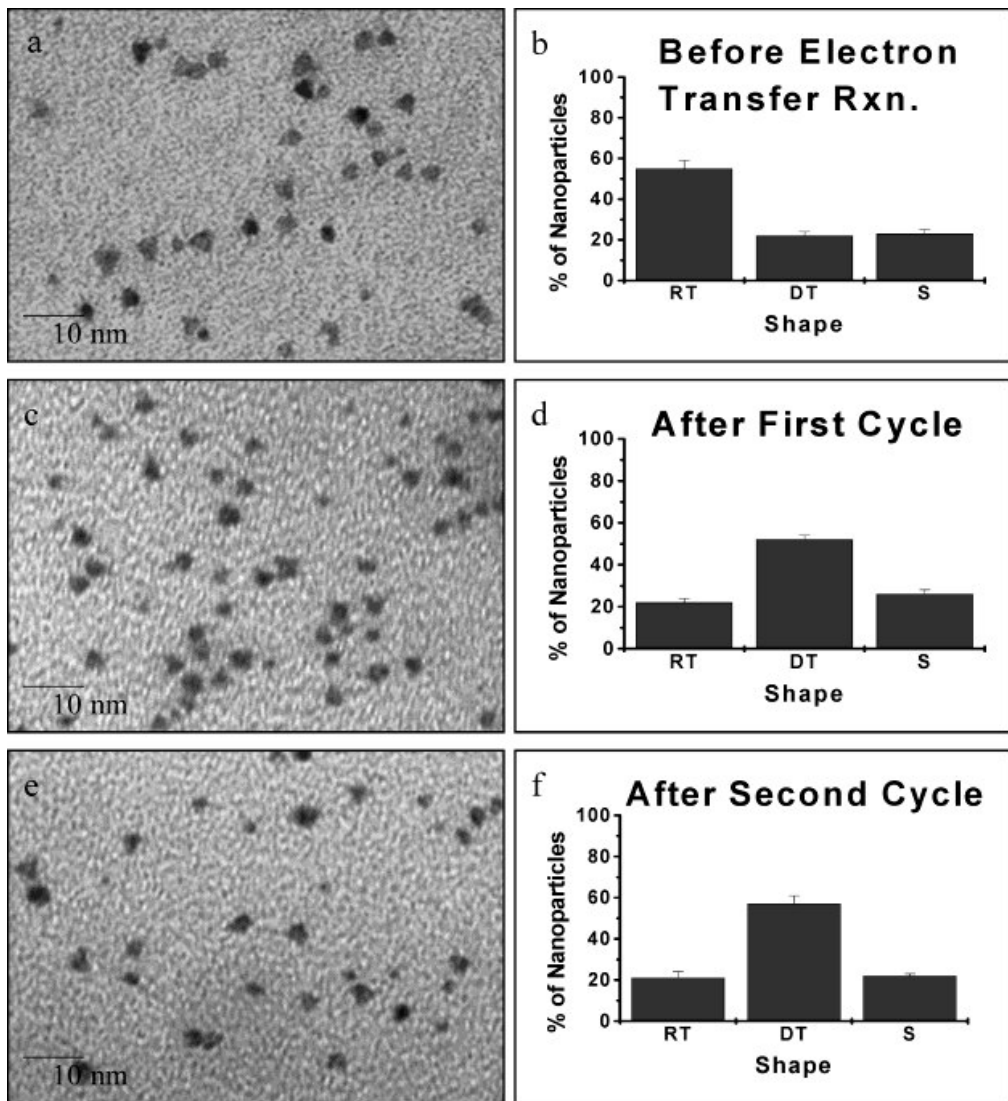


Figure 4.1—Typical TEM image and shape distribution graph of solutions containing dominantly tetrahedral PVP-Pt nanoparticles before electron transfer reaction (a-b), after first cycle of electron-transfer reaction (c-d), and after second cycle of electron-transfer reaction (e-f) [RT = regular tetrahedral, DT = distorted tetrahedral, and S = spherical].

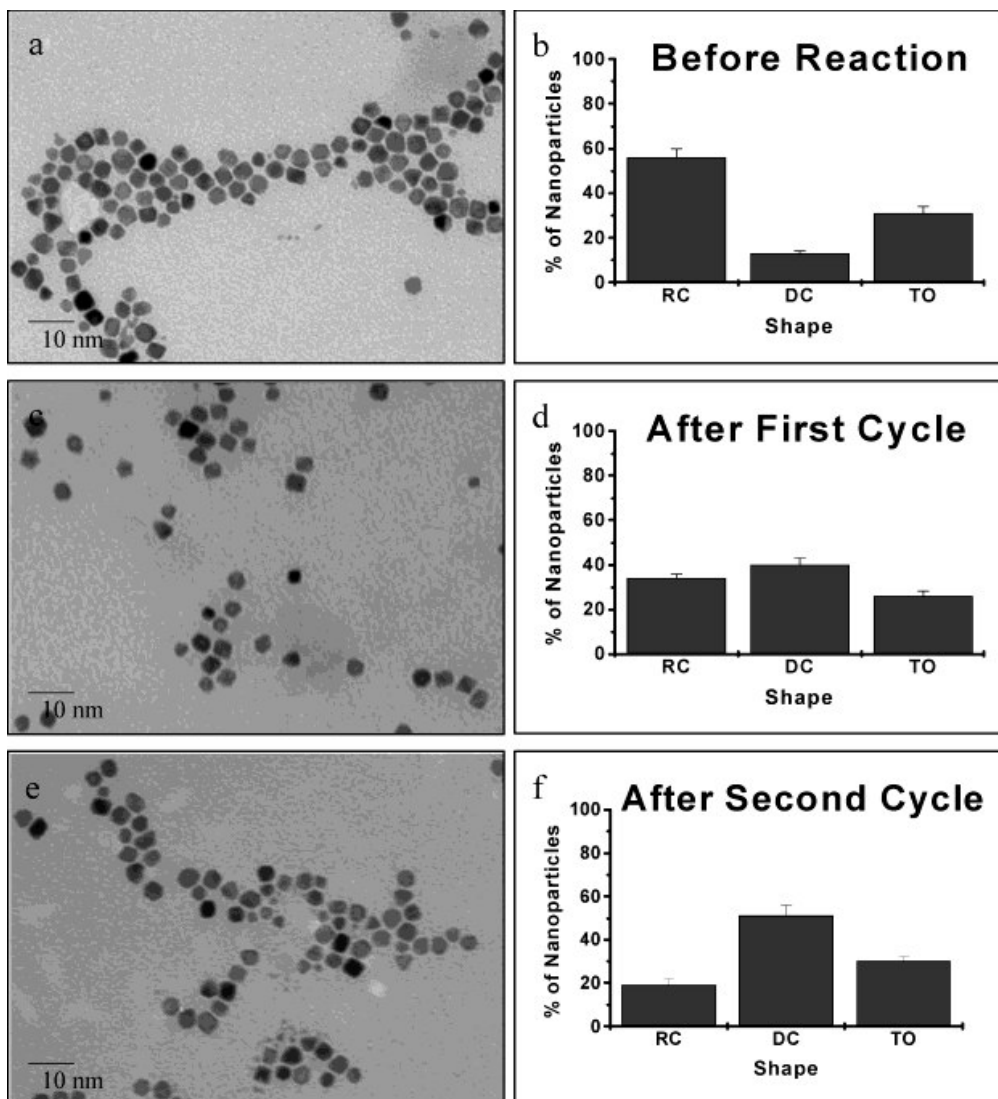


Figure 4.2—Typical TEM image and shape distribution of colloidal solutions with dominantly cubic polyacrylate stabilized platinum nanoparticles before the electron-transfer reaction (a-b), after the first cycle of electron-transfer reaction (c-d), and after the second cycle of electron-transfer reaction (e-f) [RC = regular cubes, DC = distorted cubes, and TO = truncated octahedral].

After the first cycle of the electron transfer reaction, it is observed that the percentage of regular tetrahedral nanoparticles decreases from $55 \pm 4\%$ to $22 \pm 2\%$ while the percentage of distorted tetrahedral nanoparticles increases from $22 \pm 2\%$ to $52 \pm 2\%$ (as shown in Figure 4.1c-d and Table 4.1). It can be seen that there is a greater percentage of distorted tetrahedral nanoparticles present after the first cycle of the

electron transfer reaction and that the distorted tetrahedral nanoparticles become dominant.

In the case of cubic nanoparticles, the percentage of regular cubic nanoparticles decrease from $56 \pm 4\%$ to $34 \pm 2\%$ while the percentage of distorted cubic nanoparticles increases from $13 \pm 1\%$ to $40 \pm 3\%$ (see Figure 4.2c-d and Table 4.2). It can be seen that there is a greater percentage of distorted cubic nanoparticles present after the first cycle, but they do not become the dominant shape. The observations of a greater percentage of distorted tetrahedral and cubic nanoparticles could be due to the dissolution of Pt atoms on the corners and edges of the nanoparticles by reaction with the hexacyanoferrate (III) ions. The greater percentage of distorted tetrahedral than distorted cubic nanoparticles could be due to the fact that the tetrahedral nanoparticles have sharper edges and corners that would dissolve more rapidly giving rise to the distorted tetrahedral shape. This suggests that the cubic nanoparticles with their less pointed edges are less sensitive to changes in the shape from perturbations in the reaction environment than the tetrahedral nanoparticles. As a result, dissolving the corners and edges of the cubes occur at a lower rate than for the tetrahedral nanoparticles with their (111) facets and sharper edges and corners.

After the second cycle of the reaction, it is observed that there is virtually no change in the amount of tetrahedral nanoparticles since the percentage changes from $22 \pm 2\%$ after the first cycle to $21 \pm 3\%$ after the second cycle (see Figure 4.1e-f and Table 4.1). Also, there is very little increase in the amount of distorted tetrahedral nanoparticles present since the percentage changes from $52 \pm 2\%$ after the first cycle to $57 \pm 4\%$ after the second cycle. In contrast, the relative amount of cubic nanoparticles

continues to decrease from $34 \pm 2\%$ after the first cycle to $19 \pm 3\%$ after the second cycle (see Figure 4.2e-f and Table 4.2). Meanwhile, the amount of distorted cubic nanoparticles increases from $40 \pm 3\%$ after the first cycle to $51 \pm 5\%$ after the second cycle. It can be seen that the cubic nanoparticles become more distorted after the second cycle of the reaction. This again suggests that due to the lower sensitivity of the cubic shaped nanoparticles, a longer time of exposure to the environmental perturbations is needed to induce changes in the shape. It can be seen that the distorted cubic nanoparticles are dominant only after the second cycle, while the distorted tetrahedral nanoparticles were dominant even after the first cycle of the reaction. This confirms that the rate of dissolution of the surface Pt atoms is slower for the cubic shaped nanoparticles than for the tetrahedral shaped nanoparticles.

HRTEM images of the tetrahedral and cubic shaped nanoparticles were also obtained before and after the second cycle and are shown in Figure 4.3a-d. In each image, the nanocrystal is outlined for better visualization of the shape. The lattice fringes can be clearly seen. Figure 4.3 shows an example of a high-resolution TEM image of a tetrahedral nanoparticle before the reaction (Figure 4.3a) and after the second cycle (Figure 4.3b). The same is shown for the cubic nanoparticle before the reaction (Figure 4.3c) and after the second cycle (Figure 4.3d). It can be seen that the tetrahedral nanoparticle has become more distorted, the sides are more rounded, and also the nanoparticles are smaller in size after the second cycle of the reaction. From the shape distribution data, it was also found that there are a greater percentage of distorted tetrahedral nanoparticles present after the second cycle of the reaction. In the case of the cubic nanoparticles, distortion in the corners of the nanoparticle can be observed. The

shape distribution data shows that there are a greater percentage of distorted cubic nanoparticles present after the second cycle of the reaction. The rounding of the edges and corners of the tetrahedral and cubic nanoparticles is due to the dissolution of atoms by the hexacyanoferrate (III) ions. In both cases, it can be seen that the dissolution of atoms results in a reduction in the size of the nanoparticle.

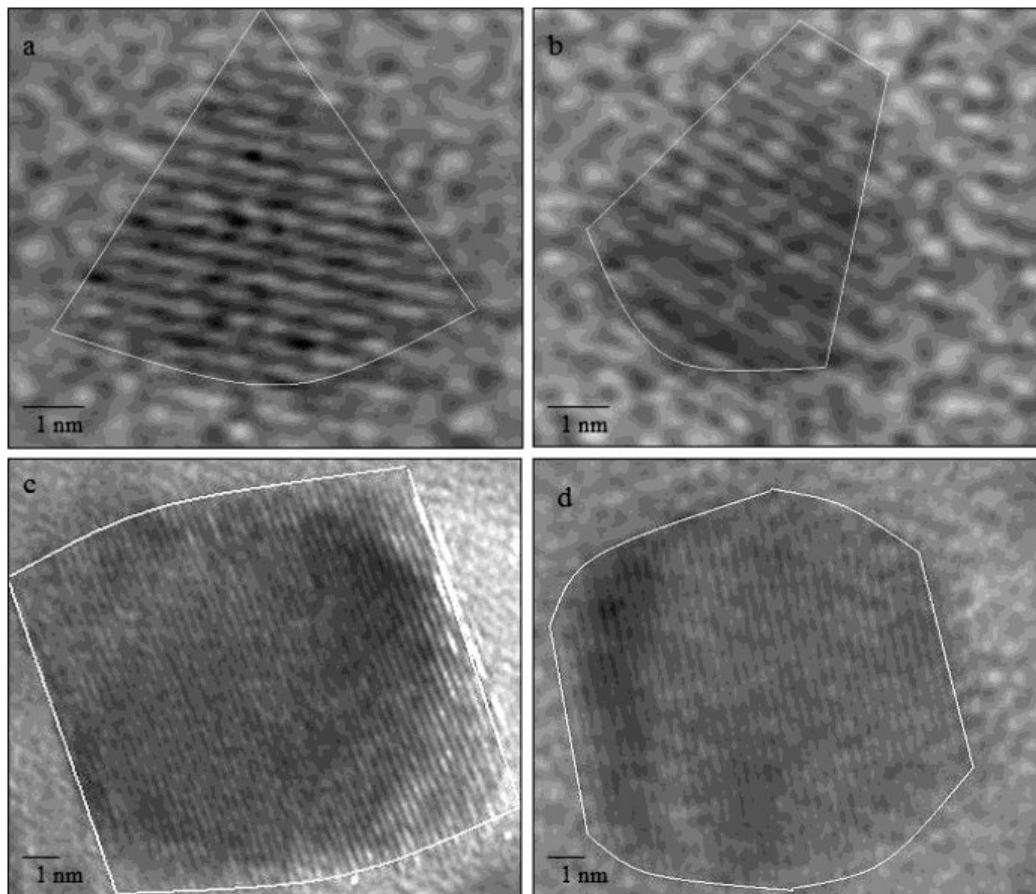


Figure 4.3—Example of a HRTEM image of a tetrahedral PVP-Pt nanoparticle before electron-transfer reaction (a), after second cycle of electron-transfer reaction (b), cubic polyacrylate capped Pt nanoparticle before electron-transfer reaction (c), and after second cycle of electron-transfer reaction (d).

4.4.1 Effect of Individual Reactants on the Nanoparticle Shape and the Nanocatalysis Mechanism

The effect of the individual reactants on the stability of the tetrahedral and cubic shapes was also investigated. Figure 4.4a-f and Figure 4.5a-f show TEM images and shape distribution graphs of the tetrahedral and cubic nanoparticles before any perturbations, after exposure to just hexacyanoferrate (III) ions and after exposure to just thiosulfate ions. Table 4.1 and 4.2 summarize the shape distribution results for the different conditions. The shape distribution of the tetrahedral and cubic nanoparticles before any perturbations are shown in Figure 4.4a-b and Figure 4.5a-b and also summarized in Table 4.1 and 4.2.

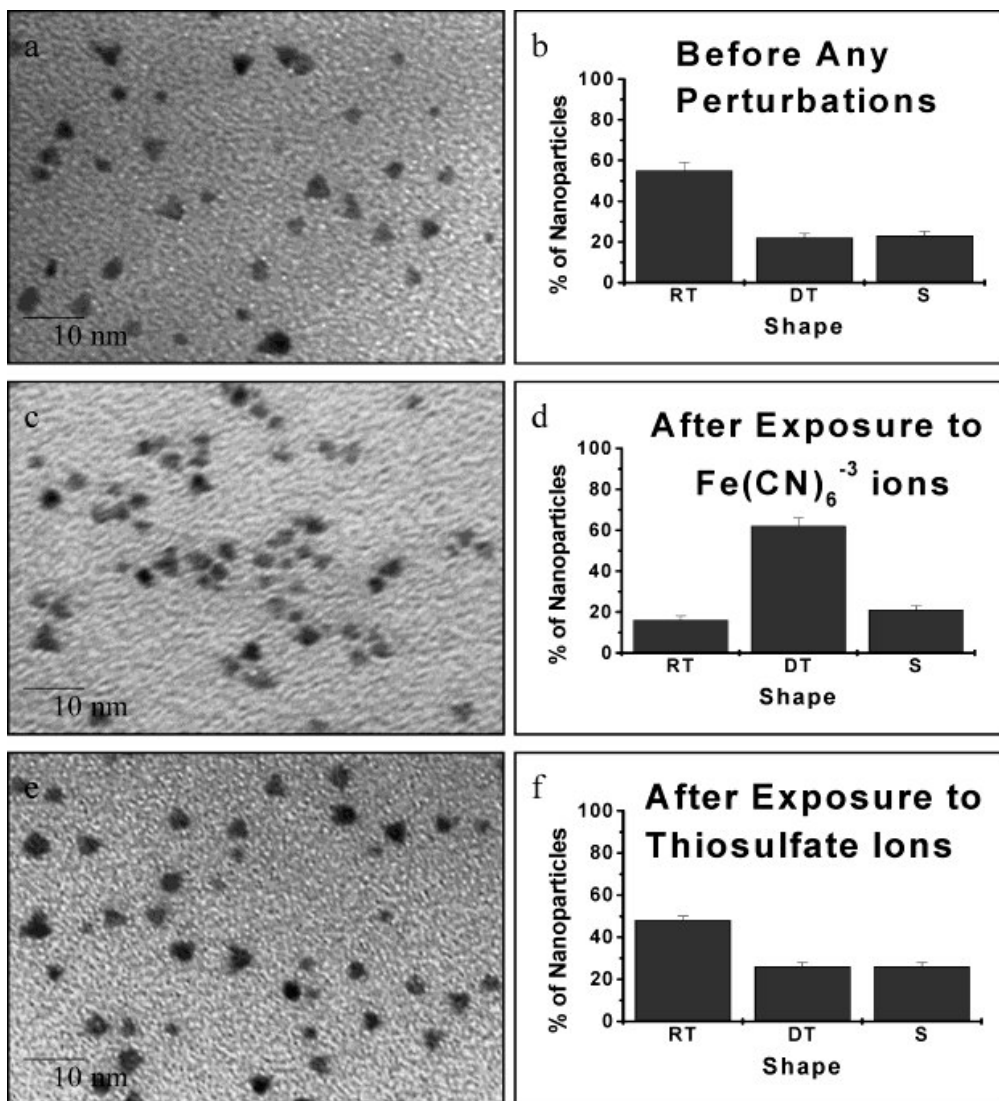


Figure 4.4—Typical TEM image and shape distribution of solutions with dominantly tetrahedral PVP-Pt nanoparticles before any perturbations (a-b), after exposure to hexacyanoferrate (III) ions for 2 days (c-d), and after exposure to thiosulfate ions for 2 days (e-f) [RT = regular tetrahedral, DT = distorted tetrahedral, and S = spherical].

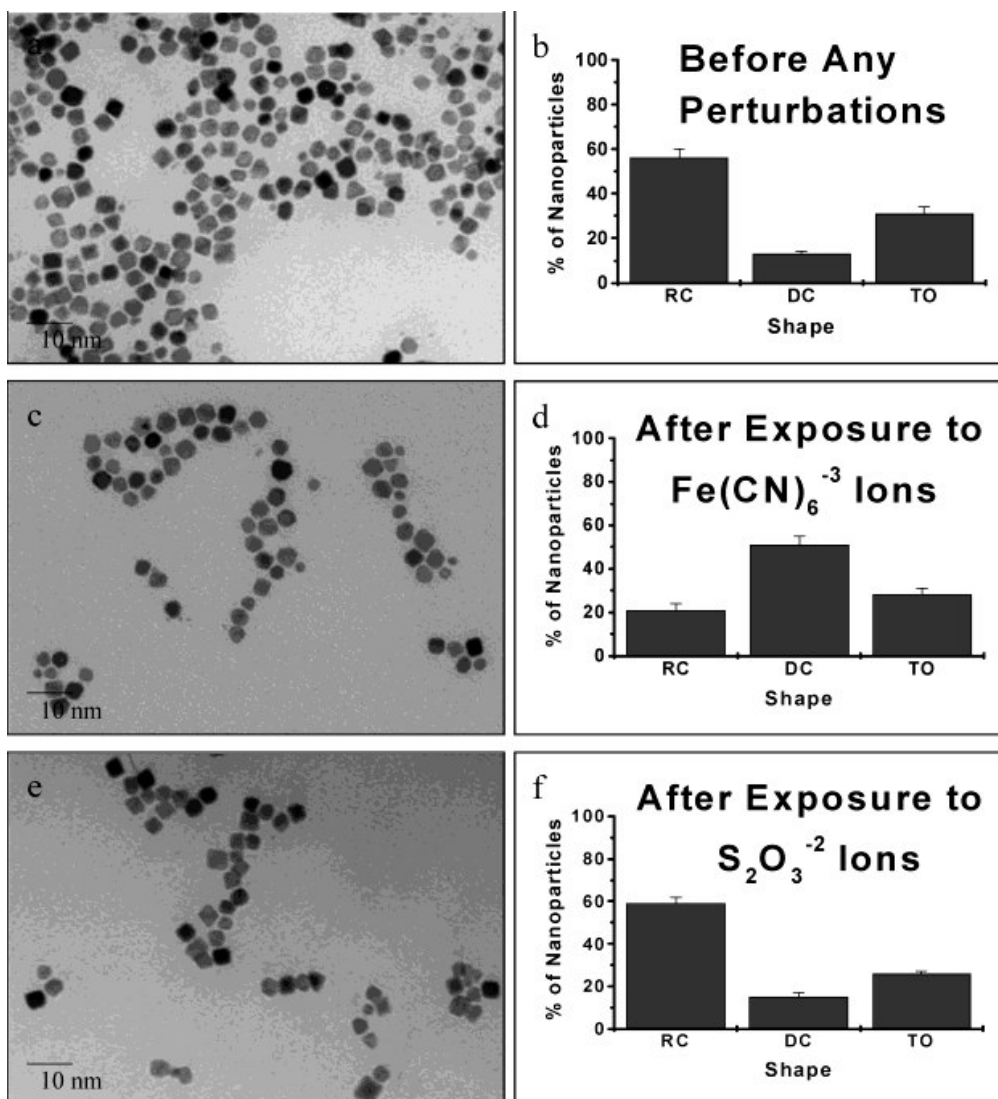


Figure 4.5—Typical TEM image and shape distribution of solutions with dominantly cubic polyacrylate capped platinum nanoparticles before any perturbations (a-b), after exposure to hexacyanoferrate (III) ions for 2 days (c-d), and after exposure to thiosulfate ions for 2 days (e-f) [RC =regular cubes, DC = distorted cubes, and TO = truncated octahedral].

In the case of the tetrahedral nanoparticles, Figure 4.4c-d and Table 4.1 show that the percentage of distorted tetrahedral nanoparticles changes from $22 \pm 2\%$ to $62 \pm 4\%$ after exposure to just hexacyanoferrate (III) ions. When cubic nanoparticles are used, Figure 4.5c-d and Table 4.2 show that the percentage of distorted cubic nanoparticles changes from $13 \pm 1\%$ to $52 \pm 4\%$ after being exposed to the hexacyanoferrate (III) ions.

It can be seen that there is a large percentage of distorted tetrahedral and distorted cubic nanoparticles present after exposure to hexacyanoferrate (III) ions for two days (same time period used for conducting the reaction). This observation confirms our previously suggested conclusion³³ on its effect on the size distribution of spherical particles in which the presence of hexacyanoferrate (III) ions dissolves some of the Pt atoms on the surface of the PVP-Pt nanoparticles. The distortions in the tetrahedral shape observed here with the tetrahedral PVP-Pt nanoparticles are probably due to more rapid dissolution of the reactive atoms on the corners and edges of the tetrahedral particles leading to their shape distortion. In the case of the cubic nanoparticles, there is dominant distorted cubic nanoparticles present, which is probably also due to the dissolution of surface Pt atoms on corners or on edges. As a result, even though the (100) facets are less sensitive to perturbations, the rate of the dissolution of the Pt atoms on the corners or the edges of the cubic nanoparticles is probably faster than that on the facets.

Figure 4.6a-b show HRTEM images of a distorted tetrahedral nanoparticle and distorted cubic nanoparticle observed after exposing the nanoparticles to just hexacyanoferrate (III) ions for two days. The lattice fringes can be seen and the nanoparticle is outlined for better visualization. It can be seen that the tetrahedral nanoparticle has become more rounded and is smaller in size. The distortions in the corners of the cubic nanoparticle are observed suggesting the dissolution of Pt atoms from these sites.

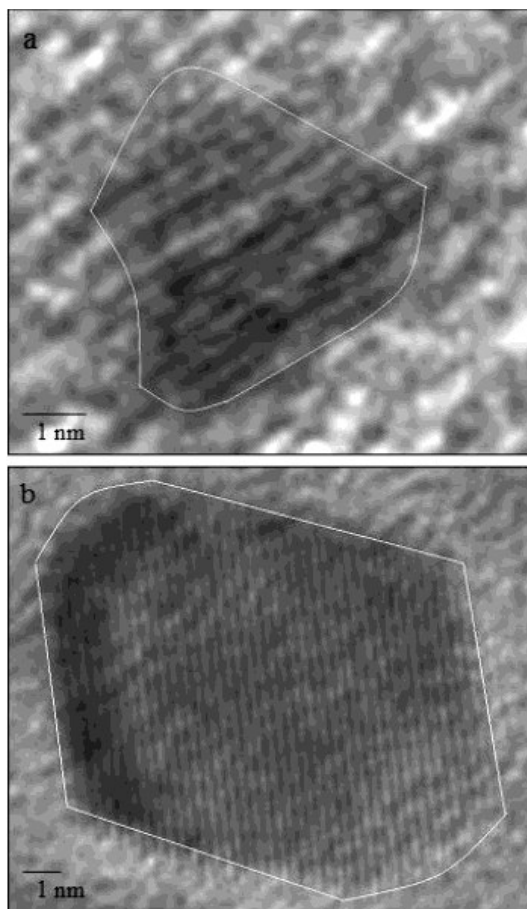


Figure 4.6—Example of a HRTEM image of a tetrahedral PVP-Pt nanoparticle after exposure to hexacyanoferrate (III) ions (a) and dominantly cubic polyacrylate capped platinum nanoparticle after exposure to hexacyanoferrate (III) ions (b).

The thiosulfate ions seem to stabilize the surface of the nanoparticles. As shown in Figure 4.4e-f and Table 4.1, it can be seen that the percentage of distorted tetrahedral nanoparticles changes from $22 \pm 2\%$ to $26 \pm 2\%$ in the presence of the thiosulfate ions alone, suggesting very little change in the distribution. The distribution remains similar to that observed before any perturbations. As shown in Figure 4.5e-f and Table 4.2, the percentage of distorted cubic nanoparticles changes from $13 \pm 1\%$ to $15 \pm 2\%$ which is also very little change in the distribution compared to before any perturbations. The results obtained using tetrahedral and cubic nanoparticles show that the presence of

thiosulfate ions does not change the shape distribution of the nanoparticles. The observations found in both the tetrahedral and cubic shaped nanoparticles is consistent with what is well known in the literature³⁹⁻⁴⁶ that thiosulfate binds to metal surfaces such as silver, cadmium, palladium, nickel, aluminum, zinc, platinum, etc. through its sulfur group. Thus, thiosulfate acts as a capping agent or stabilizer of the nanoparticle surface.

From the above results, it can be concluded that hexacyanoferrate (III) ions change the shape distribution of both the tetrahedral and cubic nanoparticles while thiosulfate ions do not. The presence of hexacyanoferrate (III) ions during the electron transfer reaction results in the Pt ions dissolving into the reaction mixture and possibly forming a complex. The stability constants for $\text{Fe}(\text{CN})_6^{-3}$ and $\text{Pt}(\text{CN})_4^{-2}$ are 10^{31} mole/L and 10^{41} mole/L respectively⁴⁷. The stability constant for the $\text{Pt}(\text{CN})_6^{-4}$ complex has not been reported in the literature. It can be seen that the stability constant for the platinum complex is 10 orders of magnitude higher than that for the iron complex. As a result, it is thermodynamically possible that the cyanide groups in hexacyanoferrate (III) ions would bind and dissolve the surface Pt atoms to form the much more stable platinum complex. Absorption spectra were obtained before and after exposing the PVP-Pt nanoparticles to hexacyanoferrate (III) ions for two days. No changes in the absorption spectra were observed. In the previous study conducted with spherical PVP-Pt nanoparticles³³, it was shown that the amount of hexacyanoferrate (III) ions used up to form the complex is so small that it couldn't be detected optically. In the cases with the tetrahedral and cubic shaped nanoparticles, it is also logical to propose that the amount of the hexacyanoferrate (III) ions lost is so small that it can't be detected. A calculation of the amount of hexacyanoferrate (III) ions that are lost would be difficult to carry out in both cases since

there is a change in the shape from tetrahedral nanoparticles to distorted tetrahedral nanoparticles and from cubic nanoparticles to distorted cubic nanoparticles. The calculation of the volume of a distorted tetrahedral or cubic nanoparticle would be difficult to do especially since the distortions are different for each nanoparticle.

Hexacyanoferrate (III) ions added alone are found to change the tetrahedral and the cubic shapes much more effectively than in the reaction mixture. This observation supports the proposal that the thiosulfate is adsorbed on the nanoparticle and is giving it more protection from the direct hexacyanoferrate attack on the surface platinum atoms. The thiosulfate protects the particle surface by capping it as well as by reacting with the hexacyanoferrate (III) ions approaching the surface. The catalytic mechanism must thus involve the reaction of hexacyanoferrate (III) ions in solution with the adsorbed thiosulfate species.

4.5 Conclusions

During catalysis, a change in the shape distribution in colloidal solutions with dominantly tetrahedral or cubic nanoparticles occurs with the change occurring faster for the tetrahedral particles. This suggests that tetrahedral nanoparticles, with sharper corners and edges, are more sensitive and more liable to shape changes during nanocatalysis than the cubic particles. Exposure to hexacyanoferrate (III) ions alone results in a larger percentage of distorted tetrahedral and distorted cubic nanoparticles than in the reaction mixture. Exposure to the other reactant, thiosulfate ions, is believed to cap and protect the nanoparticles against dissolving their surface platinum atoms on the corners and edges by the hexacyanoferrate (III) ions.

4.6 References

1. Eppler, A.; Rupprechter, G.; Guzzi, L.; Somorjai, G. A. *J. Phys. Chem. B* **1997**, *101*(48), 9973.
2. Toshima, N.; Yonezawa, T. *New J. Chem.* **1998**, *22*(11), 1179.
3. Schmid, G. *Met. Clus. Chem.* **1999**, *3*, 1325.
4. Puddephatt, R. J. *Met. Clus. Chem.* **1999**, *2*, 605.
5. Henry, C. R. *Appl. Surf. Sci.* **2000**, *164*, 252.
6. St. Clair, T. P.; Goodman, D. W. *Top. Catal.* **2000**, *13*(1,2), 5.
7. Kralik, M.; Corain, B.; Zecca, M. *Chem. Pap.* **2000**, *54*(4), 254.
8. Chusuei, C. C.; Lai, X.; Luo, K.; Goodman, D. W. *Top. Catal.* **2001**, *14*(1-4), 71.
9. Bowker, M.; Bennett, R. A.; Dickinson, A.; James, D.; Smith, R. D.; Stone, P. *Stud. Surf. Sci. Catal.* **2001**, *133*, 3.
10. Kralik, M.; Biffis, A. *J. Mol. Catal. A: Chem.* **2001**, *177*(1), 113.
11. Thomas, J. M.; Raja, R. *Chem. Rec.* **2001**, *1*(6), 448.
12. Mohr, C.; Claus, P. *Sci. Prog.* **2001**, *84*(4), 311.
13. Thomas, J. M.; Johnson, B. F. G.; Raja, R.; Sankar, G.; Midgley, P. A. *Acc. Chem. Res.* **2003**, *36*(1), 20.
14. Bradley, J. S. *Clus. Colloids* **1994**, 459.
15. Duff, D. G.; Baiker, A. *Stud. Surf. Sci. Catal.* **1995**, *91*, 505.
16. Toshima, N. *NATO ASI Ser., Ser. 3* **1996**, *12*, 371.
17. Boennermann, H.; Braun, G.; Brijoux, G. B.; Brinkman, R.; Tilling, A. S.; Schulze, S. K.; Siepen, K. *J. Organomet. Chem.* **1996**, *520*(1-2), 143.
18. Fugami, K. *Organomet. News* **2000**, *1*, 25.
19. Mayer, A. B. R. *Polym. Adv. Technol.* **2001**, *12*(1-2), 96.
20. Bonnemann, H.; Richards, R. *Syn. Meth. Organom. Inorg. Chem.* **2002**, *10*, 209.
21. Moiseev, I. I.; Vargaftik, M. N. *Russ. J. Chem.* **2002**, *72*(4), 512.

22. Collier, P. J.; Iggo, J. A.; Whyman, R. *J. Mol. Catal. A: Chem.* **1999**, *146*(1-2), 149.
23. Sculz, J.; Roucoux, A.; Patin, H. *Chem. Eur. J.* **2000**, *6*(4), 618.
24. Wang, Q.; Liu, H.; Han, M.; Li, X.; Jiang, D. *J. Mol. Catal. A: Chem.* **1997**, *118*(2), 145.
25. Kim, S.; Son, S. U.; Lee, S. S.; Hyeon, T.; Chung, Y. K.; *Chem. Commun.* **2001**, 2212.
26. Larpent, C.; Menn, B. F.; Patin, H. *J. Mol. Catal.* **1991**, *65*, L35.
27. Chechik, V.; Crooks, R. M. *J. Am. Chem. Soc.* **2000**, *122*, 1243.
28. Yeung, L. K.; Crooks, R. M. *Nano Lett.* **2001**, *1*(1), 14.
29. Dupont, J.; Fonseca, G. S.; Umpierre, A. P.; Fichtner, P. F. P.; Teixeira, S. R. *J. Am. Chem. Soc.* **2002**, *124*, 4228.
30. Hirai, H.; Chawanya, H.; Toshima, N. *Nip. Kag. Kai.* **1984**, *6*, 1027.
31. Roucox, A.; Sculz, J.; Patin, H. *Chem. Rev.* **2002**, *102*(10), 3757.
32. Narayanan, R.; El-Sayed, M. A. *J. Am. Chem. Soc.* **2003**, *125*(27), 8340.
33. Narayanan, R.; El-Sayed, M. A. *J. Phys. Chem. B*, **2003**, *107*(45), 12416.
34. Gentle, T. M.; Muetterties, E. L. *J. Phys. Chem.*, **1983**, *87*, 2469.
35. Rucker, T. G.; Logan, M. A.; Gentle, T. M.; Muetterties, E. L.; Somorjai, G. A. *J. Phys. Chem.*, **1986**, *90*, 2703.
36. Rellinghaus, B.; Stappert, S.; Acet M.; Wassermann, E. F. *Mat. Res. Soc. Symp. Proc.*, **2002**, *705*, Y9.5.1.
37. Ahmadi, T. S.; Wang, Z. L.; Green, T. C.; Henglein, A.; El-Sayed, M. A. *Science*, **1996**, *272*, 1924.
38. Li, Y.; Petroski, J.; El-Sayed, M. A. *J. Phys. Chem. B*, **2000**, *104*(47), 10956.
39. Ong, C. G.; Leckie, J. O. *Adsorpt. Met. Geo.*, **1998**, 317.
40. Baggio, S.; Pardo, M. I.; Baggio, R.; Garland, M. T. *Acta Crystallogr., Sect. C: Cryst. Struct. Commun.* **1997**, *C53*(6), 727.
41. Rizov, I.; Ilcheva, L. *Analyst* **1995**, *120*(6), 1651.

42. Aruga, R. *Inorg. Chem.* **1978**, 17(9), 2503.
43. Cusomano, M.; Giannetto, A.; Cavasino, P. F.; Sbriziolo, C. *Inorg. Chim. Acta* **1992**, 201(1), 49.
44. Itabashi, E. *Chem. Lett.* **1978**, 2, 211.
45. Foye, W. O.; Hu, J. J. *Pharm. Sci.* **1979**, 68(2), 202.
46. Foye, W. O.; Kaewchansilp, V. **1979**, 68(9), 1131.
47. Sillen, L. S.; Martell, A. E., "Stability Constants of Metal-Ion Complexes", Metcalfe & Cooper Limited, England, 1964.

CHAPTER 5

SHAPE-DEPENDENT CATALYTIC ACTIVITY OF PLATINUM NANOPARTICLES IN COLLOIDAL SOLUTION

5.1 Abstract

The activation energies and the average rate constants are determined in the 298 K – 318 K temperature range for the early stages of the nanocatalytic reaction between hexacyanoferrate (III) and thiosulfate ions using 4.8 ± 0.1 nm tetrahedral, 7.1 ± 0.2 nm cubic, and 4.9 ± 0.1 nm “near spherical” nanocrystals. These kinetic parameters are found to correlate with the calculated fraction of surface atoms located on the corners and edges in each size and shape.

5.2 Introduction

The field of nanocatalysis (in which nanoparticles are used to catalyze reactions) has been very active lately. Two types of nanocatalysis can be distinguished, the homogeneous type with catalysis in colloidal solution¹⁻⁸ and the heterogeneous type in which the nanoparticles are supported on solid surfaces catalyzing gas phase reactions⁹⁻²¹. Most of the studies in the homogeneous colloidal nanocatalysis field involve using spherical nanoparticles or nanoparticles of undetermined shapes. There are very few studies in which catalysis is conducted with nanoparticles of specific shape in colloidal solution. Truncated octahedral Pt nanoparticles have been used to catalyze the electron transfer reaction and the activation energy was determined²². The decomposition of the

oxalate capping material was studied on cubic Pt nanoparticles²³. However, these studies did not compare the nanoparticle kinetics of different shapes. A very important question to raise is whether or not the catalytic activity of atoms located on the surfaces of nanocrystals with different shapes is different. There have been no studies comparing the catalytic activity of nanoparticles of different shapes in colloidal solutions. In high vacuum surface catalysis studies with single crystals²⁴, a great deal of work has been carried out in which crystals cut with different facets are shown to catalyze different reactions. Nanoparticles of different shapes have different facets. Furthermore, they have different fractions of atoms located at different corners, edges, and at different defects (resulting from the loss of atoms at these locations). Thus, one would expect the catalytic activity to be different in catalyzing the same reaction.

In this letter, we compare the value of the activation energy and other kinetic parameters of the electron transfer reaction between hexacyanoferrate (III) ions and thiosulfate ions in colloidal solution containing dominantly tetrahedral, cubic, or “near spherical” platinum nanoparticles as catalysts during the early stages of the reaction before any shape changes occur. The “near spherical” nanoparticles have both the (111) and (100) facets with edges at their interfaces. TEM studies are conducted to determine the shape distribution and to ensure that during the early stages of the reaction, shape changes do not take place. For any size and shape, the catalytic activity of these three nanoparticles is found to correlate with the fraction of surface atoms located on corners and edges.

5.3 Experimental Section

The solutions of dominantly tetrahedral Pt nanoparticles stabilized with PVP are prepared using the H₂ reduction method described previously²⁵ with some modifications in which 0.05 g PVP is used as the capping agent and K₂PtCl₆ is the precursor salt used. The solutions of the dominantly cubic Pt nanoparticles stabilized with polyacrylate are also prepared using the H₂ reduction method described previously²⁵ with a few modifications in which the flask was thoroughly cleaned with Aqua Regia and the pH of the solution is adjusted to 9. The solutions of the dominantly “near spherical” Pt nanoparticles stabilized with PVP are synthesized by the reduction of the Pt⁺² ions with ethanol similar to a method described previously²⁶. A drop of each of the colloidal solutions is placed onto Formvar stabilized copper TEM grids and JEOL 100C TEM is used to determine the shape and size of the three different shaped nanoparticles.

For all three types of nanoparticles, the initial Pt ion concentration used for making the nanoparticles is 8×10^{-5} M. All three nanoparticle solutions are adjusted to a pH = 7 by the addition of either NaOH or HCl as appropriate. For the electron transfer reaction between hexacyanoferrate (III) ions and thiosulfate ions, 200 μ L of 0.01 M potassium hexacyanoferrate (III) and 200 μ L of 0.1 M sodium thiosulfate is added to 2 mL of the PVP-Pt nanoparticles. The kinetics of the reaction is monitored by using absorption spectroscopy with a Shimadzu UV-VIS-NIR spectrophotometer. The disappearance of the hexacyanoferrate (III) peak is monitored as a function of time by subtracting the absorbance at 500 nm from that at 420 nm. At 420 nm, both the hexacyanoferrate (III) ions and the platinum nanoparticles absorb and at 500 nm, only the platinum nanoparticles absorb with an absorption coefficient very close to that at 420 nm.

The absorbance (A) is monitored every 10 minutes for 40 minutes. The slope of the pseudo first-order plot of $-\ln A$ vs. time gives the rate constant, k. Since the concentration of the thiosulfate ions is ten times larger than that of the hexacyanoferrate ions, a pseudo first order plot is drawn from which the value of k is determined. As a result, only the concentration of the hexacyanoferrate ions is monitored. The rate constant of the reaction is determined at four different temperatures (25°C, 30°C, 40°C, and 45°C). From the slope of the graph $\ln k$ vs. $1000/T$, where T is the absolute temperature, the activation energy of the reaction is determined.

The shape distributions of the three types of nanoparticles are obtained before the reaction and after 40 minutes at 45° C using JEOL 100C TEM. The nanoparticle samples are spotted by placing a drop of the solution onto a Formvar stabilized copper grid and allowing the drop to evaporate in air. The spotted aqueous samples take approximately 2 hours to dry. Since the same deposition conditions are employed for all the samples, the evaporation rate of the solvent is fairly reproducible from one sample to another. For each experiment, the internal reproducibility of the observed nanoparticle shape distribution is examined by spotting the sample onto three separate TEM grids. Also, TEM images are taken from different sections of the TEM grids to verify the shape distribution. The general reproducibility of the observed shape distribution is verified by conducting each of the experiments three times. As a result, it is possible to compare the shape distribution changes under the various conditions used. Approximately 1800 particles are counted from enlarged TEM images for each experiment. In the case of tetrahedral nanoparticles, the shape distribution classification is regular tetrahedral, distorted tetrahedral, and spherical. For cubic nanoparticles, the distribution is regular

cubic, distorted cubic, and truncated octahedral. In the case of “near spherical” nanoparticles, the distribution classification is spherical and others. The average size of the three types of nanoparticles is determined before the reaction (initial synthesized samples).

5.4 Results and Discussion

The activation energy of the electron transfer reaction between hexacyanoferrate (III) and thiosulfate ions is determined for dominantly tetrahedral, dominantly cubic, and dominantly “near spherical” shaped platinum nanoparticles. The fraction of the surface atoms located on the corners and edges is calculated for the three different nanoparticles of different sizes and shapes. The results are correlated with the catalytic activity of each particle. In order to examine the shape dependence, the catalytic activity of the tetrahedral and “near spherical” particles that have comparable size and capped with the same capping material (PVP) is compared.

Figure 5.1 a-b, d-e, and g-h show typical TEM images and shape distribution graphs for the three nanoparticles of different shapes before the reaction. Table 5.1 also summarizes the results on the shape distribution and the average size for the three types of nanoparticles. The dominantly tetrahedral ($76 \pm 3\%$) PVP capped Pt nanoparticles have an average size of 4.8 ± 0.1 nm. The dominantly cubic ($61 \pm 4\%$) polyacrylate stabilized Pt nanoparticles have an average size of 7.1 ± 0.1 nm. The dominantly “near spherical” ($85 \pm 2\%$) PVP capped Pt nanoparticles have an average size of 4.9 ± 0.1 nm.

The shape distribution is determined after 40 minutes of the electron transfer reaction at 45°C , the highest temperature used in the study. This is conducted to

determine whether or not the shape distribution of the nanoparticles changes during the first 40 minutes of the reaction. Figure 5.1 c,f, and g show the shape distributions of the three types of nanoparticles after 40 minutes of the reaction at 45°C and the distribution results are also summarized in Table 5.1. It is clear that the shape distribution for all three types of nanoparticles is similar to that observed before the reaction. This indicates that during the beginning of the electron transfer reaction, there is very little change in the shape distribution of the nanoparticles. However, it should be mentioned that our previous studies have shown that both the size²⁶ and shape²⁷ of the nanoparticles indeed change during the full course of this reaction as well as the Suzuki reaction²⁸.

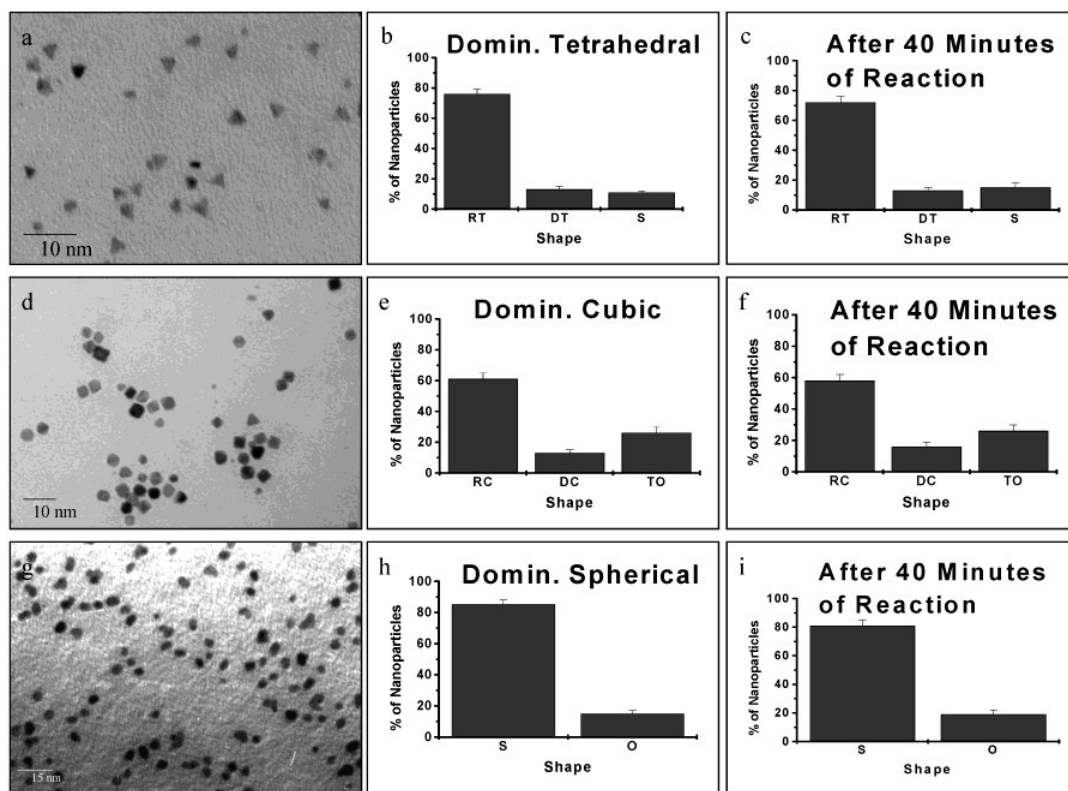


Figure 5.1—TEM images and shape distributions of dominantly tetrahedral (a-c), dominantly cubic (d-f), and dominantly “near spherical” (g-i) platinum nanoparticles before and after 40 min of electron-transfer reaction. This shows that there is no significant change in the shape of the nanoparticles resulting from the catalytic reaction at the highest temperature during the initial 40 min of the reaction.

Table 5.1—Summary of average size and shape distribution for the dominantly tetrahedral, cubic, and “near spherical” platinum nanoparticles (RT = regular tetrahedral, DT = distorted tetrahedral, S = Spherical, RC = regular cubic, DC = distorted cubic, and TO = truncated octahedral, O = other)

Nanoparticle Shape	Average Size (nm)	Shape Dist. Before Reaction	Shape Dist. After 40 Min. of Reaction at 45°C
Tetrahedral	4.8 ± 0.1	$76 \pm 3\%$ RT $13 \pm 1\%$ DT $11 \pm 1\%$ S	$72 \pm 4\%$ RT $13 \pm 2\%$ DT $15 \pm 3\%$ S
Cubic	7.1 ± 0.2	$61 \pm 4\%$ RC $13 \pm 2\%$ DC $26 \pm 4\%$ TO	$58 \pm 4\%$ RC $16 \pm 3\%$ DC $26 \pm 4\%$ TO
“Near Spherical”	4.9 ± 0.1	$85 \pm 2\%$ S $15 \pm 2\%$ O	$81 \pm 4\%$ S $19 \pm 3\%$ O

The catalytic reaction is carried out for each shape and the rate constant is determined for each shape at different temperatures during the first 40 minutes of the reaction. The activation energy is then obtained from the slope of the linear $\ln k$ vs. $1000/T$ dependence (slope = $-E_A/R$). As can be seen in Figure 5.2, the activation energy is lowest for the tetrahedral dominated nanoparticle solution (14.0 ± 0.6 kJ/mol) and highest for the cubic dominated nanoparticle solution (26.4 ± 1.2 kJ/mol). The activation energy of the “near spherically” dominated nanoparticles is intermediate (22.6 ± 1.2 kJ/mol) between that observed for the tetrahedral and cubic nanoparticles.

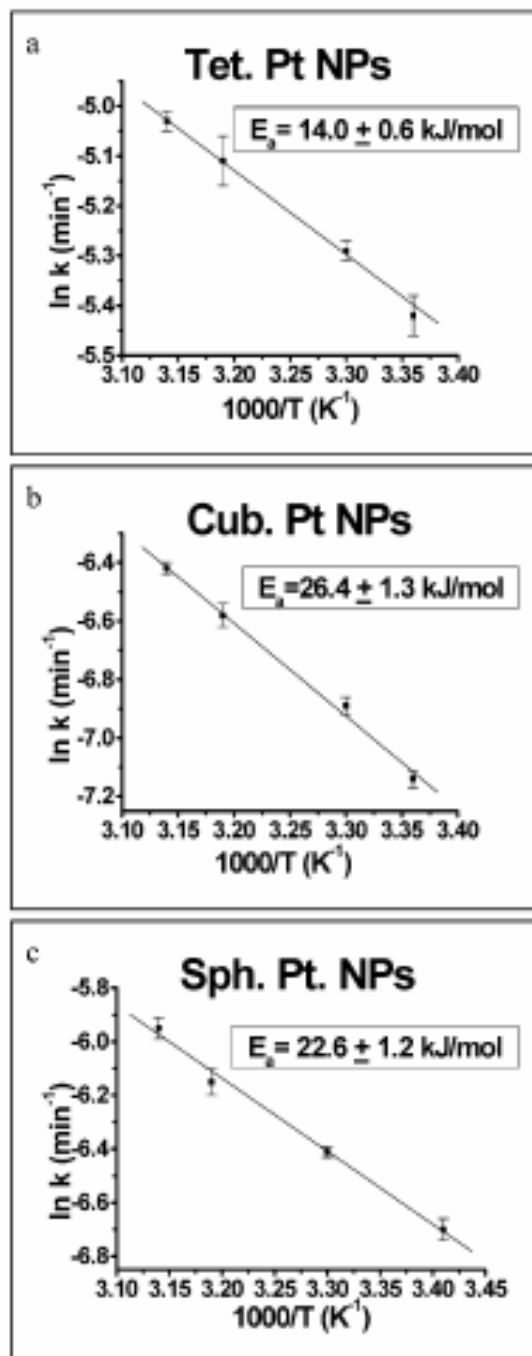


Figure 5.2—Arrhenius plots obtained using dominantly tetrahedral (a), dominantly cubic (b), and dominantly “near spherical” (c) shaped platinum nanoparticles to catalyze the electron-transfer reaction between hexacyanoferrate (III) ions and thiosulfate ions.

The tetrahedral particle is small and has sharp edges and corners. It is expected that atoms at these locations are likely to be either chemically very active or liable to

dissolve easily leaving behind atomic arrangements that has the makings of very catalytically active sites. In high vacuum surface catalysis studies²⁴, it is shown that catalysis takes place on defect sites (steps,...) The fraction of atoms in the small tetrahedral particles at these sites is probably sizable making these particles to be the most catalytically active. The cubic nanoparticles are the largest and most of its surface atoms are located on their (100) facets, which are known to be least active. This explains their high value of activation energy. The “near spherical” nanoparticles are not really spherical but have both the (111) and (100) facets with edges at the interfaces of these facets, explaining its intermediate catalytic activity.

In order to quantify the above observations and conclusions, the fraction of the surface atoms located on the corners and edges are calculated²⁹ for the different particles used in the present study. The tetrahedron, cubic, and cubo-octahedron models are used for the tetrahedral, cubic, and “near spherical” nanoparticles respectively. The models assume f.c.c. crystal structure. For each shape, formulas for the calculation of the total # of atoms, # of bulk atoms, # of surface atoms, # corner atoms, and # of vertex (edge) atoms can be obtained based on the number of shells (which depends on the size of the nanoparticles). Tetrahedral nanoparticles are small (4.8 nm), composed entirely of (111) facets with sharp edges and corners, which comprise ~28% of the total atoms and ~35% of the surface atoms (calculated using tetrahedron model²⁹). Cubic nanoparticles are larger (7.1 nm) and composed entirely of (100) facets with smaller fraction of atoms on their edges and corners, which comprises ~0.5% of total atoms and ~4% of surface atoms (calculated using cubic model²⁹). The “near spherical” nanoparticles are formed with (100) and (111) facets with numerous edges and corners. For “near spherical”

nanoparticles, we assume it to follow a cubo-octohedron structured model²⁹. For a “near spherical” particle of 4.9 nm, the number of atoms on the corners and edges comprise ~3% of the total atoms and ~13% of the surface atoms. From this analysis, if the atoms on the corners and edges (or defects resulting from them) are the dominantly active sites in the catalysis, one would predict that the 4.8 nm tetrahedral nanoparticles are the most active and the 7.1 nm cubic nanoparticles are the least active, while the 4.9 nm “near spherical” nanoparticles are in between. This is consistent with our results. The fraction of surface sites on the corners and edges of the three types of nanoparticles are also included in Table 5.2.

Table 5.2—Summary of the average rate constant, activation energy, pre-exponential factor, and entropy of activation for the dominantly tetrahedral, dominantly cubic, and dominantly “near spherical” shaped platinum nanoparticles obtained during the first 40 minutes of the electron transfer reaction

Initial Dominant Nanoparticle Shape	Average Rate Constant (min⁻¹)	Fraction of Active Surface Sites** (%)	Activation Energy (kJ/mol)	Pre-Exponential Factor (min⁻¹)	Entropy of Activation (J/mol K)
76% Tetrahedral	0.00518 ± 0.00019	35	14.0 ± 0.6	1.87 ± 1.26	2.18 ± 1.91
61% Cubic	0.00116 ± 0.00003	4	26.4 ± 1.3	35.16 ± 1.63	29.60 ± 4.04
85% “Near Spherical”	0.00184 ± 0.00008	13	22.6 ± 1.2	13.07 ± 1.58	21.37 ± 3.79

* Averaged over the temperature range used (25-45 °C)

** We are assuming that surface atoms or defects present on corners or edges are the most catalytically active.

If we carry out the above calculation for the same size of 5.0 nm (for example) for all three shapes, one finds that the fraction of surface atoms located on corners and edges to be ~35% for the tetrahedral, ~13% for the “near spherical”, and ~6% for the cubic particles suggesting that the tetrahedral nanoparticles are expected to be the most active, followed by the “near spherical” nanoparticles, and then the cubic nanoparticles. Figure 5.3a shows a plot of the average rate constant vs. % surface atoms on corners and edges of the nanoparticles. It can be seen that as the % surface atoms on corners and edges increases, the rate constant exponentially increases. This confirms that for nanoparticles of different shapes, but of the same size, the larger the percentage of edge and corner atoms that a nanoparticle has, the more catalytically active it is.

From Figure 5.3a, one can only suggest that there is a correlation between the fraction of active atoms and the average rate constant. The observed exponential dependence reflects the effect of many other factors whose contributions cannot be evaluated. For example, what is the effect of the capping material and how does it depend on the size? Is there a difference in the reactivity between sites (atoms or defects) present on corners and edges?

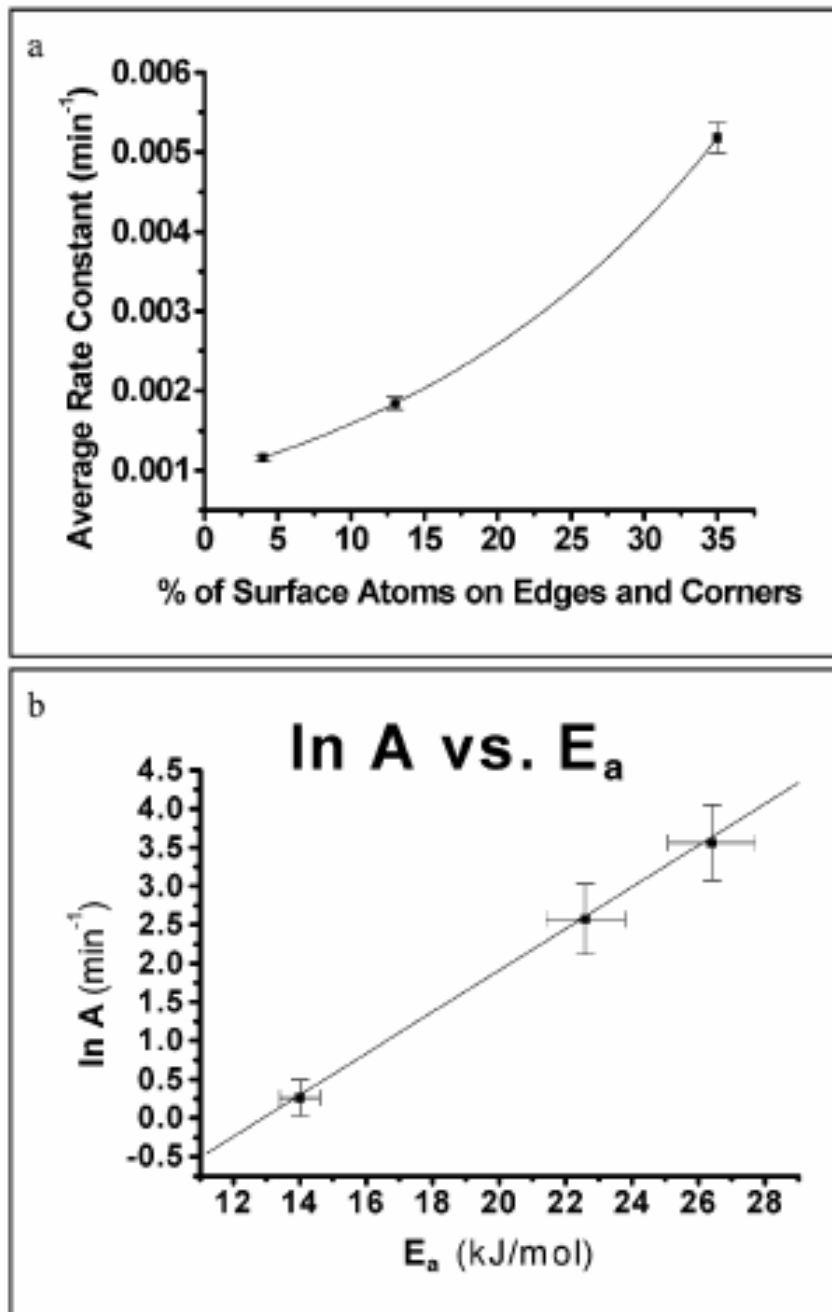


Figure 5.3—(a) Plot of average rate constant vs. % surface atoms on edges and corners on the tetrahedral, cubic, and “near spherical” shaped Pt nanoparticles and (b) plot of $\ln A$ vs E_a of the Arrhenius equation demonstrating the compensation effect in platinum nanoparticle catalysis. The activation energies and pre-exponential factors are those obtained when using the tetrahedral, cubic, and “near spherical” platinum nanoparticles to catalyze the electron-transfer reaction in the first 40 min.

In order to minimize the effect of capping material, comparison between the average rate constants and the fraction of atoms on edges and corners for catalysis with the 4.8 nm tetrahedral nanoparticles and the 4.9 nm “near spherical” nanoparticles should be made. These two particles are of the same size and PVP is used to stabilize both particles. The ratio of the average rate constants using these two particles is 2.8 while that between the corresponding fraction of atoms on the corners and edges is 2.7, suggesting a linear relationship. This relationship could result from the fact that while the atoms (or sites) on the corners are expected to be more active, they are also much smaller in number compared to those on the edges. The 4.8 nm tetrahedral nanoparticles are composed of 4 corner atoms and 42 edge atoms. The 4.9 nm “near spherical” nanoparticles are composed of 24 corner atoms and 228 edge atoms. It can be seen that for both shapes, there are ~10 times more atoms on edges than at corners. Since the tetrahedral nanoparticles have a much smaller number of corner atoms than the “near spherical” nanoparticles, the activity per corner atom must be much higher for the tetrahedral nanoparticles than for the “near spherical” nanoparticles. This makes good physical sense as the corner atoms on the tetrahedral nanoparticles are more chemically unsaturated with less next-door neighbors.

In addition to the activation energy, the pre-exponential factor (A) and the entropy of activation (ΔS^*) are also calculated during this time period. Table 5.2 summarizes the rate constant (average), activation energy, pre-exponential factor, and entropy of activation for the tetrahedral, cubic, and “near spherical” dominated nanoparticles. The pre-exponential factors are very low compared to those generally observed using metal complexes or supported metal catalysts. It is also worth mentioning that in the area of

metal nanoparticle catalyzed reactions, the pre-exponential factor has not been generally reported. Previously²⁶, we have proposed that thiosulfate binds to the Pt nanoparticle surface and reacts with hexacyanoferrate (III) ions via collisional processes. A possible reason for the low pre-exponential factors observed here is that thiosulfate binding to the heavy nanoparticles would make the collision frequency between the reactants to be much lower than in the case of homogeneous metal complexes. It can be seen that catalysis with tetrahedral nanoparticles result in the highest rate constant and that with cubic nanoparticles result in the lowest rate constant. Catalysis with “near spherical” nanoparticles results in an intermediate rate constant. It can also be seen that catalysis with tetrahedral nanoparticles has the lowest pre-exponential factor and entropy of activation while catalysis with cubic nanoparticles result in the highest pre-exponential factor and entropy of activation. The use of “near spherical” nanoparticles results in a pre-exponential factor and entropy of activation which are in between those observed for tetrahedral and cubic nanoparticles.

The graph of $\ln A$ vs. E_A , shown in Figure 5.3b, is plotted using the pre-exponential factor and the activation energy values that are obtained for the tetrahedral, cubic, and “near spherical” nanoparticles and is found to be linear. A linear relationship between $\ln A$ and the activation energy is an indication that the Meyer-Neldel rule³⁰, also called compensation law, is valid for catalysis with platinum nanoparticles. The compensation law was first discovered³¹ in the case of electron emission from a platinum surface heated in a hydrogen atmosphere. It is found to be valid in heterogeneous catalysis³²⁻³⁴ and in a large number of homogeneous and heterogeneous reactions³⁴⁻³⁶. In some cases in the literature, it has been reported that this kind of linear plot is found to

result from uncertainty in the numbers used, resulting in a false compensation effect. In our case, as can be seen in Figure 5.3b, with both horizontal and vertical error bars, there is a linear relationship between $\ln A$ and E_a , which suggests that the compensation effect we observe is genuine.

Because of the compensation effect, as the activation energy increases, the pre-exponential factor also increases. In addition, as the pre-exponential factor increases, the entropy of activation also increases since they are related by the equation³⁰: $\ln A = \Delta S^*/R$. As a result, even though the cubic nanoparticles have the lowest rate constant, the activation energy, pre-exponential factor, and entropy of activation are the highest. This would also explain the trends observed for the tetrahedral and “near spherical” Pt nanoparticles.

5.5 Conclusions

The catalytic activity is dependent on the shape of the platinum nanoparticle used during the early stages of the electron transfer reaction. The higher the fraction of surface atoms located on the edges and corners, the greater the catalytic activity. The tetrahedral nanoparticles have the highest fraction of atoms on the corners and edges and also have the lowest activation energy. As a result, the tetrahedral nanoparticles are the most catalytically active. In addition, it is observed that the catalysis with platinum nanoparticles obeys the Meyer-Neldel rule, which is also known as the compensation effect.

5.6 References

1. Bradley, J. S. *Clus. Colloids* **1994**, 459.
2. Duff, D. G.; Baiker, A. *Stud. Surf. Sci. Catal.* **1995**, 91, 505.
3. Toshima, N. *NATO ASI Ser., Ser. 3* **1996**, 12, 371.
4. Boennermann, H.; Braun, G.; Brijoux, G. B.; Brinkman, R.; Tilling, A. S.; Schulze, S. K.; Siepen, K. *J. Organomet. Chem.* **1996**, 520(1-2), 143.
5. Fugami, K. *Organomet. News* **2000**, 1, 25.
6. Mayer, A. B. R. *Polym. Adv. Technol.* **2001**, 12(1-2), 96.
7. Bonnemann, H.; Richards, R. *Syn. Meth. Organom. Inorg. Chem.* **2002**, 10, 209.
8. Moiseev, I. I.; Vargaftik, M. N. *Russ. J. Chem.* **2002**, 72(4), 512.
9. Eppler, A.; Rupprechter, G.; Gucci, L.; Somorjai, G. A. *J. Phys. Chem. B* **1997**, 101(48), 9973.
10. Toshima, N.; Yonezawa, T. *New J. Chem.* **1998**, 22(11), 1179.
11. Schmid, G. *Met. Clus. Chem.* **1999**, 3, 1325.
12. Puddephatt, R. J. *Met. Clus. Chem.* **1999**, 2, 605.
13. Henry, C. R. *Appl. Surf. Sci.* **2000**, 164, 252.
14. St. Clair, T. P.; Goodman, D. W. *Top. Catal.* **2000**, 13(1,2), 5.
15. Kralik, M.; Corain, B.; Zecca, M. *Chem. Pap.* **2000**, 54(4), 254.
16. Chusuei, C. C.; Lai, X.; Luo, K.; Goodman, D. W. *Top. Catal.* **2001**, 14(1-4), 71.
17. Bowker, M.; Bennett, R. A.; Dickinson, A.; James, D.; Smith, R. D.; Stone, P. *Stud. Surf. Sci. Catal.* **2001**, 133, 3.
18. Kralik, M.; Biffis, A. *J. Mol. Catal. A: Chem.* **2001**, 177(1), 113.
19. Thomas, J. M.; Raja, R. *Chem. Rec.* **2001**, 1(6), 448.
20. Mohr, C.; Claus, P. *Sci. Prog.* **2001**, 84(4), 311.
21. Thomas, J. M.; Johnson, B. F. G.; Raja, R.; Sankar, G.; Midgley, P. A. *Acc. Chem. Res.* **2003**, 36(1), 20.
22. Li, Y.; Petroski, J.; El-Sayed, M. A. *J. Phys. Chem. B*, **2000**, 104(47), 10956.

23. Fu, X.; Wang, Y.; Wu, N.; Gui, L.; Yang, Y. *Langmuir*, **2002**, *18*(12), 4619.
24. Somorjai, GA, "Introduction to Surface Chemistry and Catalysis", Wiley Publishers, New York, NY, 1994.
25. Ahmadi, T. S.; Wang, Z. L.; Green, T. C.; Henglein, A.; El-Sayed, M. A. *Science*, **1996**, *272*, 1924.
26. Narayanan, R.; El-Sayed, M. A. *J. Phys. Chem. B*, **2003**, *107*(45), 12416.
27. Narayanan, R.; El-Sayed, M. A. *J. Phys. Chem. B*, **2004**, *108*(18), 5726.
28. Narayanan, R.; El-Sayed, M. A. *J. Am. Chem. Soc.*, **2003**, *125*(27), 8340.
29. Hardeveld, R. V.; Hartog, F. *Surf. Sci.*, **1969**, *15*, 189.
30. Bligaard, T.; Honkala, K.; Logadottir, A.; Norskov, J. K.; Dahl, S.; Jacobsen, C. J. H. *J. Phys. Chem. B*, **2003**, *107*, 9325.
31. Wilson, H. A. *Philos. Trans. A*, **1908**, *208*, 247.
32. Palmer, W. G.; Constable, F. H. *Proc. R. Soc. London, Ser. A*, **1924**, *106*, 250.
33. Constable, F. H. *Proc. R. Soc. London, Ser. A*, **1925**, *108*, 355.
34. Leffler, J. E. *J. Org. Chem.*, **1955**, *20*, 1202.
35. Cremer, E. *Adv. Catal.*, **1955**, *7*, 75.
36. Galwey, A. K. *Adv. Catal.* **1977**, 247.

CHAPTER 6

CHANGING CATALYTIC ACTIVITY DURING COLLOIDAL PLATINUM NANOCATALYSIS DUE TO SHAPE CHANGES: ELECTRON TRANSFER REACTION BETWEEN HEXACYANOFERRATE (III) AND THIOSULFATE IONS

6.1 Abstract

The shape distribution of the catalytic nanoparticles and the activation energy of the electron transfer reaction between hexacyanoferrate (III) and thiosulfate ions were determined at different times during the course of the reaction. The activation energy is found to increase during the reaction when dominantly tetrahedral nanoparticles are used, decreases slightly when dominantly cubic nanoparticles are used, and remain almost unchanged when spherical nanoparticles are used. Corresponding changes in the tetrahedral and cubic, but not spherical, shape is observed. This is consistent with the changes in the activation energy that are observed. The shape distribution and activation energy of dominantly spherical nanoparticles is found to remain stable during the course of the reaction.

6.2 Introduction

A great interest at this time in the field of nanoscience is the dependence of the different properties of nanoparticles on their shape¹⁻⁴. Platinum nanoparticles have been synthesized with different shapes⁵. Since it is known that catalysis on transition metal crystal surfaces depends on the crystal face used⁶ and that different nanoparticles with different shapes have different facets and different ratio of the number of atoms on

corners and edges to those on the facets, one would expect catalysis to be greatly dependent on the nanoparticle shape used.

The field of catalysis using transition metal nanocatalysts in colloidal solution has been active lately with many review articles⁷⁻¹⁴ published in the last decade. In this type of catalysis, the focus has been on the use of spherical or undetermined shaped nanoparticles to catalyze reactions. There are very few studies in which catalysis is conducted with nanoparticles of known shapes, e.g. using truncated octahedral Pt nanoparticles to catalyze the electron transfer reaction¹⁵ and using cubic Pt nanoparticles for the decomposition of the oxalate capping agent¹⁶.

Being small and with surface atoms of different unsaturated valencies, nanoparticles of specific shape are more liable to change their shape in the harsh medium of chemical reactions. Surface reconstruction or dissolution of active atoms on corners or edges by one or more of the reactants or even the solvent is expected to take place during “catalysis”. We have already shown that the size of spherical nanoparticles changes during the catalysis process¹⁷⁻¹⁸. It is thus possible that not only the size, but also the shape of the nanoparticle could change during catalysis. This would screen any accurate conclusions regarding the shape dependence of the catalytic process.

In the present communication, we have determined the activation energies for the electron transfer reaction between hexacyanoferrate (III) ions and thiosulfate ions in a colloidal solution in which tetrahedral, cubic, or spherical nanoparticles are dominant. This reaction is selected because it is very “gentle” reaction that is catalyzed around room temperature. It is found that the activation energy of the reaction changes continuously

during the reaction. Using TEM, it is shown that the observed change in the reactivity of the nanoparticles is accompanied by changes in their shape distribution.

6.3 Experimental Section

The PVP stabilized dominantly tetrahedral Pt nanoparticles and the polyacrylate stabilized dominantly cubic Pt nanoparticles are prepared by using the H₂ reduction method described previously⁵ with a few modifications¹⁹. The dominantly spherical PVP-Pt nanoparticles are synthesized by the reduction of the Pt⁺² ions with ethanol as described previously¹⁸. For all three types of nanoparticles, the initial Pt ion concentration used is 8×10^{-5} M. All three nanoparticle solutions are adjusted to a pH = 7 by the addition of either NaOH or HCl as appropriate. The activation energy¹⁸ (see supporting information for details) is determined at four different time periods during the reaction (0 hr-0.67 hr, 16 hr-16.67 hr, 32-32.67 hr, and 48-48.67 hr). The shape distributions are obtained before the reaction, after 0.67 hr at 45° C, after 16.67 hrs at 45° C, after 32.67 hrs at 45° C, and after 48.67 hrs at 45° C using JEOL 100C TEM. The spotting conditions and verification of internal and general reproducibility of the shape distributions are conducted by counting 1800 nanoparticles from 9 enlarged TEM images. The shape distributions are determined for three shapes: specific shape, distorted shape, and spherical. Size distributions are determined for the initial samples of tetrahedral, cubic, and spherical nanoparticles.

6.4 Results and Discussion

Figure 6.1a-f show typical TEM images and shape distributions for the three types of nanoparticles. Table 6.1 summarizes the initial shape and size distributions for the three different types of nanoparticles. From Figure 6.2a and Table 6.1, it can be seen that the activation energy of the tetrahedral Pt nanoparticles increases during the course of the reaction while the activation energy of the cubic nanoparticles slightly decreases.

Tetrahedral nanoparticles are composed of (111) facets and are known to be the most catalytically active due to a large fraction of the surface atoms being present on edges and corners²⁰⁻²². As seen in Figure 6.2b and Table 6.1, the percentage of distorted tetrahedral nanoparticles increases during the course of the reaction. The rapid dissolution and surface reconstruction of the edge and corner atoms results in a greater percentage of distorted tetrahedral Pt nanoparticles with less sharp edges and corners and thus with higher activation energies. The cubic nanoparticles are larger in size (7 nm vs. 5 nm) and are composed of (100) facets with small fraction of their surface atoms on the edges and corners. Among other factors, the dissolution and surface reconstruction of atoms on the (100) facets of the cubic nanoparticles could take place during the reaction, and thus, creates defective and more active sites. This might explain the decrease in the activation energy observed when using the cubic nanoparticles. In the case of spherical nanoparticles composed of some (100) and (111) facets, the shape distribution, as well as the values of the activation energy, remains constant during the course of the reaction. This is consistent with the fact that the surface energy of the spherical shape is the lowest. Thus, both the tetrahedral and cubic shapes strive to become spherical, the thermodynamic reason for their shape changes during the catalytic reaction.

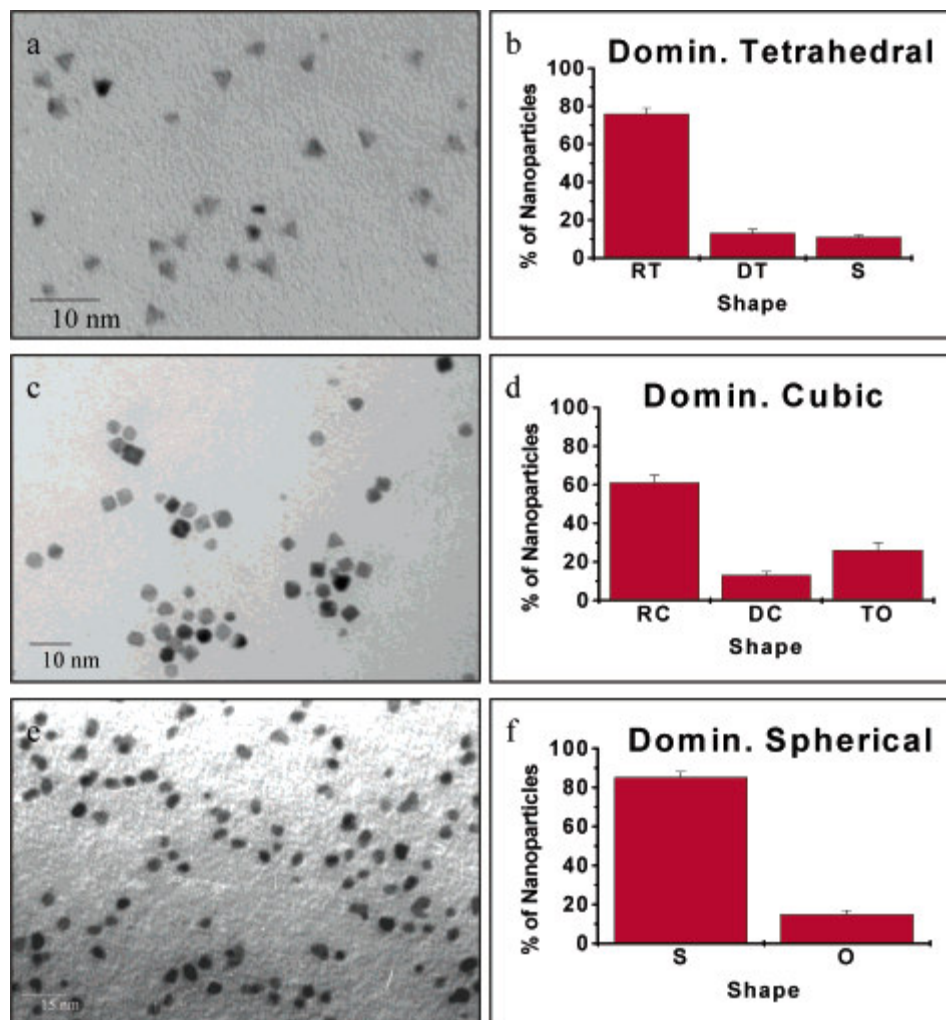


Figure 6.1—TEM images and shape distributions of the nanoparticle solutions used in the catalysis: dominantly tetrahedral (a-b), dominantly cubic (c-d), and dominantly spherical (e-f) platinum nanoparticle solutions. (RT = regular tetrahedral, DT = distorted tetrahedral, S = spherical, RC = regular cubic, DC = distorted cubic, TO = truncated octahedral, O = other.)

Table 6.1—Summary of average size and change in the shape distribution* (%D) for the dominantly tetrahedral, cubic, and spherical platinum nanoparticles (NP) and the activation energies (E_a) (kJ/mole) during the course of the catalytic reaction

NP Shape	Average Size (nm)	Initial %D	After 0.67 hr. %D and E_a	After 16.67 hr. %D and E_a	After 32.67 hr. %D and E_a	After 48.67 hr. %D and E_a
Tetra-hedral	4.8 ± 0.1	76 \pm 3 RT 13 \pm 1 DT 11 \pm 1 S	72 \pm 2 RT 13 \pm 2 DT 15 \pm 3 S 14.0 \pm 0.6 (E_a)	59 \pm 3 RT 28 \pm 3 DT 13 \pm 2 S 17.4 \pm 0.8 (E_a)	48 \pm 4 RT 39 \pm 3 DT 13 \pm 3 S 20.2 \pm 0.8 (E_a)	38 \pm 3 RT 51 \pm 4 DT 11 \pm 2 S 21.9 \pm 0.6 (E_a)
Cubic	7.1 ± 0.2	61 \pm 4 RC 13 \pm 2DC 26 \pm 4 TO	58 \pm 4 RC 16 \pm 3 DC 26 \pm 4 TO 26.4 \pm 1.3 (E_a)	52 \pm 3 RC 24 \pm 2 DC 24 \pm 3 TO 24.1 \pm 1.6 (E_a)	46 \pm 2 RC 29 \pm 4 DC 25 \pm 2 TO 23.0 \pm 1.6 (E_a)	41 \pm 3 RC 33 \pm 2 DC 26 \pm 3 TO 22.4 \pm 1.0 (E_a)
Spherical	4.9 ± 0.1	85 \pm 2 S 15 \pm 2 O	81 \pm 4 S 19 \pm 3 O 22.6 \pm 1.2 (E_a)	83 \pm 3 S 17 \pm 2 O 22.7 \pm 1.0 (E_a)	82 \pm 3 S 18 \pm 4 O 22.4 \pm 1.1 (E_a)	84 \pm 2 S 16 \pm 3 O 22.9 \pm 0.9 (E_a)

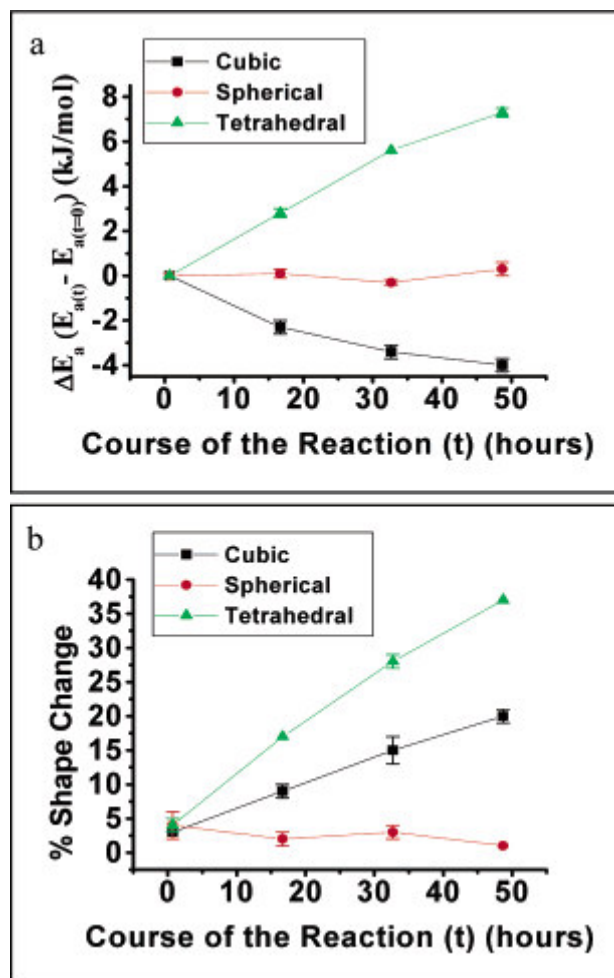


Figure 6.2—Time-dependent changes in the activation energy of the electron transfer reaction (a) and time-dependent changes of the initial shape of the platinum nanocatalysts of different shapes (b).

6.5 Conclusions

The above results suggest that indeed nanocatalysis is shape dependant.

However, the shape of the nanoparticles could change and try to assume the most stable (spherical) shape during the catalytic function. During the course of the entire electron transfer reaction, as the shape changes, there is a corresponding change in the activation energy of the reaction.

6.6 References

1. El-Sayed, M. A. *Acc. Chem. Res.* **2001**, *34*, 257.
2. Link, S.; El-Sayed, M. A. *Int. Rev. Phys. Chem.* **2000**, *19*, 409.
3. Pileni, M. P. *Supramol. Sci.* **1998**, *5*, 321.
4. Yacaman, M. J.; Ascencio, J. A.; Liu, H. B.; Gardea, T. *J. Vac. Sci. Technol., B* **2001**, *19*, 1091.
5. Ahmadi, T. S.; Wang, Z. L.; Green, T. C.; Henglein, A.; El-Sayed, M. A., *Science* **1996**, *272*, 1924.
6. Bradley, J. S. *Clusters Colloids*; VCH: Weinheim, Germany, 1994.
7. Duff, D. G.; Baiker, A. *Stud. Surf. Sci. Catal.* **1995**, *91*, 505.
8. Toshima, N. *NATO Adv. Study Inst. Ser., Ser. 3* **1996**, *12*, 371.
9. Boennermann, H.; Braun, G.; Brijoux, G. B.; Brinkman, R.; Tilling, A. S.; Schulze, S. K.; Siepen, K. *J. Organomet. Chem.* **1996**, *520*, 143.
10. Fugami, K. *Organomet. News* **2000**, *1*, 25.
11. Mayer, A. B. R. *Polym. Adv. Technol.* **2001**, *12*, 96.
12. Bonnemann, H.; Richards, R. *Synth. Methods Organomet. Inorg. Chem.* **2002**, *10*, 209.
13. Moiseev, I. I.; Vargaftik, M. N. *Russ. J. Chem.* **2002**, *72*, 512.
14. Li, Y.; Petroski, J.; El-Sayed, M. A. *J. Phys. Chem. B* **2000**, *104*, 10956.
15. Fu, X.; Wang, Y.; Wu, N.; Gui, L.; Tang, Y. *Langmuir* **2002**, *18*, 4619.
16. Narayanan, R.; El-Sayed, M. A. *J. Am. Chem. Soc.* **2003**, *125*, 8340.
17. Narayanan, R.; El-Sayed, M. A. *J. Phys. Chem. B* **2003** *107*, 12416.
18. Narayanan, R.; El-Sayed, M. A. *J. Phys. Chem. B*, published online March 2, <http://dx.doi.org/10.1021/jp037169u>.
19. Somorjai, G. A. *Introduction to Surface Chemistry and Catalysis*; Wiley: New York, 1994.
20. Falicov, L. M.; Somorjai, G. A. *Proc. Natl. Acad. Sci. U.S.A.* **1985**, *82*, 2207.
21. Somorjai, G. A.; McCrea, K. R.; Zhu, J. *Top. Catal.*, **2002**, *18*, 157.

CHAPTER 7

EFFECT OF CATALYSIS ON THE STABILITY OF METALLIC NANOPARTICLES: SUZUKI REACTION CATALYZED BY PVP-PD NANOPARTICLES

7.1 Abstract

Being small makes nanoparticles attractive in catalysis due to their large surface-to-volume ratio. However, being small raises questions about their stability in the harsh chemical environment in which these nanoparticles find themselves during their catalytic function. In the present work, we studied the Suzuki reaction between phenylboronic acid and iodobenzene catalyzed by PVP-Pd nanoparticles to investigate the effect of catalysis, recycling, and the different individual chemicals on the stability and catalytic activity of the nanoparticles during this harsh reaction. The stability of the nanoparticles to the different perturbations is assessed using TEM and the changes in the catalytic activity are assessed using HPLC analysis of the product yield.

It was found that the process of refluxing the nanoparticles for 12 hours during the Suzuki catalytic reaction increases the average size and the width of the distribution of the nanoparticles. This was attributed to Ostwald ripening in which the small nanoparticles dissolve to form larger nanoparticles. The kinetics of the change in the nanoparticle size during the 12 hour period show that the nanoparticles increase in size during the beginning of the reaction and levels off toward the end of the first cycle. When the nanoparticles are recycled for the second cycle, the average size decreases. This could be due to the larger nanoparticles aggregating and precipitating out of

solution. This process could also explain the observed loss of the catalytic efficiency of the nanoparticles during the second cycle. It is also found that the addition of biphenyl to the reaction mixture results in it poisoning the active sites and giving rise to a low product yield. The addition of excess PVP stabilizer to the reaction mixture seems to lead to the stability of the nanoparticle surface and size, perhaps due to the inhibition of the Ostwald ripening process. This also decreases the catalytic efficiency of the nanoparticles due to capping of the nanoparticle surface. The addition of phenylboronic acid is found to lead to stabilizing the size distribution as it binds to the particle surface through the O⁻ of the OH group and acts as a stabilizer. Iodobenzene is found to have no effect and thus probably does not bind strongly to the surface during the catalytic process. These two results might have an implication on the catalytic mechanism of this reaction.

7.2 Introduction

Due to their large surface to volume ratio, nanoparticles offer higher catalytic efficiency per gram than larger size materials. The field of nanocatalysis has been very active lately with numerous review articles published during the past decade in both heterogeneous catalysis in which the nanoparticles are supported on solid surfaces (e.g. silica or alumina)¹⁻¹³ and in homogeneous catalysis with colloidal nanoparticles¹⁴⁻²¹. Being small in size is expected to increase the nanoparticle surface tension. This makes surface atoms very active. The question is now raised as to how active they become. Are they active beyond their catalytic function and thus become reactants rather than catalysts? Are they active enough to change the size and shape of the nanoparticles during catalysis?

The purpose of our present research is to follow the changes in the average size, size distribution, and the shape of metallic nanoparticles as they are used in different catalytic reactions. It is expected that catalysis in high temperature colloidal solutions will affect the integrity of the particles more than gas phase-supported solid state nanoparticle catalysis. For this reason, we began examining the stability of metallic nanoparticles in catalytic reactions in colloidal solution.

In the bulk of the catalysis with colloids, TEM characterization of the nanoparticles before and after catalysis is not given. However, there are a few studies in the literature where size distribution of the nanoparticles after recycling along with the catalytic activity is reported for characterization. In these studies, reactions such as hydrogenation of ethyl pyruvate²², hydrogenation of arenes²³, carbonylation of methanol²⁴, the intra- and inter-molecular Paulson-Khand reactions²⁵, and hydrogenation of alkenes²⁶ are reported. There have also been some papers that discuss the catalytic activity of the nanoparticles upon recycling, but which do not examine the stability of the nanoparticles after catalysis. Such studies were conducted for reactions like hydrogenation of alkenes²⁷, Heck reaction between aryl halides and n-butylacrylate²⁸, hydrogenation of olefins²⁹, and hydrogenation of unsaturated fatty acid esters³⁰. In a review of transition metal colloids as reusable catalysts,³¹ it was pointed out that the major interest of reusability of the nanoparticle catalysts has not been systematically studied or published in the metal colloid literature.

For reactions catalyzed by metal nanoparticles in colloidal solution, there has not been any detailed examination in the literature of what causes the size distribution to change, the role of the individual chemicals present in the reaction mixture, and whether

the changes in the nanoparticles affects the catalytic activity upon recycling. A detailed examination is necessary in order to evaluate the nanoparticles' usefulness in catalyses and to understand in detail the mechanism of "nanocatalysis". This will enable a much better understanding of what kind of nanoparticles are the best for catalysis and also provide insight on how to make the nanoparticles more stable and maintain their catalytic activity.

It is our premise that in harsh reactions, there will be great changes in the average size (center of size distribution) and the width of the size distribution of the nanoparticles after catalysis, recycling, and in the presence of different chemicals. Also, there will be great changes in the catalytic activity of the nanoparticles upon recycling. To test this idea, the Suzuki reaction between phenylboronic acid and iodobenzene catalyzed by PVP stabilized Pd nanoparticles is chosen since it is a harsh reaction due to the need to reflux the reaction mixture at 100 degrees C for 12 hours. The Suzuki cross-coupling reaction is an effective synthetic route toward the production of biaryls by the coupling of arylboronic acids and haloarenes. It was first discovered by A. Suzuki in 1981³² and is sometimes referred to as the Suzuki-Miyaura coupling. The Suzuki cross-coupling reactions are a method of C-C bond formation that is widely used in industries. Suzuki reactions have been traditionally catalyzed using many different kinds of phosphine-based palladium catalysts and phosphine-free palladium catalysts such as Pd(PPh₃)₄, Pd(Oac)₂, [(n³-C₃H₅)PdCl]₂, and Pd₂(dba)₃ C₆H₆³³⁻³⁷. The use of palladium nanoparticles as catalysts for Suzuki reactions has been a fairly recent phenomenon. Palladium nanoparticles stabilized with tetraalkylammonium salts³⁸, PVP^{39,40}, PANAM dendrimers⁴¹, PS-b-PANa block copolymer⁴¹, 1,5-Bis(4,4'-bis(perfluorooctyl)phenyl)-

1,4-pentadien-3-one⁴², Keggin-type polyoxometalate⁴³, and cyclodextrin⁴⁴ have all been used to catalyze various Suzuki reactions.

In this paper, PVP-Pd nanoparticles are used to catalyze the Suzuki reaction between phenylboronic acid and iodobenzene. The aim of this study is to examine the effect of catalysis, recycling, and the different chemicals involved in the reaction on the stability and catalytic activity of the PVP-Pd nanoparticles.

7.3 Experimental Section

7.3.1 Synthesis of PVP-Pd Nanoparticles

The PVP-Pd nanoparticles were synthesized by the reduction of the Pd ions with ethanol similar to that described previously^{45,39,40}. The palladium precursor solution (H_2PdCl_4) was prepared by adding 0.0887 g of PdCl_2 , 6 mL of 0.2 M HCl, and diluting to 250 mL with doubly distilled water. A solution containing 15 mL of 2 mM of H_2PdCl_4 , 21 mL of doubly deionized water, 0.0667 g PVP, and 4 drops of 1 M HCl was heated. When the solution began to reflux, 14 mL of ethanol was added. The solution was then refluxed for three hours and this resulted in a dark brown colloidal Pd solution. A drop of the solution was spotted onto Formvar stabilized copper TEM grids and JEOL 100C TEM was used to characterize the size of the nanoparticles.

7.3.2 Suzuki Reaction

The Suzuki reaction between phenylboronic acid and iodobenzene was catalyzed using the PVP-Pd nanoparticles as described previously³⁹⁻⁴¹. For this reaction, 0.49 g (6

mmol) of sodium acetate, 0.37 g (3 mmol) of phenylboronic acid, and 0.20 g (1 mmol) of iodobenzene was added to 150 mL of 3:1 acetonitrile:water solvent. The solution was heated to 100 °C and 5 mL of the PVP-Pd nanoparticles was added to start the reaction. The reaction mixture was refluxed for a total of 12 hours.

7.3.3 Recycling the PVP-Pd Nanoparticles for Second Cycle of Suzuki Reaction

The same reaction mixture solution was used for recycling after the addition of fresh amounts of the reactants. For recycling, an assumption was made that all of the iodobenzene was used up since it is the limiting reactant. Initially there is 1 mmol iodobenzene and 3 mmol phenylboronic acid present in the reaction mixture. After the first cycle, it is assumed that there is no iodobenzene left and 2 mmol phenylboronic acid left. As a result, for the second cycle, 1 mmol iodobenzene and 1 mmol phenylboronic acid were added. The reaction mixture was then refluxed for another 12 hours to complete the second cycle.

7.3.4 The TEM Study to Assess Nanoparticle Stability

To examine the changes in the nanoparticles after catalysis, samples of the reaction mixture before and after refluxing for 12 hours were spotted onto Formvar stabilized copper TEM grids. The JEOL 100C TEM was used to determine the changes in the width and center of the size distributions of the PVP-Pd nanoparticles. The widths and centers of the size distributions of the PVP-Pd nanoparticles during various time periods in the first cycle such as 1 hour, 3 hours, 6 hours, and 10 hours were also obtained. The effect of recycling on the nanoparticles was also investigated using TEM.

In addition, TEM was also used to understand the roles of the different chemicals present during the Suzuki reaction. The effects of refluxing the PVP-Pd nanoparticles in the solvent, in the solvent + sodium acetate, in the solvent + sodium acetate + phenylboronic acid, and in the solvent + sodium acetate + iodobenzene were investigated. The impact of adding 0.5 g of PVP with the PVP-Pd nanoparticles solution was also investigated.

For all of the above experiments, the concentration of the Pd ions present in nanoparticles is 6.00×10^{-4} M and when 5 mL of the nanoparticles is added to 150 mL of the 3:1 acetonitrile:water solvent, the concentration of the Pd ions is 1.94×10^{-5} M. For the experiments, the samples were spotted by placing a drop of the solution onto a Formvar stabilized copper grid and allowed to evaporate in air. The spotted samples take approximately 30 minutes to dry. Since the same deposition conditions are employed for all samples, the evaporation rate of the solvent is fairly reproducible from one sample to another. For each of the experiments, the internal reproducibility of the observed particle size and distribution was verified by spotting the sample onto 3 separate TEM grids. TEM images were also obtained from different sections of the TEM grids to verify the reproducibility of the particle size and distribution. The general reproducibility of the observed particle size and distribution was verified by conducting each of the experiments 3 times. As a result, it is possible to compare the particle size and distribution changes under various conditions.

The nanoparticle size and distribution was determined by counting approximately 1800 nanoparticles from 9 enlarged TEM images (approximately 200 nanoparticles from each TEM image). The size distribution plots were fit using a Gaussian model with Microcal Origin 5.0 graphing software in order to determine the widths and centers of the

size distributions. The width of the distribution gives an idea of how narrow or wide the size distribution is and the center of the distribution is the most probable or average size of the nanoparticles (depending on the shape of the distribution).

7.3.5 HPLC Experiments to Measure Catalytic Activity

HPLC measurements were conducted on a Hitachi-4500 HPLC equipped with a L4500A diode array detector in which the absorbance was monitored at 254 nm. The separation was carried out on a reversed-phase packed column (Rainin Microsorb-MV C18, 300 Angstroms, dim 4.6 x 250 mm) using a 60:40 acetonitrile-water mixture and a flow rate of 1 mL/min. The area of the chromatographic peaks was calculated with a D-6000 interface-integrator. A calibration curve for determining the concentration of biphenyl was constructed by plotting the peak area vs. concentration of biphenyl standards. The standards prepared were 0.0005 M, 0.001 M, 0.0015 M, 0.002 M, 0.0025 M, and 0.003 M biphenyl. For HPLC measurements, all samples were diluted to $\frac{1}{4}$ of the original concentration so that the peak areas will be within the range of the calibration curve. The actual concentration was determined by taking the concentration of the diluted sample and multiplying by 4. The concentration of biphenyl was determined before the first cycle, after the first cycle, before the second cycle, and after the second cycle. Also, the effect of PVP on the amount of biphenyl formed was also determined. In addition, the impact of the presence of biphenyl in the Suzuki reaction mixture on the formation of biphenyl product was also investigated using HPLC.

7.4 Results and Discussion

In this paper, a detailed examination of the stability of the PVP-Pd nanoparticles after catalyzing the Suzuki reaction between phenylboronic acid and iodobenzene, after recycling, and in the presence of chemicals has been investigated. Also, the reasons why the changes in the width and center of the size distributions occur are discussed. Table 7.1 summarizes the widths and centers of distributions of the PVP-Pd nanoparticles before and after various conditions.

Table 7.1—Summary of Gaussian fits showing the widths and centers of size distributions of PVP-Pd nanoparticles before and after various perturbations (SA = sodium acetate, PA = phenylboronic acid, and I = iodobenzene)

Condition	Before Width (nm)	After Width (nm)	Before Center (nm)	After Center (nm)
Suzuki Reaction	1.1 ± 0.2	After first cycle 2.8 ± 0.4	2.1 ± 0.1	After first cycle 2.9 ± 0.3
		After second cycle 0.9 ± 0.2		After second cycle 2.2 ± 0.2
Suzuki Reaction in Presence of PVP	1.1 ± 0.1	1.8 ± 0.4	2.1 ± 0.1	2.4 ± 0.1
Reflux in Solvent	1.0 ± 0.1	2.2 ± 0.4	2.1 ± 0.1	4.5 ± 0.2
Reflux in Solvent + PVP	1.1 ± 0.1	1.6 ± 0.1	2.1 ± 0.1	2.5 ± 0.3
Reflux in Solvent + SA	1.0 ± 0.1	1.7 ± 0.2	2.1 ± 0.1	3.9 ± 0.1
Reflux in Solvent + SA + PA	1.0 ± 0.1	1.5 ± 0.1	2.1 ± 0.1	2.3 ± 0.1
Reflux in Solvent + SA + I	1.1 ± 0.1	1.8 ± 0.3	2.1 ± 0.1	3.6 ± 0.1

7.4.1 Effect of Catalysis and Recycling

Figure 7.1a shows a representative TEM image of the PVP-Pd nanoparticles before the first cycle of Suzuki reaction and Figure 7.1b shows the Gaussian fits of the size distributions of the nanoparticles. It can be seen that the PVP-Pd nanoparticles are monodisperse with an average size (center of distribution) of 2.1 ± 0.1 nm. Figure 7.1c shows a representative TEM image of the nanoparticles after the first cycle of the Suzuki reaction and Figure 7.1d shows the Gaussian fits of the size distributions of the nanoparticles. By comparing the Gaussian fits before and after the first cycle in Figure 7.1b, Figure 7.1d, and Table 7.1, it can be seen that both the widths and centers of the size distributions of the nanoparticles increase after the first cycle and that the size distribution shifts toward larger size. Also, the width of the size distribution after the first cycle is very broad. The observation of the increase in the size of the nanoparticles might be explained by the Ostwald ripening processes during the refluxing the reaction mixture containing the nanoparticles for 12 hours. The Ostwald ripening process is a mechanism for cluster growth. In this growth process, there is detachment of atoms from the smaller clusters then reattachment on the more stable surface of the larger clusters^{46,47}. As a result, the larger clusters grow in size while the smaller clusters shrink or dissolve altogether. Furthermore, the solution itself probably has a large concentration of atomic Pd in monomeric and different polymeric forms resulting from the reduction of the salt. These will be used to allow the growth of the nanoparticles during the 12 hours refluxing of the solution.

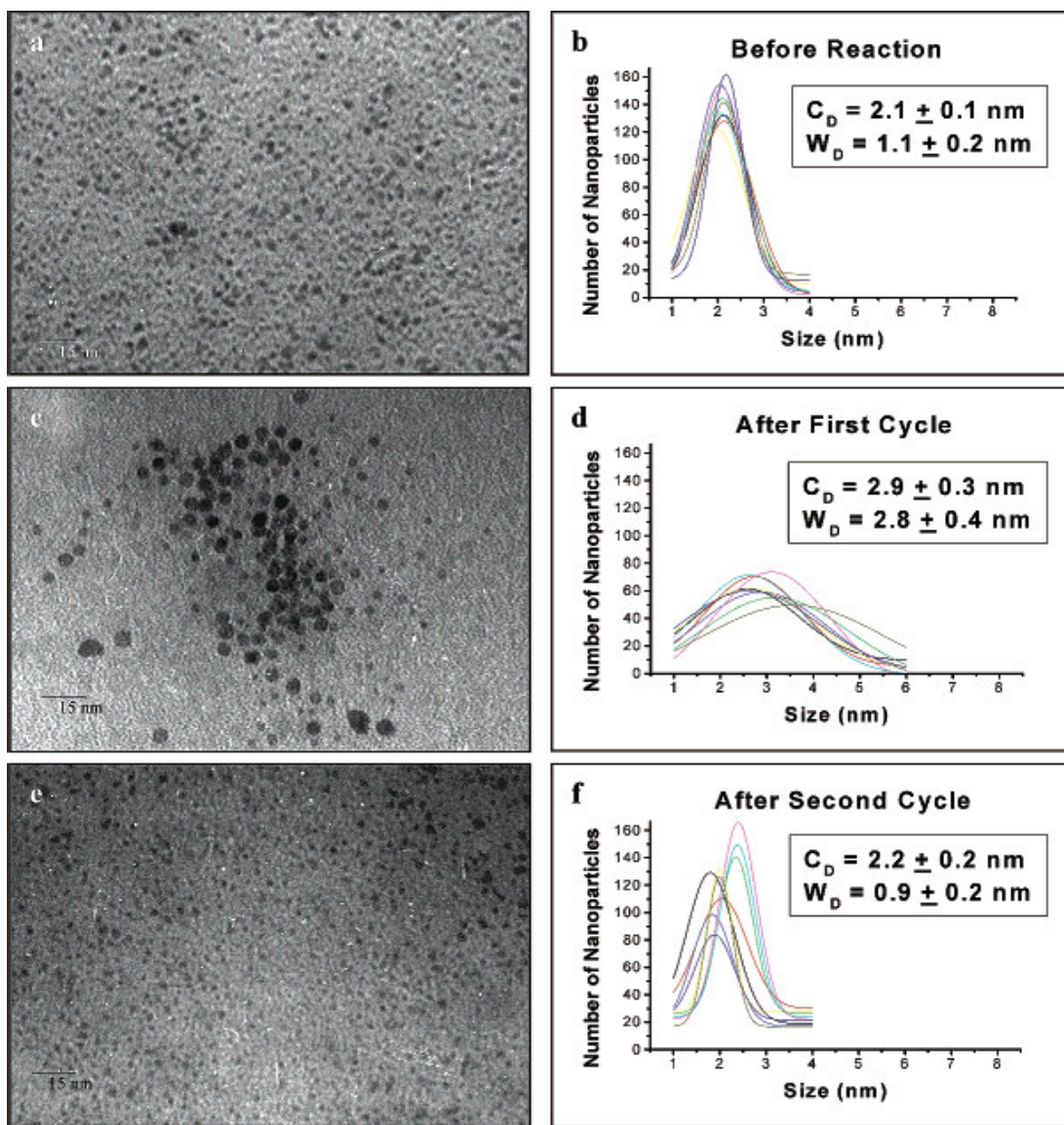


Figure 7.1—TEM images and Gaussian fits of the size distributions of PVP-Pd NPs before the Suzuki reaction (a,b), after the first cycle (c,d), and after the second cycle (e,f) Figure 7.1e shows a typical TEM image of the nanoparticles after the second cycle

Figure 7.1e shows a typical TEM image of the nanoparticles after the second cycle of the Suzuki reaction and Figure 7.1f shows the Gaussian fits of the size distributions of the nanoparticles. By comparing the Gaussian fits in Figure 7.1b, Figure 7.1d, Figure 7.1f, and Table 7.1, it can be seen that the widths and centers of the size distributions of the nanoparticles become much smaller after the second cycle of the

Suzuki reaction. This observation might be due to the aggregation and precipitation of the larger nanoparticles formed during the first cycle. As a result, the average size of the nanoparticles in solution decreases.

Table 7.2 summarizes the concentration of biphenyl formed after the first and second cycle of the Suzuki reaction and after the Suzuki reaction in the presence of 0.5 g of PVP. The percentage change in the biphenyl concentration formed is also compared. The catalytic activity of the nanoparticles after the first and second cycle of the Suzuki reaction is compared by using HPLC to find out if the nanoparticles remain catalytically active during the second cycle or if they become less catalytically active. A calibration curve of the peak area vs. concentration of biphenyl standards was constructed. The equation, $y = 5.79 * 10^6 x - 618422.75$, generated from the calibration curve is used to determine the concentration of biphenyl in the Suzuki reaction mixtures. HPLC chromatograms were obtained of the reaction mixtures before the first cycle, after the first cycle, before the second cycle, and after the second cycle. The concentration of biphenyl was determined after the first cycle and after the second cycle. After the first cycle of the reaction, there is $39 \pm 4\%$ yield of biphenyl. After the second cycle of the reaction, the overall yield of biphenyl is $54 \pm 2\%$, while the yield for the second cycle alone is $15 \pm 3\%$. Since the amount of biphenyl formed during the second cycle is much lower than the amount formed in the first cycle, the PVP-Pd nanoparticles are definitely much less catalytically active during the second cycle of the reaction. The reason why the nanoparticles are much less catalytically active during the second cycle might be due to a lower amount of nanoparticles present in the solution if due to the precipitation of larger nanoparticles. Another possibility is that if the number density has not changed,

but only the size is getting smaller, that the smaller particles might not be as catalytically active as the larger particles. In a previous paper⁴⁰, the catalytic activity of PVP-Pd nanoparticles of different sizes was examined. It was found that the catalytic activity increases with decreasing size of the nanoparticles. As a result, the latter explanation is ruled out. As a result, the lower catalytic activity observed during the second cycle is due to a lower amount of nanoparticles present in solution due to the larger nanoparticles aggregating and precipitating out of solution. In addition, surface poisoning by the products could be another reason.

Table 7.2—Concentration of the Product Biphenyl after the Various Conditions as Determined by Using HPLC

Condition	HPLC (Quantitative)
After first Cycle of Suzuki Reaction	3.00 ± 0.32 mM biphenyl (39 ± 4% yield)
After second Cycle of Suzuki Reaction	4.11 ± 0.12 mM biphenyl (54 ± 2% overall yield) (15 ± 3% yield in second cycle)
After Suzuki Reaction in Presence of 0.5 g PVP	2.28 ± 0.18 mM biphenyl (30 ± 2% yield)
Before Suzuki Reaction in Presence of 1 mmol Biphenyl	7.61 ± 0.42 mM biphenyl (started with theoretical yield of biphenyl)
After Suzuki Reaction in Presence of 1 mmol Biphenyl	10.20 ± 0.47 mM biphenyl (34 ± 6% yield)

It is noticed that yield of biphenyl in comparison to the theoretical yield is low. Experiments of conducting the Suzuki reaction in the presence of 1 mmol biphenyl were done to find out the amount of product that forms. The reason 1 mmol biphenyl is added is because that is the theoretical yield of biphenyl that can be formed. As seen by the HPLC results shown in Table 7.2, the presence of biphenyl in the reaction mixture results in inhibition of the reaction and the yield of biphenyl is $34 \pm 6\%$. As a result, the low yield of biphenyl both in the first and second cycle could be due to the biphenyl product formed itself poisoning the active sites.

The stability of the PVP-Pd nanoparticles during different time periods of the first cycle of the Suzuki reaction was also investigated. Figure 7.2a shows the nanoparticle size as a function of time. It can be seen that the PVP-Pd nanoparticles smoothly increase in size during the beginning of the reaction from 0 to 3 hours and then levels off near the end of the first cycle. This suggests that the Ostwald ripening occurs during the first three hours and then levels off toward the end of the first cycle of the Suzuki reaction due to the depletion of the small nanoparticles as well as free atoms in solution. Figure 7.2b shows the dependence of the concentration of product biphenyl as a function of time. It can be seen that there is rapid formation of biphenyl during the first hour of the reaction and then its rate of formation is greatly reduced. This reduction is probably a result of the surface poisoning by the biphenyl product as well as by the increase in the nanoparticle size.

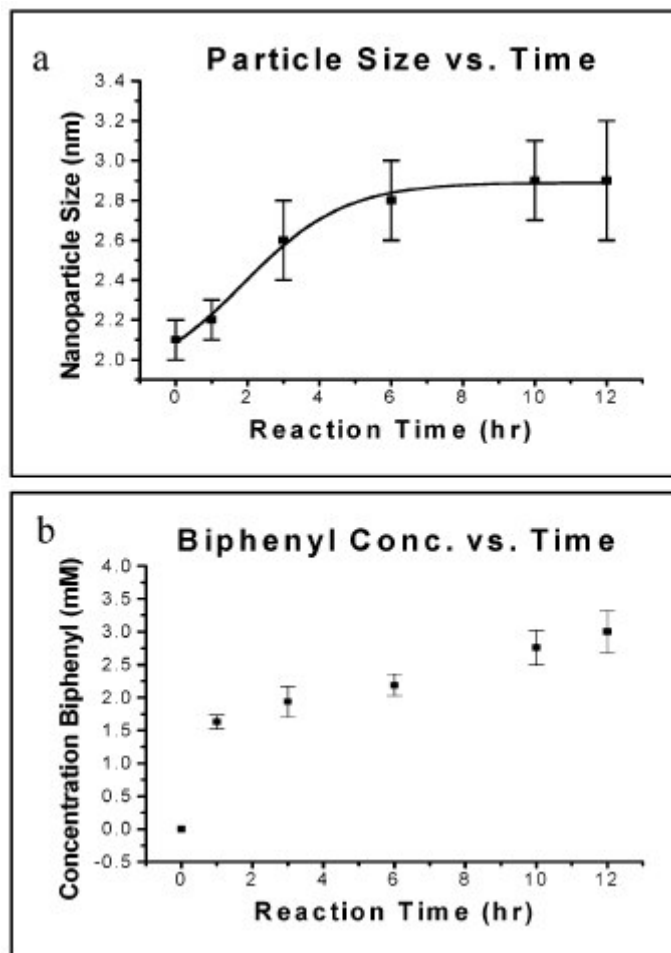


Figure 7.2—PVP-Pd nanoparticle size as a function of reaction time (a), Biphenyl concentration as a function of reaction time (b)

7.4.2 Effect of Excess PVP Stabilizer

For all the experiments, TEM images and Gaussian fits of the size distributions were obtained before each perturbation as shown in Table 7.1, but in order to concisely summarize the results in the figure, Figure 7.3a and Figure 7.3b show a typical TEM image and Gaussian fits of the PVP-Pd nanoparticles before any perturbations. Figure 7.3c and 7.3d show typical TEM image and Gaussian fits of the size distributions of the nanoparticles after the Suzuki reaction in the presence of 0.5 g PVP. By comparing the Gaussian fits in Figure 7.3b, Figure 7.3d, and in Table 7.1, it can be seen that the widths

and centers of the distributions after the reaction are slightly larger than before the reaction, but are not as large as without the presence of the PVP which is shown in Figure 7.1d and Table 7.1. Since the nanoparticles do not get as large as after a normal catalytic reaction, the presence of the excess PVP stabilizer probably diminishes the Ostwald ripening process by capping many of the free sites in the surface of the Pd nanoparticles. As a result, there are less free sites available for the Ostwald ripening process to occur.

The catalytic activity of the nanoparticles in the Suzuki reaction with 0.5 g PVP present was investigated using HPLC and compared to that of a normal catalytic mixture. It was found that there is only $30 \pm 2\%$ yield of biphenyl when excess PVP was present in the reaction mixture as shown in Table 7.2. As a result, the presence of excess PVP results in a lower amount of biphenyl formed after the reaction. The lower catalytic activity observed when the Suzuki reaction is conducted in the presence of 0.5 g PVP is due to the fact that there is less free metallic surface sites available for the catalysis since many of the free sites are capped by the excess PVP stabilizer. Figure 7.3e shows a typical TEM image of the nanoparticles after refluxing them in the 3:1 acetonitrile:water solvent for 12 hours and Figure 7.3f shows Gaussian fits of the size distributions of the nanoparticles after refluxing them in the presence of 3:1 acetonitrile:water solvent. By comparing the Gaussian fits in Figure 7.3b, Figure 7.3f, and Table 7.1, it can be seen that both the widths and the centers of the size distributions of the nanoparticles become larger after just refluxing them for 12 hours in the presence of the solvent. Also, the centers of the size distributions shift toward larger sized nanoparticles. The increase in the size of the nanoparticles observed is probably due to the Ostwald ripening process. The reason why the process is much more prominent in this case than after the first cycle

of the Suzuki reaction is because there is no phenylboronic acid present to bind to the nanoparticle surface and inhibit the Ostwald ripening process. The role of phenylboronic acid on the Ostwald ripening process of the nanoparticles is discussed later.

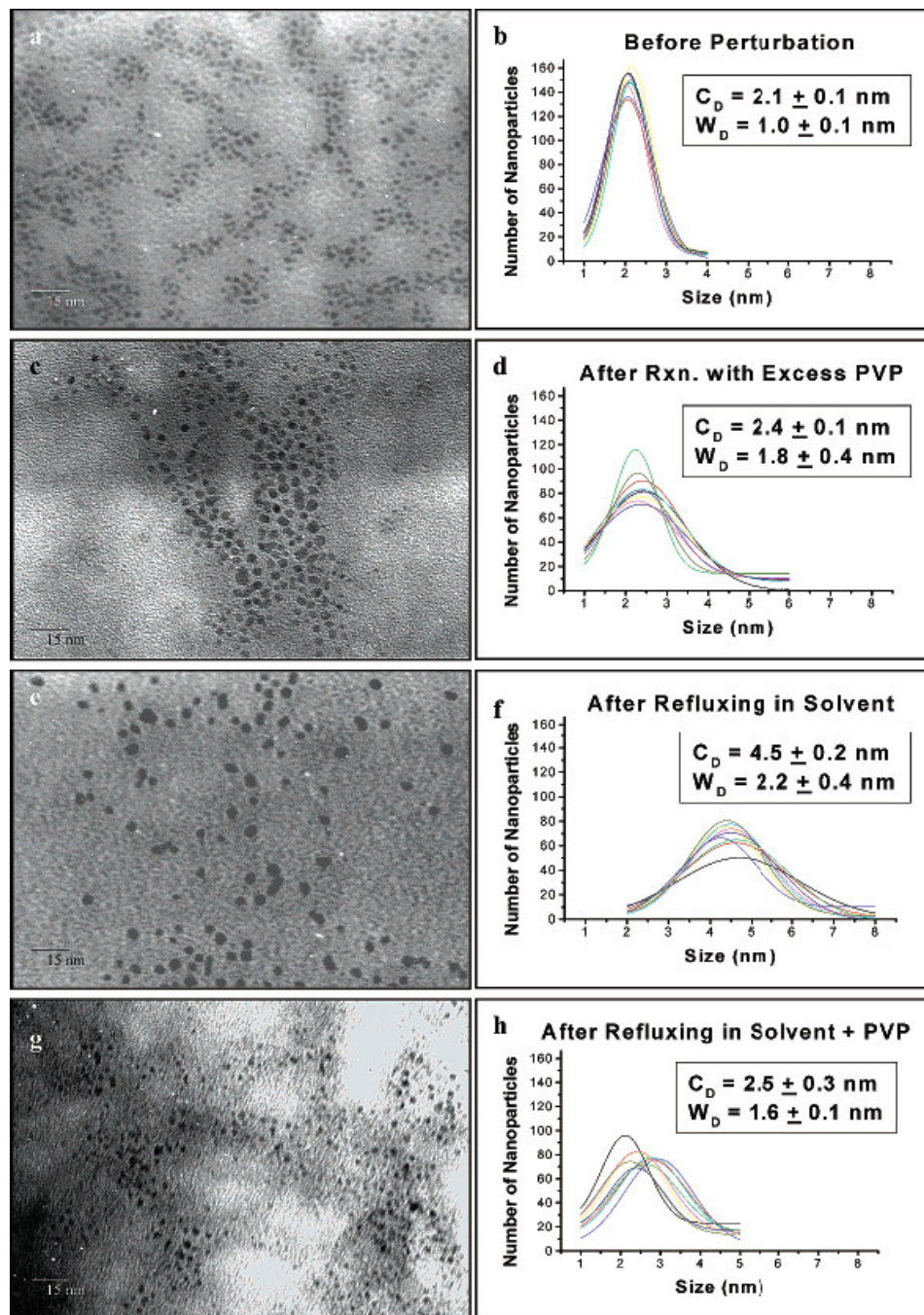


Figure 7.3—TEM images and Gaussian fits of PVP-Pd nanoparticles before any perturbations (a,b), after Suzuki reaction with excess PVP (c,d), after refluxing in just solvent (e,f), and after refluxing in just solvent + excess PVP (g,h)

Figure 7.3g shows a typical TEM image of the nanoparticles after refluxing in the presence of solvent and 0.5 g PVP and Figure 7.3h shows Gaussian fits of the size distributions. By comparing the Gaussian fits in Figure 7.3f, Figure 7.3h, and Table 7.1, it can be seen that the widths and centers of the size distributions of the nanoparticles still get larger but do not get as large as without the presence of the additional PVP which is shown in Figures 7.3e,f. It can also be seen that the addition of a large quantity of PVP (0.5 g) to the mixture greatly diminishes the Ostwald ripening process because the additional PVP present in the solution caps many of the free metallic surface sites in the nanoparticles. Since fewer sites are available for the Ostwald ripening process, the nanoparticles do not greatly increase in size.

7.4.3 Effect of Chemicals

For all the experiments, TEM images and Gaussian fits of the size distributions were obtained before each perturbation as shown in Table 7.1, but in order to concisely summarize the results in the figure, Figure 7.4a and Figure 7.4b show a typical TEM image and Gaussian fits of the PVP-Pd nanoparticles before any perturbations. Figure 7.4c shows a typical TEM image of the nanoparticles after refluxing them in the solvent + sodium acetate while Figure 7.4d shows Gaussian fits of the size distributions of the nanoparticles. As evident by comparing the Gaussian fits in Figure 7.4b, Figure 7.4d, and Table 7.1, the centers and widths of the size distributions increase after refluxing in solvent + sodium acetate. For this experiment, 0.49 g sodium acetate was added to 150 mL of 3:1 acetonitrile:water solvent. The increase in the size of the nanoparticles

observed is due to the Ostwald ripening process. Also, since there is no phenylboronic acid present to inhibit the Ostwald ripening process, the observed centers and widths of the distributions are larger than those observed after the first cycle of the Suzuki reaction. The impact of phenylboronic acid on the Ostwald ripening process is discussed next.

Figure 7.4e shows a typical TEM image of the nanoparticles after refluxing them in the presence of solvent + sodium acetate + phenylboronic acid. Figure 7.4f shows Gaussian fits of the size distributions of the nanoparticles. By comparing the Gaussian fits in Figure 7.4b, Figure 7.4f, and Table 7.1, it can be seen that the nanoparticles increase in size only slightly. The reason for this observation is that phenylboronic acid in the presence of the base sodium acetate is in the deprotonated form and as a result binds with the O⁻ of the OH group to the free sites in the Pd nanoparticles and acts as a capping material. When the phenylboronic acid binds to the free sites, it acts as a stabilizer and as a result greatly diminishes the Ostwald ripening process. The presence of phenylboronic acid also plays a role in the first cycle and second cycle of the Suzuki reaction. Because of the presence of phenylboronic acid, the Ostwald ripening process is not as prominent after the first cycle of the Suzuki reaction than in the presence of just the solvent, solvent + sodium acetate, and solvent + sodium acetate + iodobenzene. In the second cycle of the Suzuki reaction, the catalytic activity is greatly diminished which suggests that more phenylboronic acid is bound to the nanoparticles and as a result, the Ostwald ripening process is greatly diminished and the nanoparticles do not increase in size.

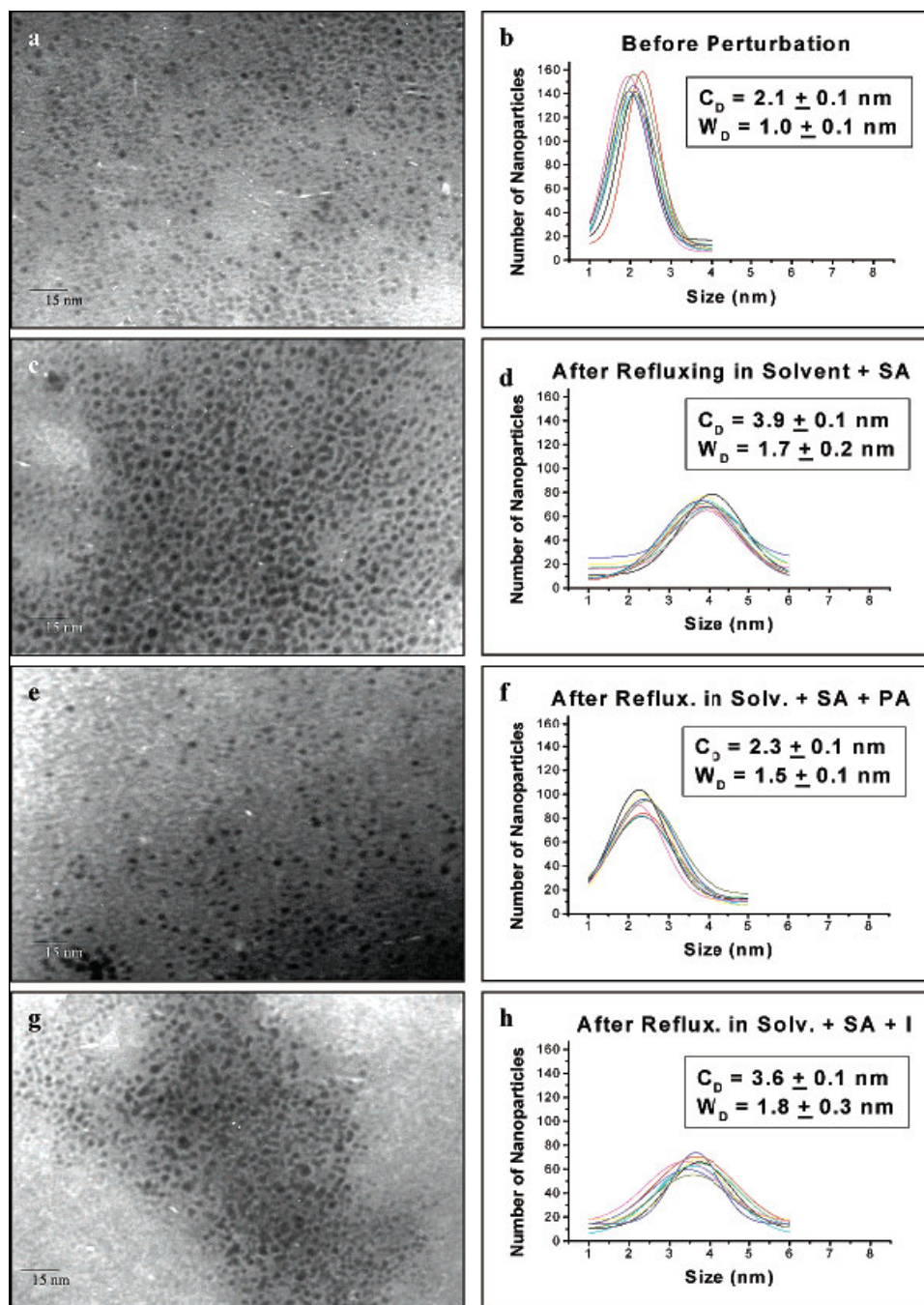


Figure 7.4—TEM images and Gaussian fits of PVP-Pd nanoparticles before any perturbations (a,b), after just solvent + sodium acetate (c,d), after just solvent + sodium acetate + phenylboronic acid (e,f), and after just solvent + sodium acetate + iodobenzene (g,h)

Figure 7.4g shows a typical TEM image of the nanoparticles after refluxing them in the presence of solvent + sodium acetate + iodobenzene and Figure 7.4h shows

Gaussian fits of the size distributions. By comparing the centers and widths of the size distributions shown in Figure 7.4b, Figure 7.4h, and Table 7.1, it can be seen that the nanoparticles do increase in size but do not get as large as after just refluxing in solvent. The Ostwald ripening process is responsible for the observed increase in the size of the nanoparticles that is observed. The iodobenzene does not bind to the surface of the nanoparticles and as a result does not inhibit the Ostwald ripening process. Also, phenylboronic acid is not present to inhibit the Ostwald ripening process.

It is evident that in the Suzuki reaction, phenylboronic acid binds to the surface of the palladium nanoparticles and iodobenzene does not. As a result, any catalytic mechanism for the Suzuki reaction between phenylboronic acid and iodobenzene has to propose that phenylboronic acid binds to the surface of the nanoparticles and then the reaction with iodobenzene occurs by collisional processes.

7.5 Conclusions

The center and width of the size distribution of the PVP-Pd nanoparticles increases after the first cycle of the Suzuki reaction. The process of refluxing the nanoparticles during the Suzuki reaction seems to cause Ostwald ripening in which the size of nanoparticles increases at the expense of the smaller ones due to atomization and diffusion between particles. The nanoparticles increase in size during the beginning of the reaction and levels off toward the end of the first cycle. After the second cycle of the reaction, the center and width of the size distribution of the nanoparticles becomes much smaller. This observation is explained by the aggregation and precipitation of the larger nanoparticles leaving the smaller nanoparticles in solution. As a result, the catalytic

efficiency of the nanoparticles during the second cycle is diminished. The smaller nanoparticles in solution do not increase in size due to the presence of a greater amount of phenylboronic acid bound to the free sites which decreases their catalytic activity. It is also found that the presence of biphenyl product in the reaction mixture results in it poisoning the active sites and giving rise to a low product yield. The addition of PVP stabilizer to the reaction mixture diminishes the Ostwald ripening process as well as diminishes the catalytic activity of the nanoparticles. This is due to the binding to the surface and prevents the adsorption of new metallic atoms or the use in catalysis.

Ostwald ripening of the nanoparticles also occurs when the sodium acetate base is present along with the solvent. The presence of phenylboronic acid, one of the reactants, inhibits the Ostwald ripening process since it binds to the nanoparticle surface through the O⁻ of its ionized OH group and acts as a stabilizer. Ostwald ripening of the nanoparticles occurs in the presence of iodobenzene, the other reactant. Thus, iodobenzene does not seem to strongly bind to the surface of the nanoparticles. As result, any catalytic mechanism for the Suzuki reaction between phenylboronic acid and iodobenzene has to consider proposing that the phenylboronic acid binds to the surface and then reacts with iodobenzene via collisional processes.

7.6 References

1. Eppler, A.; Rupprechter, G.; Guzzi, L.; Somorjai, G. A. *J. Phys. Chem. B* **1997**, *101*(48), 9973.
2. Toshima, N.; Yonezawa, T. *New J. Chem.* **1998**, *22*(11), 1179.
3. Schmid, G. *Met. Clus. Chem.* **1999**, *3*, 1325.
4. Puddephatt, R. J. *Met. Clus. Chem.* **1999**, *2*, 605.

5. Henry, C. R. *Appl. Surf. Sci.* **2000**, *164*, 252.
6. St. Clair, T. P.; Goodman, D. W. *Top. Catal.* **2000**, *13(1,2)*, 5.
7. Kralik, M.; Corain, B.; Zecca, M. *Chem. Pap.* **2000**, *54(4)*, 254.
8. Chusuei, C. C.; Lai, X.; Luo, K.; Goodman, D. W. *Top. Catal.* **2001**, *14(1-4)*, 71.
9. Bowker, M.; Bennett, R. A.; Dickinson, A.; James, D.; Smith, R. D.; Stone, P. *Stud. Surf. Sci. Catal.* **2001**, *133*, 3.
10. Kralik, M.; Biffis, A. *J. Mol. Catal. A: Chem.* **2001**, *177(1)*, 113.
11. Thomas, J. M.; Raja, R. *Chem. Rec.* **2001**, *1(6)*, 448.
12. Mohr, C.; Claus, P. *Sci. Prog.* **2001**, *84(4)*, 311.
13. Thomas, J. M.; Johnson, B. F. G.; Raja, R.; Sankar, G.; Midgley, P. A. *Acc. Chem. Res.* **2003**, *36(1)*, 20.
14. Bradley, J. S. *Clus. Colloids* **1994**, 459.
15. Duff, D. G.; Baiker, A. *Stud. Surf. Sci. Catal.* **1995**, *91*, 505.
16. Toshima, N. *NATO ASI Ser., Ser. 3* **1996**, *12*, 371.
17. Boennermann, H.; Braun, G.; Brijoux, G. B.; Brinkman, R.; Tilling, A. S.; Schulze, S. K.; Siepen, K. *J. Organomet. Chem.* **1996**, *520(1-2)*, 143.
18. Fugami, K. *Organomet. News* **2000**, *1*, 25.
19. Mayer, A. B. R. *Polym. Adv. Technol.* **2001**, *12(1-2)*, 96.
20. Bonnemann, H.; Richards, R. *Syn. Meth. Organom. Inorg. Chem.* **2002**, *10*, 209.
21. Moiseev, I. I.; Vargaftik, M. N. *Russ. J. Chem.* **2002**, *72(4)*, 512.
22. Collier, P. J.; Iggo, J. A.; Whyman, R. *J. Mol. Catal. A: Chem.* **1999**, *146(1-2)*, 149.
23. Sculz, J.; Roucoux, A.; Patin, H. *Chem. Eur. J.* **2000**, *6(4)*, 618.
24. Wang, Q.; Liu, H.; Han, M.; Li, X.; Jiang, D. *J. Mol. Catal. A: Chem.* **1997**, *118(2)*, 145.
25. Kim, S.; Son, S. U.; Lee, S. S.; Hyeon, T.; Chung, Y. K.; *Chem. Commun.* **2001**, 2212.
26. Larpent, C.; Menn, B. F.; Patin, H. *J. Mol. Catal.* **1991**, *65*, L35.

27. Chechik, V.; Crooks, R. M. *J. Am. Chem. Soc.* **2000**, *122*, 1243.
28. Yeung, L. K.; Crooks, R. M. *Nano Lett.* **2001**, *1(1)*, 14.
29. Dupont, J.; Fonseca, G. S.; Umpierre, A. P.; Fichtner, P. F. P.; Teixeira, S. R. *J. Am. Chem. Soc.* **2002**, *124*, 4228.
30. Hirai, H.; Chawanya, H.; Toshima, N. *Nip. Kag. Kai.* **1984**, *6*, 1027.
31. Roucox, A.; Sculz, J.; Patin, H. *Chem. Rev.* **2002**, *102(10)*, 3757.
32. Miyaura, N.; Yanagi, T.; Suzuki, A. *Synth. Commun.* **1981**, *11*, 513.
33. Suzuki, A. In *Metal-Catalyzed Cross-Coupling Reactions*; Diederich, F., Stang, P. J., Eds.; VCH: Weinheim, 1998, pp 49.
34. Alo, B. I.; Kandil, A.; Patil, P. A.; Sharp, M. J.; Siddiqui, M. A.; Snieckus, V. *J. Org. Chem.* **1991**, *56*, 3763.
35. Wallow, T. I.; Novak, B. M.; *J. Org. Chem.* **1994**, *59*, 5034.
36. Bumagin, N. A.; Bykov, V. V.; Beletskaya, I. P.; *Dokl. Akad. Nauk. SSSR* **1990**, *315*, 1133.
37. Marck, G.; Villiger, A.; Buchecker, R. *Tetrahedron Lett.* **1994**, *35*, 3277.
38. Reetz, M. T.; Breinbauer, R.; Wanninger, K. *Tetrahedron Lett.* **1996**, *26*, 4499.
39. Li, Y.; Hong, X. M.; Collard, D. M.; El-Sayed, M. A. *Org. Lett.* **2000**, *2(15)*, 2385.
40. Li, Y.; Boone, E.; El-Sayed, M. A. *Langmuir* **2002**, *18*, 4921.
41. Li, Y.; El-Sayed, M. A. *J. Phys. Chem. B* **2001**, *105*, 8938.
42. Moreno-Manas, M.; Pleixats, R.; Villarroja, S. *Organomet.* **2001**, *20(22)*, 4524.
43. Kogan, V.; Aizenshtat, Z.; Popovitz-Biro, R.; Neumann, R. *Org. Lett.* **2002**, *4(20)*, 3529.
44. Strimbu, L.; Liu, J.; Kaifer, A. E. *Langmuir* **2003**, *19*, 483.
45. Teranishi, T.; Miyake, M. *Chem. Mat.*, **1998**, *10*, 594.
46. Howard, A.; Mitchell, C. E. J.; Egdell, R. G. *Surf. Sci.* **2002**, *515*, L504.

47. Imre, A.; Beke, D. L.; Gontier-Moya, E.; Szabo, I. A.; Gillet, E. *Appl. Phys. A* **2000**, *71*, 19.

CHAPTER 8

EFFECT OF COLLOIDAL CATALYSIS ON THE NANOPARTICLE SIZE DISTRIBUTION: DENDRIMER-PD VS. PVP-PD NANOPARTICLES CATALYZING THE SUZUKI REACTION

8.1 Abstract

A comparison of the stability and catalytic activity of PAMAM-OH Generation 4 dendrimer-Pd nanoparticles (1.3 ± 0.1 nm) with the previously studied PVP-Pd nanoparticles (2.1 ± 0.1 nm) in the Suzuki coupling reaction between phenylboronic acid and iodobenzene is conducted. After the first cycle, the average size of the PVP-Pd nanoparticles increases by 38% and the dendrimer-Pd nanoparticles increase by 54%. After the second cycle, the PVP-Pd nanoparticles decrease in size by 24% while the dendrimer-Pd nanoparticles continue to increase in size by 35%. The strong encapsulating action of the PAMAM-OH Generation 4 dendrimer-Pd nanoparticles could make the rate of conversion to the full nanoparticle size slow resulting in a large excess Pd metal atom concentration in solution resulting in the continuous growth of the nanoparticles during the catalytic reaction.

The effect of the individual reactants on the stability of the dendrimer-Pd nanoparticles have also been investigated and found to be similar to that observed for the PVP-Pd nanoparticles previously. It was found that the nanoparticle size growth occurs while refluxing in the presence of only the solvent, sodium acetate, or iodobenzene. However, the presence of phenylboronic acid is found to inhibit the particle growth, suggesting that it acts as a capping agent. Thus, the surface catalytic mechanism must

involve the adsorption of phenylboronic acid to the nanoparticle surface which subsequently reacts with the iodobenzene in solution. This is similar to the catalytic mechanism found previously on PVP-Pd nanoparticles, suggesting that the mechanism of surface catalysis is insensitive to the capping material used.

The ratio of the yield of biphenyl formed in the second cycle to that in the first cycle is higher for the dendrimer-Pd nanoparticles catalyzed reaction than for the PVP-Pd nanoparticles. This could be due to the greater stability of the dendrimer-Pd nanoparticles and the increase in its size during the reaction. The larger PVP-Pd nanoparticles studied previously is believed to aggregate and precipitate out of solution during the second cycle. The presence of excess dendrimer is found to severely diminish the catalytic activity of the dendrimer-Pd nanoparticles and also diminishes the change in the Pd nanoparticle size during the catalysis.

8.2 Introduction

Due to their large surface to volume ratio, nanoparticles offer higher catalytic efficiency per gram than a larger size material. The field of nanocatalysis has been very active lately with numerous review articles published during the past decade in both heterogeneous catalysis in which the nanoparticles are supported on solid surfaces (e.g. silica or alumina)¹⁻¹³ and in homogeneous catalysis with colloidal nanoparticles¹⁴⁻²¹. Being small in size is expected to increase the nanoparticle surface tension. This makes surface atoms very active. Are they active enough to change the size and shape of the nanoparticles during catalysis? In the bulk of the catalysis with colloids, TEM characterization of the nanoparticles before and after catalysis is not given. However,

there are a few studies in the literature where size distribution of the nanoparticles after recycling along with the catalytic activity is reported for characterization²²⁻²⁸. There have also been some papers that discuss the catalytic activity of the nanoparticles upon recycling, but which do not examine the stability of the nanoparticles after catalysis²⁹⁻³². In a review of transition metal colloids as reusable catalysts,³³ it was pointed out that the major interest of the reusability of nanoparticle catalysts has not been systematically studied or published in the metal colloid literature.

There have been very few detailed studies in the literature that examine the stability and catalytic activity of metal nanoparticles in colloidal solution which are used to catalyze various organic and inorganic reactions. In our previous study²² conducted with PVP-Pd nanoparticles catalyzing the Suzuki reaction between phenylboronic acid and iodobenzene, it was found that after the first cycle of the reaction, the nanoparticles increased in size, and this was attributed to the Ostwald ripening process. After the second cycle of the reaction, the nanoparticle size decreases and this was attributed to the larger nanoparticles aggregating and precipitating out of solution. It was also found that the Ostwald ripening process occurs in the presence of iodobenzene, while in the presence of phenylboronic acid, the process is greatly diminished. As a result, it was proposed that the surface catalytic mechanism involves phenylboronic acid binding to the nanoparticle surface and reacting with iodobenzene in solution.

The previous study with PVP-Pd nanoparticles raises some additional interesting questions. Does the method of preparing the nanoparticles used to catalyze the Suzuki reaction affect the particle growth process? Does the capping agent used affect the proposed catalytic mechanism of the Suzuki reaction? How does the change in the size

of the nanoparticles during the second cycle of the reaction affect the biphenyl product yield?

In order to shed light to these questions, the stability and catalytic activity of PAMAM-OH Generation 4 dendrimer capped Pd nanoparticles is examined and compared to those of the PVP-Pd nanoparticles studied previously. The use of dendrimer stabilized nanoparticles for catalyzing reactions has been a fairly recent activity. The first report of the use of dendrimers as capping agents in the preparation of metal nanoparticles is by the Crooks group³⁴. A few examples of reactions catalyzed by dendrimer encapsulated nanoparticles include hydrogenation of olefins³⁵⁻³⁷, Heck reactions³⁸, oxidation reactions³⁹, reduction reactions⁴⁰, and Suzuki reactions⁴¹. In a previous study⁴¹, PAMAM-OH Generation 2, 3, and 4 dendrimers have been used as stabilizers for Pd nanoparticles in an effort to understand the effect of dendrimer generation on the catalytic activity of the nanoparticles catalyzing the Suzuki reaction. It was found that Generation 2 dendrimers do not provide effective protective action while Generation 3 and 4 dendrimers are good stabilizers. Palladium in PAMAM-OH Generation 4 dendrimers is found to be the best catalyst because the dendrimer stabilizes the metal nanoparticles by preventing their agglomeration but it does not fully passivate the metal surface. A desirable property in a colloidal catalyst is to be small and stable, but with a nanoparticle surface that is not fully passivated so that reactants can access the encapsulated clusters.

The PAMAM-OH Generation 4 dendrimer-Pd nanoparticles are prepared using the sodium borohydride reduction method while the PVP-Pd nanoparticles in the previous study²² were prepared using the ethanol reduction method. The aim of this

paper is to study how the method of synthesizing the nanoparticles affects the particle growth process, how the capping agent affects the mechanism of surface catalysis, and how the size of the nanoparticles during the second cycle of the reaction affects the biphenyl product yield.

8.3 Experimental Section

8.3.1 Synthesis of PAMAM-OH Dendrimer Stabilized Pd Nanoparticles

The PAMAM-OH dendrimer stabilized Pd nanoparticles were synthesized in a similar manner to that described previously⁴¹. The dendrimer solution was rotovaped to remove the methanol solvent. A 1 mM aqueous solution of the dendrimer and a 3 mM solution of K_2PdCl_4 were prepared. To prepare the nanoparticles, 90 mL of the dendrimer solution was added to 30 mL of the K_2PdCl_4 solution. The solution is stirred under nitrogen for five minutes. Then, 2 mL of 0.36 M of sodium borohydride is added to the solution. The solution is stirred vigorously under nitrogen atmosphere for 1 hour. The 120 mL volume of nanoparticle solution was diluted to a total volume of 150 mL by adding 30 mL of doubly deionized water. The dilution was done so that the concentration of the initial Pd ions in the dendrimer capped nanoparticles would be the same as for the PVP-Pd nanoparticles studied previously for comparison purposes. The diluted dendrimer-Pd nanoparticle solution was used for all of the experiments conducted. JEOL 100C TEM is used to determine the average size and distribution of the nanoparticles.

8.3.2 Suzuki Reaction between Phenylboronic Acid and Iodobenzene

The Suzuki reaction between phenylboronic acid and iodobenzene was catalyzed using the PAMAM-OH Generation 4 dendrimer capped Pd nanoparticles as described previously⁴¹⁻⁴³. For this reaction, 0.49 g (6 mmol) of sodium acetate, 0.37 g (3 mmol) of phenylboronic acid, and 0.20 g (1 mmol) of iodobenzene was added to 150 mL of 3:1 acetonitrile:water solvent. The solution was heated to 100 °C and 5 mL of the dendrimer capped Pd nanoparticles was added to start the reaction. The reaction mixture was refluxed for a total of 12 hours.

The same reaction mixture solution was used for recycling after the addition of fresh amounts of the reactants. For recycling, an assumption was made that all of the iodobenzene was used up since it is the limiting reactant. Initially there is 1 mmol iodobenzene and 3 mmol phenylboronic acid present in the reaction mixture. After the first cycle, it is assumed that there is no iodobenzene left and that there are 2 mmol phenylboronic acid left. As a result, for the second cycle, 1 mmol iodobenzene and 1 mmol phenylboronic acid were added. The reaction mixture was then refluxed for another 12 hours to complete the second cycle.

8.3.3 TEM Studies

To examine the changes in the size distribution of the nanoparticles during the catalysis, samples of the reaction mixture before and after refluxing for 12 hours were spotted onto Formvar stabilized copper TEM grids. The JEOL 100C TEM was used to determine the average widths and centers of the size distributions of the dendrimer-Pd

nanoparticles after the first and second catalytic cycles. The effect of the amount of reduction time in synthesizing the nanoparticles is also examined. In addition, TEM was also used to examine the effect of the different chemicals present during the Suzuki reaction. The effects of refluxing for 12 hours on the nanoparticle size distribution of the dendrimer-Pd nanoparticles in the presence of the solvent alone, in the solvent + sodium acetate, in the solvent + sodium acetate + phenylboronic acid, and in the solvent + sodium acetate + iodobenzene were investigated. The impact of adding excess dendrimer to the Pd nanoparticle solution before the reaction was also investigated.

For all of the above experiments, the concentration of the Pd ions present initially in the nanoparticles is 6.00×10^{-4} M and when 5 mL of the nanoparticles is added to 150 mL of the 3:1 acetonitrile:water solvent, the concentration of the Pd ions present initially is 1.94×10^{-5} M. For the experiments, the samples were spotted by placing a drop of the solution onto a Formvar stabilized copper grid and allowed to evaporate in air. The spotted samples take approximately 30 minutes to dry. Since the same deposition conditions are employed for all samples, the evaporation rate of the solvent is fairly reproducible from one sample to another. For each of the experiments, the internal reproducibility of the observed particle size and distribution was verified by spotting the sample onto 3 separate TEM grids. TEM images were also obtained from different sections of the TEM grids to verify the reproducibility of the particle size and distribution. The general reproducibility of the observed particle size and distribution was verified by conducting each experiment 3 times. As a result, it is possible to compare the particle size and distribution changes under various conditions.

The nanoparticle size and distribution was determined by counting approximately 1800 nanoparticles from 9 enlarged TEM images (approximately 200 nanoparticles from each TEM image). The size distribution plots were fit using a Gaussian model with Microcal Origin 5.0 graphing software in order to determine the widths and centers of the size distributions. The width of the distribution gives an idea of how narrow or wide the size distribution is and the center of the distribution is the most probable or average size of the nanoparticles (depending on the shape of the distribution).

8.3.4 HPLC Studies

The determination of the concentration of biphenyl product and thus the reaction yield were carried out by using the Hitachi-4500 HPLC equipped with a L4500A diode array detector in which the absorbance at 254 nm was monitored. The separation was carried out on a reversed-phase packed column (Rainin Microsorb-MV C18, 300 Angstroms, dim 4.6 x 250 mm) using a 60:40 acetonitrile-water mixture and a flow rate of 1 mL/min. The area of the chromatographic peaks was calculated with a D-6000 interface-integrator. A calibration curve for determining the concentration of biphenyl was constructed by plotting the peak area vs. concentration of biphenyl standards. The standards prepared were 0.0005 M, 0.001 M, 0.0015 M, 0.002 M, 0.0025 M, and 0.003 M biphenyl. For HPLC measurements, all samples were diluted to $\frac{1}{4}$ of the original concentration so that the peak areas will be within the range of the calibration curve. The concentration of biphenyl was determined before the first cycle, after the first cycle, before the second cycle, and after the second cycle. Also, the effect of the presence of excess dendrimer on the amount of biphenyl formed was also determined.

8.4 Results and Discussion

8.4.1 Effect of Nanoparticle Preparation Method on the Particle Size Growth

In our previous study of the Suzuki reaction between phenylboronic acid and iodobenzene conducted using PVP-Pd nanoparticles²², it was found that after the first cycle of the reaction, the center of distribution increased by $38 \pm 10\%$ and the width of distribution increased by $155 \pm 18\%$. This was attributed to Ostwald ripening²² of the nanoparticles i.e. a result of dissolving the small sized nanoparticles to feed the growth of the larger ones that have lower surface tension. It also could result from the presence of metal atoms in solution which continues to deposit on the nanoparticle surface. Of course, if the mechanism of the particle growth involves the reduction of the metal ions on the surface of the nanoparticle, excess metal ions in solution could lead to the observed nanoparticle size during the catalytic reaction.

After the second cycle of the reaction, the centers of distribution actually decreases by $24 \pm 3\%$ and the widths of distributions decrease by 68% compared to the size during the first cycle. This decrease in size was attributed to the aggregation of larger Pd nanoparticles leading to its precipitating out of solution leaving only the smaller nanoparticles in solution. Table 1 summarizes the center and width of the size distribution before and after the different conditions. The percentage increase/decrease in the centers and widths of distributions after the first and second cycle are summarized in Table 8.2.

Table 8.1—Summary of widths and centers of size distributions of PAMAM-OH generation 4 dendrimer capped Pd nanoparticles before and after different perturbations (SA = sodium acetate, PA = phenylboronic acid, and I = iodobenzene)

Condition	Before Width (nm)	After Width (nm)	Before Center (nm)	After Center (nm)
Suzuki Reaction	0.7 ± 0.1	After first cycle 2.2 ± 0.2	1.3 ± 0.1	After first cycle 2.0 ± 0.1
		After second cycle 2.5 ± 0.1		After second cycle 2.7 ± 0.1
Suzuki Reaction in Presence of Dendrimer	0.7 ± 0.1	1.3 ± 0.2	1.4 ± 0.1	1.7 ± 0.1
Reflux in Solvent	0.7 ± 0.1	1.6 ± 0.2	1.3 ± 0.1	2.5 ± 0.1
Reflux in Solvent + Dendrimer	0.7 ± 0.1	1.5 ± 0.2	1.3 ± 0.1	1.7 ± 0.1
Reflux in Solvent + SA	0.8 ± 0.1	2.0 ± 0.2	1.3 ± 0.1	2.1 ± 0.3
Reflux in Solvent + SA + PA	0.7 ± 0.1	0.8 ± 0.1	1.3 ± 0.1	1.5 ± 0.1
Reflux in Solvent + SA + I	0.7 ± 0.1	1.3 ± 0.2	1.3 ± 0.1	2.3 ± 0.2

Table 8.2—Comparison of the percentage change in the centers and widths of distributions for the PVP-Pd nanoparticles and the PAMAM-OH Generation 4 Dendrimer-Pd nanoparticles as a result of catalyzing the Suzuki reaction

Condition	% Increase (+)/% Decrease (-) in C_D and W_D of PVP-Pd Nanoparticles (Initially: 2.1 ± 0.1 nm) ²²	% Increase (+)/% Decrease (-) in C_D and W_D of Dendrimer-Pd Nanoparticles (Initially: 1.3 ± 0.1 nm)
First Cycle of Suzuki Reaction	$(C_D = +38 \pm 10\%)$ $(W_D = +155 \pm 18\%)$	$(C_D = +54\%)$ $(W_D = +186\%)$
Second Cycle of Suzuki Reaction	$(C_D = -24 \pm 3\%)$ $(W_D = -68\%)$	$(C_D = +35\%)$ $(W_D = +14\%)$

The stability of the PAMAM-OH Generation 4 dendrimer capped Pd nanoparticles after the first and second cycle of the Suzuki reaction was also investigated to gain a better understanding of the nanoparticle growth process. Table 8.1 summarizes the centers and widths of the distributions determined from Gaussian fits for various perturbations that were conducted. Figure 8.1a and 8.1b show typical TEM image and Gaussian fits of the size distributions of PAMAM-OH Generation 4 dendrimer capped Pd nanoparticles before the Suzuki reaction. It can be seen that the nanoparticles are very small in size (1.3 ± 0.1 nm) and also reasonably monodisperse. These nanoparticles are smaller in size than the PVP-Pd nanoparticles²² (2.1 ± 0.1 nm) studied previously. Figure 8.1c and 8.1d show typical TEM image and Gaussian fits of the dendrimer capped Pd nanoparticles after the first cycle of the Suzuki reaction. Table 8.2 summarizes the percentage increase/decrease in the centers and widths of distributions after the first and second cycle. Both the centers and widths of the size distributions increase by 54% and 186% respectively, after the first cycle of the reaction. This increase in size of the nanoparticles could be attributed to Ostwald ripening of the nanoparticles. Figure 8.1e and 8.1f show representative TEM image and Gaussian fits of the nanoparticles after the second cycle of the Suzuki reaction. During the second cycle, the dendrimer-Pd nanoparticles continue to increase in size with a 35% increase in the center and a 14% increase in the width of the distribution compared to the first cycle. This suggests that when the dendrimer-Pd nanoparticles are used, the growth process continues during the second cycle of the Suzuki reaction. The mechanism of the growth of the palladium nanoparticles is discussed in the next section.

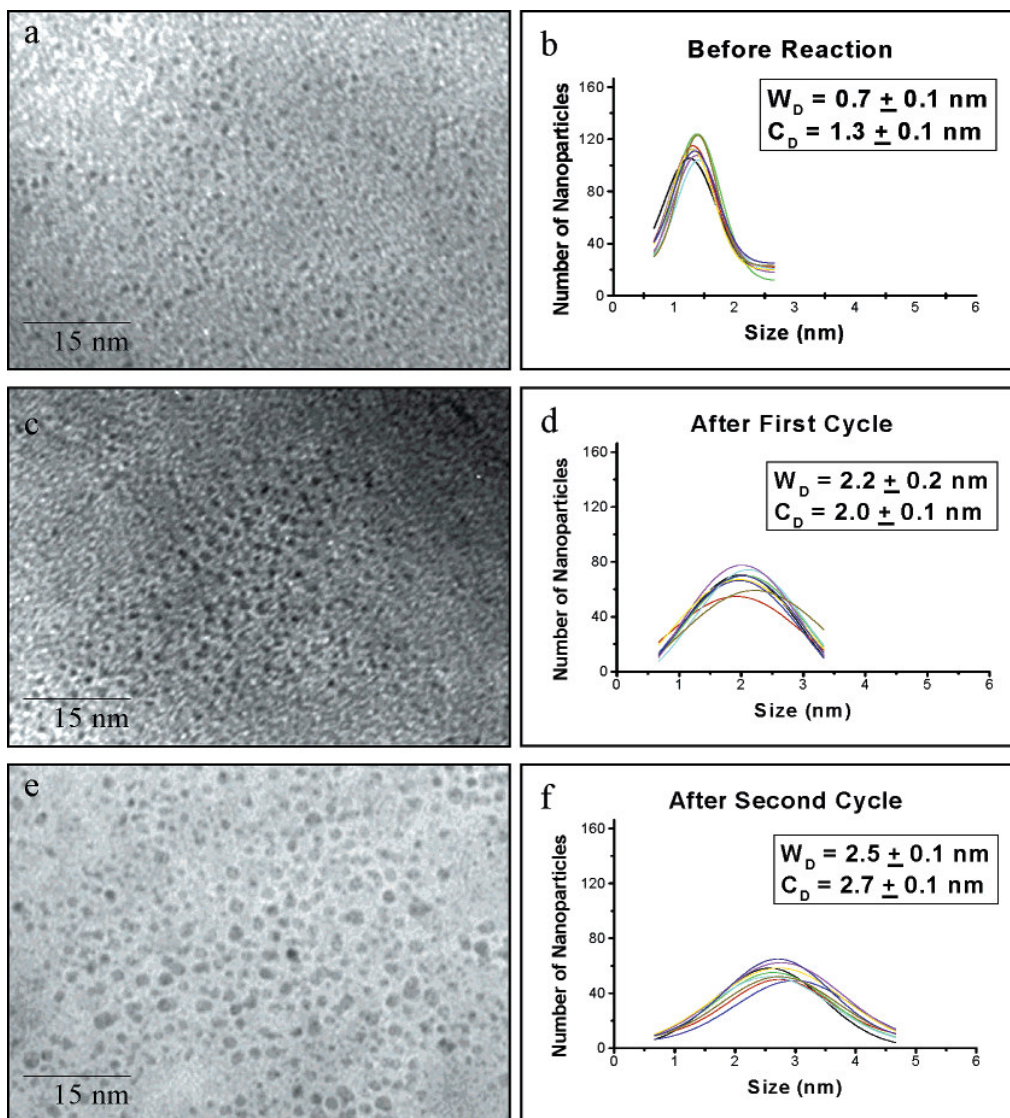


Figure 8.1—TEM images and Gaussian fits of size distributions of PAMAM-OH dendrimer-capped Pd nanoparticles before the Suzuki reaction (a, b), after the first cycle (c, d), and after the second cycle (e, f).

8.4.2 Mechanism of Growth of the Palladium Nanoparticles

There are several possibilities that could result in the large growth of the dendrimer-Pd nanoparticles such as high metal or metal ion concentration in solution resulting from the synthetic procedure, a large nanoparticle distribution in the beginning, and better capping making the rate of conversion to full nanoparticles slow, thus leading

to an increase in the metal or metal ion concentration in the final solution. The large initial particle distribution could result in growth by Ostwald ripening processes. The Ostwald ripening process is a mechanism for cluster growth in which there is detachment of atoms from the smaller clusters and attachment to the lower energy surfaces of the larger clusters. The smaller clusters shrink or disappear completely while the larger clusters grow in size and will eventually lead to larger nanoparticles with smaller width of distribution (more monodisperse).

It is worth noting that the PVP-Pd nanoparticles we studied previously²² were synthesized using the ethanol reduction method while the PAMAM-OH Generation 4 dendrimer capped Pd nanoparticles were synthesized using the sodium borohydride reduction method. The two types of nanoparticles were synthesized using two different reduction methods. Different methods of preparing nanoparticles vary in their degree of conversion of the metal ion into capped nanoparticles. PAMAM-OH Generation 4 dendrimer-Pd nanoparticles are known to be very strong encapsulators of metal clusters⁴⁰. Since the synthesis of the dendrimer-Pd nanoparticles occurs at room temperature, it is quite possible that the rate of conversion to full nanoparticle is slow, thus leading to an increase in the metal or metal ion concentration in the final solution. This could also explain why the dendrimer-Pd nanoparticles are very small to begin with. During the Suzuki reaction, it is possible that the nanoparticles continue to grow in size since the rate of conversion to full nanoparticle is greater due to the high temperature and long reflux time period involved. This can also explain the continued growth of the nanoparticle size during the second cycle. The growth of the nanoparticles is expected to continue until the source of free metal is depleted. Since the widths of the size distributions of the

dendrimer-Pd nanoparticles are broad both during the first and second cycle as shown in Figure 8.1c-f, Table 8.1, and Table 8.2, the growth of the nanoparticles is not dominantly due to Ostwald ripening process, but is largely due to the excess atoms or ions in solution during the catalytic reaction.

In order to test our hypothesis that the growth of the nanoparticles is due to the presence of unreduced ions, partly reduced ions, and metal atoms in solution after the synthesis of the nanoparticles, we conducted the reaction with dendrimer-Pd nanoparticles synthesized by reduction for 30 minutes and 3 hours at room temperature. We also conducted the reaction with dendrimer-Pd nanoparticles synthesized by reduction for 1 hour at 100 degrees Celsius. The standard procedure reported in the literature⁴¹⁻⁴³ for synthesizing dendrimer-Pd nanoparticles involves reduction for 1 hour at room temperature, which is what we based all of our experiments on. The goal now is to see if the growth process is affected by the amount of reduction time or the reduction temperature at which the nanoparticles are initially synthesized. Table 8.3 summarizes the average size and widths of distributions of the dendrimer-Pd nanoparticles before the reaction, after the first cycle, and after the second cycle for the following synthetic conditions (reduction for 30 minutes at room temperature, reduction for 1 hour at room temperature (standard procedure), reduction for 3 hours at room temperature, and reduction for 1 hour at 100 degrees Celsius). Figure 8.2 a-h shows typical TEM images and Gaussian fits of the size distributions of the dendrimers-Pd nanoparticles after the second cycle for the four different synthetic conditions. The entry for 1 hour at room temperature in Table 8.3 is repeated from Table 8.1 and the TEM image and Gaussian fits in Figure 8.2c-d is repeated from Figure 8.1e-f for comparison purposes. It can be seen

that the general trend observed is that the growth of the dendrimer-Pd nanoparticles is the greatest using the nanoparticles reduced for only 30 minutes and the growth is the lowest when the nanoparticles are reduced for 1 hour at 100 degrees Celsius. This suggests that reduction at room temperature for a longer time period and reduction at 100 degrees Celsius results in a more complete reduction of the precursor palladium salt. As a result, there are less free metal atoms and ions present in solution to contribute to the growth during the reaction. This trend supports our hypothesis that the growth process is dependant on the amount of free atoms or ions present after the synthetic process.

Table 8.3—Comparison of center and width of size distributions of dendrimer-Pd nanoparticles synthesized with various reduction times and temperatures before the reaction, after the first cycle, and after the second cycle

Condition	Before Reaction (nm)	After First Cycle (nm)	After Second Cycle (nm)
Reduced 30 minutes at room temperature	$C_D = 1.4 \pm 0.1$ $W_D = 0.7 \pm 0.1$	$C_D = 2.1 \pm 0.1$ $W_D = 2.4 \pm 0.2$	$C_D = 2.9 \pm 0.1$ $W_D = 2.8 \pm 0.4$
Reduced 1 hour at room temperature	$C_D = 1.3 \pm 0.1$ $W_D = 0.7 \pm 0.1$	$C_D = 2.0 \pm 0.1$ $W_D = 2.2 \pm 0.2$	$C_D = 2.7 \pm 0.1$ $W_D = 2.5 \pm 0.1$
Reduced 3 hours at room temperature	$C_D = 1.4 \pm 0.1$ $W_D = 0.7 \pm 0.1$	$C_D = 2.0 \pm 0.2$ $W_D = 1.9 \pm 0.1$	$C_D = 2.5 \pm 0.1$ $W_D = 2.2 \pm 0.2$
Reduced 1 hour at 100 degrees C	$C_D = 1.5 \pm 0.1$ $W_D = 0.7 \pm 0.1$	$C_D = 1.8 \pm 0.1$ $W_D = 1.7 \pm 0.2$	$C_D = 2.1 \pm 0.1$ $W_D = 2.0 \pm 0.2$

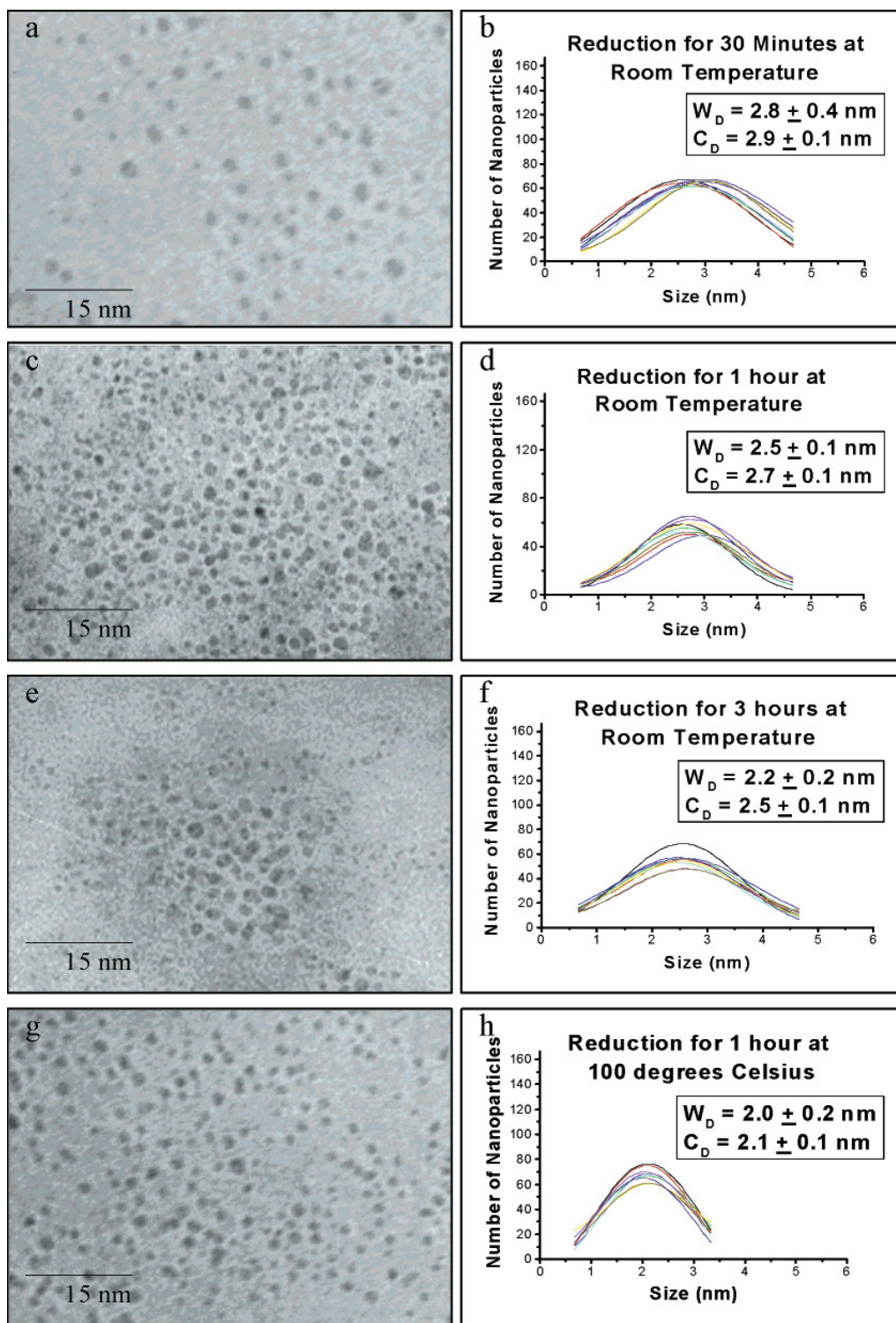


Figure 8.2—Typical TEM images and Gaussian fits of the size distributions after the second cycle of the Suzuki reaction for dendrimer-Pd nanoparticles synthesized in the following manners: reduction for 30 min at room temperature (a, b), reduction for 1 h at room temperature (c, d), reduction for 3 h at room temperature (e, f), and reduction for 1 h at 100 °C (g, h).

8.4.3 Effect of Capping Agent on Catalytic Mechanism of Suzuki Reaction

For the PVP-Pd nanoparticles catalyzing the Suzuki reaction studied previously²², it was determined that the Ostwald ripening process occurred when refluxing in the presence of iodobenzene, while refluxing in the presence of phenylboronic acid results in the inhibition of the nanoparticle size growth. It was proposed that phenylboronic acid binds to the nanoparticle surface and acts as a capping agent, which protects the particles from increasing in size. The catalytic mechanism was proposed to involve the phenylboronic acid binding to the nanoparticle surface while reaction with iodobenzene occurs via collisional processes.

The stability of the PAMAM-OH Generation 4 dendrimer capped palladium nanoparticles in the presence of various chemicals involved in the Suzuki reaction (solvent, sodium acetate, phenylboronic acid, and iodobenzene) was investigated to find out if the surface catalytic mechanism is affected by the capping agent that is used on the palladium nanoparticles. TEM images and Gaussian fits of the size distributions of the nanoparticles were obtained before each perturbation and the results are summarized in Table 8.1. In order to concisely summarize the results, the TEM images and Gaussian fits of the size distributions of the dendrimer-Pd nanoparticles after the different perturbations are shown in Figure 8.3.

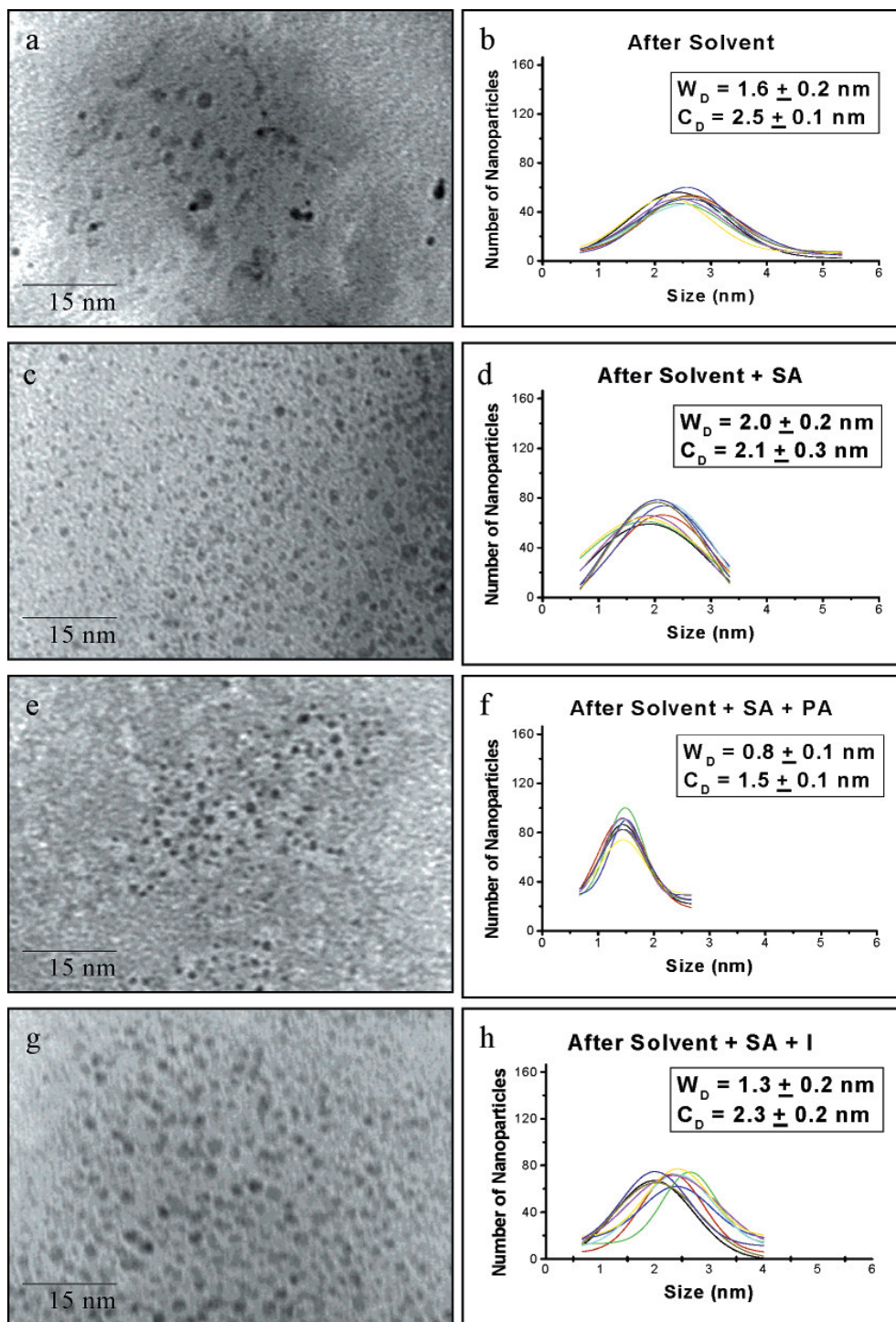


Figure 8.3—TEM images and Gaussian fits of the size distributions of PAMAM-OH generation 4 dendrimer-Pd nanoparticles after refluxing in solvent (a, b), after refluxing in solvent + SA (c, d), after refluxing in solvent + SA + PA (e, f), and after refluxing in solvent + SA + I (g, h).

Figure 8.3a and 8.3b show a representative TEM image and Gaussian fits for the nanoparticles after refluxing in solvent alone and Figure 8.3c and 8.3d show a typical TEM image and Gaussian fits of the nanoparticles after refluxing in solvent + sodium acetate. In both cases, the growth of the nanoparticles is evident since the widths and centers of the size distributions of the nanoparticles increases. Figure 8.3e and 8.3f show a representative TEM image and Gaussian fits of the nanoparticles after refluxing in solvent + sodium acetate + phenylboronic acid. It can be seen that the growth of the nanoparticles is inhibited since the nanoparticle size does not increase much. This was also observed with the PVP-Pd nanoparticles previously²². The phenylboronic acid in its deprotonated form acts as a capping agent and binds to many of the free Pd sites on the nanoparticles and inhibits the growth process. Figure 8.3g and 8.3h show representative TEM image and Gaussian fits of the nanoparticles after refluxing in solvent + sodium acetate + iodobenzene. Growth of the nanoparticles occurs in this case since iodobenzene probably does not bind to the nanoparticle surface.

Based on the results, it can be seen that the surface catalytic mechanism of phenylboronic acid binding to the nanoparticle surface and reacting with iodobenzene in solution also occurs when the PAMAM-OH Generation 4 dendrimer capped Pd nanoparticles are used to catalyze the Suzuki reaction. Since the catalytic mechanism observed is the same for both the PVP-Pd nanoparticles studied previously²² and for the dendrimer-Pd nanoparticles studied presently, it can be concluded that the mechanism of surface catalysis is insensitive to the capping agent used.

8.4.4 Effect of Nanoparticle Size during Second Cycle on Biphenyl Yield

For the PVP-Pd nanoparticles studied previously²², the yield of biphenyl after the first and second cycle was determined using HPLC and it was observed that the catalytic activity of the nanoparticles is greatly diminished during the second cycle of the Suzuki reaction. The results obtained previously are reported in Table 8.4 as concentration of biphenyl and % yield of biphenyl. The % yield is obtained based on the amount of biphenyl actually formed compared to the theoretical amount of biphenyl that can be formed. The theoretical yield of biphenyl is 1 mmol since iodobenzene is the limiting reagent and there is only 1 mmol iodobenzene present at the beginning of the reaction. The ratio of (biphenyl yield_{2nd})/(biphenyl yield_{1st}) when the PVP-Pd nanoparticles are used is 0.38 ± 0.08 as shown in Table 8.5. The diminished catalytic activity observed was attributed to two effects. The aggregation and precipitation of the larger nanoparticles out of solution could result in the smaller nanoparticles remaining in solution, and the biphenyl product itself could poison some of the active sites of the PVP-Pd nanoparticles. It is also worth mentioning that precipitation of the nanoparticles was observed in the bottom of the solution after catalysis.

Table 8.4—Comparison of concentration and reaction yield of biphenyl in the Suzuki reaction catalyzed by the PVP-Pd nanoparticles and dendrimer-Pd nanoparticles

Condition	Concentration and % Biphenyl Yield using PVP-Pd Nanoparticles ²²	Concentration and % Biphenyl Yield Using PAMAM-OH Generation 4 Dendrimer-Pd Nanoparticles
First Cycle	3.00 ± 0.32 mM $39 \pm 4\%$ yield	2.61 ± 0.21 mM $34 \pm 3\%$ yield
Second Cycle	1.11 ± 0.20 mM $15 \pm 3\%$ yield	1.31 ± 0.25 mM $17 \pm 3\%$ yield
After First Cycle with Excess Stabilizer	2.28 ± 0.18 mM $30 \pm 2\%$ yield	0.42 ± 0.05 mM $6 \pm 1\%$ yield

The catalytic activity of the PAMAM-OH Generation 4 dendrimer capped Pd nanoparticles was also studied using HPLC and compared to that of the PVP-Pd nanoparticles. The HPLC results on the concentration and % biphenyl yield obtained using the PAMAM-OH Generation 4 dendrimer capped Pd nanoparticles as the catalyst is summarized in Table 8.4. When the dendrimer-Pd nanoparticles are used as the catalyst, the catalytic activity is also diminished during the second cycle of the Suzuki reaction but not as much as observed with the PVP-Pd nanoparticles. As shown in Table 8.5, the ratio of (biphenyl yield_{2nd})/(biphenyl yield_{1st}) when the PAMAM-OH Generation 4 dendrimer capped Pd nanoparticles are used to catalyze the Suzuki reaction is 0.50 ± 0.09 . A possible reason why the ratio of biphenyl yields is higher when the dendrimer-Pd nanoparticles are used is that the nanoparticles continue to grow during the second cycle resulting in more active sites. Since the nanoparticles continue to increase in size, precipitation of the nanoparticles might not be taking place. This is also supported by the absence of the black metallic powder at the bottom of the reaction mixture after catalysis. This is expected to be the case as the dendrimer is a strong and stable capping agent. As a result, the diminished yield observed is probably due to poisoning of the active sites by the biphenyl product. The larger size of the dendrimer-Pd nanoparticles during the second cycle could also contribute to the higher ratio of biphenyl yield with the dendrimer-Pd than with the PVP-Pd nanoparticles. The larger sized dendrimer-Pd nanoparticles have more active sites available for catalysis because these sites are less likely to be poisoned by biphenyl.

Table 8.5—Ratios of biphenyl yields obtained using PVP-Pd nanoparticles and PAMAM-OH Generation 4 Dendrimer-Pd nanoparticles

Nanoparticle Type	Biphenyl Yield Ratio (2 nd cycle/1 st cycle)
PVP-Pd Nanoparticles ²²	0.38 ± 0.08
PAMAM-OH Generation 4 Dendrimer-Pd Nanoparticles	0.50 ± 0.09

8.4.5 Effect of Excess Capping Agent

For the PVP-Pd nanoparticles studied previously²², the effect of the addition of excess PVP to the reaction mixture was found to diminish the growth processes as well as diminish the catalytic activity of the nanoparticles. The effect of adding excess dendrimer to the Suzuki reaction mixture was investigated with the PAMAM-OH Generation 4 dendrimer-Pd nanoparticles and the HPLC results are summarized in Table 8.4. It can be seen that the addition of excess dendrimer severely diminishes the catalytic activity of the dendrimer-Pd nanoparticles. This is probably due to the strong encapsulating action of the Generation 4 dendrimer on the nanoparticles. In addition, the dendrimer-Pd nanoparticles are smaller than the PVP-Pd nanoparticles studied previously and as a result, will have a smaller concentration of active sites on the surface that are available. The addition of excess dendrimer will thus, result in much lower number of active sites available for the catalysis to occur.

Figure 8.4 shows typical TEM images and Gaussian fits of the size distributions of the dendrimer-Pd nanoparticles before any perturbations (a,b), after refluxing in presence of solvent and excess dendrimer (c,d), and after Suzuki reaction in the presence of excess dendrimer (e,f). It can be seen that the presence of excess dendrimer diminishes the growth of the nanoparticles when refluxed in solvent alone and when

added to the Suzuki reaction mixture. This is also observed previously²² with the PVP-Pd nanoparticles.

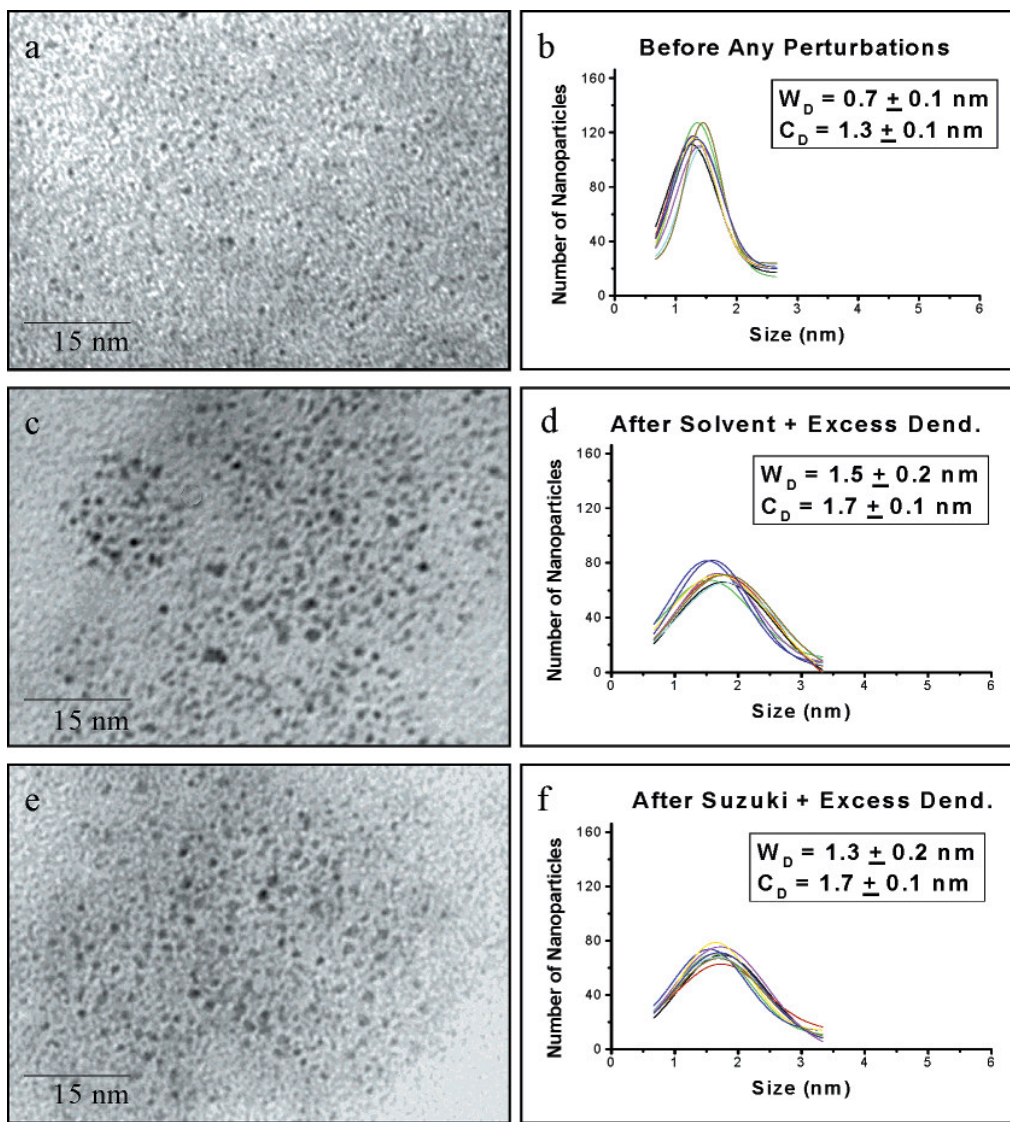


Figure 8.4—TEM images and Gaussian fits of the size distributions of PAMAM-OH generation 4 dendrimer-Pd nanoparticles before any perturbations (a, b), after refluxing in solvent + excess dendrimer (c, d), and after Suzuki reaction in the presence of excess dendrimer (e, f).

8.5 Conclusions

The nanoparticle growth process observed in the reaction by refluxing in the solvent is governed by the amount of free metal present in solution after the preparation of the nanoparticles. Different methods of preparing nanoparticles result in varying amounts of free metal in solution. Since PAMAM-OH Generation 4 dendrimer is a strong encapsulator, the rate of conversion to full nanoparticle is slow resulting in the large concentration of metal in solution. It is shown that the catalytic mechanism of the Suzuki reaction in which phenylboronic acid binds to the nanoparticle surface and reacts with iodobenzene in solution is insensitive to the capping agent used. This is because the growth of the nanoparticles in the presence of iodobenzene and the inhibition of the growth in the presence of phenylboronic acid occurs for both the dendrimer-Pd nanoparticles and the PVP-Pd nanoparticles studied previously²². The biphenyl ratio (second cycle/first cycle) is higher for the dendrimer-Pd nanoparticles than the PVP-Pd nanoparticles. This could be due to the dendrimer-Pd nanoparticles being larger during the second cycle and thus having more active sites and also due to the nanoparticles not precipitating out of solution yet. However, the biphenyl product itself probably still does poison some of the active sites on the nanoparticle surface. It is also found that the presence of excess dendrimer severely diminishes the catalytic activity of the nanoparticles and this is probably due to the strong encapsulating action of the Generation 4 dendrimer to the nanoparticles resulting a much lower number of sites available for catalysis. The presence of excess dendrimer is also found to diminish the growth process.

8.6 References

1. Eppler, A.; Rupprechter, G.; Guzzi, L.; Somorjai, G. A. *J. Phys. Chem. B* **1997**, *101*(48), 9973.
2. Toshima, N.; Yonezawa, T. *New J. Chem.* **1998**, *22*(11), 1179.
3. Schmid, G. *Met. Clus. Chem.* **1999**, *3*, 1325.
4. Puddephatt, R. J. *Met. Clus. Chem.* **1999**, *2*, 605.
5. Henry, C. R. *Appl. Surf. Sci.* **2000**, *164*, 252.
6. St. Clair, T. P.; Goodman, D. W. *Top. Catal.* **2000**, *13*(1,2), 5.
7. Kralik, M.; Corain, B.; Zecca, M. *Chem. Pap.* **2000**, *54*(4), 254.
8. Chusuei, C. C.; Lai, X.; Luo, K.; Goodman, D. W. *Top. Catal.* **2001**, *14*(1-4), 71.
9. Bowker, M.; Bennett, R. A.; Dickinson, A.; James, D.; Smith, R. D.; Stone, P. *Stud. Surf. Sci. Catal.* **2001**, *133*, 3.
10. Kralik, M.; Biffis, A. *J. Mol. Catal. A: Chem.* **2001**, *177*(1), 113.
11. Thomas, J. M.; Raja, R. *Chem. Rec.* **2001**, *1*(6), 448.
12. Mohr, C.; Claus, P. *Sci. Prog.* **2001**, *84*(4), 311.
13. Thomas, J. M.; Johnson, B. F. G.; Raja, R.; Sankar, G.; Midgley, P. A. *Acc. Chem. Res.* **2003**, *36*(1), 20.
14. Bradley, J. S. *Clus. Colloids* **1994**, 459.
15. Duff, D. G.; Baiker, A. *Stud. Surf. Sci. Catal.* **1995**, *91*, 505.
16. Toshima, N. *NATO ASI Ser., Ser. 3* **1996**, *12*, 371.
17. Boennermann, H.; Braun, G.; Brijoux, G. B.; Brinkman, R.; Tilling, A. S.; Schulze, S. K.; Siepen, K. *J. Organomet. Chem.* **1996**, *520*(1-2), 143.
18. Fugami, K. *Organomet. News* **2000**, *1*, 25.
19. Mayer, A. B. R. *Polym. Adv. Technol.* **2001**, *12*(1-2), 96.
20. Bonnemann, H.; Richards, R. *Syn. Meth. Organom. Inorg. Chem.* **2002**, *10*, 209.
21. Moiseev, I. I.; Vargaftik, M. N. *Russ. J. Chem.* **2002**, *72*(4), 512.

22. Narayanan, R.; El-Sayed, M. A. *J. Am. Chem. Soc.*, **2003**, *125*(27), 8340.
23. Collier, P. J.; Iggo, J. A.; Whyman, R. *J. Mol. Catal. A: Chem.* **1999**, *146*(1-2), 149.
24. Sculz, J.; Roucoux, A.; Patin, H. *Chem. Eur. J.* **2000**, *6*(4), 618.
25. Wang, Q.; Liu, H.; Han, M.; Li, X.; Jiang, D. *J. Mol. Catal. A: Chem.* **1997**, *118*(2), 145.
26. Kim, S.; Son, S. U.; Lee, S. S.; Hyeon, T.; Chung, Y. K.; *Chem. Commun.* **2001**, 2212.
27. Larpent, C.; Menn, B. F.; Patin, H. *J. Mol. Catal.* **1991**, *65*, L35.
28. Sidorov, S. N.; Volkov, I. V.; Davankov, V. A.; Tsyurupa, M. P.; Valetsky, P. M.; Bronstein, L. M.; Karlinsey, R.; Zwanziger, J. W.; Matveeva, V. G.; Sulman, E. M.; Lakina, N. V.; Wilder, E. A.; Spontak, R. J. *J. Am. Chem. Soc.* **2001**, *123*(43), 10502.
29. Chechik, V.; Crooks, R. M. *J. Am. Chem. Soc.* **2000**, *122*, 1243.
30. Yeung, L. K.; Crooks, R. M. *Nano Lett.* **2001**, *1*(1), 14.
31. Dupont, J.; Fonseca, G. S.; Umpierre, A. P.; Fichtner, P. F. P.; Teixeira, S. R. *J. Am. Chem. Soc.* **2002**, *124*, 4228.
32. Hirai, H.; Chawanya, H.; Toshima, N. *Nip. Kag. Kai.* **1984**, *6*, 1027.
33. Roucox, A.; Sculz, J.; Patin, H. *Chem. Rev.* **2002**, *102*(10), 3757.
34. Zhao, M.; Sun, L.; Crooks, R. M. *J. Am. Chem. Soc.* **1998**, *120*, 4877.
35. Zhao, M.; Crooks, R. M. *Angew. Chem., Int. Ed. Engl.* **1999**, *38*(3), 364.
36. Chechik, V.; Zhao, M.; Crooks, R. M. *J. Am. Chem. Soc.* **1999**, *121*, 4910.
37. Chechik, V.; Crooks, R. M. *J. Am. Chem. Soc.* **2000**, *122*, 1243.
38. Rahim, E. H.; Kamounah, F. S.; Frederiksen, J.; Christensen, J. B. *Nano Lett.* **2001**, *1*(9), 499.
39. Zhao, M.; Crooks, R. M. *Adv. Mater.* **1999**, *11*(3), 217.
40. Kunio, E.; Keiko, M.; Tomokazu, Y. *J. Coll. Interf. Sci.* **2002**, *254*(2), 402.
41. Li, Y.; El-Sayed, M. A. *J. Phys. Chem. B* **2001**, *105*, 8938.

42. Li, Y.; Hong, X. M.; Collard, D. M.; El-Sayed, M. A. *Org. Lett.* **2000**, *2*(15), 2385.

43. Li, Y.; Boone, E.; El-Sayed, M. A. *Langmuir* **2002**, *18*, 4921.

CHAPTER 9

EFFECT OF COLLOIDAL NANOCATALYSIS ON THE METALLIC NANOPARTICLE SHAPE: THE SUZUKI REACTION

9.1 Abstract

Dominantly tetrahedral shaped PVP-Pt nanoparticles are shown to catalyze the Suzuki reaction between phenylboronic acid and iodobenzene, but are not as active as the spherical palladium nanoparticles studied previously. The dominantly tetrahedral PVP-Pt nanoparticles ($55 \pm 4\%$ regular tetrahedral, $22 \pm 2\%$ distorted tetrahedral, and $23 \pm 2\%$ spherical nanoparticles) are synthesized by using the hydrogen reduction method. The TEM results show that a transformation of shape from tetrahedral to spherical Pt nanoparticles takes place three hours into the first cycle of the reaction. After the first cycle, the spherical nanoparticles have a similar size distribution to that of the tetrahedral nanoparticles before the reaction and the observed shape distribution is $18 \pm 6\%$ regular tetrahedral, $28 \pm 5\%$ distorted tetrahedral, and $54 \pm 5\%$ spherical nanoparticles. After the second cycle of the Suzuki reaction, the shape distribution is $13 \pm 5\%$ regular tetrahedral, $24 \pm 5\%$ distorted tetrahedral, and $63 \pm 7\%$ spherical nanoparticles. After the second cycle, the transformed spherical nanoparticles continue to grow and this could be due to the strong capping action of the higher molecular weight PVP (mw = 360,000), which makes the nanoparticles more resistant to aggregation and precipitation unlike the Pd particles capped with the lower molecular weight PVP (mw = 40,000) used previously. The transformation in shape also occurs when the nanoparticles are refluxed in the presence of the solvent, sodium acetate, and iodobenzene and results in spherical

nanoparticles with similar size distribution to that of the tetrahedral nanoparticles before any perturbations. However, in the presence of phenylboronic acid, the regular tetrahedral nanoparticles remain dominant ($51 \pm 6\%$) and maintain their size. These results support our previous studies in which we proposed that phenylboronic acid binds to the nanoparticle surface and thus acts as a capping stabilizer material for the particle and reacts with the iodobenzene. Recycling the nanoparticles results in a drastic reduction of the catalytic activity, and this must be due to the transformation of shape from the dominantly tetrahedral to the larger dominantly spherical nanoparticles. This also supports results in the literature that show that spherical platinum nanoparticles do not catalyze this reaction.

9.2 Introduction

The nanocatalysis field has undergone an explosive growth during the past decade with many review articles in heterogeneous catalysis with supported nanoparticles¹⁻¹³ and in homogeneous catalysis with nanoparticles in colloidal solution¹⁴⁻²¹. The large surface-to-volume ratio of metallic nanoparticles makes them very attractive to use as catalysts for chemical reactions compared to other bulk catalytic materials. This attractive property of metallic nanoparticles results in the surface atoms being very active. This raises a very important question on whether the surface atoms are so active that they result in changes in the size or shape of the nanoparticles during their catalytic function. In the bulk of catalysis with colloids, TEM characterization of the nanoparticles before and after catalysis is not usually given. However, there have been a few studies²²⁻²⁸ where the size distribution of the nanoparticles after recycling along with the catalytic

activity is reported for characterization and also some studies²⁹⁻³² that discuss the catalytic activity of the nanoparticles upon recycling, but which do not examine the stability of the nanoparticles after catalysis. In a review of transition metal colloids as reusable catalysts,³³ it was pointed out that the major interest of reusability of the nanoparticle catalysts has not been systematically studied or published in the metal colloid literature.

There have been very few detailed studies in the literature that examine the stability and catalytic activity of metal nanoparticles in colloidal solution which are used to catalyze organic and inorganic reactions. This kind of examination is necessary to evaluate nanoparticles' usefulness in catalysis and to quantitatively understand the mechanism of "nanocatalysis". We have conducted a few detailed studies on the stability of the nanoparticles after catalysis, recycling, and in the presence of individual reactants using spherical PVP-Pd²⁷ and spherical dendrimer-Pd³⁴ nanoparticles to catalyze the Suzuki reaction. We have also used spherical²⁸ PVP-Pt nanoparticles to catalyze the electron transfer reaction. In these studies, we have examined the effect of individual reactants on the size distribution of the nanoparticles which have provided possible insights in the surface catalytic mechanisms of the reactions. We have also conducted a study on the effect of the tetrahedral and cubic shape on the stability of Pt nanoparticles used to catalyze the electron transfer reaction, which is a gentle reaction conducted at room temperature³⁵. For this reaction, it was observed that distortions in the corners and edges of the tetrahedral and cubic nanoparticles occur during the course of the reaction. We have also shown that as the tetrahedral and cubic shape changes during the course of the reaction, the activation energy of the reaction also changes. During the early stages

of the electron transfer reaction (first 40 minutes), it was observed that there are no changes in the shape of the tetrahedral and cubic nanoparticles. Also, it was observed that the activation energy is correlated to the fraction of surface atoms located on the corners and edges of the nanoparticles and that the tetrahedral nanoparticles are the most catalytically active while the cubic nanoparticles are the least catalytically active³⁶. However, during the course of the entire reaction, it was observed that there are distortions in the corners and edges of the nanoparticles and also there was a corresponding change in the activation energy³⁷.

Suzuki cross-coupling reactions have been traditionally catalyzed using many different kinds of phosphine-based palladium catalysts and phosphine-free palladium catalysts such as Pd(PPh₃)₄, Pd(OAc)₂, [(n³-C₃H₅)PdCl]₂, and Pd₂(dba)₃ C₆H₆³⁸⁻⁴². Recently, there have been many reports on the use of palladium nanoparticles^{6, 43-49} as catalysts for Suzuki reactions. A number of other metallic nanoparticles such as copper nanoparticles⁵⁰, ruthenium nanoparticles⁵⁰, and also various bimetallic, trimetallic, and multi-metallic nanoparticles⁵⁰ have also been reported to catalyze Suzuki reactions. Very recently, it has been reported that platinum complexes such as [PtCl₂-(NPh)₂] and K₂[PtCl₄] can also be used as catalysts for the Suzuki reaction⁵¹. There have been no reports on the successful use of platinum nanoparticles to catalyze the Suzuki reaction. There has been one study⁵⁰ on the use of *spherical* platinum nanoparticles stabilized with TOAF in which it was found that the Pt nanoparticles do not catalyze the reaction. The aim of our study is to find out if tetrahedral PVP-Pt nanoparticles can catalyze the Suzuki cross-coupling reaction between phenylboronic acid and iodobenzene since we have

already shown³⁶ that tetrahedral nanoparticles are more active in catalyzing the electron transfer reaction between hexacyanoferrate (III) ions and thiosulfate ions.

Tetrahedral shaped nanoparticles have [111] facets which are known to be the most catalytically active⁵²⁻⁵⁴. Furthermore, these particles have sharp edges and corners, the atoms on which are expected to be chemically and dynamically active. As a result, they change their position, causing shape changes that could occur during the chemical reaction as recently suggested by our results on the electron transfer reaction^{35,37}. The PVP-Pt nanoparticles used in this study are dominantly tetrahedral in shape and as a result, it can be determined what the effect that the shape has on the catalytic activity of the nanoparticles. Thus, another important aim of the present study is to study the effect of the Suzuki reaction on the shape stability of the PVP capped tetrahedral platinum nanoparticles. In addition, it is also important to understand what happens to the size of nanoparticles when they change shape during the reaction. As a result, we have monitored the size distribution of the dominant shape as well as the shape distribution for the different conditions.

9.3 Experimental

9.3.1 Synthesis of Tetrahedral PVP-Pt Nanoparticles

The PVP stabilized Pt nanoparticles were prepared using the H₂ reduction method described previously⁵⁵ with some modifications³⁵⁻³⁷. The precursor platinum salt used is K₂PtCl₆ and the stabilizer is PVP (mw = 360,000). A 500 mL 3-neck flask equipped with a gas trap is used for the synthesis. Two hundred fifty mL of doubly deionized water, 5

mL of 0.01 M K_2PtCl_6 , and 0.25 g of PVP is added to the flask. After the solution is thoroughly mixed, argon is bubbled for 20 minutes and then hydrogen gas is bubbled for 5 minutes. Then the flask is sealed, wrapped in aluminum foil, and stored in the dark for 24 hours. The resulting colloidal solution is light brown. A drop of the colloidal solution is placed onto a Formvar stabilized carbon grid and allowed to evaporate in air. JEOL 100C TEM is used to characterize the nanoparticle size and shape.

9.3.2 Catalyzing Suzuki Reaction

Figure 9.1 shows a schematic of the Suzuki reaction between phenylboronic acid and iodobenzene catalyzed with platinum nanoparticles in the presence of sodium acetate base.

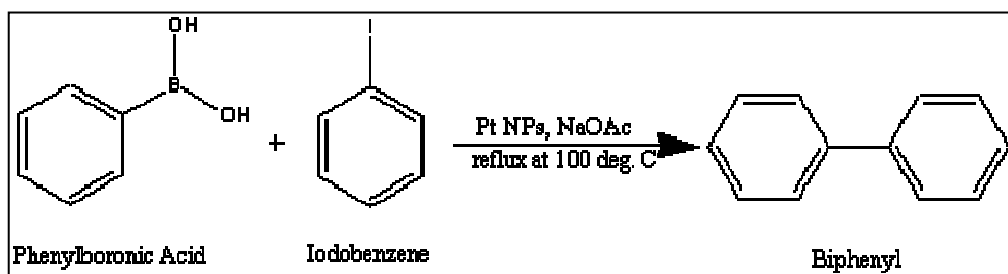


Figure 9.1—Schematic of the Suzuki reaction between phenylboronic acid and iodobenzene to yield biphenyl

Tetrahedral PVP-Pt nanoparticles are used to catalyze the Suzuki reaction. In this reaction, 0.49 g sodium acetate, 0.37 g phenylboronic acid, and 0.20 g iodobenzene is added to 150 mL of the 3:1 acetonitrile:water solvent. The reaction mixture is heated to 100° C. Once the mixture refluxes, 15 mL of the tetrahedral PVP-Pt nanoparticles are added to the reaction mixture. The reaction mixture is refluxed for a total of 12 hours. The same reaction mixture solution was used for recycling after the addition of fresh

amounts of the reactants. For recycling, an assumption was made that all of the iodobenzene was used up since it is the limiting reactant. Initially there is 1 mmol iodobenzene and 3 mmol phenylboronic acid present in the reaction mixture. After the first cycle, it is assumed that there is no iodobenzene left and 2 mmol phenylboronic acid left. As a result, for the second cycle, 1 mmol iodobenzene and 1 mmol phenylboronic acid are added. The reaction mixture is then refluxed for another 12 hours to complete the second cycle.

9.3.3 TEM Studies on Shape and Size Stability of Tetrahedral PVP-Pt Nanoparticles

The concentration of the stock solution of PVP-Pt nanoparticles is 1×10^{-4} M. When 15 mL of the nanoparticles are added, the total volume for all of the experiments is 165 mL. As a result, the initial concentration of Pt ions for all of the experiments is 9.09×10^{-6} M. For the experiments, the samples are spotted by placing a drop of the solution onto a Formvar stabilized copper grid and allowing the drop to evaporate in air. The spotted samples take approximately 30 minutes to dry. Since the same deposition conditions are employed for all samples, the evaporation rate of the solvent is fairly reproducible from one sample to another. For each of the experiments, the internal reproducibility of the observed shape is verified by spotting the sample onto 3 separate TEM grids. TEM images are also obtained from different sections of the TEM grids to verify the reproducibility of the shape. The general reproducibility of the shape is verified by conducting each of the experiments 3 times. The nanoparticle shape distribution is determined by counting approximately 1800 nanoparticles from 9 enlarged TEM images (approximately 200 nanoparticles from each TEM image). The shapes are

categorized as regular tetrahedral, distorted tetrahedral, and spherical nanoparticles. Size distributions of the dominant shape (either tetrahedral or spherical) after each condition are also conducted. The size distributions of distorted tetrahedral nanoparticles are not conducted since the size of these types of nanoparticles depends on the type of distortion.

9.3.4 HPLC Studies on Catalytic Activity of Nanoparticles

HPLC measurements are conducted on a Hitachi-4500 HPLC equipped with a L4500A diode array detector in which the absorbance is monitored at 254 nm. The separation is carried out on a reversed-phase packed column (Rainin Microsorb-MV C18, 300 Angstroms, dim 4.6 x 250 mm) using a 60:40 acetonitrile-water mixture and a flow rate of 1 mL/min. The area of the chromatographic peaks is calculated with a D-6000 interface-integrator. A calibration curve for determining the concentration of biphenyl is constructed by plotting the peak area vs. concentration of biphenyl standards. The standards prepared are 0.0005 M, 0.001 M, 0.0015 M, 0.002 M, 0.0025 M, and 0.003 M biphenyl. For HPLC measurements, all samples are diluted to $\frac{1}{4}$ of the original concentration so that the peak areas will be within the range of the calibration curve. The actual concentration is determined by taking the concentration of the diluted sample and multiplying by 4. The concentration of biphenyl is determined before the first cycle, after the first cycle, before the second cycle, and after the second cycle.

9.4 Results and Discussion

Spherical palladium nanoparticles have been shown to catalyze the Suzuki reaction previously^{6, 41-47}. The spherical shaped nanoparticles are really “near spherical”

since the nanoparticles are really composed of numerous (100) and (111) facets and appear to be spherical in TEM images. As a result, we will refer to them as “near spherical” nanoparticles. One goal of the present study is to determine the relative catalytic activity of tetrahedral shaped PVP-Pt nanoparticles for the Suzuki cross-coupling reaction relative to the spherical PVP-Pd nanoparticles. We also determine the effect of various perturbations on the tetrahedral shape in colloidal solution. HPLC is used to compare the catalytic activity of the tetrahedral PVP-Pt nanoparticles with the “near spherical” PVP-Pd nanoparticles studied previously²⁷. TEM and HRTEM are used to examine the shape stability by examining the shape distribution of the nanoparticles during the reaction and under different conditions. The size distribution of the dominant shape present after each condition is also determined.

9.4.1 Catalytic Activity of Tetrahedral PVP-Pt Nanoparticles for Suzuki Reaction

HPLC studies are conducted in order to compare the catalytic activity of the tetrahedral PVP-Pt nanoparticles with the “near spherical” PVP-Pd nanoparticles studied previously²⁷. Table 9.1 shows the percent yield of biphenyl for the two types of nanoparticles (tetrahedral PVP-Platinum nanoparticles and “near spherical” PVP-Palladium nanoparticles studied previously²⁷) during the first and second cycle. The % yield of biphenyl is calculated by dividing the number of moles of biphenyl actually formed by the number of moles of biphenyl that can be theoretically formed and multiplying by 100. It can be seen that the % yield of biphenyl formed is lower (almost one third as active) for the tetrahedral PVP-Pt nanoparticles (5.0 nm) than for the “near spherical” PVP-Pd nanoparticles (2.1 nm). It is worth noting that the PVP-Pd

nanoparticles are really “near spherical”, in which they are composed of numerous (100) and (111) facets and appear to be spherical in TEM images. As a result for the calculation of the fraction of atoms on the corners and edges of the “near spherical” nanoparticles, we used the cubo-octahedron model⁵⁶. The tetrahedral Pt nanoparticles have 164 surface atoms and 52 corner + edge atoms (calculated using tetrahedron model⁵⁶) while the “near spherical” Pd nanoparticles have 122 surface atoms and 60 corner + edge atoms (calculated using cubo-octahedral model⁵⁶). As a result, the fraction of surface atoms in the tetrahedral Pt nanoparticles is 0.32, while the fraction of surface atoms in the “near spherical” Pd nanoparticle is 0.49. A possible reason for the reduction in activity that is observed with the tetrahedral nanoparticles could be due to the lower fraction of atoms on corners and edges for the tetrahedral nanoparticles compared to the “near spherical” nanoparticles due to the differences in their sizes. The reduction in activity can also be partly due to the differences in the reactivity of the two different metals used to catalyze the reaction. In addition, the tetrahedral Pt nanoparticles are capped by the larger PVP which covers its surface better. Poisoning of the platinum nanoparticles could also account for some of the loss of catalytic activity that is observed.

Table 9.1—Summary of the concentration and % yield of biphenyl obtained using the tetrahedral PVP-Pt nanoparticles and the “near spherical” PVP-Pd nanoparticles studied previously

Condition	Concentration (mM) and % Yield of Biphenyl Using PVP-Pt Nanoparticles	Concentration (mM) and % Yield of Biphenyl Using PVP-Pd Nanoparticles
First Cycle of Suzuki Reaction	1.07 ± 0.05 mM 14 ± 5%	3.00 ± 0.32 mM 39 ± 4%
Second Cycle of Suzuki Reaction	0.36 ± 0.03 mM 5 ± 2%	1.11 ± 0.20 mM 15 ± 3%

We also conducted a study comparing the yield of biphenyl obtained by first refluxing the nanoparticles in solvent alone and then conducting the Suzuki reaction to that obtained during the second cycle of a “normal” Suzuki reaction. During the second cycle of a “normal” Suzuki reaction, the biphenyl yield is 0.36 ± 0.03 mM ($5 \pm 2\%$ yield). In the case of conducting the Suzuki reaction after refluxing the tetrahedral nanoparticles in solvent for 12 hours, the biphenyl yield is 0.43 ± 0.02 mM ($6 \pm 1\%$ yield). It can be seen that in both cases, the biphenyl yield is very low. Also, in both cases, the tetrahedral nanoparticles have transformed into dominantly “near spherical” ones before the reaction proceeds. It is also worth noting that the fraction of atoms located on the corners and edges of the transformed “near spherical” platinum nanoparticles is 0.11. This is dramatically lower than that of the initial tetrahedral platinum nanoparticles, which has a fraction of 0.32. These observations provide additional evidence that the transformation of the tetrahedral nanoparticles into “near spherical” ones contributes to the great reduction in catalytic activity that is observed.

Li and El-Sayed have shown that the more stable the nanoparticles are due to its better capping, the lower the catalytic activity⁴⁶. The tetrahedral PVP-Pt nanoparticles do yield biphenyl unlike the unsuccessful use of spherical TOAF stabilized Pt nanoparticles to catalyze the Suzuki reaction that was reported in the literature previously⁴⁸. This points out to the fact that tetrahedral shape is a more catalytically active shape. It can be seen that in terms of actual percent yield, both the “near spherical” PVP-Pd and the tetrahedral PVP-Pt nanoparticles have poor recycling potential. However, the PVP-Pt nanoparticles have a much lower recycling potential than the PVP-Pd nanoparticles. As will be discussed in the next section, the tetrahedral PVP-Pt nanoparticles transform into

a more stable and larger “near spherical” shape after the first cycle of the Suzuki reaction. We propose that the transformation from tetrahedral to the larger “near spherical” shaped PVP-Pt nanoparticles could account for the drastic loss of catalytic activity observed during the second cycle of the Suzuki reaction. This is supported by the previously reported study in the literature⁴⁸ which showed that “near spherical” platinum nanoparticles do not catalyze the Suzuki reaction.

“Near spherical” platinum nanoparticles are composed of numerous (100) and (111) facets while tetrahedral platinum nanoparticles are composed entirely of (111) facets. The Pt-Pt distances for both the Pt (111) and the Pt (100) surface are both 0.2772 nm⁵⁷. However, the number of Pt neighbors for the Pt (111) surface is 6, while the number of Pt neighbors for the Pt (100) surface is 4. As a result, the electron densities of the two surfaces are different. This could account for why there are differences in the reactivity for the “near spherical” and tetrahedral platinum nanoparticles for catalyzing the Suzuki reaction.

9.4.2 Effect of Catalysis and Recycling on Stability of Tetrahedral Shape

The PVP-Pt nanoparticles used are dominantly tetrahedral in shape. We have examined the effect of the Suzuki reaction on the tetrahedral shape with its (111) facets and sharp edges and corners known to be the most catalytically active and which could also be the most sensitive to changes in the shape of the nanoparticles. Table 9.2 summarizes the shape distribution results and the size distribution results (for the dominant shape) for the different conditions. Figure 9.2a-c shows a typical TEM image, shape distribution of the PVP-Pt nanoparticles before any perturbations, and the size

distribution of the dominant tetrahedral shape. The shape distribution is reported as a percentage of regular tetrahedral, distorted tetrahedral, and “near spherical” nanoparticles. As can be seen, the regular tetrahedral nanoparticles ($55 \pm 4\%$) are dominant with some distorted tetrahedral ($22 \pm 2\%$) and “near spherical” nanoparticles ($23 \pm 2\%$) also present. The tetrahedral nanoparticles have an average size of 5.0 ± 0.1 nm and are monodisperse. Figure 9.2d-f show a typical TEM image, shape distribution of the nanoparticles after the first cycle of the Suzuki reaction, and the size distribution of the dominant “near spherical” shape. It can be seen that there is a transformation in the shape of the nanoparticles from tetrahedral to “near spherical” in which there are $54 \pm 5\%$ “near spherical” nanoparticles present. The “near spherical” nanoparticles become the dominant shape after the first cycle of the Suzuki reaction and have an average size of 5.2 ± 0.1 nm. This suggests that the tetrahedral shaped Pt nanoparticles with their (111) facets and sharp edges and corners are sensitive to its chemical environment. The process of dissolving (or reacting) the unstable atoms on the edges and corners tends to transform the nanoparticles to the more stable “near spherical” shape. Also, it can be seen that the tetrahedral nanoparticles transform into “near spherical” nanoparticles of comparable size.

Table 9.2—Summary of number (#) of PVP-Pt nanoparticles counted, number and percentage of regular tetrahedral, distorted tetrahedral, and “near spherical” nanoparticles under various conditions

Condition	# Particles Counted	# and % Regular Tetrahedral NPs	# and % Distorted Tetrahedral NPs	# and % “Near Spherical” NPs	C _D and W _D of Size Dist. of Dominant Shape (nm)
Before Suzuki Reaction	1735	953 ± 68 55 ± 4	382 ± 37 22 ± 2	401 ± 34 23 ± 2	C _D = 5.0 ± 0.1 W _D = 0.9 ± 0.1
After First Cycle of Suzuki Reaction	1821	326 ± 110 18 ± 6	508 ± 93 28 ± 5	985 ± 91 54 ± 5	C _D = 5.2 ± 0.1 W _D = 1.0 ± 0.1
After Second Cycle of Suzuki Reaction	1798	234 ± 91 13 ± 5	433 ± 88 24 ± 5	1131 ± 125 63 ± 7	C _D = 5.7 ± 0.2 W _D = 1.6 ± 0.2
After Just Solvent	1739	244 ± 89 14 ± 5	381 ± 51 22 ± 3	1113 ± 71 64 ± 4	C _D = 5.2 ± 0.1 W _D = 1.0 ± 0.1
After Solvent + Sodium Acetate	1832	292 ± 76 16 ± 4	456 ± 93 25 ± 5	1082 ± 108 59 ± 6	C _D = 5.1 ± 0.1 W _D = 1.1 ± 0.1
After Solvent + Sodium Acetate + Phenylboronic Acid	1804	921 ± 109 51 ± 6	522 ± 73 29 ± 4	359 ± 52 20 ± 3	C _D = 5.1 ± 0.1 W _D = 1.1 ± 0.1
After Solvent + Sodium Acetate + Iodobenzene	1786	266 ± 70 15 ± 4	374 ± 107 21 ± 6	1141 ± 91 63 ± 5	C _D = 5.1 ± 0.1 W _D = 1.0 ± 0.1

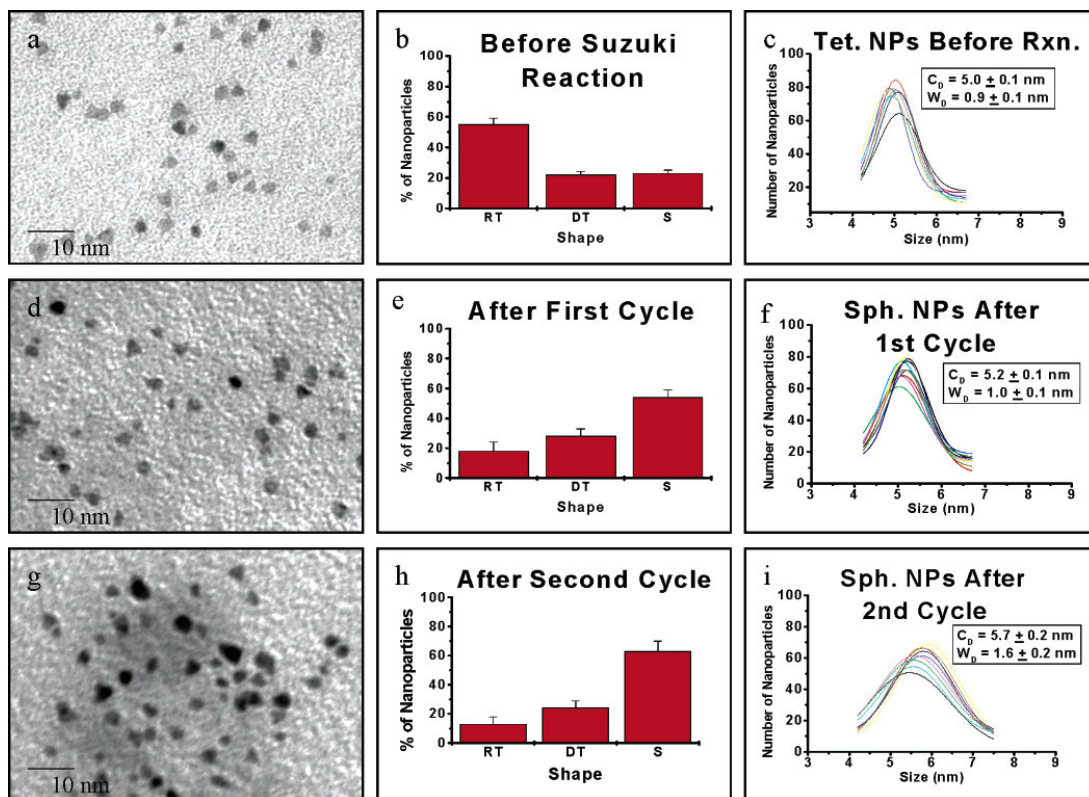


Figure 9.2—TEM images, shape distributions, and size distributions (dominant shape) of PVP-Pt nanoparticles before the Suzuki reaction (a-c), after the first cycle of the Suzuki reaction (d-f), and after the second cycle of the Suzuki reaction (g-i).

Figure 9.2g-i show a representative TEM image of the PVP-Pt nanoparticles after the second cycle of the Suzuki reaction, the shape distribution of the nanoparticles, and the size distribution of the dominant “near spherical” shape. After the second cycle, the “near spherical” nanoparticles remain dominant ($63 \pm 7\%$) and the shape distribution remains similar to that observed after the first cycle of the Suzuki reaction. It can also be seen that the size of the “near spherical” nanoparticles increases after the second cycle (average size = 5.7 ± 0.2 nm) and that the width of distribution is broader (width = 1.6 ± 0.2 nm). This suggests that the tetrahedral nanoparticles transform to the more stable “near spherical” shape and continue to grow in size by Ostwald ripening processes.

In a previous study with “near spherical” shaped PVP-Pd nanoparticles²⁷, we observed that the nanoparticles grew larger after the first cycle of the reaction due to the Ostwald ripening process. During the second cycle, we proposed that the nanoparticles aggregated and precipitated out of solution leaving the smaller nanoparticles behind. In another previous study with PAMAM Generation 4 dendrimer-capped Pd nanoparticles³⁴, it is observed that the nanoparticles continue to increase in size during the second cycle suggesting that aggregation and precipitation does not take place due to the better capping action of the dendrimer. The growth process was attributed to both the Ostwald ripening process and also the presence of palladium atoms and partly reduced palladium ions remaining in solution. It is worth noting that in the previous study with “near spherical” shaped PVP-Pd nanoparticles, we used PVP with a molecular weight of 40,000. In the current study with tetrahedral shaped PVP-Pt nanoparticles, we use PVP with a molecular weight of 360,000. The higher the molecular weight of the PVP used, the better its capping action. This could explain why after the second cycle of the reaction, the transformed “near spherical” PVP-Pt continue to grow larger in size while in the case of the PVP-Pd nanoparticles studied previously²⁷, the larger nanoparticles that are formed aggregated and precipitated out of solution. The PVP (mw = 360, 000), with better capping action, results in the nanoparticles being more resistant to aggregation and precipitation. This result is also consistent with the results obtained previously³⁴ with the PAMAM Generation 4 dendrimer capped Pd nanoparticles, which have strong encapsulating action.

Figure 9.3 shows the % regular tetrahedral nanoparticles as a function of time during the first cycle of the Suzuki reaction and during the process of refluxing the

nanoparticles in solvent alone. It can be seen that in both cases, the % of regular tetrahedral nanoparticles decreases exponentially over time. When the nanoparticles are refluxed in solvent alone, it can be seen that the shape transformation occurs slightly faster than during the course of the first cycle of the Suzuki reaction. This suggests that perhaps the phenylboronic acid, which can bind to the nanoparticle surface, has some effect in slowing the shape transformation process. When the nanoparticles are refluxed in solvent alone, there is no phenylboronic acid present so the transformation occurs slightly faster. The transformation in shape occurs three hours into the Suzuki reaction. Figure 9.4 shows a HRTEM image of a tetrahedral nanoparticle before the Suzuki reaction (a) and a transformed “near spherical” nanoparticle after the second cycle of the Suzuki reaction (b). It can be seen that there is a complete transformation in shape from tetrahedral to “near spherical”.

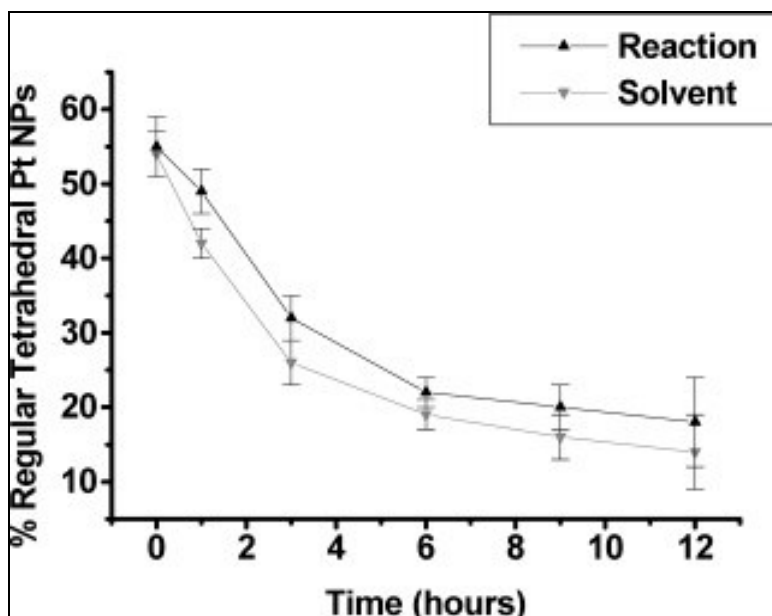


Figure 9.3—Graph of the percentage of regular tetrahedral platinum nanoparticles during the course of the first cycle of the Suzuki reaction and during the course of refluxing the nanoparticles in just the solvent.

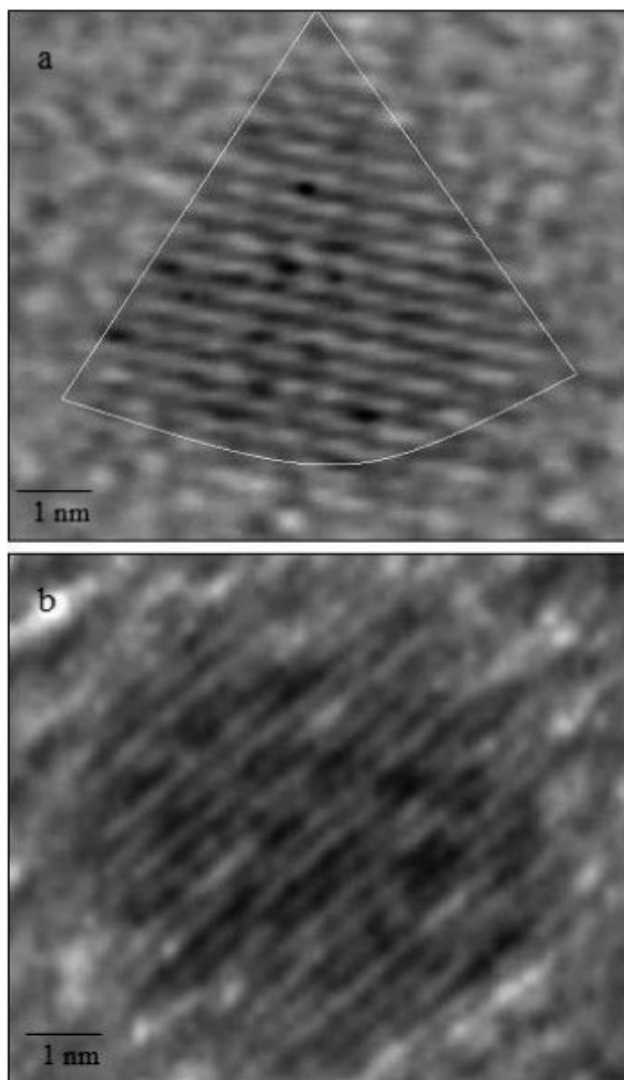


Figure 9.4—HRTEM images of the PVP-Pt nanoparticles before the Suzuki reaction (a) and after the second cycle of the Suzuki reaction (b).

9.4.3 Effect of the Individual Chemicals Involved in Reaction on Stability of the Tetrahedral Shape

The effect of the *individual* chemicals involved in the reaction on the stability of the nanoparticle shape is also investigated. Table 9.2 summarizes the shape distribution and the size distribution (of the dominant shape) under different conditions. Figure 9.5a-c show a typical TEM image, shape distribution of the nanoparticles after refluxing them in the 3:1 acetonitrile:water solvent alone, and size distribution of the dominant “near spherical” shape. It is observed that after refluxing in just the solvent, there is a greater percentage of “near spherical” nanoparticles present ($54 \pm 4\%$) than that present in the initial synthesized sample. The process of refluxing the nanoparticles transforms the tetrahedral nanoparticles into the more stable “near spherical” shape. It is also observed that the size of the dominant “near spherical” nanoparticles is similar to that of the tetrahedral nanoparticles before any perturbations, suggesting that the shape transformation process results from surface atomic reorganization, i.e. the atoms on the corners and edges reconstruct and dynamically move and construct the (100) facets present on the spheres but not on the tetrahedral nanoparticles. The “near spherical” particles are slightly larger than the tetrahedral nanoparticles. This is undoubtedly due to Ostwald ripening in which the small nanoparticles dissolve and adsorb on the surface of the larger one. Excess metallic atoms in solution might also deposit on the surface of the larger nanoparticles. Since atoms on the corners and edges are the least stable, these positions might not be the most favorable position for condensing atoms. The adsorbed atoms begin to make the (100) facets and are assisted by the reconstruction of the host atoms in the original tetrahedral atoms.

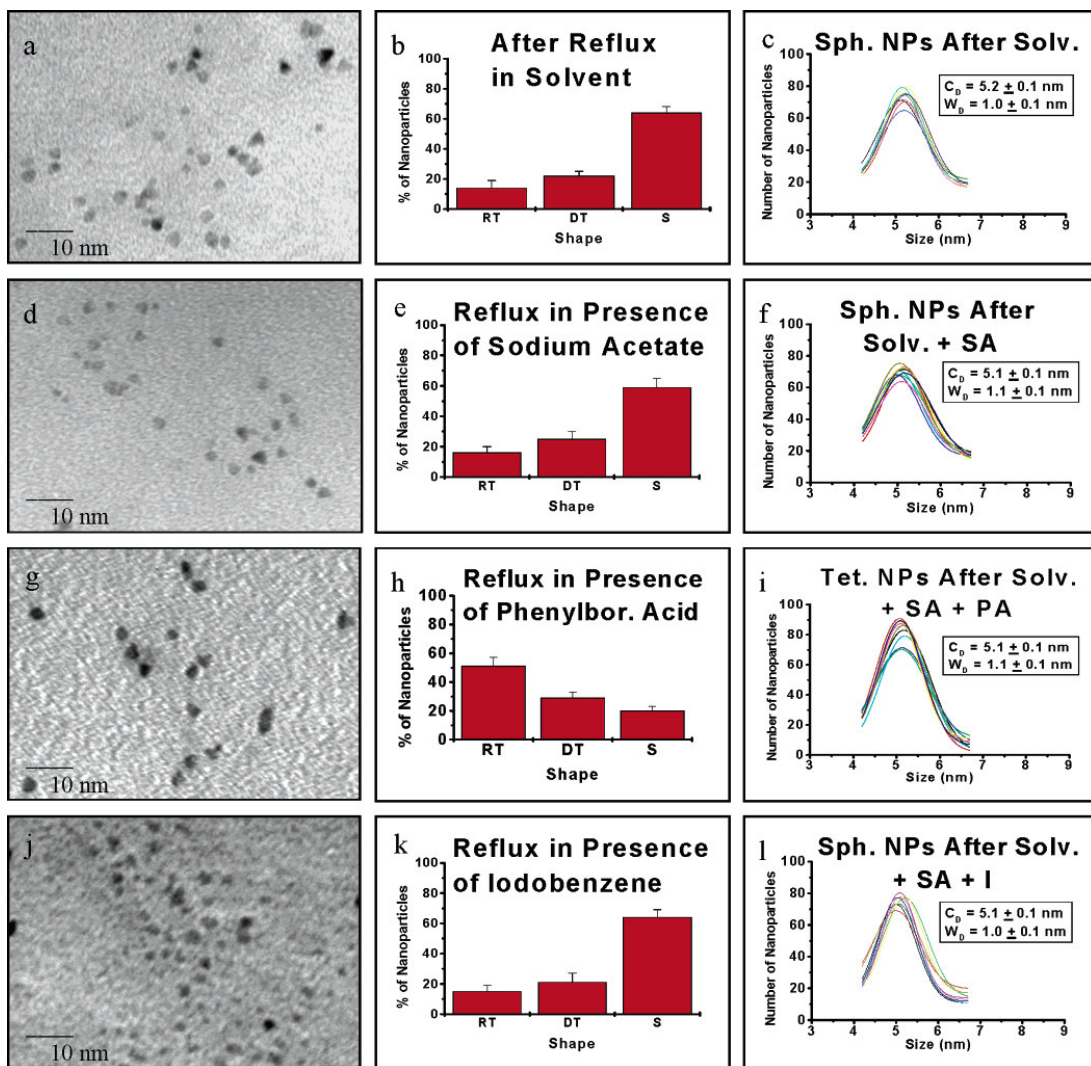


Figure 9.5—TEM images, shape distributions, and size distributions (dominant shape) of the PVP-Pt nanoparticles after refluxing in solvent alone (a-c), after refluxing in solvent + sodium acetate (d-f), after refluxing in solvent + sodium acetate + phenylboronic acid (g-i), and after refluxing in solvent + sodium acetate + iodobenzene (j-l).

Figure 9.5d-f show typical TEM image, shape distribution of the nanoparticles after refluxing the nanoparticles in solvent + sodium acetate, and the size distribution of the dominant “near spherical” shape. In this case, it is found that there are a greater percentage of “near spherical” nanoparticles ($63 \pm 6\%$) present and that the size of the “near spherical” nanoparticles is similar to that of the tetrahedral nanoparticles before any perturbations. Figure 9.5g-i show a typical TEM image, shape distribution of the

nanoparticles after refluxing in the presence of phenylboronic acid, and size distribution of the dominant tetrahedral shape. Under these conditions, it is observed that the tetrahedral nanoparticles ($64 \pm 9\%$) remain the dominant shape, which supports previous studies with “near spherical” nanoparticles^{27,34} in which the size distribution is found not to change in the presence of phenylboronic acid and we proposed that phenylboronic acid acts as a capping (stabilizing) agent by binding to the nanoparticle surface. In this manner, it stabilizes not only the size, but also the tetrahedral shape of the platinum nanoparticles.

Figure 9.5j-1 show a typical TEM image, shape distribution of the PVP-Pt nanoparticles after refluxing in the presence of iodobenzene, and size distribution of the dominant “near spherical” shape. It is observed that “near spherical” nanoparticles are dominant ($68 \pm 10\%$) and this is probably because iodobenzene does not bind to the nanoparticle surface and thus does not protect the nanoparticle shape. This result also supports the catalytic mechanism that we proposed in previous studies^{27,34} in which the phenylboronic acid binds to the nanoparticles surface and reacts with iodobenzene in solution via collisional processes. Also, it can be seen that the “near spherical” nanoparticles are similar in size to that of the tetrahedral nanoparticles before any perturbations.

9.5 Conclusions

It is found that the 5.0 nm tetrahedral PVP-Pt nanoparticles catalyze the Suzuki reaction between phenylboronic acid and iodobenzene while they are only one-third as efficient as PVP-Pd “near spherical” palladium nanoparticles, but are certainly better than

“near spherical” platinum nanoparticles which are known not to catalyze this reaction. However, due to the loss of the tetrahedral shape in the drastic chemical and thermal environment at which the Suzuki reaction takes place, the catalytic activity rapidly decreases. The transformation of shape results in surface atomic reconstruction of the atoms on the corners and edges as well as Ostwald ripening process which form the (100) facets which are not present in the tetrahedral nanoparticles. This results in the formation of “near spherical” nanoparticles, which grow larger during the second cycle of the reaction. The continued growth of the nanoparticles during the second cycle is due to the strong capping action of the PVP (mw = 360,000) making the nanoparticles more resistant to aggregation and precipitation and is consistent with previous results observed with PAMAM Generation 4 dendrimer capped Pd nanoparticles³⁴, which are strong encapsulators. It is observed that the shape transformation is minimized in the presence of phenylboronic acid and this is proposed to be due to its binding to the nanoparticle surface and thus acting as a capping (stabilizing) agent. This result supports our proposed surface catalytic mechanism of the Suzuki reaction in our previous studies^{27,34} in which the phenylboronic acid binds to the nanoparticle surface and reacts with iodobenzene in solution via collisional processes.

9.6 References

1. Eppler, A.; Rupprechter, G.; Gucci, L.; Somorjai, G. A. *J. Phys. Chem. B* **1997**, *101(48)*, 9973.
2. Toshima, N.; Yonezawa, T. *New J. Chem.* **1998**, *22(11)*, 1179.
3. Schmid, G. *Met. Clus. Chem.* **1999**, *3*, 1325.
4. Puddephatt, R. J. *Met. Clus. Chem.* **1999**, *2*, 605.

5. Henry, C. R. *Appl. Surf. Sci.* **2000**, *164*, 252.
6. St. Clair, T. P.; Goodman, D. W. *Top. Catal.* **2000**, *13(1,2)*, 5.
7. Kralik, M.; Corain, B.; Zecca, M. *Chem. Pap.* **2000**, *54(4)*, 254.
8. Chusuei, C. C.; Lai, X.; Luo, K.; Goodman, D. W. *Top. Catal.* **2001**, *14(1-4)*, 71.
9. Bowker, M.; Bennett, R. A.; Dickinson, A.; James, D.; Smith, R. D.; Stone, P. *Stud. Surf. Sci. Catal.* **2001**, *133*, 3.
10. Kralik, M.; Biffis, A. *J. Mol. Catal. A: Chem.* **2001**, *177(1)*, 113.
11. Thomas, J. M.; Raja, R. *Chem. Rec.* **2001**, *1(6)*, 448.
12. Mohr, C.; Claus, P. *Sci. Prog.* **2001**, *84(4)*, 311.
13. Thomas, J. M.; Johnson, B. F. G.; Raja, R.; Sankar, G.; Midgley, P. A. *Acc. Chem. Res.* **2003**, *36(1)*, 20.
14. Bradley, J. S. *Clus. Colloids* **1994**, 459.
15. Duff, D. G.; Baiker, A. *Stud. Surf. Sci. Catal.* **1995**, *91*, 505.
16. Toshima, N. *NATO ASI Ser., Ser. 3* **1996**, *12*, 371.
17. Boennermann, H.; Braun, G.; Brijioux, G. B.; Brinkman, R.; Tilling, A. S.; Schulze, S. K.; Siepen, K. *J. Organomet. Chem.* **1996**, *520(1-2)*, 143.
18. Fugami, K. *Organomet. News* **2000**, *1*, 25.
19. Mayer, A. B. R. *Polym. Adv. Technol.* **2001**, *12(1-2)*, 96.
20. Bonnemann, H.; Richards, R. *Syn. Meth. Organom. Inorg. Chem.* **2002**, *10*, 209.
21. Moiseev, I. I.; Vargaftik, M. N. *Russ. J. Chem.* **2002**, *72(4)*, 512.
22. Collier, P. J.; Iggo, J. A.; Whyman, R. *J. Mol. Catal. A: Chem.* **1999**, *146(1-2)*, 149.
23. Sculz, J.; Roucoux, A.; Patin, H. *Chem. Eur. J.* **2000**, *6(4)*, 618.
24. Wang, Q.; Liu, H.; Han, M.; Li, X.; Jiang, D. *J. Mol. Catal. A: Chem.* **1997**, *118(2)*, 145.
25. Kim, S.; Son, S. U.; Lee, S. S.; Hyeon, T.; Chung, Y. K.; *Chem. Commun.* **2001**, 2212.
26. Larpent, C.; Menn, B. F.; Patin, H. *J. Mol. Catal.* **1991**, *65*, L35.

27. Narayanan, R.; El-Sayed, M. A. *J. Am. Chem. Soc.* **2003**, *125*(27), 8340.
28. Narayanan, R.; El-Sayed, M. A. *J. Phys. Chem. B*, **2003**, *107*(45), 12416.
29. Chechik, V.; Crooks, R. M. *J. Am. Chem. Soc.* **2000**, *122*, 1243.
30. Yeung, L. K.; Crooks, R. M. *Nano Lett.* **2001**, *1*(1), 14.
31. Dupont, J.; Fonseca, G. S.; Umpierre, A. P.; Fichtner, P. F. P.; Teixeira, S. R. *J. Am. Chem. Soc.* **2002**, *124*, 4228.
32. Hirai, H.; Chawanya, H.; Toshima, N. *Nip. Kag. Kai.* **1984**, *6*, 1027.
33. Roucox, A.; Sculz, J.; Patin, H. *Chem. Rev.* **2002**, *102*(10), 3757.
34. Narayanan, R.; El-Sayed, M. A., *J. Phys. Chem. B*, **2004**, *108*(25), 8572.
35. Narayanan, R.; El-Sayed, M. A. *J. Phys. Chem. B*, **2004**, *108*(18), 5726.
36. Narayanan, R.; El-Sayed, M. A. *Nano Lett.*, **2004**, *4*(7), 1343.
37. Narayanan, R.; El-Sayed, M. A. *J. Am. Chem. Soc.*, **2004**, *126*(23), 7194.
38. Suzuki, A. In *Metal-Catalyzed Cross-Coupling Reactions*; Diederich, F., Stang, P. J., Eds.; VCH: Weinheim, 1998, pp 49.
39. Alo, B. I.; Kandil, A.; Patil, P. A.; Sharp, M. J.; Siddiqui, M. A.; Snieckus, V. *J. Org. Chem.* **1991**, *56*, 3763.
40. Wallow, T. I.; Novak, B. M.; *J. Org. Chem.* **1994**, *59*, 5034.
41. Bumagin, N. A.; Bykov, V. V.; Beletskaya, I. P.; *Dokl. Akad. Nauk. SSSR* **1990**, *315*, 1133.
42. Marck, G.; Villiger, A.; Buchecker, R. *Tetrahedron Lett.* **1994**, *35*, 3277.
43. Reetz, M. T.; Breinbauer, R.; Wanninger, K. *Tetrahedron Lett.* **1996**, *26*, 4499.
44. Li, Y.; Hong, X. M.; Collard, D. M.; El-Sayed, M. A. *Org. Lett.* **2000**, *2*(15), 2385.
45. Li, Y.; Boone, E.; El-Sayed, M. A. *Langmuir* **2002**, *18*, 4921.
46. Li, Y.; El-Sayed, M. A. *J. Phys. Chem. B* **2001**, *105*, 8938.

47. Moreno-Manas, M.; Pleixats, R.; Villarroya, S. *Organomet.* **2001**, *20*(22), 4524.
48. Kogan, V.; Aizenshtat, Z.; Popovitz-Biro, R.; Neumann, R. *Org. Lett.* **2002**, *4*(20), 3529.
49. Strimbu, L.; Liu, J.; Kaifer, A. E. *Langmuir* **2003**, *19*, 483.
50. Thathagar, M. B.; Beckers, J.; Rothenberg, G. *J. Am. Chem. Soc.* **2002**, *124*(40), 11858.
51. Colacot, T. J.; Qian, H.; Cea-Olivares, R.; Hernandez-Ortega, S. *J. Organomet. Chem.* **2001** 637-639, 691.
52. Gentle, T. M.; Muetterties, E. L. *J. Phys. Chem.*, **1983**, *87*, 2469.
53. Rucker, T. G.; Logan, M. A.; Gentle, T. M.; Muetterties, E. L.; Somorjai, G. A. *J. Phys. Chem.*, **1986**, *90*, 2703.
54. Rellinghaus, B.; Stappert, S.; Acet M.; Wassermann, E. F. *Mat. Res. Soc. Symp. Proc.*, **2002**, *705*, Y9.5.1.
55. Ahmadi, T. S.; Wang, Z. L.; Green, T. C.; Henglein, A.; El-Sayed, M. A. *Science*, **1996**, *272*, 1924.
56. Hardeveld, R. V.; Hartog, F. *Surf. Sci.*, **1969**, *15*, 189.
57. Xiong, L.; Manthiram, A., *J. Mater. Chem.*, **2004**, *14*, 1454.

CHAPTER 10

FTIR STUDY OF THE MODE OF BINDING OF THE REACTANTS ON THE Pd NANOPARTICLE SURFACE DURING THE CATALYSIS OF THE SUZUKI REACTION

10.1 Abstract

In the Suzuki reaction between phenylboronic acid and iodobenzene catalyzed by palladium nanoparticles, our previous studies suggested that the phenylboronic acid adsorbs on the nanoparticle surface and then interacts with the iodobenzene that is present in solution. In the present study, FTIR is used to examine the change in the vibrational frequencies of phenylboronic acid in films with and without the addition of palladium nanoparticles. The large change in the B-O stretching frequency of phenylboronic acid from 1348 cm^{-1} to 1376 cm^{-1} in the presence of sodium acetate and palladium nanoparticles strongly suggests that the mode of binding of phenylboronic acid to the Pd nanoparticle surface involves a B-O-Pd type of bonding. Shifts in the B-C stretching mode and the out-of-plane phenyl C-C ring deformation bands associated with phenylboronic acid provide additional confirmations of the binding process. It is also shown that the phenylboronic acid needs to be in the deprotonated form in the presence of sodium acetate (phenylboronate anion) in order to bind to the palladium nanoparticle surface. No changes in the characteristic bands of iodobenzene were observed in films made in the presence of the palladium nanoparticles. The FTIR studies provide proof of the mode of binding that occurs in the nanoparticle surface for the first time and also

confirms the surface catalytic mechanism of the Suzuki reaction that we proposed previously.

10.2 Introduction

Studies on catalysis with transition metal nanoparticles in colloidal solution has been very active recently and is described in many review articles published during the past decade¹⁻⁸. There have been very few studies conducted on the stability of the nanoparticle catalysts during the course of the reaction⁹⁻¹³. We have previously¹⁴⁻¹⁹ studied the effect of catalysis on the size and shape of transition metal nanoparticles that are used as catalysts. One particular reaction that we studied is the electron transfer reaction between hexacyanoferrate (III) ions and thiosulfate ions using spherical¹⁴⁻¹⁶, tetrahedral¹⁵⁻¹⁷, and cubic¹⁵⁻¹⁷ platinum nanoparticles as catalysts. It was observed that there is a slight reduction in the size of the spherical platinum nanoparticles after the first and second cycle of the electron transfer reaction¹⁴. Also, there is a great reduction in the size of the nanoparticles when they are exposed to just the hexacyanoferrate (III) ions while they maintain their size in the presence of just the thiosulfate ions. Based on these observations, it was suggested that the catalytic mechanism involves the thiosulfate ions binding to the nanoparticle surface and reacting with hexacyanoferrate (III) ions in solution. We found that the catalytic activity is shape-dependent during the early stages of the reaction in which the tetrahedral nanoparticles are found to be the most catalytically active and the cubic nanoparticles are the least catalytically active for particles of comparable size¹⁵. During the course of the reaction, it was observed that dissolution of platinum atoms occurred at the corners and edges of the tetrahedral and cubic nanoparticles, which also resulted in corresponding changes in the activation

energy¹⁶. It was also observed that the dissolution of atoms on the corners and edges of the platinum nanoparticles occurs faster for the tetrahedral nanoparticles than the cubic nanoparticles¹⁷.

Another reaction that we studied was the Suzuki reaction between phenylboronic acid and iodobenzene using PVP-Pd nanoparticles^{18, 20-22} and PAMAM-OH Generation 4 dendrimer capped Pd nanoparticles^{19, 22}. We found that the size of the nanoparticles became larger as a result of Ostwald ripening processes as well as the presence of excess palladium atoms and partly reduced palladium ions. These processes occur in the presence of the solvent, sodium acetate, and iodobenzene^{18, 19}. We observed that the growth process is inhibited in the presence of phenylboronic acid. Due to these observations, we proposed that when the phenylboronic acid is in the deprotonated form (due to presence of sodium acetate), it binds to the nanoparticle surface through the O⁻ of the OH group. We also proposed that the surface catalytic mechanism of the Suzuki reaction involves the phenylboronic acid binding to the nanoparticle surface and reacting with iodobenzene that is present in solution.

FTIR is used to determine the mode of binding of the phenylboronic acid to the Pd nanoparticle surface. One major characteristic vibrational mode of the phenylboronic acid that is greatly shifted upon the addition of the nanoparticles and sodium acetate is the B-O vibration. This suggests a mode of binding that involves the B-O-Pd structure. The FTIR studies provide proof of the mode of binding that occurs in the nanoparticle surface for the first time and also confirms the mechanism of surface catalysis in the Suzuki reaction that we proposed previously.

10.3 Experimental

10.3.1 Synthesis of PVP-Pd Nanoparticles

The PVP-Pd nanoparticles are synthesized as described previously^{18, 20-23} by the reduction of the Pd ions with ethanol. The palladium precursor solution (H_2PdCl_4) is prepared by adding 0.0887 g of PdCl_2 , 6 mL of 0.2 M HCl, and diluting to 250 mL with doubly distilled water. A solution containing 15 mL of 2 mM of H_2PdCl_4 , 21 mL of doubly deionized water, 0.0667 g PVP, and 4 drops of 1 M HCl is heated. When the solution begins to reflux, 14 mL of ethanol is added. The solution is then refluxed for three hours and a dark brown colloidal Pd solution is formed. A drop of the solution is spotted onto Formvar stabilized copper TEM grids and JEOL 100C TEM is used to characterize the size of the nanoparticles. For the FTIR studies, it is necessary to have concentrated nanoparticle solutions. As a result, the nanoparticles are rotovaped to concentrate the nanoparticle solution from 50 mL to 2 mL.

10.3.2 FTIR Studies of Dried Films

Films of sodium acetate (SA), phenylboronic acid (PA), SA + PA, PVP-Pd nanoparticles, PVP-Pd nanoparticles + PA, and PVP-Pd nanoparticles + SA + PA are prepared and dried in the oven for 30 minutes in order to investigate how the phenylboronic acid interacts with the palladium nanoparticle surface. In addition, films of iodobenzene (I), SA + I, and PVP-Pd nanoparticles + SA + I are also prepared in order to investigate how the iodobenzene interacts with the palladium nanoparticle surface.

FTIR spectra of the films are recorded in the range of 4000-400 cm^{-1} at a resolution of 4 cm^{-1} using the Nicolet 860 Magna-IR with DTGS detector and zinc selenide windows.

10.4 Results and Discussion

10.4.1 FTIR Studies on Phenylboronic Acid

FTIR studies are conducted to find out if there are shifts in the characteristic vibrational modes associated with phenylboronic acid upon exposure to sodium acetate and the PVP-Pd nanoparticles. Table 10.1 summarizes the important vibrational modes and the frequencies observed in phenylboronic acid, phenylboronic acid + sodium acetate, phenylboronic acid + PVP-Pd nanoparticles, and phenylboronic acid + sodium acetate + PVP-Pd nanoparticles.

Table 10.1—Frequencies of different vibration modes* in phenylboronic acid (PA), PA + sodium acetate (SA), PVP-Pd NPs + PA, and PVP-Pd NPS + PA + SA

Vibration Mode	Frequency in PA (cm^{-1})	Frequency in PA + SA (cm^{-1})	Frequency in PVP-Pd + PA (cm^{-1})	Frequency in PVP-Pd + PA + SA (cm^{-1})
B-O Stretching	1348	1348	1349	1376
B-C Stretching	1087	1087	1087	1086
B-C Stretching	1102	1103 1112	1103	1118
Out-of-plane phenyl ring deformation	700	698	700	706
Shoulder next to out-of-plane phenyl ring deformation	688	687	687	681

Figure 10.1a shows the FTIR spectra in the region of 1800-1200 cm^{-1} obtained from dried films of sodium acetate (SA), phenylboronic acid (PA), SA + PA, PVP-Pd nanoparticles, PVP-Pd nanoparticles + PA, and PVP-Pd nanoparticles + PA + SA. Band assignments for PA are obtained from a previous infrared spectral study in the literature²⁴. It can be seen that the B-O stretching band shifts from 1348 cm^{-1} in the presence of PA to 1376 cm^{-1} when the nanoparticles are added to PA + SA in solution before drying. In the spectra of PA + SA without the presence of PVP-Pd nanoparticles, it is observed that the B-O stretching band occurs at 1348 cm^{-1} , and this suggests that deprotonation does not occur in the film due to the loss of water upon drying and thus does not result in a shift in the B-O stretching mode. The large shift in the B-O stretching frequency that occurs when the PVP-Pd nanoparticles are added to PA and SA prior to evaporation of the solution is an important indication that the phenylboronate anion (formed from PA due to the presence of SA) binds to the nanoparticle surface through the B-O⁻ group. In the case of the PVP-Pd nanoparticles + PA, it is observed that the B-O stretching mode occurs at 1349 cm^{-1} , suggesting that the addition of PA to the palladium nanoparticles prior to drying the solution into a film does not result in it binding to the palladium nanoparticle surface. This provides additional evidence that the phenylboronic acid must be in the form of phenylboronate anion by the presence of sodium acetate in order to bind to the palladium nanoparticle surface.

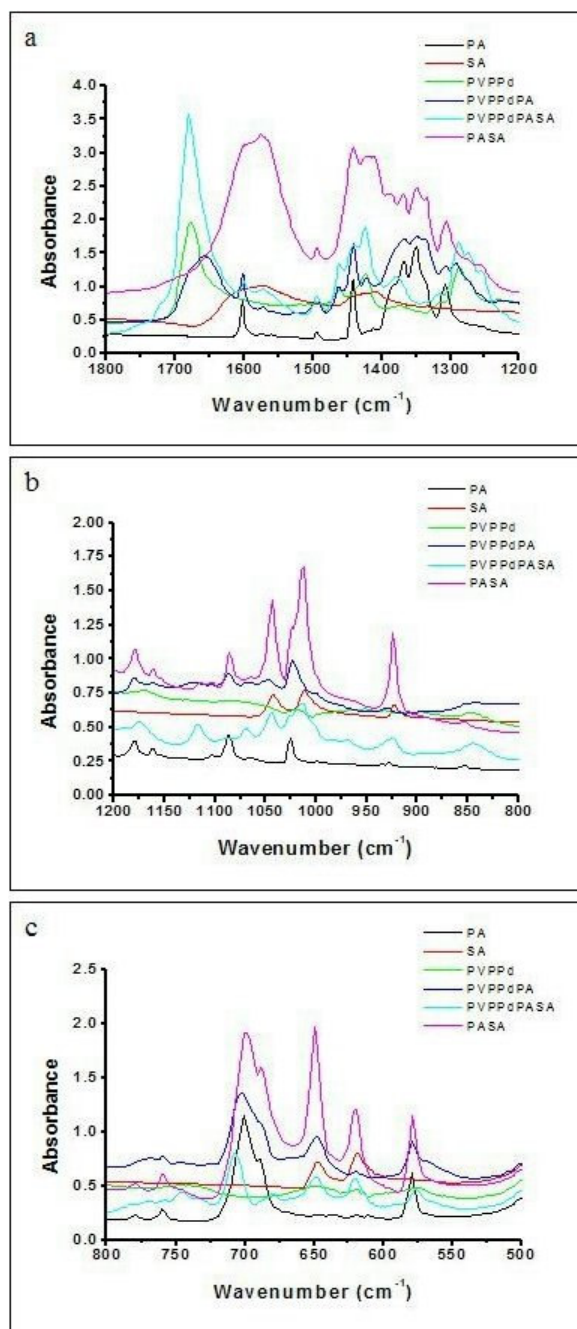


Figure 10.1— FTIR spectra of PA, SA, SA + PA, PVP-Pd nanoparticles, PVP-Pd nanoparticles + PA, and PVP-Pd nanoparticles + SA + PA in 1800-1200 cm⁻¹ region (a), 1200-800 cm⁻¹ region (b), and 800-500 cm⁻¹ region (c)

An interesting question involves determining how the boronate group (BO_2^-) of phenylboronate anion binds to the nanoparticle surface and Figure 10.2 illustrates two possible binding modes. The phenylboronate anion can bind to the palladium nanoparticle surface through a single bond between its B-O^- group and the Pd atom (terminal binding) or through both of its B-O^- groups to two Pd atoms (bridged binding). Terminal binding would result in bands existing in both the 1348 cm^{-1} and the 1376 cm^{-1} regions since one B-O^- group would be bound to the palladium nanoparticles while the other B-O^- group would be free. The blue shift in the B-O stretching mode that occurs when the nanoparticles are exposed to PA + SA is relatively large ($\sim 28\text{ cm}^{-1}$). Since there is no band in the 1348 cm^{-1} region and only one shifted band is observed at 1376 cm^{-1} , the phenylboronate anion most likely binds through a bridge involving two B-O-Pd bonds.

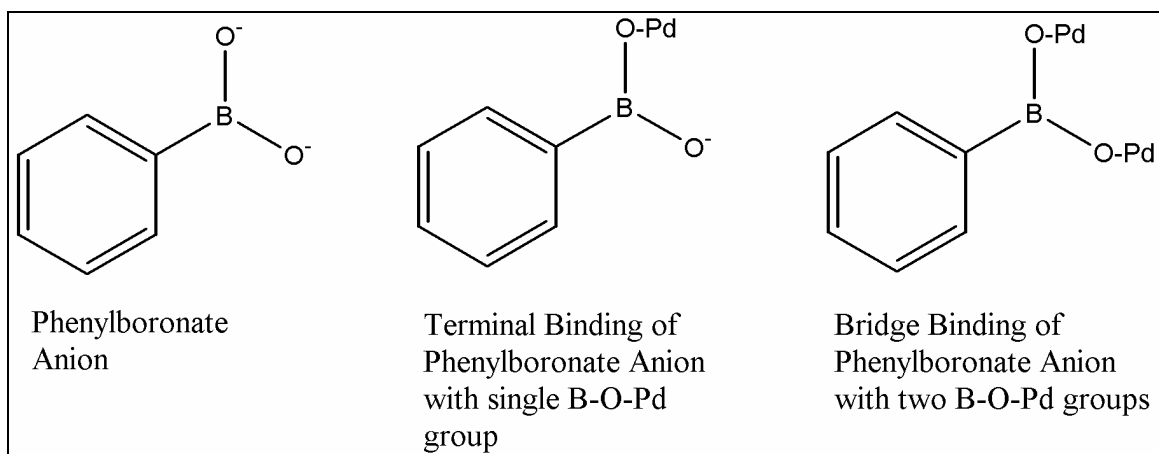


Figure 10.2—Illustration of phenylboronate anion and the two possibilities of binding to the palladium nanoparticle surface which can occur. The binding can occur through one B-O^- group or through both B-O^- groups.

Figure 10.1b shows the FTIR spectra in the region of $1200\text{--}800\text{ cm}^{-1}$ for the different systems. In the case of PA and PA + SA, the B-C stretching mode occurs at 1087 cm^{-1} . This suggests that deprotonation of phenylboronic acid does not occur in a

film made by adding SA and then drying the solution due to the loss of water that occurs during the evaporation process. When the PVP-Pd nanoparticles are added to PA + SA prior to drying the solution into a film, it is observed that the B-C stretching mode is very weak. In the case where the PVP-Pd nanoparticles are added to PA, it is also observed that the B-C stretching mode occurs at 1086 cm^{-1} . It is also observed that the band at 1102 cm^{-1} in PA and 1103 cm^{-1} in PA + SA is shifted and enhanced when the nanoparticles are added to PA + SA before drying and appears at 1118 cm^{-1} . In the literature^{24, 25}, it was shown that the infrared spectra of phenylboronic anhydride has two B-C stretching bands (doublet), one at 1087 cm^{-1} and the other at 1104 cm^{-1} . It is possible that the weak band we observe at 1102 cm^{-1} for PA by itself and 1103 cm^{-1} for PA + SA is also due to the B-C stretching mode. In the case of PA + SA, it is observed that there is also a band at 1112 cm^{-1} , which could be due to the deprotonation of the phenylboronic acid causing a shift in the B-C stretching mode. In this case, it can also be seen that the shift in the B-C stretching mode is incomplete. When the nanoparticles are added to PA + SA in solution before evaporation, the shift in the B-C stretching mode is complete with a band at 1118 cm^{-1} being present and the band at 1103 cm^{-1} being absent. The complete shift in the B-C stretching mode observed when the nanoparticles are added to PA + SA suggests that the phenylboronate anion binds to the nanoparticle surface. In the case when the nanoparticles are added to PA prior to drying the solution into a film, there is no shift in the B-C stretching mode since it occurs at 1103 cm^{-1} . This provides additional evidence that the phenylboronate anion (formed by the presence of sodium acetate) binds to the nanoparticle surface in solution prior to drying.

Figure 10.1c shows the FTIR spectra in the region of 800-500 cm^{-1} . When comparing spectra obtained when the PVP-Pd nanoparticles are mixed with PA + SA to the spectra obtained of PA by itself, it is observed that there is a shift in the out-of-plane phenyl C-C ring deformation band and its shoulder from 700 cm^{-1} and 688 cm^{-1} to 706 cm^{-1} and 681 cm^{-1} , respectively. The shoulder has not been reported in the literature. In the spectra of PA + SA without the presence of the PVP-Pd nanoparticles, the out-of-plane phenyl C-C ring deformation band and its shoulder occur at 698 cm^{-1} and 687 cm^{-1} . In this case, it can be seen that the ring deformation band and its shoulder occur at frequencies similar to those observed in PA. This might be explained by the fact that the OH is unionized in both cases due to the loss of water that occurs in the process of preparing dried films. This means that deprotonation of the phenylboronic acid might not occur in the films of the two samples and thus does not result in a shift in the out-of-plane phenyl C-C ring deformation band and its shoulder. In the case of PVP-Pd NPs + PA + SA, it is observed that there is a shift in the ring deformation band to higher frequencies. The shifts in the out-of plane phenyl C-C ring deformation vibration and its shoulder could be due to the phenylboronate anion (formed from PA by the presence of SA) binding to the palladium nanoparticle surface. In the structure of the Ph-B-O-Pd, one would expect that the phenyl deformation would be different from that for the Ph-B-OH, which is present in a film made from drying a solution of PA and PA + SA. In the case of Ph-B-OH, the out-of-plane ring deformation can occur much more easily and freely than in the case of Ph-B-O-Pd, where the presence of the heavy nanoparticles makes the Ph-B bond stiffer. As a result, when the heavy phenylboronic acid is bound to the nanoparticle surface, the out-of-plane phenyl C-C ring deformation process does not

occur as readily and is more difficult to do so. This would result in this vibrational mode occurring at a higher frequency, which correlates with our observation that the frequency shifts from 700 cm^{-1} to 706 cm^{-1} . When the PVP-Pd nanoparticles are added to PA in solution before drying, it is observed that the ring deformation band occurs at 700 cm^{-1} and its shoulder occurs at 687 cm^{-1} , which is similar to that observed in PA. This shows that the phenylboronic acid does not bind to the nanoparticle surface when it is not in the presence of sodium acetate before drying. This also provides additional proof that the phenylboronate anion formed in the presence of sodium acetate binds to the nanoparticle surface.

10.4.2 FTIR Studies on Films of Iodobenzene and the Pd Nanoparticles

Figure 10.3a-c show FTIR spectra in the region of $1800\text{-}1200\text{ cm}^{-1}$, $1200\text{-}800\text{ cm}^{-1}$, and $800\text{-}500\text{ cm}^{-1}$ respectively, for the following conditions involving iodobenzene: iodobenzene (I), sodium acetate (SA), I + SA, PVP-Pd NPs, and PVP-Pd NPs + I + SA. The band assignments for iodobenzene were obtained from infrared spectral studies conducted in the literature²⁶. It can be seen that there are no shifts in the bands that are associated with characteristic vibrational modes of iodobenzene. There are no shifts in the four C-C stretching modes at 1571 cm^{-1} , 1471 cm^{-1} , 1438 cm^{-1} , and 1321 cm^{-1} . There are no shifts in the C-I stretching mode at 1059 cm^{-1} and the CCH in-plane bending mode at 1014 cm^{-1} . There are also no shifts in the ring breathing mode at 997 cm^{-1} or in the two CH out-of-plane bending modes at 903 cm^{-1} and 729 cm^{-1} . Finally, there is also no shift in the CCC nonplanar twist mode at 685 cm^{-1} . Since there are no shifts in the bands associated with the characteristic vibrational modes of iodobenzene, it is concluded

that iodobenzene does not have specific bonding to the surface of the palladium nanoparticles.

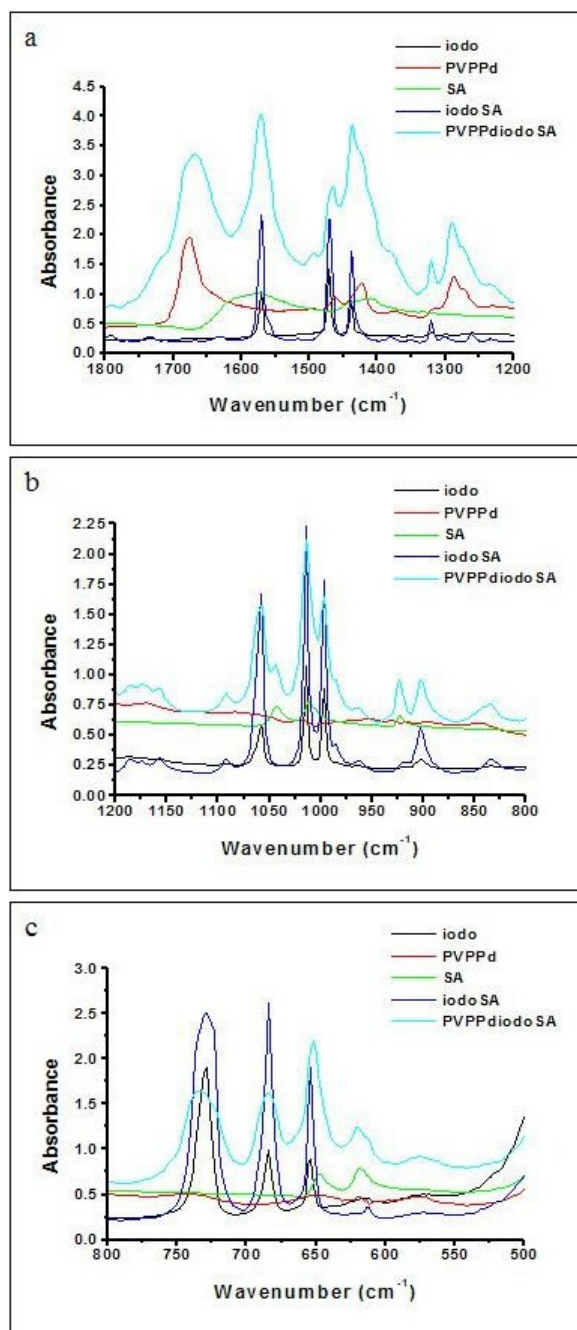


Figure 10.3— FTIR spectra of I, SA, SA + I, PVP-Pd nanoparticles, and PVP-Pd nanoparticles + SA + I in 1800-1200 cm⁻¹ region (a), 1200-800 cm⁻¹ region (b), and 800-500 cm⁻¹ region (c).

10.4.3 Catalytic Mechanism of the Suzuki Reaction

The results obtained from the FTIR studies on the interaction of phenylboronic acid and iodobenzene to the palladium nanoparticle surface show that our proposed surface catalytic mechanism of the Suzuki reaction reported previously^{18, 19} is correct. The phenylboronate anion does indeed bind to the nanoparticle surface through both B-O⁻ groups. Since the iodobenzene does not bind to the nanoparticle surface, the mechanism of surface catalysis must involve the phenylboronic acid binding to the nanoparticle surface in the form of phenylboronate anion followed by its reaction with the iodobenzene present in solution.

10.5 Conclusions

FTIR studies have shown that phenylboronate anion (which is formed from PA in the presence of SA) does indeed bind to the Pd nanoparticle surface. Shifts in the B-O stretching mode, the B-C stretching mode, and the out-of-plane phenyl C-C ring deformation band and its shoulder associated with phenylboronic acid are observed when the PVP-Pd nanoparticles are exposed to PA + SA. When the PVP-Pd nanoparticles are added to PA without the presence of SA, shifts in the characteristic bands associated with PA are not observed, suggesting that in this case, the phenylboronic acid must be in the protonated form and that the binding process involves its conjugate base (phenylboronate anion). The phenylboronate anion binds to the nanoparticle through a B-O-Pd bridge. It has also been shown that iodobenzene does not have specific binding to the nanoparticle surface since no shifts in the characteristic vibrational modes associated with iodobenzene are observed upon exposure to the nanoparticles. These results provide

support to the surface catalytic mechanism of the Suzuki reaction that involves the phenylboronate anion binding to the nanoparticle surface and then reacting with the iodobenzene present in solution.

10.6 References

1. Bradley, J. S. *Clus. Colloids* 1994, 459.
2. Duff, D. G.; Baiker, A. *Stud. Surf. Sci. Catal.* 1995, 91, 505.
3. Toshima, N. *NATO ASI Ser., Ser. 3* 1996, 12, 371.
4. Boennermann, H.; Braun, G.; Brijoux, G. B.; Brinkman, R.; Tilling, A. S.; Schulze, S. K.; Siepen, K. *J. Organomet. Chem.* 1996, 520(1-2), 143.
5. Fugami, K. *Organomet. News* 2000, 1, 25.
6. Mayer, A. B. R. *Polym. Adv. Technol.* 2001, 12(1-2), 96.
7. Bonnemann, H.; Richards, R. *Syn. Meth. Organom. Inorg. Chem.* 2002, 10, 209.
8. Moiseev, I. I.; Vargaftik, M. N. *Russ. J. Chem.* 2002, 72(4), 512.
9. Collier, P. J.; Iggo, J. A.; Whyman, R. *J. Mol. Catal. A: Chem.* 1999, 146(1-2), 149.
10. Sculz, J.; Roucoux, A.; Patin, H. *Chem. Eur. J.* 2000, 6(4), 618.
11. Wang, Q.; Liu, H.; Han, M.; Li, X.; Jiang, D. *J. Mol. Catal. A: Chem.* 1997, 118(2), 145.
12. Kim, S.; Son, S. U.; Lee, S. S.; Hyeon, T.; Chung, Y. K.; *Chem. Commun.* 2001, 2212.
13. Larpent, C.; Menn, B. F.; Patin, H. *J. Mol. Catal.* 1991, 65, L35.
14. Narayanan, R.; El-Sayed, M. A. *J. Phys. Chem. B*, 2003, 107(45), 12416.
15. Narayanan, R.; El-Sayed, M. A. *Nano Lett.*, 2004, 4(7), 1353.
16. Narayanan, R.; El-Sayed, M. A. *J. Am. Chem. Soc.*, 2004, 126(23), 7419.

17. Narayanan, R.; El-Sayed, M. A. *J. Phys. Chem. B*, 2004, *108*(18), 5726.
18. Narayanan, R.; El-Sayed, M. A. *J. Am. Chem. Soc.*, 2003, *125*(27), 8340.
19. Narayanan, R.; El-Sayed, M. A. *J. Phys. Chem. B*, 2004, *108*(25), 8572.
20. Li, Y.; Hong, X. M.; Collard, D. M.; El-Sayed, M. A. *Org. Lett.* 2000, *2*(15), 2385.
21. Li, Y.; Boone, E.; El-Sayed, M. A. *Langmuir* 2002, *18*, 4921.
22. Li, Y.; El-Sayed, M. A. *J. Phys. Chem. B* 2001, *105*, 8938.
23. Teranishi, T.; Miyake, M. *Chem. Mat.*, 1998, *10*, 594.
24. Faniran, J. A.; Shurvell, H. F. *Canadian J. Chem.* 1968, *46*, 2089.
25. Aubrey, D. W.; Lappert, M. F.; Pyszora, H. *J. Chem. Soc.* 1961, 1931.
26. Syomin, D.; Koel, B. E. *Surf. Sci.*, 2001, *490*, 265.

CHAPTER 11

CARBON SUPPORTED SPHERICAL PALLADIUM NANOPARTICLES AS POTENTIAL RECYCLABLE CATALYSTS FOR THE SUZUKI REACTION

11.1 Abstract

Carbon supported spherical PVP-Pd nanoparticles are prepared by the adsorption of colloidal PVP-Pd nanoparticles onto activated carbon and used as catalysts for the Suzuki cross-coupling reaction between phenylboronic acid and iodobenzene to form biphenyl. HPLC studies show that the use of the carbon supported Pd nanoparticles result in a lower amount of biphenyl formed during the first cycle than the colloidal Pd nanoparticles we studied previously. The carbon supported spherical palladium nanoparticles retain 69% of its activity during the second cycle while the colloidal spherical palladium nanoparticles we studied previously retain only 37% of its activity during the second cycle. As a result, it can be seen that the carbon supported spherical Pd nanoparticles have almost double the recycling potential compared to the colloidal spherical Pd nanoparticles we studied previously. Perhaps the large amount of carbon support on which the palladium nanoparticles are adsorbed helps to preserve its catalytic activity for longer periods of time. The effect of catalyzing the Suzuki reaction and recycling on the nanoparticle size has also been investigated for the carbon supported spherical Pd nanoparticles. The supported nanoparticles are monodisperse with an initial average size of 1.9 ± 0.1 nm. The average size of the carbon supported spherical palladium nanoparticles is 2.6 ± 0.1 nm after the first cycle of the Suzuki reaction and 3.1

± 0.1 nm after the second cycle. The continued growth of the supported nanoparticles suggests that the large amount of carbon support helps to protect the palladium nanoparticles during the harsh Suzuki reaction and helps to prevent aggregation and precipitation unlike the behavior of the colloidal palladium nanoparticles we studied previously. In addition, it is observed that catalysis with the supported nanoparticles retains its observed narrow size distribution. The adsorption method used to prepare the carbon supported Pd nanoparticles could account for this observation since in this preparation method, excess unaggregated palladium atoms will not be present since they will not be adsorbed onto the carbon support. The growth of the nanoparticles after the first and second cycle of the Suzuki reaction strictly occurs via the Ostwald ripening process in which there is detachment of atoms from the smaller nanoparticles and reattachment of these atoms to the more stable surfaces of the larger nanoparticles.

11.2 Introduction

The nanocatalysis field has undergone an explosive growth during the past decade since nanoparticles are attractive to use as catalysts compared to other bulk catalytic materials due to their high surface tension. Nanoparticles in colloidal solution as well as supported nanoparticles have been used as catalysts and there have been over 2800 papers published in this vast field. Approximately 15-20% of the work in this field is conducted using colloidal metal nanoparticles as catalysts. Majority of the work has been conducted using supported metal nanoparticles as catalysts for a variety of organic and inorganic reactions. Supported metal nanoparticles have been prepared by adsorption¹⁻¹⁰, grafting¹¹⁻¹², or by lithographic fabrication using electron beam lithography¹³⁻¹⁶. There

have been numerous review articles that have been published which describe the use of supported nanoparticles as catalysts for a variety of reactions¹⁷⁻²⁹.

While the nanocatalysis field is vast, there have not been many studies on understanding what happens to the nanoparticles during the course of the catalytic process. There have been a few studies that have characterized the nanoparticles after the catalytic process for colloidal metal nanoparticles³⁰⁻³⁴ as well as supported metal nanoparticles³⁵⁻³⁹. There have also been a few studies that have investigated the recycling potential of colloidal metal nanoparticles⁴⁰⁻⁴³ and supported metal nanoparticles⁴⁴⁻⁴⁷. Overall, it can be seen that there has not been many studies conducted on the stability of the nanoparticles after its catalytic function as well as their recycling potential in both the colloidal metal nanoparticles and the supported metal nanoparticles. **Detailed** studies are necessary in order to try to design the best catalyst to use for a particular kind of reaction.

We have previously conducted several studies on the effect of the catalytic process on the shape^{49-51, 54} and size^{48, 52-53} of colloidal metal nanoparticles. We have used tetrahedral⁴⁹⁻⁵¹, cubic⁴⁹⁻⁵¹, and spherical⁴⁸⁻⁵⁰ shaped platinum nanoparticles to catalyze the electron transfer reaction. We found that catalysis is shape-dependent during the early stages of the reaction, in which no large shape changes take place⁴⁹. The activation energy of the catalytic reaction is found to decrease as the fraction of surface platinum atoms present in the corners and edges increases. During the long reaction time in the full course of the electron transfer reaction (2 days), we observe changes in the platinum nanoparticle shape and corresponding changes in the activation energy that take place⁵⁰. Dissolution of atoms from the corners and edges of the tetrahedral and cubic platinum nanoparticles occur, resulting in the formation of distorted tetrahedral and

distorted cubic platinum nanoparticles. The rate of shape change was found to occur faster for the tetrahedral platinum nanoparticles than the cubic platinum nanoparticles⁵¹.

We also conducted studies on the effect of catalyzing the Suzuki reaction on the size of spherical palladium nanoparticles⁵²⁻⁵³. The Suzuki reaction is a more harsh reaction since it requires the reaction mixture to be refluxed at 100 °C for 12 hours. It was observed that the spherical PVP-palladium nanoparticles grew larger in size after the first cycle of the Suzuki reaction due to the Ostwald ripening process. After the second cycle, the palladium nanoparticles are much smaller in size due to the aggregation and precipitation of the larger nanoparticles that were formed during the first cycle of the reaction⁵². In the case of the dendrimer-Pd nanoparticles, it was observed that the growth process continues to occur during the second cycle and this could be due to the dendrimer being a strong encapsulating agent and protecting the nanoparticle surface well⁵³. This makes the nanoparticles more resistant to aggregation and precipitation. It was also found that the reduction method used to prepare the nanoparticles also plays an important role in the growth of the palladium nanoparticles during the Suzuki reaction. In addition, colloidal tetrahedral platinum nanoparticles have also been used as catalysts for the Suzuki cross-coupling reaction⁵⁴. It was observed that the tetrahedral platinum nanoparticles transform into spherical shaped platinum nanoparticles after the Suzuki reaction is complete and these transformed spherical nanoparticles grew larger in size upon recycling (after the second cycle).

We have shown in our previous studies that **colloidal** metal nanoparticles are unstable and undergo changes in their morphology (size and shape) in order to survive in the reaction mixture. As a result, it can be seen that there is a need to try to find better

types of nanocatalysts to use that can withstand the reaction conditions in which catalytic processes take place. Some possibilities include the use of better stabilizers to stabilize colloidal metal nanoparticles or the use of supported metal nanoparticles as catalysts. Previously, Li et al⁵⁵ has examined the effect of the capping material in colloidal solution. They found that as the capping material stabilizes the nanoparticles, it decreases its catalytic efficiency.

In the present study, we explore the possibility of using supported metal nanoparticles as good potential catalysts. We used carbon supported nanoparticles to catalyze the Suzuki reaction. One very common type of substrate that has been used in the preparation of supported nanoparticles is carbon⁵⁶⁻⁶⁴. Suzuki cross-coupling reactions have traditionally been catalyzed with different phosphine based and phosphine-free palladium complexes⁶⁵⁻⁶⁹. There have also been many cases of palladium complexes supported on various substrates such as silica^{70-71, 73, 77}, resin^{72, 78}, chitosan⁷⁴, alumina⁷⁵, carbon⁷⁶, etc. that have also been used to catalyze this type of reaction. Recently, many different types of colloidal palladium nanoparticles have been used as catalysts for the Suzuki reaction^{52-53, 79-87}. It is worth noting that there have been very few cases of supported palladium nanoparticles being used as catalysts for this reaction⁸⁸⁻⁸⁹ and the substrates that have been used in these cases are silica⁸⁸, titania⁸⁸, and alumina⁸⁹. More importantly, there have not been any studies on the use of carbon supported palladium nanoparticles as catalysts for the Suzuki cross-coupling reaction.

One aim in this paper is to determine if carbon supported spherical PVP-Pd nanoparticles are more catalytically active for the Suzuki reaction than the colloidal spherical PVP capped palladium nanoparticles that we studied previously⁵². Another

goal is to investigate the effect of the catalytic process on the size of the carbon supported spherical palladium nanoparticles and compare the results with those obtained for the colloidal spherical palladium nanoparticles studied previously⁵². The Suzuki reaction is chosen to test the stability of the carbon supported spherical nanoparticles since it is a relatively harsh reaction that takes place at 100 °C for 12 hours. In addition, it is also very important to assess the recycling potential of the carbon supported spherical palladium nanoparticles in order to provide additional information on its usefulness in catalysis.

11.3 Experimental Section

11.3.1 Synthesis of Colloidal Spherical PVP-Pd Nanoparticles

The colloidal spherical PVP-Pd nanoparticles are synthesized by the reduction of the Pd ions with ethanol similar to that described previously³⁶. The palladium precursor solution (H_2PdCl_4) is prepared by adding 0.0887 g of PdCl_2 , 6 mL of 0.2 M HCl, and diluting to 250 mL with doubly distilled water. A solution containing 15 mL of 2 mM of H_2PdCl_4 , 21 mL of doubly deionized water, 0.0667 g PVP, and 4 drops of 1 M HCl is heated. When the solution begins to reflux, 14 mL of ethanol is added. The solution is then refluxed for three hours and a dark brown colloidal Pd solution is formed. A drop of the solution is spotted onto Formvar stabilized copper TEM grids and JEOL 100C TEM is used to characterize the size of the nanoparticles.

11.3.2 Synthesis of Carbon Supported Spherical PVP-Pd Nanoparticles

The carbon supported spherical PVP-Pd nanoparticles are prepared using the adsorption method. First, 25 mL of the nanoparticle solution is diluted to 50 mL by adding 25 mL of doubly distilled water. Next, 50 mL of the diluted palladium nanoparticles is mixed with 1.0 g of activated carbon. The solution is then stirred vigorously at room temperature for 24 hours. After this, the solution is centrifuged at 19,000 rpm for 30 minutes at 25° C in order to separate the liquid from the carbon support containing the adsorbed Pd nanoparticles. The centrifugation process is continued for two more cycles in order to make sure that only the adsorbed nanoparticles remain in the carbon support. The carbon support containing the adsorbed Pd nanoparticles is poured onto a piece of filter paper and is allowed to dry overnight. The resulting powder is the spherical PVP-Pd nanoparticles adsorbed onto the activated carbon support. In order to observe the nanoparticles by HRTEM, it is necessary to place a small amount of the powder in ethanol and sonicate it for an hour prior to spotting the solution onto a Formvar stabilized copper TEM grid. The carbon-supported palladium nanoparticles are imaged by using the JEM 4000EX HRTEM since the use of high-resolution transmission electron microscopy results in the supported nanoparticles being seen much more clearly than in the case of conventional transmission electron microscopy.

11.3.3 Catalyzing Suzuki Reaction (First and Second Cycles)

The carbon supported spherical PVP-Pd nanoparticles are used to catalyze the Suzuki reaction between phenylboronic acid and iodobenzene to form biphenyl. In this

reaction, 0.49 g sodium acetate, 0.37 g phenylboronic acid, and 0.20 g iodobenzene is added to 150 mL of the 3:1 acetonitrile:water solvent. The reaction mixture is heated to 100° C. Once the mixture refluxes, 0.05 g of the carbon supported spherical PVP-Pd nanoparticles is added to the reaction mixture. The reaction mixture is refluxed for a total of 12 hours. The same reaction mixture solution was used for recycling after the addition of fresh amounts of the reactants. For recycling, an assumption was made that all of the iodobenzene was used up since it is the limiting reactant. Initially there is 1 mmol iodobenzene and 3 mmol phenylboronic acid present in the reaction mixture. After the first cycle, it is assumed that there is no iodobenzene left and 2 mmol phenylboronic acid left. As a result 1 mmol iodobenzene and 1 mmol phenylboronic acid are added in order to start the second cycle of the Suzuki reaction. The reaction mixture is then refluxed for another 12 hours to complete the second cycle. A control experiment is also conducted in which the Suzuki reaction mixture is refluxed for 12 hours without the presence of any catalyst. In addition, another control experiment is conducted in which the Suzuki reaction mixture is refluxed for 12 hours in the presence of just the activated carbon support without the nanoparticles.

11.3.4 HPLC Studies on Catalytic Activity of the Carbon Supported Spherical Pd Nanoparticles

HPLC measurements are conducted on a Hitachi-4500 HPLC equipped with a L4500A diode array detector in which the absorbance is monitored at 254 nm. The separation is carried out on a reversed-phase packed column (Rainin Microsorb-MV C18, 300 Angstroms, dim 4.6 x 250 mm) using a 60:40 acetonitrile-water mixture and a flow rate of 1 mL/min. The area of the chromatographic peaks is calculated with a D-6000

interface-integrator. A calibration curve for determining the concentration of biphenyl is constructed by plotting the peak area vs. concentration of biphenyl standards. The standards prepared are 0.0005 M, 0.001 M, 0.0015 M, 0.002 M, 0.0025 M, and 0.003 M biphenyl. For HPLC measurements, all samples are diluted to $\frac{1}{4}$ of the original concentration so that the peak areas will be within the range of the calibration curve. The actual concentration is determined by taking the concentration of the diluted sample and multiplying by 4. The concentration of biphenyl is determined before the first cycle, after the first cycle, before the second cycle, and after the second cycle. In addition, the biphenyl concentration is also determined after the three control experiments: Suzuki reaction with no catalyst, Suzuki reaction in the presence of the activated carbon support without the nanoparticles, and biphenyl by itself vs. biphenyl in presence of activated carbon.

11.3.5 HRTEM Studies on the Size Distribution of the Carbon Supported Spherical Palladium Nanoparticles Before and After Catalysis and Recycling

The reaction mixture solutions containing the carbon supported spherical PVP-Pd nanoparticles are sonicated for an hour before spotting them onto TEM grids. A drop of the solution is placed onto a Formvar stabilized copper grid and the drop is allowed to evaporate in air. The spotted samples take approximately 30 minutes to dry. Since the same deposition conditions are employed for all samples, the evaporation rate of the solvent is fairly reproducible from one sample to another. For each of the experiments, the internal reproducibility of the observed size distribution is verified by spotting the sample onto three separate TEM grids. HRTEM images are also obtained from different

sections of the TEM grids in order to verify the reproducibility of the size distribution. The general reproducibility of the size distribution is verified by conducting each of the experiments three times. The nanoparticle size distribution is determined by counting approximately 1800 nanoparticles from nine enlarged HRTEM images (approximately 200 nanoparticles from each HRTEM image). Gaussian fits of the size distributions determined from the Origin 5.0 software are used to determine the average size and the width of the size distribution.

11.4 Results and Discussion

11.4.1 Catalytic Activity of the Carbon Supported Spherical Palladium Nanoparticles

The catalytic activity of the carbon supported spherical palladium nanoparticles is compared to that of the colloidal spherical palladium nanoparticles studied previously⁵². In addition, control experiments in which the Suzuki reaction is conducted without the presence of any catalyst and in which the Suzuki reaction is conducted in the presence of the activated carbon support without the nanoparticles are also done. In both cases, it is found that there is no biphenyl product that is detected from the HPLC studies. Thus, it is safe to conclude that the Suzuki reaction does not proceed without a catalyst and that the presence of activated carbon alone does not catalyze the Suzuki reaction.

Table 11.1 summarizes the HPLC results on the biphenyl yields obtained during the first and second cycles of the Suzuki reaction for both the carbon supported spherical palladium nanoparticles and the colloidal spherical palladium nanoparticles we studied previously³⁶. It can be seen that the carbon supported spherical palladium nanoparticles

do catalyze the Suzuki cross-coupling reaction, but results in a lower amount of biphenyl formed after the first cycle compared to the amount produced with the colloidal palladium nanoparticles we studied previously⁵². This could be a result of the adsorption of some of the biphenyl on the activated carbon or that the catalytic efficiency of the nanoparticles on carbon is not as good as in colloidal solution. In order to test for the possible adsorption of biphenyl on the activated carbon, a control experiment was conducted in which the concentration of biphenyl was determined when it is present in 150 mL acetonitrile:water by itself and after refluxing the biphenyl in the presence of 0.05 grams of activated carbon. It is observed that the biphenyl concentration is $12.5 \pm 1.4\%$ lower after refluxing in the presence of activated carbon when compared to the initial biphenyl concentration. This suggests that that the activated carbon adsorbs a small quantity of biphenyl and as a result, during the reaction, the actual quantity of biphenyl produced is slightly higher. As a result, the biphenyl concentration after the first and second cycle is corrected by multiplying by 114.3% in order to reflect the actual concentration of biphenyl present and this is also shown in Table 11.1. A possible reason for the catalytic efficiency of carbon supported nanoparticles being lower than that of the colloidal nanoparticles could be due to the better capping by large quantities of the carbon support (1 gram). As a result, it is possible that there is a much lower fraction of sites available for the catalytic process since many free sites are used in the adsorption process. It can be seen that even after correcting for the biphenyl that gets adsorbed onto the carbon support, the biphenyl concentration is still lower than that observed previously for the colloidal palladium nanoparticles. This suggests that the catalytic efficiency of

carbon supported nanoparticles being lower than that of the colloidal nanoparticles is the dominant cause for the lower biphenyl yield observed after the first cycle.

Table 11.1—Biphenyl Yield Obtained with the Carbon Supported Spherical PVP-Pd nanoparticles vs. Colloidal Spherical PVP-Pd nanoparticles studied previously³⁶. In the case of carbon supported spherical PVP-Pd nanoparticles, the raw biphenyl concentrations as well as the concentration corrected for biphenyl adsorbed onto the carbon support is reported.

Condition	Carbon Supported Spherical PVP-Pd Nanoparticles	Colloidal Spherical PVP-Pd Nanoparticles ³⁶
First Cycle of Suzuki Reaction	1.54 ± 0.07 mM $20 \pm 1\%$ <u>Corrected for Adsorption</u> 1.76 ± 0.07 mM $23 \pm 1\%$	3.00 ± 0.32 mM $39 \pm 4\%$
Second Cycle of Suzuki Reaction	1.07 ± 0.20 mM $14 \pm 3\%$ <u>Corrected for Adsorption</u> 1.22 ± 0.20 mM $16 \pm 3\%$	1.11 ± 0.20 mM $15 \pm 3\%$

It is interesting to note that during the second cycle of the reaction, the carbon supported spherical palladium nanoparticles do produce a high quantity of biphenyl relative to the amount that is produced during the first cycle. The colloidal spherical PVP-Pd nanoparticles we studied previously⁵² do not have a good recycling potential. Table 11.2 summarizes the biphenyl yield ratios obtained for both types of palladium nanoparticles. The biphenyl yield ratio is calculated by dividing the biphenyl yield obtained during the second cycle by that formed during the first cycle. In the case of the carbon supported palladium nanoparticles, the biphenyl concentration corrected for the

adsorption of biphenyl on the carbon is used to conduct the calculation of the biphenyl yield ratio. It can be seen that the biphenyl yield ratio for the carbon supported spherical palladium nanoparticles is quite high at 0.69 and this is due to the relatively high recycling potential of these nanoparticles. In the case of the colloidal spherical PVP-Pd nanoparticles we studied previously⁵², the biphenyl yield ratio of 0.37 is relatively low suggesting that the colloidal palladium nanoparticles have a low recycling potential. Overall, the carbon-supported spherical PVP-Pd nanoparticles have almost twice the recycling potential than that for the colloidal spherical PVP-Pd nanoparticles⁵². The high recycling potential for the carbon supported spherical PVP-Pd nanoparticles is probably due to the presence of a large amount of the carbon support around the palladium nanoparticles thus stabilizing the palladium nanoparticles. It is worth noting that the biphenyl product formation is approximately 70% and not close to 100% and this could be due to the slightly lower catalytic activity of the larger capped and stabilized palladium nanoparticles that are formed and also due to some poisoning effect that could occur due to the biphenyl product itself. The carbon supported palladium nanoparticles are not as catalytically active as the colloidal nanoparticles, but its active sites are more stable. This is a result of a good stabilizing effect of the carbon around the nanoparticles.

Table 11.2—Ratio of biphenyl yields (yield in 2nd cycle/yield in 1st cycle) for the case of the carbon supported spherical PVP-Pd nanoparticles and the colloidal spherical PVP-Pd nanoparticles studied previously³⁶. In the case of the carbon supported nanoparticles, the corrected biphenyl concentrations are used for the calculation.

Type of Nanoparticles	Ratio of Biphenyl Yields
Carbon Supported Spherical PVP-Pd Nanoparticles	0.69
Colloidal Spherical PVP-Pd Nanoparticles ³⁶	0.37

11.4.2 Effect of Catalyzing the Suzuki Reaction on the Size of Carbon Supported Spherical Palladium Nanoparticles

The effect of catalyzing the Suzuki reaction on the size of carbon supported spherical palladium nanoparticles is investigated and compared to that obtained with the colloidal spherical palladium nanoparticles. Figure 11.1 shows HRTEM images and Gaussian fits of the size distributions of the carbon supported spherical palladium nanoparticles before and after the first and second cycle of the Suzuki reaction. Table 11.3 summarizes the results on the center and width of the size distribution of the carbon supported spherical palladium nanoparticles and the colloidal spherical palladium nanoparticles studied previously⁵² before and after the first and second cycle.

It can be seen that the carbon supported spherical palladium nanoparticles are monodisperse with an average size of 1.9 ± 0.1 nm. They are similar in size to that of the colloidal spherical palladium nanoparticles we studied previously (2.1 ± 0.1 nm)⁵². After the first cycle of the Suzuki reaction, it is observed that the nanoparticles grow in size and the average size becomes 2.6 ± 0.1 nm. After the second cycle, the carbon supported nanoparticles continue to grow to an average size of 3.1 ± 0.1 nm. The continued growth of the carbon supported palladium nanoparticles and the high catalytic activity observed with these nanoparticles during the second cycle suggest that the carbon support is effective in preventing aggregation and precipitation of the nanoparticles unlike the colloidal spherical palladium nanoparticles in which the larger nanoparticles that were formed aggregated and precipitated out of solution leaving the smaller nanoparticles left in solution⁵².

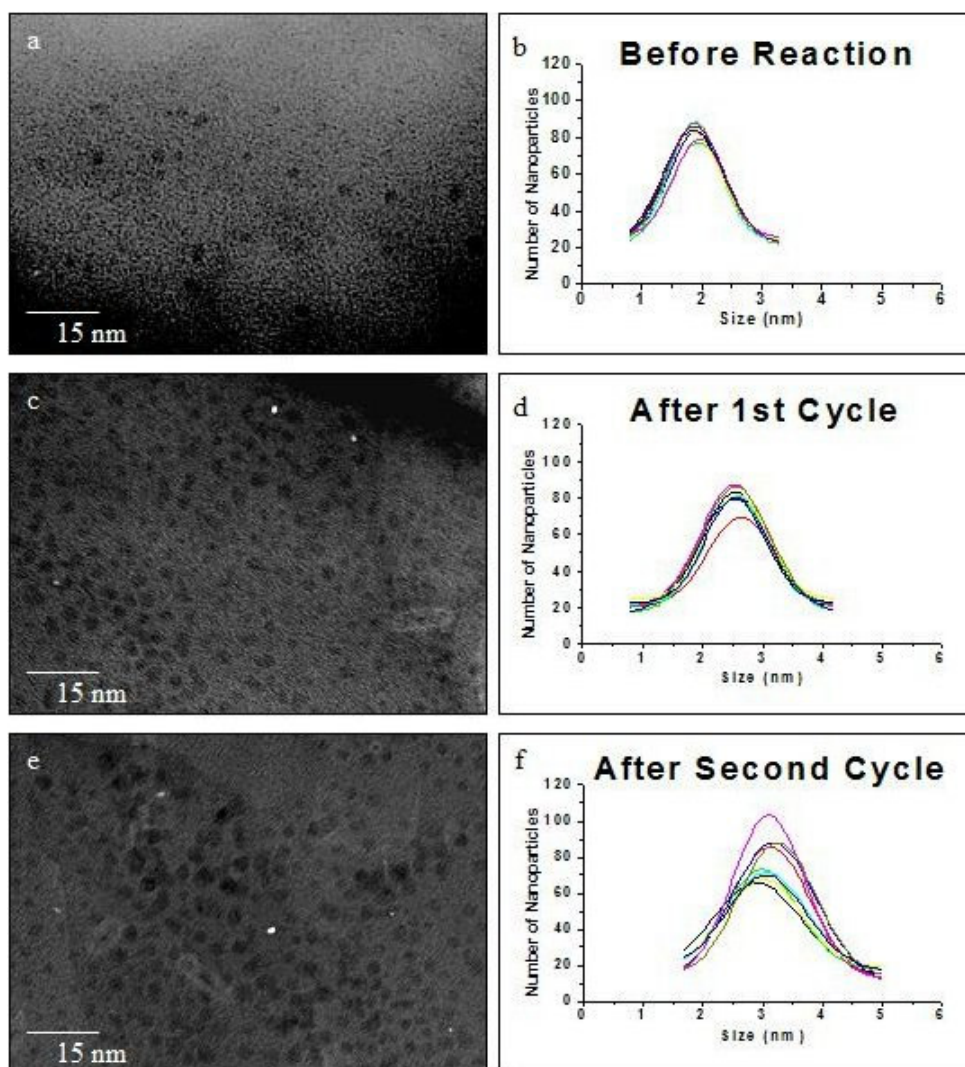


Figure 11.1—HRTEM images and Gaussian fits of the size distributions of the carbon supported spherical palladium nanoparticles before any perturbations (a-b), after the first cycle of the Suzuki reaction (c-d), and after the second cycle of the Suzuki reaction (e-f)

Table 11.3—Size distributions of the carbon supported spherical PVP-Pd nanoparticles and the colloidal spherical PVP-Pd nanoparticles studied previously³⁶ before the reaction, after the first cycle, and after the second cycle.

Condition	Carbon Supported Spherical PVP-Pd NPs	Colloidal Spherical PVP-Pd NPs ³⁶
Before Suzuki Reaction	$C_D = 1.9 \pm 0.1$ nm $W_D = 0.9 \pm 0.1$ nm	$C_D = 2.1 \pm 0.1$ nm $W_D = 1.1 \pm 0.2$ nm
After First Cycle of Suzuki Reaction	$C_D = 2.6 \pm 0.1$ nm $W_D = 1.1 \pm 0.1$ nm	$C_D = 2.9 \pm 0.3$ nm $W_D = 2.8 \pm 0.4$ nm
After Second Cycle of Suzuki Reaction	$C_D = 3.1 \pm 0.1$ nm $W_D = 1.3 \pm 0.1$ nm	$C_D = 2.2 \pm 0.2$ nm $W_D = 0.9 \pm 0.2$ nm

It is also worth noting that the width of the size distribution of the carbon supported palladium nanoparticles is not as broad as that of the colloidal spherical palladium nanoparticles. This might be due to the repetitive centrifugation and decanting techniques used to prepare the nanoparticles in the carbon samples. The method of preparing the carbon supported palladium nanoparticles also results in very little, if any, free palladium atoms in the sample. This is because the centrifugation process would have effectively removed these atoms as well as unaggregated palladium atoms and colloidal palladium nanoparticles that are not adsorbed onto the support. In addition, the ethanol is also removed during the centrifugation process and as a result, no further reduction of any remaining palladium ions can occur. As a result, the growth of the nanoparticles during the reaction must then occur by the detachment of atoms from the smaller palladium nanoparticles and reattachment of these atoms to the more stable surfaces of the larger palladium nanoparticles. This would explain why the size

distribution is not very broad compared to the colloidal spherical palladium nanoparticles we studied previously⁵².

11.5 Conclusions

It is observed that while the carbon supported spherical palladium nanoparticles are less catalytically active compared to the colloidal spherical palladium nanoparticles we studied previously³⁶, the carbon supported nanoparticles have almost double the recycling potential than the colloidal palladium nanoparticles. This is probably due to the stabilizing effect of carbon as a possible capping agent. The carbon supported spherical palladium nanoparticles grow in size during the first and second cycle of the reaction and the width of the size distribution is not very broad. The presence of the carbon support makes the nanoparticles resistant to aggregation and precipitation and also helps to preserve its catalytic activity during the second cycle. In addition, the adsorption method of preparing the supported palladium nanoparticles effectively favors the adsorption of larger palladium against the very small ones as well as the palladium atoms. This results in the Ostwald ripening growth mechanism occurring only between the nanoparticles present on the carbon support. Overall, the carbon supported spherical palladium nanoparticles are potentially better recyclable catalysts for the Suzuki reaction than colloidal palladium nanoparticles.

11.6 References

1. Chen, S.; Kucernak, A., *J. Phys. Chem. B*, **2004**, *108*(10), 3262.
2. Liu, Z.; Ling, X. Y.; Lee, J. Y.; Su, X.; Gan, L. M., *J. Mat. Chem.*, **2003**, *13*(12), 3049.

3. Fachini, E. R.; Diaz-Ayala, R.; Casado-Rivera, E.; File, S.; Cabrera, C. R., *Langmuir*, **2003**, *19*(21), 8986.
4. Lang, H.; May, R. A.; Iversen, B. L.; Chandler, B. D., *J. Am. Chem. Soc.*, **2003**, *125*(48), 14832.
5. Bianchini, C.; Dal Santo, V.; Meli, A.; Moneti, S.; Moreno, M.; Oberhauser, W.; Psaro, R.; Sordelli, L.; Vizza, F., *J. Catal.*, **2003**, *213*(1), 47.
6. Yoo, J. W.; Hathcock, D. J.; El-Sayed, M. A., *J. Catal.*, **2003**, *214*(1), 1.
7. Yoo, J. W.; Hathcock, D.; El-Sayed, M. A., *J. Phys. Chem. A*, **2002**, *106*(10), 2049.
8. Marconi, G.; Pertici, P.; Evangelisti, C.; Caporusso, A. M.; Vitulli, G.; Capannelli, G.; Hoang, M.; Turney, T. W., *J. Organomet. Chem.*, **2004**, *689*(3), 639.
9. Bowker, M.; Stone, P.; Bennett, R.; Perkins, N., *Surf. Sci.*, **2002**, *511*(1-3), 435.
10. Claus, P.; Hofmeister, H., *J. Phys. Chem. B*, **1999**, *103*(14), 2766.
11. Chen, C.-W.; Serizawa, T.; Akashi, M. *Chem. Mater.* **1999**, *11*, 1381.
12. Hirai, H.; Ohtaki, M.; Komiyama, M. *Chem. Lett.* **1986**, 269.
13. Jacobs, P. W.; Wind, S. J.; Ribeiro, F. H.; Somorjai, G. A., *Surf. Sci.*, **1997**, *372*(1-3), L249.
14. Eppler, A.; Rupprechter, G.; Guzzi, L.; Somorjai, G. A., *J. Phys. Chem. B*, **1997**, *101*(48), 9973.
15. Eppler, A. S.; Rupprechter, G.; Anderson, E. A.; Somorjai, G. A., *J. Phys. Chem. B*, **2000**, *104*(31), 7286.
16. Grunes, J.; Zhu, J.; Anderson, E. A.; Somorjai, G. A., *J. Phys. Chem. B*, **2002**, *106*(44), 11463.
17. Eppler, A.; Rupprechter, G.; Guzzi, L.; Somorjai, G. A. *J. Phys. Chem. B* **1997**, *101*(48), 9973.
18. Toshima, N.; Yonezawa, T. *New J. Chem.* **1998**, *22*(11), 1179.
19. Schmid, G. *Met. Clus. Chem.* **1999**, *3*, 1325.
20. Puddephatt, R. J. *Met. Clus. Chem.* **1999**, *2*, 605.
21. Henry, C. R. *Appl. Surf. Sci.* **2000**, *164*, 252.

22. St. Clair, T. P.; Goodman, D. W. *Top. Catal.* **2000**, *13*(1,2), 5.
23. Kralik, M.; Corain, B.; Zecca, M. *Chem. Pap.* **2000**, *54*(4), 254.
24. Chusuei, C. C.; Lai, X.; Luo, K.; Goodman, D. W. *Top. Catal.* **2001**, *14*(1-4), 71.
25. Bowker, M.; Bennett, R. A.; Dickinson, A.; James, D.; Smith, R. D.; Stone, P. *Stud. Surf. Sci. Catal.* **2001**, *133*, 3.
26. Kralik, M.; Biffis, A. *J. Mol. Catal. A: Chem.* **2001**, *177*(1), 113.
27. Thomas, J. M.; Raja, R. *Chem. Rec.* **2001**, *1*(6), 448.
28. Mohr, C.; Claus, P. *Sci. Prog.* **2001**, *84*(4), 311.
29. Thomas, J. M.; Johnson, B. F. G.; Raja, R.; Sankar, G.; Midgley, P. A. *Acc. Chem. Res.* **2003**, *36*(1), 20.
30. Collier, P. J.; Iggo, J. A.; Whyman, R. *J. Mol. Catal. A: Chem.* **1999**, *146*(1-2), 149.
31. Sculz, J.; Roucoux, A.; Patin, H. *Chem. Eur. J.* **2000**, *6*(4), 618.
32. Wang, Q.; Liu, H.; Han, M.; Li, X.; Jiang, D. *J. Mol. Catal. A: Chem.* **1997**, *118*(2), 145.
33. Kim, S.; Son, S. U.; Lee, S. S.; Hyeon, T.; Chung, Y. K.; *Chem. Commun.* **2001**, 2212.
34. Larpent, C.; Menn, B. F.; Patin, H. *J. Mol. Catal.* **1991**, *65*, L35.
35. Hansen, P. L.; Wagner, J. B.; Helveg, S.; Rostrup-Nielsen, J. R.; Clausen, B. S.; Topsoe, H., *Science* **2002**, *295*(5562), 2053.
36. Hayek, K.; Goller, H.; Penner, S.; Rupprechter, G.; Zimmermann, C., *Catal. Lett.* **2004**, *92*, (1-2), 1.
37. Liu, R.-J.; Crozier Peter, A.; Smith, C. M.; Hucul Dennis, A.; Blackson, J.; Salaita, G., *Micros. Microanal.* **2004**, *10*, (1), 77.
38. Balint, I.; Miyazaki, A.; Aika, K.-i., *Phys. Chem. Chem. Phys.* **2004**, *6*, (9), 2000.
39. Rupprechter, G.; Eppler, A. S.; Avoyan, A.; Somorjai, G. A., *Stud. Surf. Sci. Catal.* **2000**, *130A*, 215.
40. Chechik, V.; Crooks, R. M. *J. Am. Chem. Soc.* **2000**, *122*, 1243.

41. Yeung, L. K.; Crooks, R. M. *Nano Lett.* **2001**, *1*(1), 14.
42. Dupont, J.; Fonseca, G. S.; Umpierre, A. P.; Fichtner, P. F. P.; Teixeira, S. R. *J. Am. Chem. Soc.* **2002**, *124*, 4228.
43. Hirai, H.; Chawanya, H.; Toshima, N. *Nip. Kag. Kai.* **1984**, *6*, 1027.
44. Brook, M. A.; Ketelson, H. A.; LaRonde, F. J.; Pelton, R., *Inorg. Chim. Acta* **1997**, *264*, (1-2), 125.
45. Ketelson, H. A.; Brook, M. A.; Pelton, R.; Heng, Y. M., *Chem. Mat.* **1996**, *8*, (9), 2195.
46. Priyanto, U.; Sakanishi, K.; Okuma, O.; Mochida, I., *Fuel Process. Tech.* **2002**, *79*, (1), 51.
47. Yoon, T.-J.; Lee, W.; Oh, Y.-S.; Lee, J.-K., *New J. Chem.* **2003**, *27*, (2), 227.
48. Narayanan, R.; El-Sayed, M. A. *J. Phys. Chem. B*, **2003**, *107*(45), 12416.
49. Narayanan, R.; El-Sayed, M. A. *Nano Lett.*, **2004**, *4*(7), 1353.
50. Narayanan, R.; El-Sayed, M. A. *J. Am. Chem. Soc.*, **2004**, *126*(23), 7419.
51. Narayanan, R.; El-Sayed, M. A. *J. Phys. Chem. B*, **2004**, *108*(18), 5726.
52. Narayanan, R.; El-Sayed, M. A. *J. Am. Chem. Soc.*, **2003**, *125*(27), 8340.
53. Narayanan, R.; El-Sayed, M. A. *J. Phys. Chem. B*, **2004**, *108*(25), 8572.
54. Narayanan, R.; El-Sayed, M. A. *Langmuir*, **2005**, *21*(5), 2027.
55. Li, Y.; El-Sayed, M. A. *J. Phys. Chem. B* **2001**, *105*, 8938.
56. Bulushev, D. A.; Yuranov, I.; Suvorova, E. I.; Buffat, P. A.; Kiwi-Minsker, L., *J. Catal.*, **2004**, *224*(1), 8.
57. Lopez, N.; Janssens, T. V. W.; Clausen, B. S.; Xu, Y.; Mavrikakis, M.; Bligaard, T.; Norskov, J. K., *J. Catal.*, **2004**, *223*(1), 232.
58. Chen, S.; Kucernak, A., *J. Phys. Chem. B*, **2004**, *108*(10), 3262.
59. Liu, Z.; Lee, J. Y.; Chen, W.; Han, M.; Gan, L. M., *Langmuir*, **2004**, *20*(1), 181.

60. Nakagawa, K.; Yamagishi, M.; Nishimoto, H.; Ikenaga, N.; Suzuki, T.; Kobayashi, T.; Nishitani-Gamo, M.; Ando, T., *Chem. Mat.*, **2003**, *15*(24), 4571.
61. Fachini, E. R.; Diaz-Ayala, R.; Casado-Rivera, E.; File, S.; Cabrera, C. R., *Langmuir*, **2003**, *19*(21), 8986.
62. Takasu, Y.; Itaya, H.; Kawaguchi, T.; Sugimoto, W.; Murakami, Y., *Stud. Surf. Sci. Catal.*, **2003**, *145*, 279.
63. Li, F.; Zou, J.; Yuan, G., *Catal. Lett.*, **2003**, *89*(1-2), 115.
64. Carretin, S.; McMorn, P.; Johnston, P.; Griffin, K.; Kiely, C. J.; Hutchings, G. J., *Phys. Chem. Chem. Phys.*, **2003**, *5*(6), 1329.
65. Suzuki, A. In *Metal-Catalyzed Cross-Coupling Reactions*; Diederich, F., Stang, P. J., Eds.; VCH: Weinheim, 1998, pp 49.
66. Alo, B. I.; Kandil, A.; Patil, P. A.; Sharp, M. J.; Siddiqui, M. A.; Snieckus, V. J. *Org. Chem.* **1991**, *56*, 3763.
67. Wallow, T. I.; Novak, B. M.; *J. Org. Chem.* **1994**, *59*, 5034.
68. Bumagin, N. A.; Bykov, V. V.; Beletskaya, I. P.; *Dokl. Akad. Nauk. SSSR* **1990**, *315*, 1133.
69. Marck, G.; Villiger, A.; Buchecker, R. *Tetrahedron Lett.* **1994**, *35*, 3277.
70. Baleizao, C.; Corma, A.; Garcia, H.; Leyva, A., *Chem. Comm.*, **2003**, *5*, 606.
71. Bedford, R. B.; Cazin, C. S. J.; Hursthouse, M. B.; Light, M. E.; Pike, K. J.; Wimperis, S., *J. Organomet. Chem.*, **2001**, *633*(1-2), 173.
72. Chamoin, S.; Houldsworth, S.; Kruse, C. G.; Bakker, W. I.; Snieckus, V., *Tetrahed. Lett.* **1998**, *39*(24), 4179.
73. Gurbuz, N.; Ozdemir, I.; Cetinkaya, B.; Seckin, T., *Appl. Organomet. Chem.* **2003**, *17*(10), 776.
74. Hardy, J. J. E.; Hubert, S.; Macquarrie, D. J.; Wilson, A. J., *Green Chem.* **2004**, *6*(1), 53.
75. Kabalka, G. W.; Pagni, R. M.; Hair, C. M., *Org. Lett.* **1999**, *1*, (9), 1423.

76. Marck, G.; Villiger, A.; Buchecker, R., *Tetrahed. Lett.* **1994**, 35, (20), 3277.
77. Paul, S.; Clark, J. H., *Green Chem.* **2003**, 5, (5), 635.
78. Uozumi, Y.; Nakai, Y., *Org. Lett.* **2002**, 4, (17), 2997.
79. Gopidas, K. R.; Whitesell, J. K.; Fox, M. A., *Nano Lett.* **2003**, 3, (12), 1757.
80. Li, Y.; Boone, E.; El-Sayed, M. A., *Langmuir*, **2002**, 18, (12), 4921.
81. Li, Y.; El-Sayed, M. A., *J. Phys. Chem. B* **2001**, 105, (37), 8938.
82. Li, Y.; Hong, X. M.; Collard, D. M.; El-Sayed, M. A., *Org. Lett.* **2000**, 2, (15), 2385.
83. Liu, Y.; Khemtong, C.; Hu, J., *Chem. Commun.*, **2004**, 4, 398.
84. Lu, F.; Ruiz, J.; Astruc, D., *Tetrahed. Lett.* **2004**, 45, (51), 9443.
85. Moreno-Manas, M.; Pleixats, R.; Villarroya, S., *Organomet.* **2001**, 20, (22), 4524.
86. Pittelkow, M.; Moth-Poulsen, K.; Boas, U.; Christensen, J. B., *Langmuir* **2003**, 19, (18), 7682.
87. Strimbu, L.; Liu, J.; Kaifer, A. E., *Langmuir* **2003**, 19, (2), 483.
88. Kim, N.; Kwon, M. S.; Park, C. M.; Park, J., *Tetrahed. Lett.* **2004**, 45, (38), 7057.
89. Kogan, V.; Aizenshtat, Z.; Popovitz-Biro, R.; Neumann, R., *Org. Lett.* **2002**, 4, (20), 3529.

APPENDIX A

LIST OF PUBLICATIONS

1. Narayanan, R.; El-Sayed, M. A. “Effect of Catalysis on the Stability of Metallic Nanoparticles: Suzuki Reaction Catalyzed by PVP-Palladium Nanoparticles” *J. Am. Chem. Soc.*, **2003**, *125*(27), 8340-8347.
2. Narayanan, R.; El-Sayed, M. A. “Effect of Catalytic Activity on the Size Distribution of Metallic Nanoparticles: Electron Transfer Reaction Catalyzed by PVP-Platinum Nanoparticles” *J. Phys. Chem. B*, **2003**, *107*(45), 12416-12424.
3. Narayanan, R.; El-Sayed, M. A. “Effect of Catalysis in Colloidal Solution on the Tetrahedral and Cubic Nanoparticle SHAPE: Electron Transfer Reaction Catalyzed by Platinum Nanoparticles”, *J. Phys. Chem. B.*, **2004**, *108*(18), 5726-5733.
4. Narayanan, R.; El-Sayed, M. A. “Changing Catalytic Activity During Colloidal Platinum Nanocatalysis Due to Shape Changes: Electron Transfer Reaction”, *J. Am. Chem. Soc.*, **2004**, *126*(23), 7194-7195.
5. Narayanan, R.; El-Sayed, M. A. “Effect of Colloidal Catalysis on the Nanoparticle Size Distribution: Dendrimer-Pd vs. PVP-Pd Nanoparticles Catalyzing the Suzuki Coupling Reaction”, *J. Phys. Chem. B*, **2004**, *108*(25), 8572-8580 (Special Issue honoring Dr. Alvin L. Kwiram).
6. Narayanan, R.; El-Sayed, M. A. “Shape-Dependent Catalytic Activity of Platinum Nanoparticles in Colloidal Solution”, *Nano Lett.*, **2004**, *4*(7), 1343-1348.
7. Burda, C.; Chen, X.; Narayanan, R.; El-Sayed, M. A. “The Chemistry and Properties of Nanocrystals of Different Shapes”, *Chem. Rev.*, **2005**, in press. (**Invited Review Article**)
8. Narayanan, R.; El-Sayed, M. A. “Effect of Colloidal Nanocatalysis on the Metallic Nanoparticle Shape: The Suzuki Reaction”, *Langmuir*, **2005**, *21*(5), 2074.
9. Narayanan, R.; El-Sayed, M. A. “FTIR Study of the Mode of Binding of the Reactants on the Pd Nanoparticle Surface during the Catalysis of the Suzuki Reaction”, *J. Phys. Chem. B*, **2005**, ASAP Article.
10. Narayanan, R.; El-Sayed, M. A. “Colloidal Catalysis with Transition Metal Nanoparticles: Effect of Nanoparticle Shape on Catalysis and the Effect of Catalysis

on the Nanoparticle Shape and Size“, submitted to *J. Phys. Chem. B.* (**Invited Feature Article**)

11. Narayanan, R.; El-Sayed, M. A. “Carbon Supported Palladium Nanoparticles as Potential Recyclable Catalysts for the Suzuki Reaction”, in preparation for submission.

VITA

Radha Narayanan was born in Savannah, GA in 1978. She attended Windsor Forest High School and was the class valedictorian when she graduated in 1996. Afterwards, she attended Armstrong Atlantic State University in Savannah, GA to pursue a B. S. degree in chemistry with a minor in psychology and she graduated in May 2000. In addition to obtaining numerous scholarships and awards, she graduated *summa cum laude* and as an Honors program graduate at Armstrong. She then attended Georgia Institute of Technology to pursue the Ph.D. program in chemistry and received numerous fellowships and awards. She worked for Dr. Mostafa A. El-Sayed and conducted research on shape-dependent nanocatalysis and the effect of the catalytic process on the size and shape of colloidal metal nanocatalysts. Her thesis work has so far resulted in 8 publications and she has presented her thesis work in numerous local, regional, and national meetings.